"*Ortho*- and *Edge*-Functionalization of Ryleneimides"

Dissertation

zur Erlangung des Grades

"Doktor der Naturwissenschaften"

im Promotionsfach Chemie

am Fachbereich Chemie, Pharmazie und Geowissenschaften

der Johannes Gutenberg-Universität

in Mainz

vorgelegt von

Glauco Battagliarin

geboren in Milano, Italien

Mainz, 2013

Dekan: Prof. Dr. ██████████

1. Berichterstatter: Prof. Dr. ████████

2. Berichterstatter: Prof. Dr. ██████████

Tag der mündlichen Prüfung: 23.09.2013

A Giordy

Die vorliegende Dissertation wurde unter Betreuung durch Herrn Prof. Dr. ███████ am Max Planck Institut für Polymerforschung in Mainz in der Zeit vom 01. Oktober 2008 bis zum 15. Juli 2012 angefertigt.

Danksagung

Table of Contents

List of Abbreviations

a.u.	arbitrary unit
d	doublet (NMR)
DBN	1,5-diazabicyclo[4.3.0]-non-5-en
DBU	1,8-diazabicyclo[5,4,0]undec-7-en
DCM	dichloromethane
DFT	density functional theory
DMF	N,N-dimethylformamide
DMSO	dimethylsulfoxide
DSSC	dye-sensitized solar cell
FD	field desorption
FET	field-effect transistor
h	hour
HAC	acetic acid
HBC	hexa-*peri*-hexabenzocoronene
HOMO	highest occupied molecular orbital
ICT	intramolecular charge-transfer
IR	infrared
I_{sc}	short-circuit current
LED	light emitting diode
LUMO	lowest unoccupied molecular orbital
m	multiplett (NMR)
MALDI-TOF	matrix-assisted laser desorption/ionization time-of-flight
Me	methyl
min	minute
MS	mass spectrometry
NIR	near-infrared
NMR	nuclear magnetic resonance
NMP	1-methyl-2-pyrrolidone
PCE	power conversion efficiency
PDI	perylenediimide
Ph	phenyl
PL	photoluminescence
PMI	perylenemonoimide
ppm	parts per million
PV	photovoltaic
s	singlet (NMR)
sDSSCs	solid-state dye-sensitized solar cell
t	triplet (NMR)
TBAF	tetra-iso-butyl ammonium fluoride
TDI	terrylenediimide
THF	tetrahydrofuran
TGA	thermo-gravimetry analysis
TLC	thin layer chromatography
TOF	time-of-flight
UV	ultraviolet
vis	visible
V_{oc}	open circuit voltage

1 Introduction

The birth of dyestuff chemistry dates back to 1865, when William Henry Perkin serendipitously discovered the synthesis of mauvine.[1] Since then, hundreds of dyes and pigments have been reported and produced on an industrial scale. While colorants have been for a long time only applied for simple aesthetic purposes, in recent times they found novel fields of applications, experiencing a renaissance as "functional dyes".[2] Their structural features, which determine their color, have made them very interesting platforms for the design and synthesis of functional materials. Their π-conjugated structure, responsible for the absorption in the visible region, provides the scaffold on which charge carriers can hop, making them suitable as organic semiconductors.[3] Their absorption properties play a fundamental role when incorporated into optical filters or organic solar cells, where light harvesting is critical.[4] Their fluorescence and phosphorescence is used to generate light within organic light emitting devices[5] or for the development of probes for bioimiaging.[6] All these desirable properties can be tailored via targeted chemical modifications to fit the application requirements, taking advantage of the precious expertise developed in the colorant industry. Nevertheless such expertise provides a first set of synthetic tools that must be constantly broadened and extended to fulfill the ambitious requirements of the market. Therefore chemists are challenged day by day in developing and implementing new synthetic instruments to optimize the performances of known colorants, making dye chemistry an ever-young field of research. Without doubt, ryleneimides (RIs) belong to the most investigated systems in the field of colorants and functional dyes.[7] RIs have found many applications ranging from the colorant industry[8] to photonics as dyes for electrophotographic devices[9], fluorescent solar collectors[10], dye lasers[11] or bioimaging[12], to the more recent use in organic electronics as electron transporting materials in field effect transistors[13] and heterojunction solar cells[14] or as light absorbers in dye sensitized solar cells[15].

1.1 Ryleneimides: Definition and Synthesis

Ryleneimides are obtained combining two simple ingredients: 1) a conjugated core composed of fused naphthalene units linked between their *peri*-positions (1 and 1' and the 8 and 8' positions) to give the scaffold of the oligo-*peri*-naphtylene, known with the abbreviation "rylene";[16] 2) one or two six-membered dicarboxylic imide rings introduced at the *peri*-positions of the terminal naphthalene units, as depicted in Figure 1.
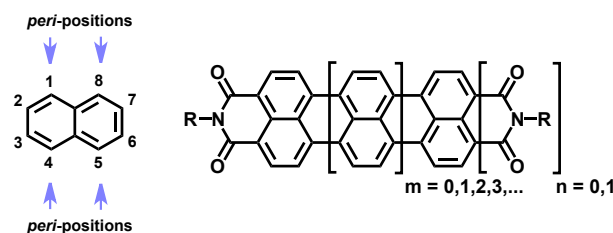
Figure 1 The "monomer" naphthalene (left) and the general structure of a ryleneimide. For n=0 or 1 a monoimide or diimide is obtained, respectively. The rylene series features of perylene (m=0), terrylene (m=1), quaterrylene (m=2), pentarylene (m=3), hexarylene (m=4) heptarylene (m=5) and octarylene (m=6).

The research on ryleneimides starts historically and synthetically with the discovery of perylenediimide (PDI), the first member of the family reported by Kardos in the beginning of the 1910s.[17] Nowadays perylenediimides are produced on an industrial scale as high performance pigments, following the synthesis shown in Scheme 1. In this production process, the perylenediimide lead structure is obtained after a homocoupling reaction using naphthalene monoimide and converted into perylenedianhydride (PDA).
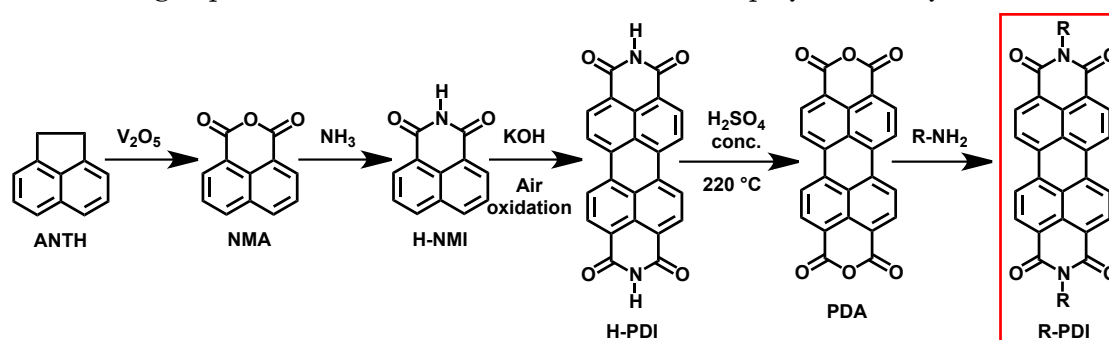
Scheme 1 Industrial synthesis of perylenediimide (**PDI**) and perylenedianhydride (**PDA**), starting from the oxidation of acenaphthylene, followed by the imidization of the naphthalenemonoanhydride with ammonia to obtain the naphthalenemonoimide. Further reaction in alkali melt leads to the formation of the perylenediimide structure.

PDA can be considered as the fundamental building block in the chemistry of ryleneimides.[18] In fact PDIs bearing different imide substituents can be synthesized by simple imidization of PDA.[19] Perylene dianhydride represents also the first step toward the synthesis of the other members of the ryleneimide family.[20] Via an imidization-decarboxylation reaction, a perylenemonoimide (PMI) is obtained.[21] This asymmetric molecule can then be further coupled with other rylenes or rylenemonoimides to obtain the higher homologues of the series. The two most popular synthetic routes towards the second homologue of the series of rylenediimides, terrylenediimide (TDI) are shown in Scheme 2. The first route is the multistep synthesis starting from the bromination of perylenemonoimide, the second procedure is the one-pot coupling of perylenemonoimide with naphthalenemonomide.[22] These two protocols can be easily extended for the synthesis of the higher ryleneimides, by simply varying the rylenes or rylenemonoimides used in the reactions.[23] The limited number of steps needed for the synthesis of the more extended ryleneimide derivatives and the commercial availability at affordable prices of PDIs and more importantly of **PDA** represents one the first reasons making ryleneimides-based materials so successful.
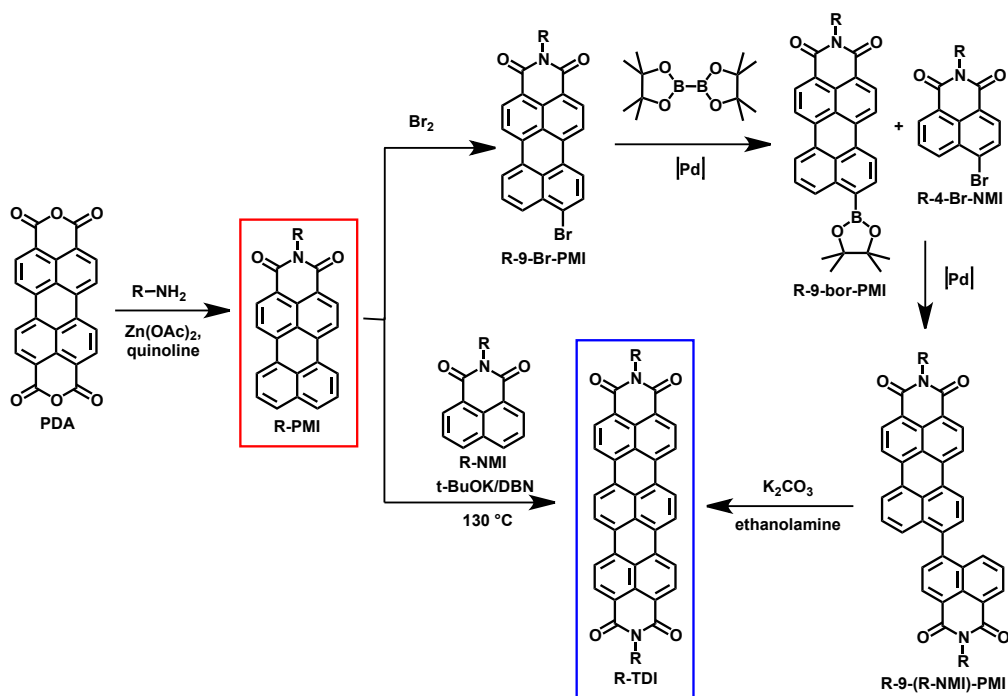
Scheme 2 Synthesis of perylenemonoimide (PMI) and terrylenediimide (TDI).

1.2 Properties of Ryleneimides

Unsubstituted ryleneimides are attractive basic structures for the creation of functional dyes, not only due to their synthetic accessibility, but also because of their outstanding properties. Among them their impressive chemical, thermal and photochemical stability exceeding those of most of the organic dyes known in the literature plays a major role.[24] Such stability is particularly accentuated for the diimide derivatives and is maintained throughout the rylene series, even in the case of the higher homologues possessing smaller HOMO-LUMO gaps. This persistence of stability is a result of their low lying LUMO energies and the little impact that the extension of the conjugated core has on them. In fact the introduction of additional naphthalene units into the conjugated core leads only to minor changes in the energy of the LUMO level, while the HOMO rises considerably.[25] Therefore ryleneimides are ideal materials for applications requiring long-term stability and small alteration of their initial properties. Perylenediimides are nowadays an important class of high performance pigments with high color strength, weather fastness and migration stability, finding application in the coloration of automotive, of plastics and engineering resins.[8]

The second attractive feature of ryleneimides is connected to their optical properties. RIs normally show high extinction coefficients with strong vibronically structured absorptions. The unsubstituted lower homologues PDIs and PMIs for example possess molar extinction coefficients in the order of 10^4 M^{-1}cm^{-1} in the region between 400 and 550 nm.[26] The extension of the conjugated core by successive introduction of naphthalene units causes an increase of the absorptivities and a bathochromic shift. If rylenediimides are considered, the energy of the absorption maximum correlates in a nearly linear

manner with the inverse square length of the π-conjugated system. A linear correlation is also observed between the number of naphthalene units composing the core and the maximum absorptivity.[23c]

Additionally some of the rylenediimides exhibit outstanding fluorescence. Unsubstituted perylenediimides may show quantitative quantum yields, which remain nearly unchanged also in the case of terrylenediimides (90 %). Their emission spectrum typically exhibits only a small Stokes shift and appears as a mirror image of the absorption curve. The higher homologues, beginning from quaterrylenediimide, lose their fluorescence dramatically.[20]

The outstanding photostability combined with the high fluorescence quantum yields makes PDI and TDI ideal probes for single molecule spectroscopy investigations. In particular TDI, that thanks to its absorption above 600 nm, can be excited with inexpensive and effective sources, such as HeNe laser (633 nm) or the krypton-ion laser (647, 676 nm). Furthermore TDI derivatives showed record stabilities, which allowed tracking of single molecules for several minutes before photobleaching. The combination of these desirable properties allowed the use of TDI in a variety of applications such as biomimetic models of photosynthesis[27], bioimaging[28] and multichromophoric arrays.[29]

Last, but not least, rylenediimides possess large electron affinities and they can undergo reversible double reductions. Their relatively low lying LUMO energies render these molecules rather easy to be reduced and this property is very appealing in particular in the field of n-type semiconductors, where low LUMO energies are required to stabilize the molecules in their reduced forms.[30]

This set of outstanding properties of ryleneimides can be further tuned via chemical modifications of their basic structure to obtain tailor-made materials. The extraordinary chemical, thermal and photochemical stability allows to maintain the molecular scaffold and perform post-functionalization. This strategy permits straightforward modifications, without the need for tedious multistep syntheses and is an added value of ryleneimides as compared to other dyes. The functionalization strategies can be mainly divided into two: imide variation (Figure 2, red arrows) and core modification (Figure 2, blue and orange arrows).
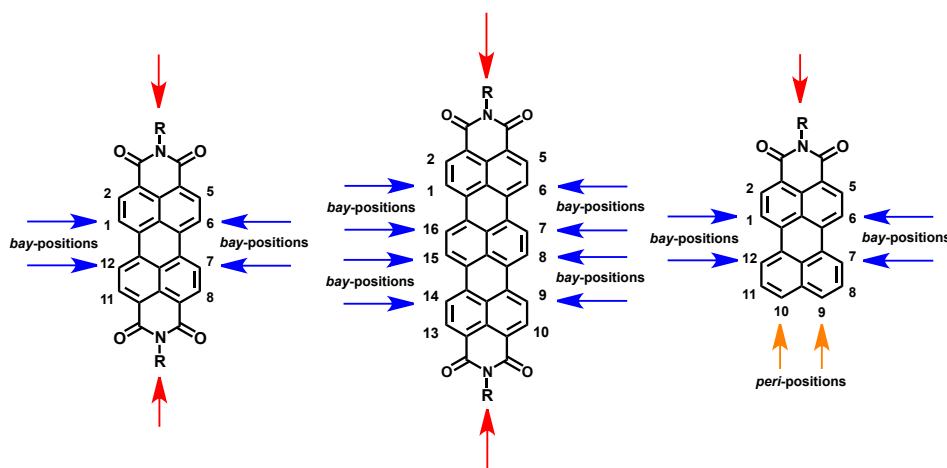
Figure 2 Accessible positions of ryleneimides: the imide positions (red arrows), the *bay*-positions (blue arrows) and *peri*-positions (orange arrows).

1.3 Chemistry of Ryleneimides: Imide Functionalization

Variation of the imide substituents is typically used to tune the solubility and solid-state packing of rylene molecules and does not consistently affect the optical and electrochemical properties. In fact, both HOMO and LUMO orbitals of unsubstituted ryleneimides exhibit a nodal plane bisecting the molecule along its long symmetry axis, on which the imide nitrogens are located.[26] Therefore the effect of imide substitution on the frontier orbital energies is expected to be inductive in nature and, therefore, similar for both HOMO and LUMO, leading to little change in the optical properties.[19] The calculated frontier molecule orbitals of perylenediimide are shown in Figure 3 as example.

HOMO   **LUMO**
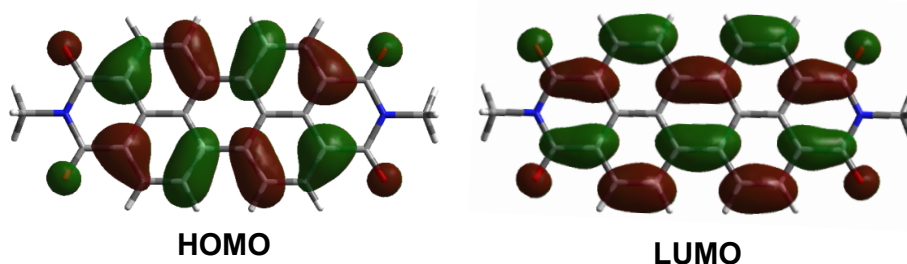
Figure 3 Frontier molecular orbitals of N,N'-dimethyl-perylenediimide, obtained via DFT calculations.

The chemistry of the imide represents the historically more consolidated functionalization, beginning already with the ground research in the pigment chemistry. In this field systematic variation of the imide substituents is used to influence the solid-state packing and thus the color of the bulk material.[31] This phenomenon, typical for PDI pigments, is called crystallochromy and it derives from the different intermolecular π-π stacking. [32]

During the 1980s Langhals based a successful solubilizing strategy of perylenediimides on imide functionalization, which determined the transition from perylenediimde pigments to dyes. This approach relied upon the introduction of bulky α-branched alkyl chains (also known as swallow-tail substituents, Figure 4) at the imidic nitrogen with the possibility to modulate solubility.[33] Other typical solubilizing groups used for this scope are *ortho*-substituted aryls, as the 2,6-diisopropylphenyl group depicted in Figure 4.[34]
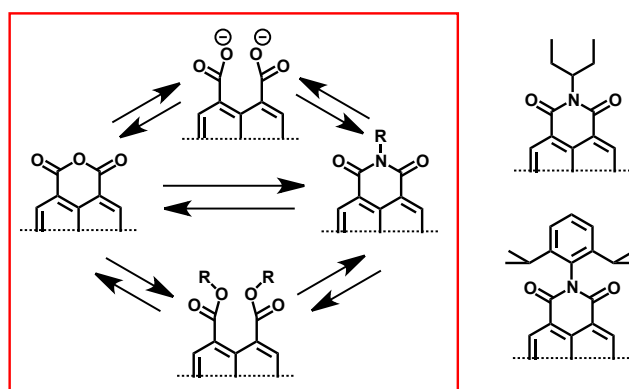
Figure 4 Chemistry of the imide (red box). Examples of α-branched alkyl chains and *ortho*-substituted phenyl ring (right).

The attractive future of the chemistry of the imide is the reversibility of most of the reactions allowing the introduction and removal of substituents according to different needs via simple acid or base-catalyzed reactions. Solubility and reactivity can be greatly influenced switching from the imide to the anhydride derivative or the dicarboxylic acids or esters.[35]

1.4 Core Functionalization via Halogenation

The second important functionalization of ryleneimides is the decoration of the aromatic core. Introduction of different substituents directly into the conjugated system allows to not only influence solubility and solid-state packing, but, more importantly, to tune the optical and electronic properties as desired. Since the rylene core exhibits multiple accessible positions, pattern and number of substituents can be varied, with different consequences i.e. on the energy of the molecular orbitals, optical properties and other molecular and supramolecular features.

Access to the aromatic core of ryleneimides is typically achieved via halogenation. In the case of the diimide derivatives, halogenation is favored at the so-called *bay*-positions (Figure 2). Chlorination of the 1,6,7,12-positions (*bay*-positions) of perylenediimides was first reported by BASF as a solubilizing strategy.[34] In fact the introduction of halogen atoms in the *bay*-region causes a geometric distortion of the aromatic core, which reduces the aggregation of the molecules and allows the transition from insoluble pigments to soluble dyes. While the geometrical distortion of the molecular structure is beneficial for solubilizing reasons, it may not be desirable for some applications where close stacking is crucial.
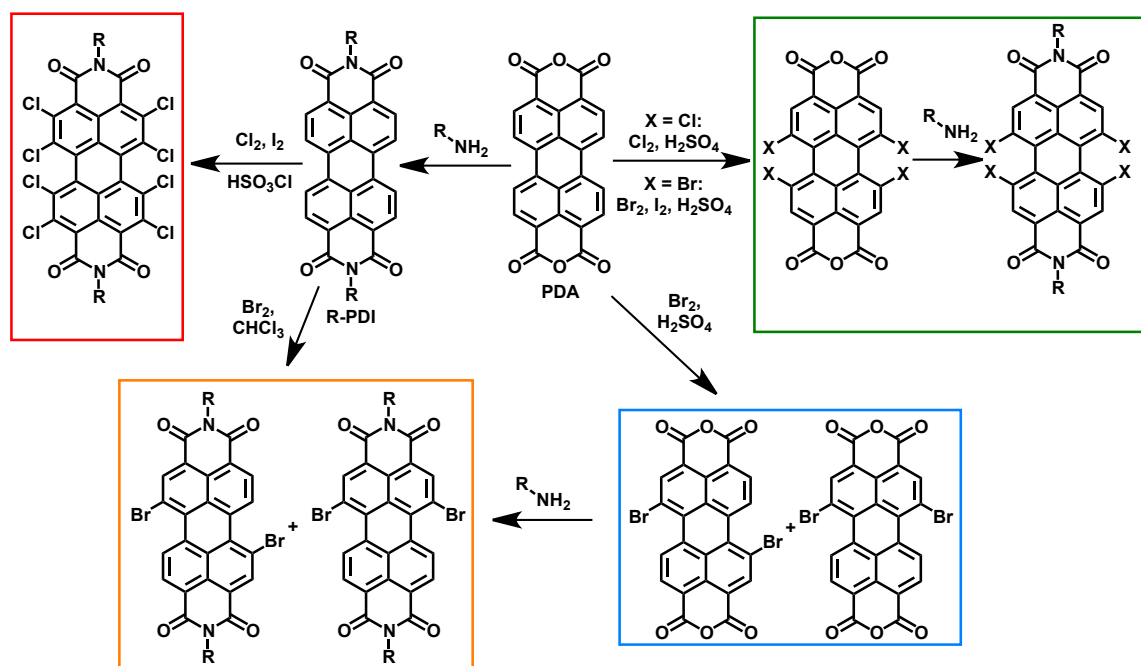
Scheme 3 Halogenation of perylenediimides and perylenedianhydride.

Halogenation of the aromatic core can be done either on the imide derivatives or on their corresponding anhydrides, as can be seen in Scheme 3 for the perylene-based dyes. Control of the reaction conditions allows the possibility to introduce a varying number of halogen substituents. In the case of perylenediimides the number of substituents ranges typically from one to four, since halogenation occurs preferentially at the *bay*-positions. In the case of difunctionalization, the 1,6 and 1,7-halogenated isomers are obtained, separable only via recrystallization methods.[36] Halogenation of all the eight positions was also reported using quite drastic reaction conditions by Würthner and coworkers. In the case of the higher rylenediimides, bromination occurs preferentially at the *bay*-positions of the terminal naphthalene units.[22,23]

In the case of rylenemonoimides, the reactivity is slightly modified. For perylenemonoimide the first site to undergo bromination is the 9-position, followed by the 1,6-positions and finally the 10-position.[15] Selective bromination of both *peri*-positions was recently reported by ▮▮▮▮▮▮▮▮, starting from *bay*-tetrachloro-perylenedianhydride.[37]
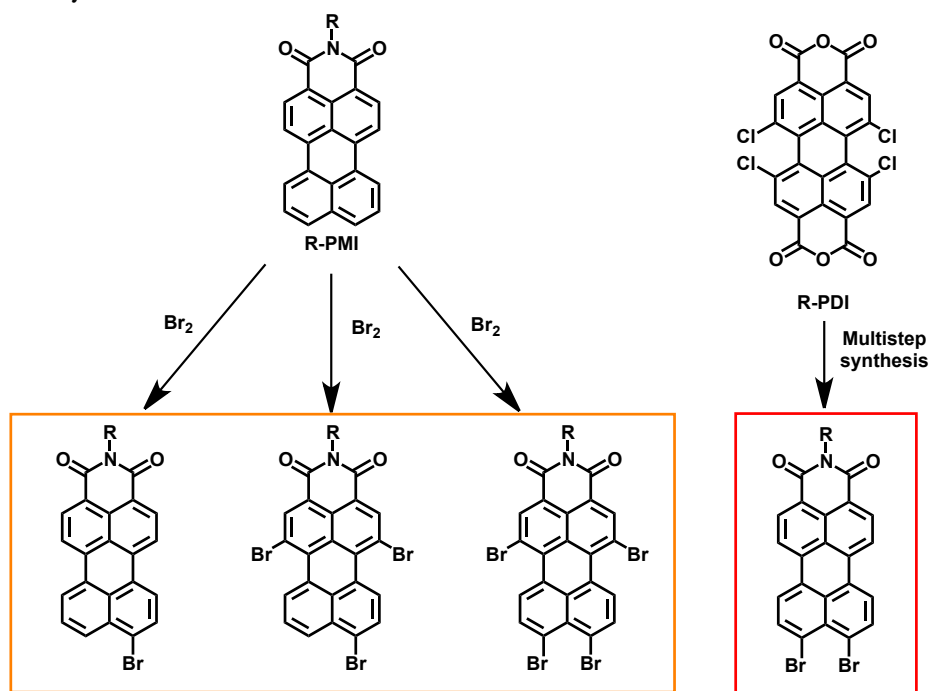
Scheme 4 Synthesis of halogenated perylenemonoimides.

Peri- and *bay*-functionalized higher rylenemonoimides are also known, but for these molecules the substituents are usually introduced already on the smaller rylene segments used for the synthesis of the more extended conjugated core.

Halogenated ryleneimides are multi-purpose building-blocks for the chemistry of the *peri-* and *bay*-positions. Numerous reports describe the use of these dyes for the introduction of substituents to obtain derivatives with tailored electro-optical properties. Due to the rather electron-poor nature of the aromatic core, *bay*-halogenated ryleneimides undergo straightforward nucleophilic substitution. Alternatively, modifications can be obtained via metal-catalyzed reactions, such as Suzuki, Ullmann or

Sonogashira coupling reactions, some of which are reported for perylenediimides in Scheme 5.
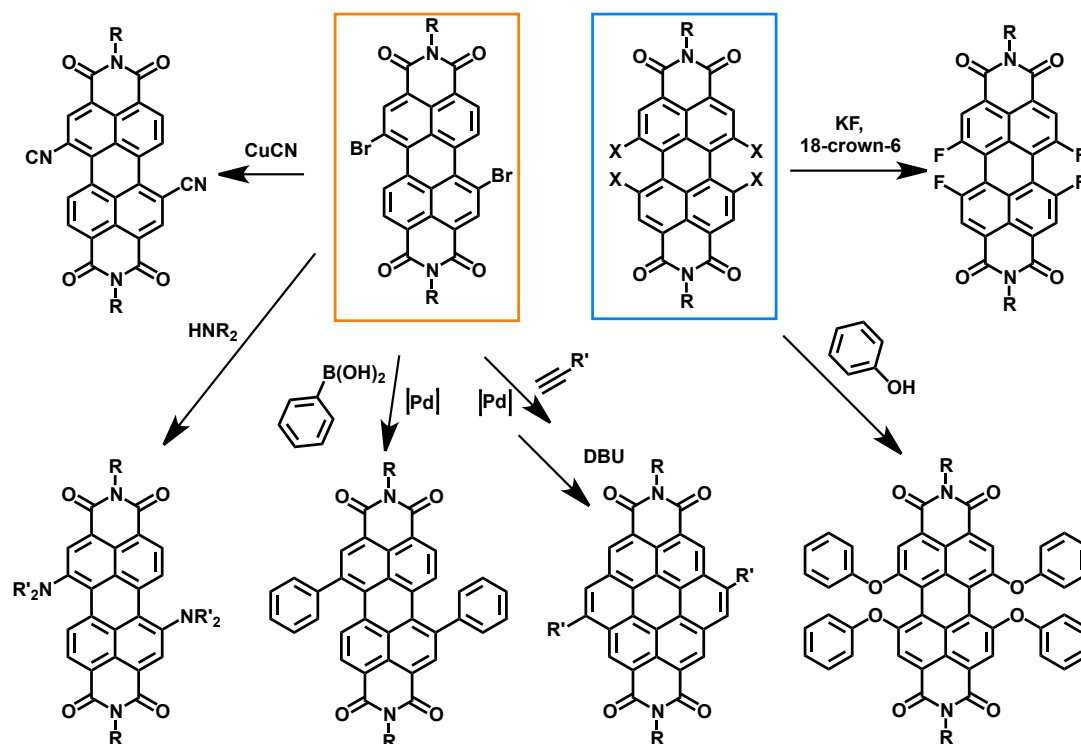
Scheme 5 Examples of the structures accessible starting from the *bay*-halogenated-PDI.

Among the most famous examples of core-substituted rylenediimides are tetraphenoxy rylenediimides.[26] These dyes are obtained via nucleophilic substitution of the halogen atoms with phenols and the substituents are used to tune the solubility of the molecules. Via this strategy, largely investigated in our group, water-soluble fluorescent probes could be obtained possessing outstanding photochemical stability. [38]

The absorption of ryleneimides can instead be tuned via the introduction of amino substituents in the *bay-* or *peri*-positions via nucleophilic substitution or Buchwald coupling. In this way the absorption can be strongly shifted toward the near-infrared region and the energy of HOMO level raised. Notable examples are the investigations reported by ▮▮▮▮▮▮ and ▮▮▮▮▮▮, who synthesized a series of perylenemonoimides for the application in dye sensitized solar cells with tailored absorption and tuned frontier molecular orbitals.[39] Lowering of the energy of the LUMO level can on the other hand be achieved via the introduction of electron withdrawing groups, as in the case of the *bay*-dicyano PDI derivatives, which exhibit LUMO levels between the -4.3 and -4.5 eV, among the lowest reported for ryleneimide derivatives.[40]

1.5 The Functionalization of the *Ortho*-Positions to the Imide

Despite the established chemistry of ryleneimides, in the most recent years new functionalization methods have been reported, opening new fields of opportunities. One of the most interesting novelties is the work published by the Shinokubo group in 2009, which for the first time demonstrated the possibility to selectively functionalize the 2,5,8,11-positions of perylenediimides.[41] The synthesic protocol used is based on the work of the Murai and Chatani group for the alkylation and arylation of the *ortho*-positions of aromatic ketones. [42, 43] This reaction, catalyzed by the Murai catalyst RuH$_2$(CO)(PPh$_3$)$_3$, allows the introduction of alkyl substituents via a reaction with olefins, while aryl substituents can be introduced using aryl boronic esters, as shown in Scheme 6. High yields were reported for both fourfold functionalizations. In the case of the alkylated derivatives, enhanced solid-state fluorescence was observed for all the derivatives while through the introduction of aryl substituents a weak influence on the energies of the frontier molecular orbitals was observed.
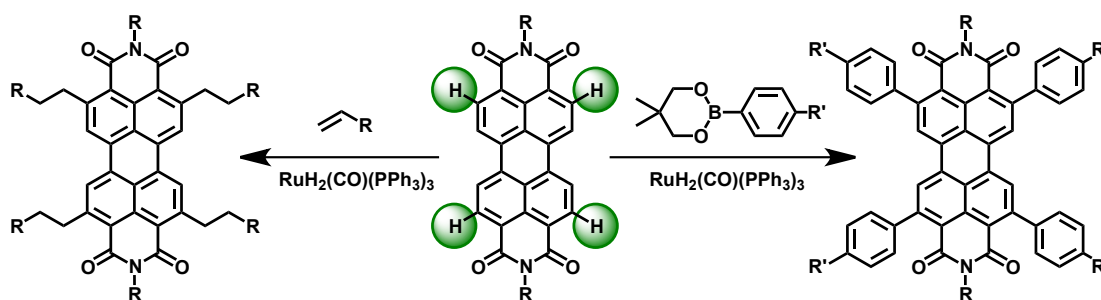
Scheme 6 The functionalization of the 2,5,8,11-positions of perylenediimides reported by Shinokubo and coworkers: alkylation and arylation reaction (left and right, respectively).

Besides the striking novelty of the functionalization pattern, the work of Shinokubo highlighted an important feature of the 2,5,8,11-functionalization: the possibility to substitute the perylene core preserving its planarity. In fact, even the introduction of the bulky phenyl substituents leaves the geometry of the π-system unmodified, as it was demonstrated by the X-ray diffraction data. This possibility represents an absolute innovation in the chemistry of rylenediimides, where the core functionalization was always achieved through the established *bay*-functionalization. In this case, as above mentioned, steric factors limit the number of substituents that can be introduced on the aromatic core and cause geometrical alterations, affecting solid-state packing and electro-optical properties, not always desirable. Therefore the functionalization of the positions *ortho* to the imide group may allow the tuning of the optical and electrochemical properties of ryleneimides, while preserving the planarity of the core.

1.6 References

[1] Travis, A. S. (1990), *Technology and culture*, *31*(1), 51-82.

[2] Zollinger, H. (2003). Color Chemistry. *Verlag Helvetica Chimica Acta*.

[3] Wang, C., Dong, H., Hu, W., Liu, Y., & Zhu, D. (2012), *Chemical Reviews*, 112(4), 2208-2267.

[4] Dong, H., Zhu, H., Meng, Q., Gong, X., & Hu, W. (2012),*Chemical Society Reviews*, *41*(5), 1754–1808.

[5] Shinar, J. (2004). *Organic light–emitting devices: a survey*. Springer Verlag.

[6] Terai, T., & Nagano, T. (2008),*Current opinion in chemical biology*, *12*(5), 515-521.

[7] Herrmann, A., & Mullen, K. (2006), *Chemistry Letters*, *35*(9), 978-985.

[8] Herbst, W., & Hunger, K. (2006). *Industrial organic pigments*. Wiley-VCH.

[9] Law, K. Y. (1993),*Chemical Reviews*, *93*(1), 449-486.

[10] Mansour, A. F., El-Shaarawy, M. G., El-Bashir, S. M., El-Mansy, M. K., & Hammam, M. (2002), *Polymer international*, *51*(5), 393-397.

[11] Ford, W. E., & Kamat, P. V. (1987), *Journal of Physical Chemistry*, *91*(25), 6373-6380.

[12] Weil, T., Vosch, T., Hofkens, J., Peneva, K., & Müllen, K. (2010), *Angewandte Chemie International Edition*, *49*(48), 9068–9093.

[13] Zhan, X., Facchetti, A., Barlow, S., Marks, T. J., Ratner, M. A., Wasielewski, M. R., & Marder, S. R. (2011), *Advanced Materials*, *23*(2), 268–284.

[14] Lin, Y., Li, Y., & Zhan, X. (2012), *Chemical Society Reviews*.

[15] Li, C., & Wonneberger, H. (2012), *Advanced Materials*, *24*(5), 613–636.

[16] E. Clar, *Chem. Ber.* 1948, 81, 52.

[17] Kardos, M. *D.R.P. 276 357* 1913.

[18] Faulkner, E. B., & Schwartz, R. J. (Eds.). (2009). *High performance pigments*. Wiley-VCH.

[19] Huang, C., Barlow, S., & Marder, S. R. (2011), *The Journal of Organic Chemistry*, *76*(8), 2386–2407.

[20] Avlasevich, Y., Li, C., & Müllen, K. (2010), *Journal of Materials Chemistry*, *20*(19), 3814.

[21] Müller, S. (2006), Ph. D. Thesis, Johannes Gutenberg University (Mainz).

[22] Nolde, F., Qu, J., Kohl, C., Pschirer, N. G., Reuther, E., & Müllen, K. (2005),*Chemistry – A European Journal*, *11*(13), 3959–3967.

[23] a) Quante, H., & Müllen, K. (1995), *Angewandte Chemie International Edition in English*, *34*(12), 1323-1325. b) Avlasevich, Y., & Müllen, K. (2007), *The Journal of Organic Chemistry*, *72*(26), 10243-10246. c) Pschirer, N. G., Kohl, C., Nolde, F., Qu, J., & Müllen, K. (2006), *Angewandte Chemie International Edition*, *45*(9), 1401-1404.

[24] Nagao, Y. (1997), *Progress in organic Coatings*, *31*(1), 43-49.

[25] a) Lee, S. K., Zu, Y., Herrmann, A., Geerts, Y., Müllen, K., & Bard, A. J. (1999), *Journal of the American Chemical Society*, *121*(14), 3513-3520. b) Adachi, M., & Nagao, Y. (2001), *Chemistry of materials*, *13*(2), 662-669.

[26] Würthner, F. (2004), *Chemical Communications*, (14), 1564.

[27] Wolf-Klein, H., Kohl, C., Müllen, K., & Paulsen, H. (2002). *Angewandte Chemie International Edition*, *41*(18), 3378-3380.

[28] Jung, C., Müller, B. K., Lamb, D. C., Nolde, F., Müllen, K., & Bräuchle, C. (2006). *Journal of the American Chemical Society*, *128*(15), 5283-5291.

[29] Oesterling, I., & Müllen, K. (2007). *Journal of the American Chemical Society*, *129*(15), 4595-4605.

[30] Anthony, J. E., Facchetti, A., Heeney, M., Marder, S. R., & Zhan, X. (2010), *Advanced Materials*, *22*(34), 3876–3892.

[31] a)Graser, F., & Hädicke, E. (1980). *Liebigs Annalen der Chemie*, *1980*(12), 1994-2011. b) Hadicke, E., & Graser, F. (1986), *Acta Crystallographica Section C: Crystal Structure Communications*, *42*(2), 189-195.

[32] a) Klebe, G., Graser, F., Hadicke, E., & Berndt, J. (1989), *Acta Crystallographica Section B: Structural Science*, *45*(1), 69-77. b) Kazmaier, P. M., & Hoffmann, R. (1994), *Journal of the American Chemical Society*, *116*(21), 9684-9691.

[33] H. Langhals, *Heterocycles* (1995), 40, 1, 477

[34] G. Seybold, G. Wagenblast, (1989), *Dyes and Pigments*, 11, 303.

[35] a) Hassheider, T., Benning, S. A., Kitzerow, H. S., Achard, M. F., & Bock, H. (2001), *Angewandte Chemie International Edition*, *40*(11), 2060-2063. b) Xue, C., Sun, R., Annab, R., Abadi, D., & Jin, S. (2009), *Tetrahedron Letters*, *50*(8), 853-856.

[36] a) Böhm, A., Arms, H., Henning, G., Blaschka, P., & AG, B. (1997). German Pat. DE 19547209 A1, 1997. In *Chem. Abstr* (Vol. 127, p. 96569g). b) Würthner, F.; Stepanenko, V.; Chen, Z.; Saha-Moller, C. R.; Kocher, N.; Stalke, D. (2004), *Journal of Organic Chemistry*, 69, 7933–7939.

[37] Zagranyarski, Y., Chen, L., Zhao, Y., Wonneberger, H., Li, C., & Müllen, K. (2012), *Organic letters*, *14*(21), 5444-5447.

[38] Kohl, C., Weil, T., Qu, J., & Müllen, K. (2004), *Chemistry-A European Journal*, *10*(21), 5297-5310.

[39] a) Li, C. (2008), Ph. D. Thesis, Johannes Gutenberg University (Mainz). b) Wonneberger, H. (2012), Ph. D. Thesis, Johannes Gutenberg University (Mainz).

[40] a) Ahrens, M. J., Fuller, M. J., & Wasielewski, M. R. (2003). *Chemistry of materials*, *5*(14), 2684-2686. b) Jones, B. A., Ahrens, M. J., Yoon, M. H., Facchetti, A., Marks, T. J., & Wasielewski, M. R. (2004), *Angewandte Chemie*, *116*(46), 6523-6526. c) Jones, B. A., Facchetti, A., Wasielewski, M. R., & Marks, T. J. (2007), *Journal of the American Chemical Society*, *129*(49), 15259-15278.

[41] a) Nakazono, S.; Imazaki, Y.; Yoo, H.; Yang, J.; Sasamori, T.; Tokitoh, N.; Cédric, T.; Kageyama, H.; Kim, D.; Shinokubo, H.; Osuka, (2009), *Chemistry-A European Journal*, *15*(31), 7530-7533. b) Nakazono, S., Easwaramoorthi, S., Kim, D., Shinokubo, H., & Osuka, A. (2009), *Organic letters*, *11*(23), 5426-5429.

[42] a) Murai, S., Kakiuchi, F., Sekine, S., Tanaka, Y., Kamatani, A., Sonoda, M., & Chatani, N. (1993), *Nature*, *366*(6455), 529-531. b) Kakiuchi, F., Sekine, S., Tanaka, Y., Kamatani, A., Sonoda, M., Chatani, N., & Murai, S. (1995), *Bulletin of the Chemical*

24

Society of Japan, *68*(1), 62-83.c) Kakiuchi, F., & Murai, S. (2002), *Accounts of chemical research*, *35*(10), 826-834..

[43] Kakiuchi, F., & Chatani, N. (2003), *Advanced Synthesis & Catalysis*, *345*(9-10), 1077-1101.

Kakiuchi, F., Matsuura, Y., Kan, S., & Chatani, N. (2005), *Journal of the American Chemical Society*, *127*(16), 5936-5945.

2 Motivation

Ryleneimides belong to the most extensively investigated systems in the field of conjugated molecules. Due to their desirable properties, they have found numerous fields of applications and the number of reports featuring these molecules, in particular perylenediimides, has been permanently increasing. However, in 2009 the first report about the functionalization of the 2,5,811-positions of PDIs has demonstrated and highlighted one fact: in the ryleneimide chemistry there are positions, which have been ignored for long time and still remain largely unexplored, mainly due to the limited number of suitable synthetic methods to access them. Nevertheless, due to the attractive properties of RIs, new functionalization patterns may broaden the instruments to tune their molecular and supramolecular properties, further consolidating their importance in the field of functional dyes.

Main goal of this thesis work is the development of synthetic methods for the selective functionalization of the "unconventional" positions of ryleneimides. Such positions are those molecular sites that cannot be addressed via the established bromination and imidization reactions. In this investigation, three main molecular structures will be considered: perylenediimide, perylenemonoimide and terrylenediimide, as highlighted in Figure 5. For these molecules, the "unconventional" positions can be subdivided into two categories:

- the sites *ortho* to the imide groups (2,5,8,11 for the PDI molecule, 2,5 for PMI and 2,5,10,13 for TDI) that will be simply defined as *ortho*-positions;
- the 8,11-positions of perylenemonoimides, that we will define as *edge*-positions.
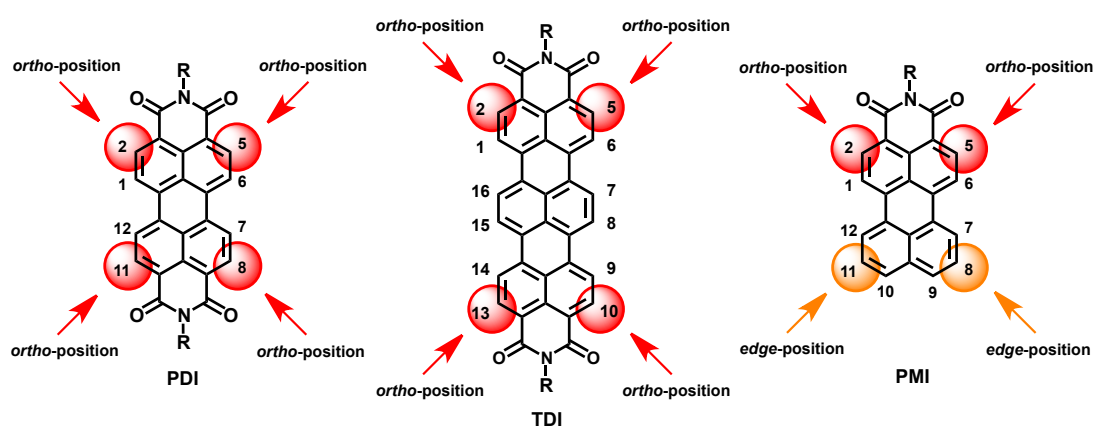
Figure 5 Molecular structures and schematic representation of the molecular sites, which will be focus of this thesis work.

The reason to focus exclusively on PDI, TDI and PMI derivatives is due to the key role of these molecules in the ryleneimide chemistry. PDIs represent without any doubt the most important structure of the family, subject of hundreds of reports. Due to their

popularity new functionalization routes may greatly contribute to further development of the chemistry of these molecules. As compared to the higher rylenes, PDIs exhibit a less extended conjugated core, but still a strong tendency to aggregate, which represents one of the major obstacles in the ryleneimide chemistry. Being commercially available materials, they are also ideal model compounds for explorative experiments.

Terrylenediimides have been chosen as representative of the higher rylene homologues. Their more elongated scaffold consistently increases the tendency to aggregate as compared to PDIs, posing challenges for the synthesis and purification. Successful extension of the synthetic methods developed on PDIs to TDIs would demonstrate their validity. More importantly, despite the limited number of reports in literature, TDIs have the potential to outperform PDI dyes in several application fields, as they already did for example in the field of single molecule spectroscopy. Unfortunately not being commercially available and relatively difficult to be synthesized and purified, the work on TDIs still remains limited and further investigations may help attracting the attention of the scientific community on this unfairly disregarded molecular structures.

Finally perylenemonoimides have been selected as an accessible rylenemonoimide model. Monoimides present an asymmetric structure, with different reactivity as compared to the diimides. The absence of the second imide group completely changes the structural environment of the terminal naphthalene unit, requiring new synthetic concepts to reach the above-mentioned *edge*-positions. Additionally perylenemonoimides are a class of outstanding light absorbers in the field of dye-sensitized solar cells and new unconventional functionalization patterns should be beneficial for further improving their performances.

The work is subdivided in six main chapters (from 3 to 8). In chapter 3 the alkylation of the *ortho*-positions reported by the Shinokubo group will be investigated as a starting point. Potential and limitations of this functionalization will be explored using a model olefin. Additionally the impact of the alkylation on the electro-optical properties of PDI, PMI and TDI will be investigated. Later on, *ortho*-alkylated PDIs will be used as electron acceptors for bulk-heterojunction solar cells. Finally, a library of *ortho*-alkylated PDIs will be synthesized to better understand the influence of the substitution pattern on the performances of the solar cells.

In Chapter 4 and 5 the alkylation of the *ortho*-positions will be envisioned as solubilizing approach. As previously mentioned, due to their extended π-conjugated system, RIs tend to strongly aggregate and the transition from dye to insoluble pigment is often caused by minimal structural changes. For this reason, tuning of the solubility has been among the most investigated topics in the ryleneimide chemistry. Historically, the solubilization strategies used in ryleneimide chemistry have been exclusively based on imide and *bay*-functionalization. However the introduction of alkyl chains onto the *ortho*-positions may represent an attractive alternative, able to enhance solubility and leave the optical properties of the materials virtually unmodified. To explore this approach, *ortho*-alkylation will be applied in two different fields of the ryleneimide chemistry: the synthesis of a stable quinoidal perylenemonoimide derivative as NIR-absorbing dye

(Chapter 4) and for the synthesis of PDI-based water-soluble fluorescent probes with high fluorescence quantum yields (Chapter 5).

Chapter 6 constitutes a crucial point of this thesis work and more generally for the functionalization of the *ortho*-positions of ryleneimides. The first two reports of the Shinokubo group demonstrated the possibility to selectively address such molecular sites. However the synthetic protocols allow introduction of only a limited number of substituents. If these functionalization methods are compared to the routes followed for the modification of the imide and *bay*-positions, a major difference can be discovered: the access to the *ortho*-modified RIs does not proceed through generic building-blocks. In the more established functionalization methods, anhydride groups and halogen atoms guarantee a variety of alternative functionalizations of imide and *bay*-positions and the extension of a similar approach to the *ortho*-positions could really make this chemistry competitive.
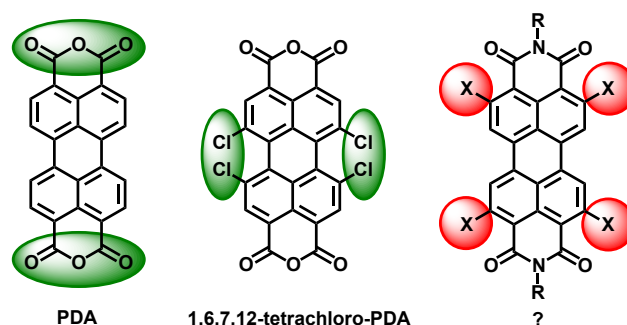
Figure 6 Building blocks in the perylenediimide chemistry.

Therefore in the Chapter 6 the focus will be set on the synthesis of a class of universal building blocks for the chemistry of the *ortho*-positions. First a protocol to access such building blocks will be described, developed initially on perylenediimdes and then extended to PMI and TDI. Successively the fundamental role of these molecules in the chemistry of the *ortho*-positions will be demonstrated, by introducing a variety of functional groups, which will undoubtedly prove the efficacy of the approach allowing further modifications and tuning of the electro-optical properties.

In chapter 7 the synthetic instruments developed in Chapter 3 will be used to lower the energy of LUMO levels of perylenediimides and terrylenediimides via the introduction of cyano-substituents onto the *ortho*-positions. The increase of electron affinities plays a major role in the chemistry of n-type semiconductors to improve air stability in operating devices. *Bay*-dicyanation of PDIs has already proven to be an extremely effective strategy to synthsize outstanding air-stable n-type semiconductors. However cyanation of the *ortho*-positions would offer two main advantages: 1) allow fourfold substitution to achieve stronger electron acceptors; 2) preserve the planarity of the molecules, which may lead to better π-π stacking and possibly to better charge carrier mobilities. At first *ortho*-fourfold cyanation will be explored on perylenediimides, to be then extended to terrylenediimides. Using TDI, a direct comparison of the differences between fourfold *bay* and *ortho*-cyanation will be done.

In chapter 8 the functionalization of the *edge*-positions of perylenemonoimides will be considered. These molecular sites, after the report about the *ortho*-functionalization of PDIs, are virtually the only remaining positions of RIs that cannot be selectively addressed. Their functionalization would provide additional solutions for the tuning of the electro-optical properties of PMIs and further extend the manifold chemistry of these molecules. Similarly to the approach followed in Chapter 6, a synthetic protocol will be developed, not only to achieve selective functionalization, but also to provide suitable building blocks for further modification.

3 *Ortho*-Alkylated Ryleneimides: Chemistry, Properties and Application in Organic Solar Cells

3.1 Introduction

The explorative work about the functionalization of the unconventional sites of the core of ryleneimides starts in this chapter with the alkylation of the *ortho*-positions. As previously mentioned in the introduction, the Shinokubo group reported the synthetic protocol in 2009.[44] According to the authors the alkylation reaction proceeds in high yields and the functionalization greatly enhances solubility and solid-state fluorescence, while preserving the planarity of the aromatic core. These features would render the *ortho*-alkylation a very interesting alternative to the more established methods focusing on the imide group and *bay*-positions to reduce aggregation and improve the processability of ryleneimides. Therefore a deeper understanding about the reactivity, advantages and limitations of this functionalization would be of high interest.

In this chapter the reaction will be explored using a model olefin and three differerent ryleneimides. Later on the consequences on the electro-optical properties of the dyes will be investigated. Finally, *ortho*-alkylated perylenediimides will be applied as electron acceptors in bulk heterojunction solar cells.

3.2 *Ortho*-Alkylation of Ryleneimide Derivatives

The synthetic route for the alkylation of the *ortho*-positions of PDIs was inspired by the work of the Murai group, which reported in 1993 the first protocol for a highly efficient and selective aromatic C-H olefin coupling.[45] In the reaction an aromatic ketone reacts with a terminal double bond in presence of a ruthenium catalyst ($RuH_2(CO)(PPh_3)_3$), also known as Murai catalyst, to yield the *ortho*-alkylated compounds in high yields (Scheme 7). The reaction involves the cleavage of an *ortho* C-H bond of the aromatic ketone and the formation of a C-C bond by addition of an olefin. The key role in this reaction is played by the directing carbonyl group. Its coordination to the ruthenium brings the metal center into close proximity to the *ortho* C-H bonds and allows the selective functionalization of this position. The synthetic protocol can be applied to various olefins and the major limitation in the choice of the terminal double bond is the presence of allylic protons, which are known to cause isomerization side reaction, lowering the yields.
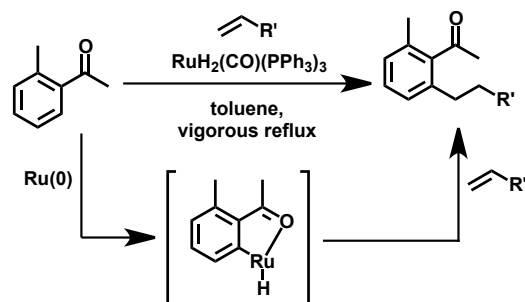
Scheme 7. An example of Murai type alkylation reaction, showing the cyclometallated intermediate.

Among the olefins known to undergo Murai type alkylation reaction, 3,3-dimethyl-1-butene appears to be a suitable candidate for the synthesis of *ortho*-substituted rylene imide. From a chemical point of view, the absence of allylic hydrogen atoms precludes parasitic isomerization reaction of the olefin, guaranteeing high reaction yields. The commercial availability at economic price of 3,3-dimethyl-1-butene allows its use as standard material even for large scale reactions. Furthermore its terminal bulky groups would be capable to reduce the aggregation between the planar conjugated cores of RIs, improving the solubility in organic solvents and enhancing solid-state fluorescence.

The suitability of 3,3-dimethyl-1-butene for Murai type alkylation was initially tested following the reaction conditions reported in the literature for perylenediimide derivatives, using mesitylene as solvent and **C2SW-PDI** as model compound (Scheme 8).[44] This PDI derivative is known to undergo the *ortho*-alkylation reaction in high yields and could be easily synthesized in large scale. The fourfold alkylation reaction ran overnight and the formation of the desired product was detected by FD-MS spectroscopy and confirmed by TLC. Besides the target compound, no other major side products were formed and only traces of trialkylated PDI were still present after reaction. **C2SW-alk-PDI** could be purified by column chromatography and isolated as a bright orange powder in good yields (75-87 %). The solubility of the alkylated derivative in organic solvents appears to be greatly enhanced as compared to the unsubstituted material: in dichloromethane under ambient conditions, concentrations up to 35 mg/mL can be achieved with **C2SW-alk-PDI**, while for **C2SW-PDI** only partial dissolution is obtained above 15 mg/mL. Further, the strong solid-state fluorescence of the tetraalkylated PDI provides proof for the beneficial effect of the *ortho*-alkylation in limiting the solid-state aggregation.

C2SW-PDI   **C2SW-alk-PDI**
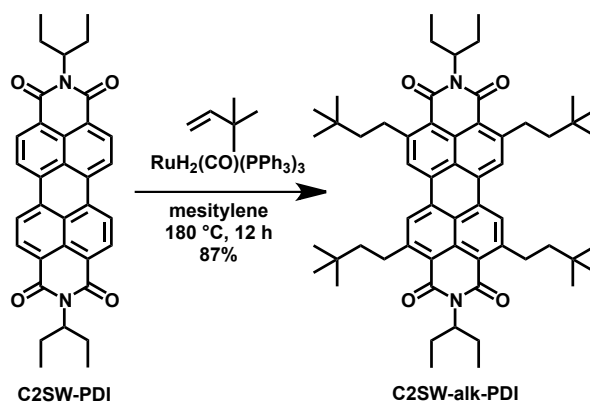
Scheme 8. *Ortho*-alkylation reaction of **C2SW-PDI**.

The high symmetry of **C2SW-alk-PDI** is evidenced in the ^{1}H-NMR spectrum of Figure 7. The aromatic region shows exclusively a singlet, which can be assigned to the aromatic protons in the *bay*-region. The peaks ascribable to the *ortho*-alkyl groups are highlighted in red, while the proton signals of the 3-pentyl imide substituent are reported in yellow. The splitting of the signals of the b protons, originating from the interaction with the carbonyl group, is typical for swallow-tail N-substituted ryleneimides, as previously described.[46]
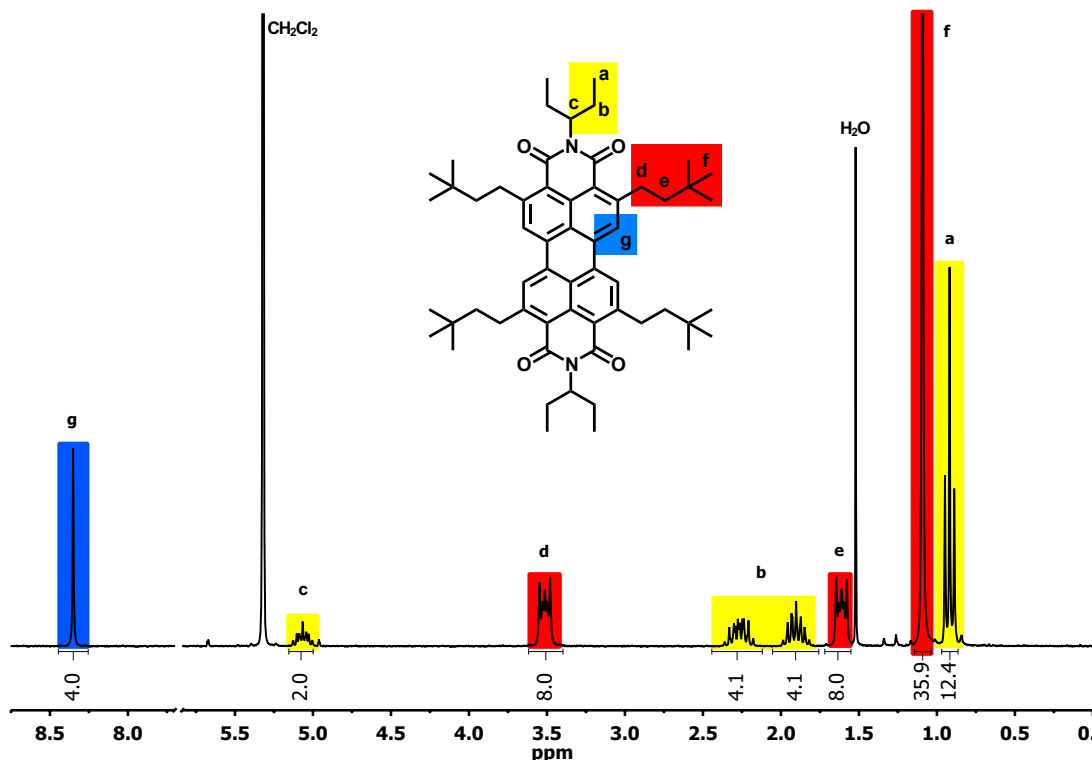
Figure 7. ^{1}H-NMR in CD_2Cl_2 of **C2SW-alk-PDI**.

Encouraged by the high yields of the reaction, demonstrating the suitability of 3,3-dimethyl-1-butene for the *ortho*-functionalization of perylenediimides, the reaction was tested also on two other rylene derivatives: a terrylenediimide and a perylenemonoimide. TDI and PMI find application as dyes for organic solar cells and bioimaging and further functionalizations possibilities may enlarge the number of synthetic solutions to tune their solubility and opto-electrochemical properties. More importantly, terrylenediimides and perylenemonoimides were chosen as model compounds to explore the possibility to apply the Murai alkylation to the higher rylenediimides (RDIs) and rylenemonoimides (RMIs), respectively. RDIs and RMIs may exhibit a different reactivity as compared to PDIs and no reports were known in the literature at the time featuring these dyes as substrates for the Murai-type alkylation reaction.

Among the different terrylenediimide derivatives, **C7SW-TDI** was selected as model compound. **C7SW-TDI** shows superior solubility as compared to many other core unsubstituted terrylenediimide derivatives, therefore providing an extremely versatile platform for further functionalization. However, terrylenediimides are not commercially available materials and their synthesis is rather challenging. In fact, the uneven number of

naphthalene units composing the core of TDI requires the coupling of two different monoimides, PMI and NMI. Furthermore the extended conjugated terrylene core is responsible for a strong tendency to aggregation, which makes gram scale synthesis rather demanding, especially when chromatographic purification is required. Therefore, in order to make of **C7SW-TDI** a standard material available for a series of experiments that will be described later on in this thesis, a synthetic protocol enabling gram scale synthesis with only a limited number of chromatographic purifactions was developed.

In the case of **C7SW-TDI**, the one-pot reaction starting from NMI and PMI and leading directly to TDI cannot be applied, due to the presence of imide substituents that can be easily saponified under the strongly basic conditions of the reaction (DBN and sodium tert-butylate at 130 °C). Therefore the material was synthesized following an optimized version of the six-step protocol published by ▮▮▮▮.[47a] The synthesis started from the imidization of 4-bromo-naphthalenemonoanhydride (Scheme 9) and perylenemonoanhydride (**PMA**) (Scheme 10) with 1-heptyl-octyl amine in molten imidazole.
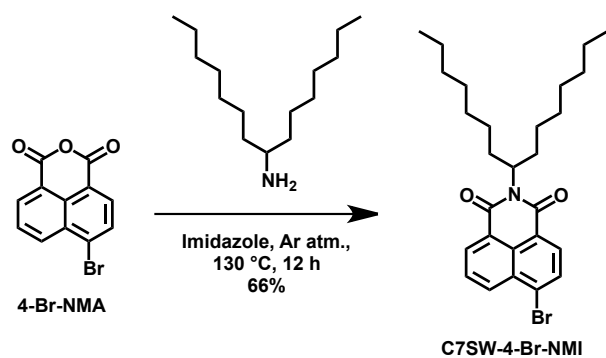
Scheme 9 Synthesis of **C7SW-4-Br-NMI**.

Both materials, **C7SW-4-Br-NMI** and **C7SW-PMI** were isolated after column chromatography in good yields (66 % and 60 % respetively).
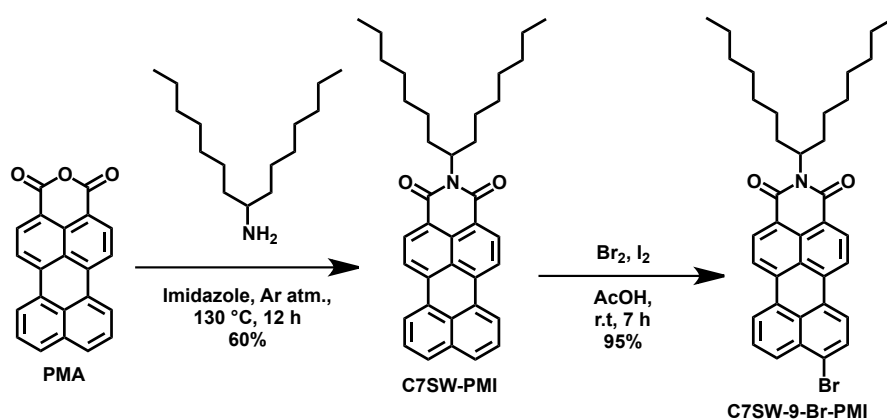
Scheme 10 Synthesis of **C7SW-9-Br-PMI**.

---

[a] The final optimized synthesis reported in the experimental part was performed by ▮▮▮▮▮▮▮, supervised during the thesis period.

Successively, **C7SW-PMI** was monobrominated at room temperature in acetic acid in presence of catalytic amounts of iodine. Careful monitoring via FD-MS and TLC was required, to achieve selective halogenation of the 9-position and avoid overbromination of the less activated 1- and 6-positions in the *bay*-region. Also in this case multigram scale was possible and the material was used for the next step without further purification.

Following the Miyaura borylation protocol, **C7SW-9-Br-PMI** was then converted into the monoboronate **C7SW-9-bor-PMI**. The reaction afforded also the debromination product **C7SW-PMI** in about 15 % yields, which was not separated from the target monoboronate. In fact, the subsequent step features a Suzuki coupling with **C7SW-4-Br-NMI**, in which **C7SW-PMI** cannot react and is also formed as side product. Therefore, the borylation reactions mixture was simply precipitated in methanol to remove the catalyst and other side product and used for the next step.
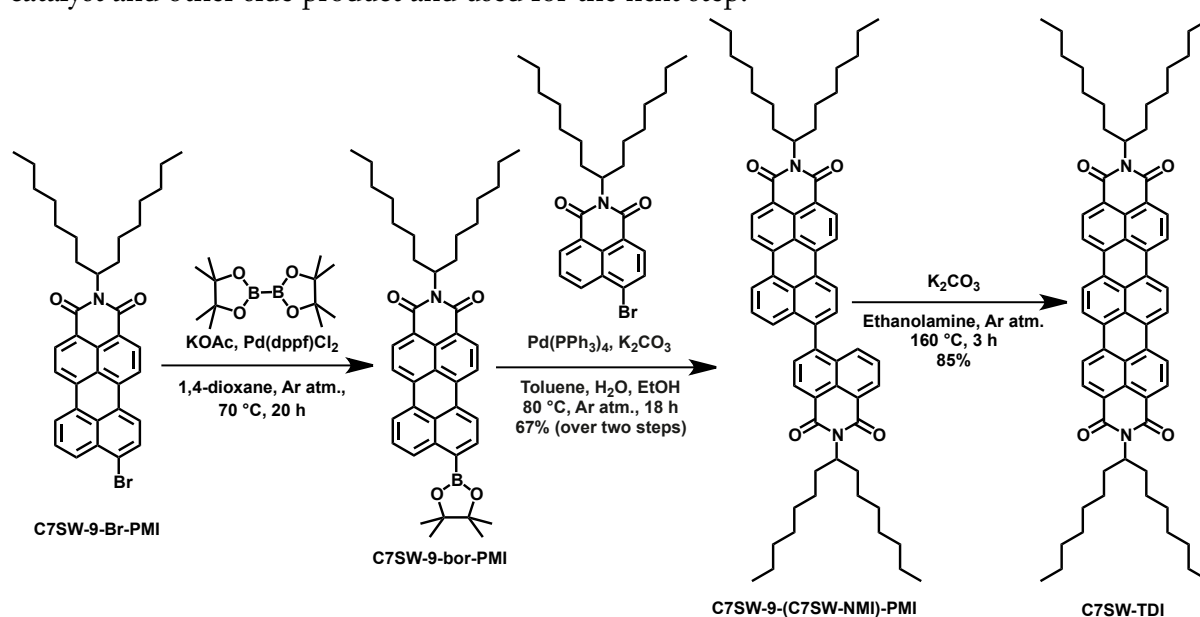
Scheme 11 Synthesis of **C7SW-TDI**.

The Suzuki coupling reaction between **C7SW-9-bor-PMI** and **C7SW-4-Br-NMI** lead to **C7SW-9-(C7SW-NMI)-PMI**, the open form of the terrylenediimide **C7SW-TDI**. The reaction afforded not only the desired molecule, but also **C7SW-PMI** and **C7SW-NMI** as products of the deborylation and debromination. Furthermore, the homocoupling product of the perylene monoboronate was also isolated after column chromatography. This material is a precious precursor for the synthesis of quaterrylenediimide and it was isolated for other experiments performed in the group, but not reported in this thesis.

The target compound **C7SW-TDI** was finally obtained after cyclodehydrogenation, achieved using potassium carbonate and ethanolamine. Drastic color change was observed upon heating at 160 °C, distinctive sign of the formation of the terrylene dye. The target compound was isolated in good yields (85 %) after a last chromatographic purification.

Among the perylenemonoimide derivatives, **DiPP-PMI** was chosen to investigate the ruthenium-catalyzed alkylation reaction. This material can be readily synthesized starting from perylenedianhydride and is a standard precursor for the synthesis of

perylenemonoimide based dyes, as described in the Introduction. Therefore understanding its reactivity could be of high interest for the PMI-chemistry. In this case **DiPP-PMI** was provided by BASF SE.

The reaction conditions used for the synthesis of **C2SW-alk-PDI** were applied to the two above-mentioned rylenes and in both cases the desired products could be obtained (Scheme 12 and Scheme 13).
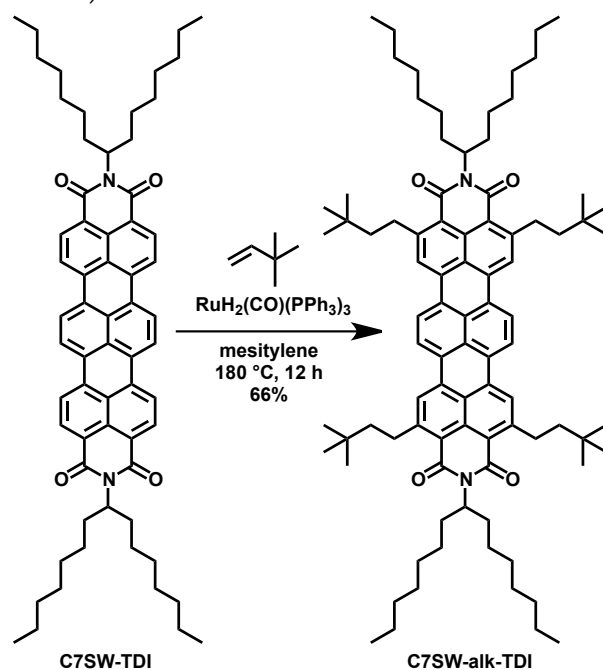
Scheme 12 *Ortho*-alkylation reaction of **C7SW-TDI**.

High yields were achieved for the TDI derivative. The *ortho*-alkylation of PMI worked only in moderate yields, instead, probably due to the presence of the sterically demanding di-isopropyl phenyl imide substituent, which partially hinders the catalyst from coordinating at the carbonyl group. The mono alkylated derivative could also be isolated from the reaction. For both **DiPP-alk-PMI** and **C7SW-alk-TDI**, no major change in the color of the powder of the material was observed, as compared to **C7SW-PDI** and **DiPP-PMI**. The introduction of the alkyl substituents also led to an enhanced lipophilicity for both derivatives, soluble in non-polar solvents such as petroleum ether and hexane, in which the unsubstituted starting materials usually can be precipitated.
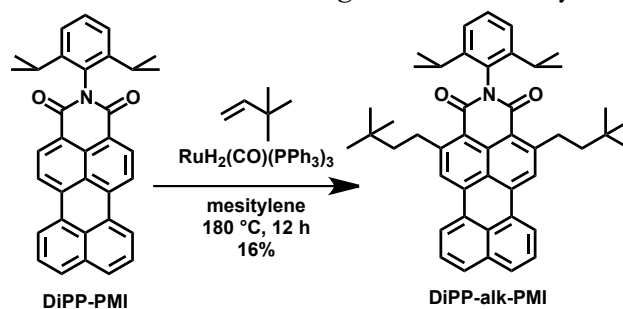
Scheme 13 *Ortho*-alkylation reaction of **DiPP-PMI**

Ideally, to be used as a means to improve solubility and processability the functionalization of the *ortho*-positions should have only a minor impact on the optical

and electrochemical properties of rylenediimides, as compared to the unsubstituted derivatives. Indeed, the introduction of the 3,3-dimethyl-butyl groups has only marginal effects on the absorption and fluorescence in solution of the rylene imides. The data are summarized in Table 1. The extinction coefficients are comparable with those of the unsubstituted derivatives as well as the fluorescence quantum yields.

Molecule	λ_{max} [nm]	ε [M^{-1}cm^{-1}]	λ_{em} [nm]	Φ_F (λ_{ex} [nm])
C2SW-alk-PDI	521	58500	535	0.55 (521), 1.00 (501)
DiPP-alk-PMI	473	33700	525	0.49 (473)
C7SW-alk-TDI	643	105000	657	0.95 (632)

Table 1 Optical properties of the *ortho*-alkylated RDIs measured in toluene. Φ_F measured using as standards Rhodamine 6G in ethanol, Rhodamine 110 in ethanol and Cresyl violet in methanol for **C2SW-alk-PDI**, **DiPP-alk-PMI** and **C7SW-alk-TDI** respectively.

In Figure 8, the absorption and fluorescence spectra of the *ortho*-alkylated derivatives are compared with those of the parent unsubstituted compounds. A slight hypsochromic shift of both absorption and fluorescence curves was observed for all the core-substituted molecules. The typical shape of the spectrum is retained, with a slight decrease of the intensity of the S$_0$→S$_2$ transition compared to the S$_0$→S$_1$.
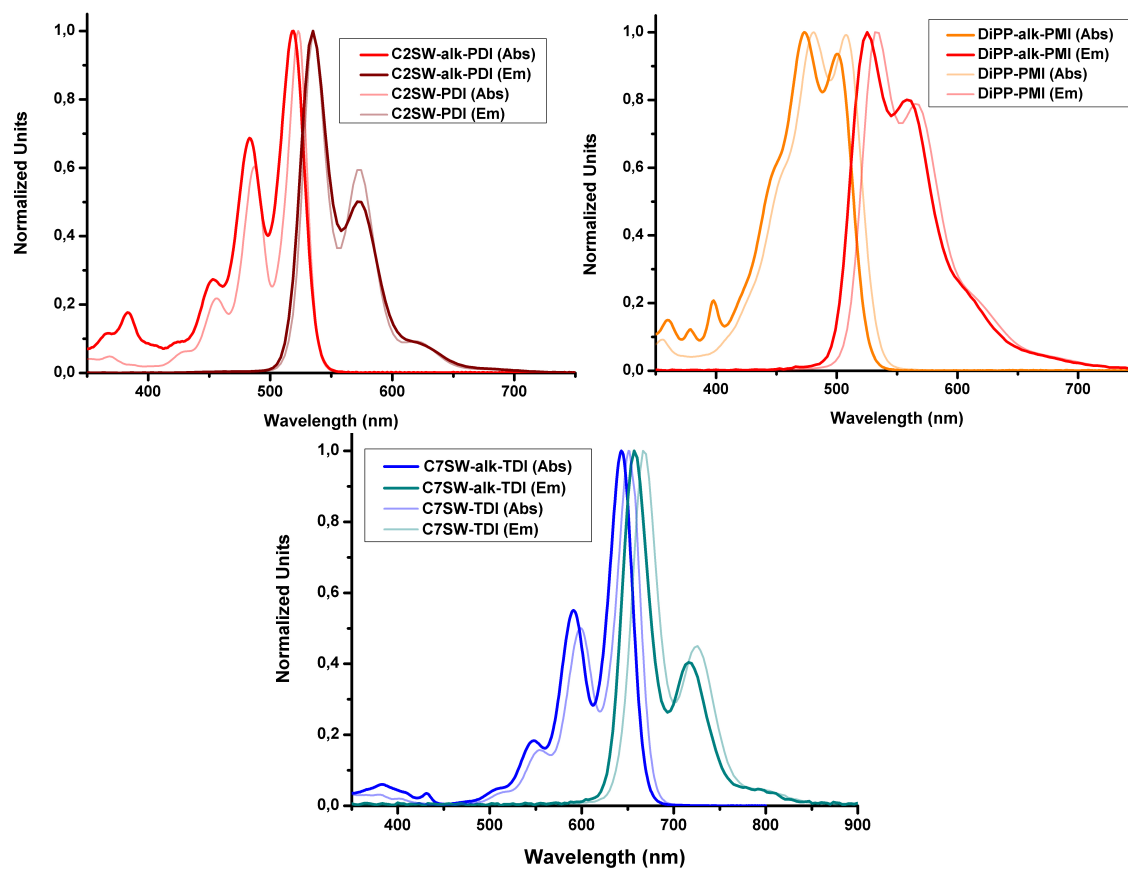
Figure 8 Absorption and emission spectra in toluene of: **C2SW-alk-PDI** and **C2SW-PDI** (top left), **DiPP-alk-PMI** and **DiPP-PMI** (top right) and **C7SW-alk-TDI** and **C7SW-TDI** (bottom). The spectra heve been normalized to highlight the effect of the *ortho*-substitution on the absorption and emission curves.

To determine the HOMO and LUMO levels of the *ortho*-alkylated rylenes, cyclovoltammetric measurements were performed, assuming a direct correlation between the energy levels and the oxidation and reduction potentials in solution. The cyclovoltammograms are presented in Figure 9 and the reduction and oxidation potentials summarized in Table 2.
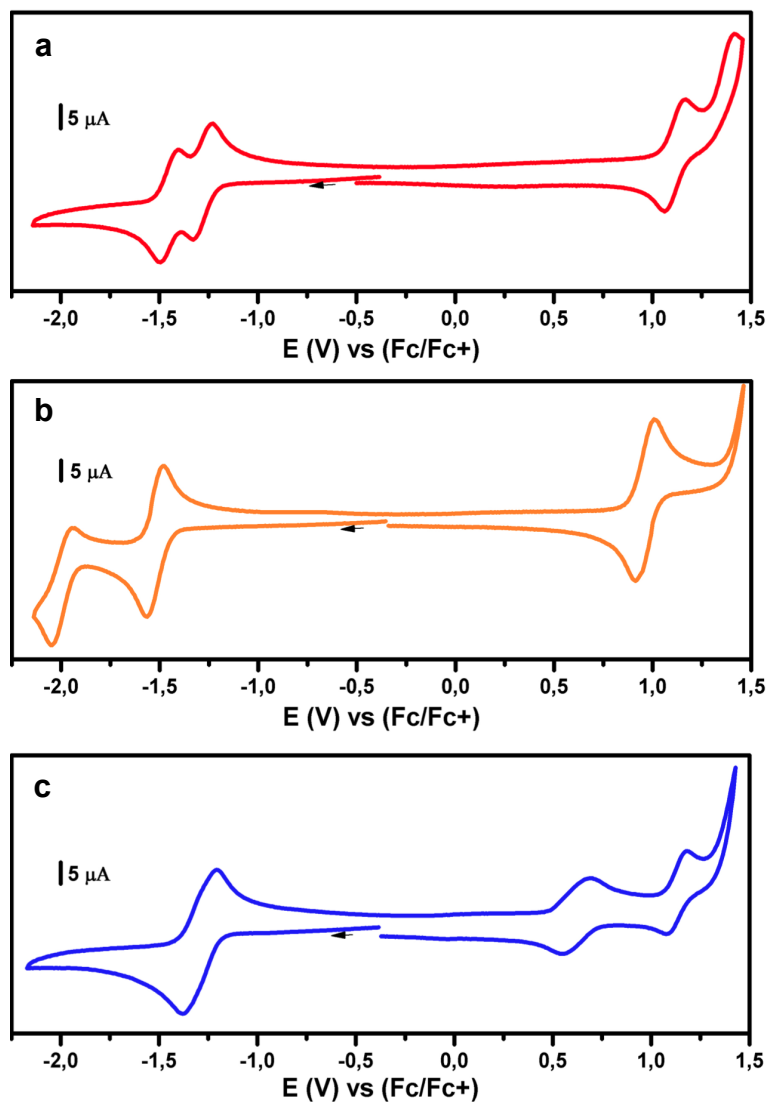
Figure 9 Cyclic voltammetric measurement for **C2SW-alk-PDI** (red), **DiPP-alk-PMI** (orange) and **C7SW-alk-TDI** (blue).

Molecule	E_{red2}	E_{red1}	E_{ox1}	E_{ox2}	HOMO[a]	LUMO[b]
C2SW-alk-PDI	-1.80	-1.28	1.12	-	-5.92	-3.52
DiPP-alk-PMI	-2.01	-1.55	0.91	-	-5.71	-3.25
C7SW-alk-TDI	-	-1.30	0.63	1.15	-5.43	-3.50

Table 2. Electrochemical properties of the reported alkyted-ryleneimides determined by cyclic voltammetric measurement in 0,1 M solution of Bu_4NPF_6 in CH_2Cl_2: vs Fc/Fc^+. The values reported are referred to half wave potentials. a) Estimated vs. vacuum level from $E_{HOMO} = 4.80$ eV + E_{ox1}. b) Estimated vs. vacuum level from $E_{LUMO} = 4.80$ eV - E_{red1}.

The *ortho*-alkylation impacts only marginally the energies of the HOMO and LUMO levels of the unsubstituted ryleneimides. More precisely the levels are slightly higher in energy, in agreement with the weak donating effect of the alkyl substituents. Consequently the HOMO-LUMO gap remains practically unmodified, in good agreement with the minor changes in the absorption. In the case of **C7SW-alk-TDI** the potentials for the first and second reduction are degenerate, as already observed for unsubstituted TDIs. The experimental data agree with the results reported by the Wasielevski group,[48] published in the time period in which these experiments were performed.

Summarizing, the introduction of alkyl-substituents in the *ortho*-positions has only minor consequences on the electro-optical properties of the ryleneimide core. Additionally the solubility of the dyes is improved, thanks to the reduced solid-state aggregation, as proved by the strong enhancement of the solid-state fluorescence of **C2SW-alk-PDI**. Therefore alkylated ryleneimides may prove to be useful for applications in which their strong aggregation has detrimental effects. One of these applications is in bulk heterojunction solar cells.

3.3 Application of an *Ortho*-Alkylated PDI in Bulk-Heterojunction Solar Cells[b]

Solution processed bulk hetero-junction (BHJ) organic solar cells have attracted significant attention since they have been first reported in 1995.[49] Such systems exhibit very interesting properties from a commercial point of view, due to their low costs of production, with consequently reduced payback times, as well as flexibility and roll to roll fabrication.[50] In this field, perylenediimides have been investigated as electron acceptors in blends with conjugated donor polymers.[51] PDIs exhibit strong absorption in the visible, large electron affinities, high charge carrier mobilities and low cost of productions.[52] These properties combined with the outstanding thermal, chemical and photo-stability would make of PDIs ideal electron acceptors, alternative to the most investigated fullerene-based materials.[53] However the application of PDIs in BHJ solar cells remains limited.

One of the reasons affecting the performances of PDI-based systems is the strong tendency of perylenediimides to aggregate in solution and in the solid-state. The negative consequences are first of morphological nature with the formation of micrometric domains, too extended for the realization of efficient bulk heterojunction solar cells.[54] The second negative aspect, which derives from the strong aggregation in the solid-state, is the formation of intermolecular states upon the absorption of light leading to non-radiative relaxation mechanisms, representing an important loss channel. [55]

As above mentioned, the use of a 2,5,8,11-alkylated perylenediimide as electron acceptor could have beneficial effects on the performances of BHJ solar cells for several reasons: 1) *ortho*-alkylated PDIs exhibit enhanced solubility in organic solvents, which could suppress the undesired formation of large domains in the blend of the solar cell; 2) the planarity of the aromatic core of the PDI is preserved upon substitution and the alkyl substituents are either linear or γ-substituted. These two attributes leave the possibility to the aromatic cores to π-π stack, necessary condition for the obtainment of good electron mobilities and high power conversion efficiencies; 3) the *ortho*-alkylation has a tremendous impact on the solid-state fluorescence as compared to the parent unsubstituted PDIs. This property would not appear to be relevant for bulk heterojunction solar cells. However high fluorescence quantum yields in the solid-state are usually obtained for PDIs with reduced aggregation and strong solid-state emission can be achieved only if non-radiative relaxation mechanisms are suppressed.[56] Those non-radiative relaxation mechanisms that are also responsible for the low power conversion efficiencies in PDI-based BHJ solar cells.

In the work in collaboration with the group of █████████████████ investigated the performances of BHJ solar cells featuring **C2SW-alk-PDI** as electron acceptor. Photovoltaic devices were fabricated using the *ortho*-alkylated-PDI and as comparison also the core unsubstituted **C7SW-PDI** and **C2SW-PDI**. **C7SW-PDI** was considered for the similar molecular weight and solubility to the alkylated derivative. **C2SW-PDI** provided instead a direct comparison, since it differs from **C2SW-alk-PDI** exclusively for the absence of the *ortho*-substituents. The commercially available regioregular poly(3-hexylthiophene) (rr-P3HT) was selected as polymeric donor material.[57]
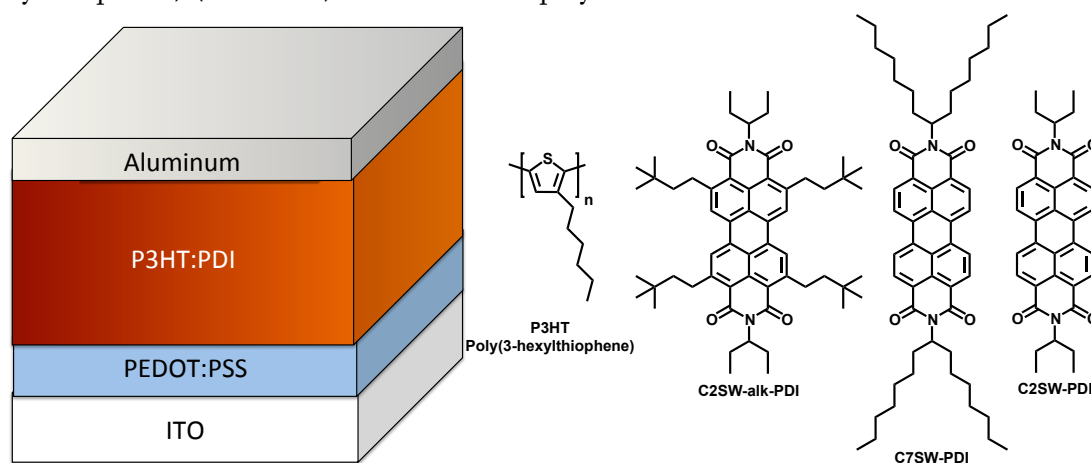
Figure 10. (left) Schematic representation of the photovoltaic devices fabricated by ████. (right) Chemical structure of P3HT and the investigated PDI derivatives.

A photovoltaic device structure equivalent to ITO/PEDOT:PSS/P3HT:PDI/Al was used for testing the photovoltaic parameters. The P3HT used for all devices was BASF SepiolidTM P100 (rr ~ 94 %). Figure 11 shows the IV-curves measured under AM1.5 solar illumination conditions of three different devices: rr-P3HT:**C7SW-PDI** (1:1), rr-P3HT:**C2SW-PDI** (1:1) and rr-P3HT:**C2SW-alk-PDI** (1:1). The first two solar cells were prepared from chloroform, the third from chlorobenzene solution. As it can be seen

from the different IV curves displayed in Figure 11, the *ortho*-alkylation of PDI has a significant impact on the photovoltaic properties of the system.
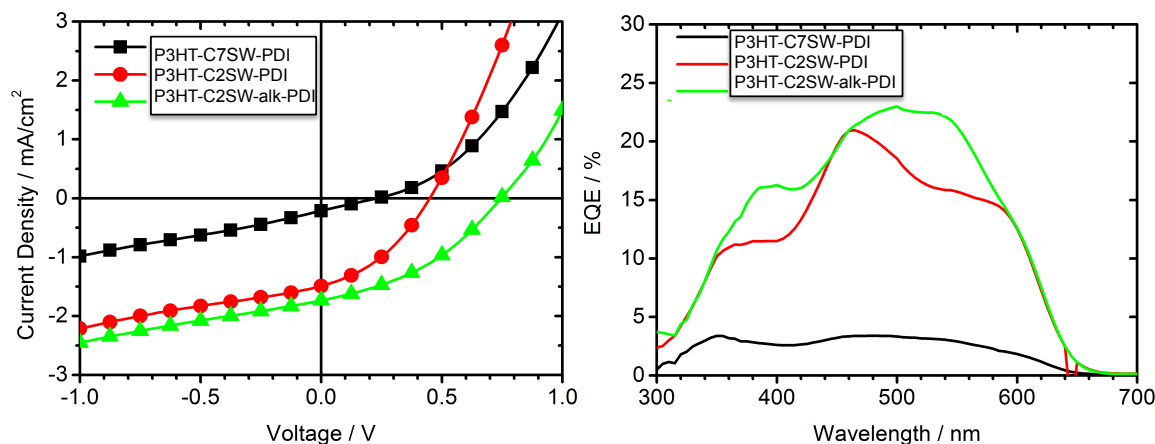
Figure 11 (left): IV-curves of photovoltaic devices using rr-P3HT:PDI as active layers. The curves correspond to: P3HT:**C7SW-PDI** (filled squares), P3HT:**C2SW-PDI** (filled circles) and P3HT:**C2SW-alk-PDI** (up triangles). The first two were prepared from chloroform, the latter from chlorobenzene solution. (right): External quantum efficiencies of rr-P3HT:PDI devices all prepared from chloroform solution.

The power conversion efficiencies (PCE) of the investigated blend films are reported in Table 3. As it can be seen, for all the derivatives PCEs below 1 % were measured. The low performances are to be attributed most probably to the strong tendency of PDIs to form large crystalline domains within the polymer phase, which act as electron traps, decreasing the photocurrents. This problem was already reported in the literature for **C2SW-PDI**.[58] In the case of **C7SW-PDI**, the PCE is not higher than 0.1 %, which may be a consequence either of the poor phase separation between the donor and acceptor, both bearing long alkyl chains which may favor intermixing, or of the low n-type mobilities of **C7SW-PDI**. In fact, the bulky α-branched imide substituents may be responsible for a poor π-π overlap between the PDI molecules, detrimental for the charge transport properties of the system. Nevertheless the performances of **C2SW-alk-PDI** are clearly superior to those of **C7SW-PDI** and **C2SW-PDI**. This is a consequence of an improved short circuit current of the devices using **C2SW-alk-PDI** as electron acceptor compared to those using the two unsubstituted derivatives, if cast from chloroform, and in addition a higher open circuit voltage (V_{OC}) and larger fill factor, if cast from chlorobenzene.

Sample	I_{SC} [mA/cm²]	V_{OC} [V]	FF [%]	PCE [%]
P3HT:**C7SW-PDI**[a]	0.21	0.25	22	0.01
P3HT:**C2SW-PDI**[a]	1.49	0.48	35	0.25
P3HT:**C2SW-alk-PDI**[a]	2.05	0.45	31	0.29
P3HT:**C2SW-alk-PDI**[b]	1.74	0.75	38	0.50

Table 3 Comparison of the photovoltaic parameters, namely short circuit current I_{SC}, open circuit voltage V_{OC}, fill factor FF and power conversion efficiency PCE, of rr-P3HT:PDI blend films. [a] Blended films (1:1) prepared from chloroform solution. [b] Blended film (1:1) prepared from chlorobenzene solution.

In fact the best devices using **C2SW-alk-PDI** exhibit a V_{OC} of 0.75 V, which is higher than typically available from rr-P3HT:PCBM devices and close to the diagonal band-gap of 0.8 V, i.e., the offset between the HOMO of the donor polymer P3HT and the LUMO of the *ortho*-alkylated PDI electron acceptor. Additionally the external quantum efficiency (EQE) values of blend films of rr-P3HT:**C2SW-alk-PDI** are significantly increased throughout the region between 350 and 600 nm compared to those of rr-P3HT:**C7SW-PDI** and rr-P3HT:**C2SW-PDI** devices, despite similar absorption of the blends. The power conversion efficiency of 0.5 % was the highest PCE reported for P3HT:PDI solar cells at the time.

In the previous section the electro-optical characterization didn't reveal any major difference between the properties of **C2SW-alk-PDI** and **C2SW-PDI**. Therefore the improved performances must be originating from the reduced solid-state aggregation of the alkylated derivative as compared to the unsubstituted material. In order to demonstrate this hypothesis, the PDI derivatives were blended in a polystyrene passive matrix at a concentration of 50.0 wt.% to measure their photoluminescence and absorption spectra in the solid. Due to the almost identical optical properties of the two unsubstituted derivatives, the discussion will be limited to only on of them, **C7SW-PDI**, and **C2SW-alk-PDI**. The absorption and fluorescence curves are shown in Figure 12. Indeed a substantially different situation can be observed in the solid-state for the spectra of the unsubstituted PDI as compared to the *ortho*-alkylated derivative.
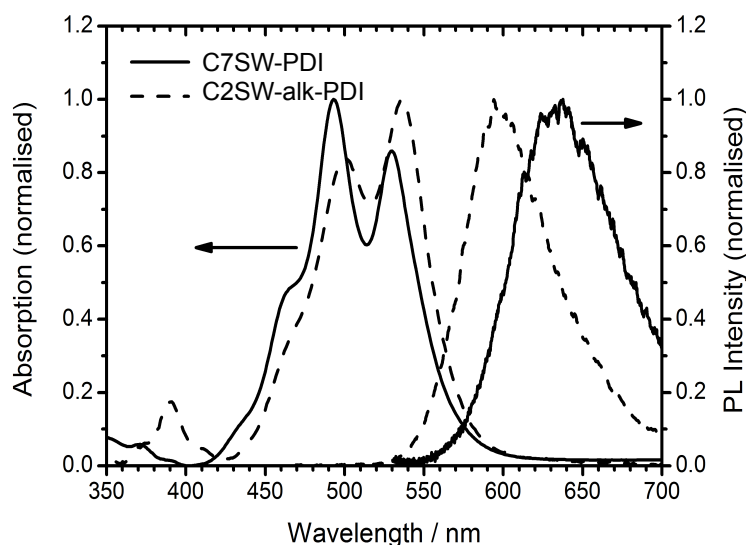
Figure 12 Normalised absorption and fluorescence spectra of PS:**C7SW-PDI** (50 wt. %) (solid line) and PS:**C2SW-alk-PDI** (50wt. %) (dashed line). Note the blue-shifted fluorescence of the intermolecular excited state in the case of **C2SW-alk-PDI** and the different shape of the absorption spectra.

In the absorption spectrum of **C7SW-PDI** a more intense band can be observed corresponding to the 0-1 transition, compared to the 0-0 transition. This is a distinctive sign of the formation of aggregates and has previously been assigned to PDI H-aggregates. The absorption of **C2SW-alk-PDI** maintains instead the typical fine structure of the PDI spectra in solution, most probably due to a decreased interaction in the solid-state between the different molecules. In both cases the emission appears to be

broad and featureless as a consequence of the formation of intermolecular excited states due to PDI aggregation.[59] Nevertheless the more blue-shifted emission of the alkylated PDI compared to the **C7SW-PDI** corresponds to an increase of the energy level of the intermolecular excited states by 160 meV. This may result in a decreased exciton trapping in aggregates and an increase of the charge generation efficiency.

Additional investigations of the PL-lifetimes of the two PDI derivatives gave further proof of the beneficial role of the *ortho*-alkylation in reducing solid-state aggregation. In solution typical lifetimes of 4.7 ns could be measured for all the PDIs, demonstrating a similar photophysical behavior at the molecular level. However, in the solid-state the alkylated derivative showed substantially shorter decay times as compared to the other two derivatives (10 ns vs. the 20 ns observed for the two unsubstituted derivatives). This discrepancy is a direct consequence of the different intermolecular interactions in the bulk. In the case of the unsubstituted PDIs, the strong solid-state aggregation gives rise to the already mentioned long lived intermolecular excited states, which are also responsible for the relaxation mechanisms leding to major energy losses in the organic solar cells. The introduction of the *ortho*-alkyl substituents appears instead to limit the formation of such detrimental relaxation pathways, resulting in shorter decay times and higher power conversion efficiencies.
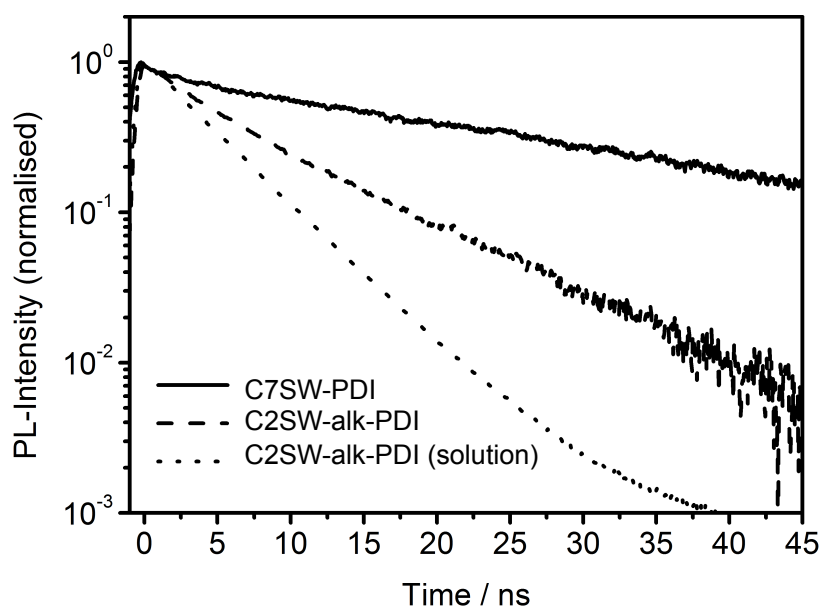
Graphic 1 Fluorescence transients of PS:**C7SW-PDI** (50 wt. %) (solid line), PS: **C2SW-alk-PDI** (50 wt. %) (dashed line) and of **C2SW-alk-PDI** in toluene solution (dotted line).

Summarizing, the introduction of alkyl substituents at the *ortho*-position led to a reduction of the aggregation of the PDI molecules in the solid-state with positive consequences for the photovoltaic performances of devices based on P3HT:PDI blends. However, a more systematic screening of *ortho*-alkylated PDIs would be needed to better understand the beneficial role of the alkylation on the photovoltaic performances. Therefore, a series of *ortho*-alkylated PDIs was synthesized and tested as electron acceptors in BHJ solar cells, work that will be described in the next sections.

3.4 Synthesis of a Series of *Ortho*-Alkylated Perylenediimides

Due to the above mentioned positive effect of the introduction of *ortho*-3,3-dimethyl-butyl substituents, in the investigation which will be here described the core substitution pattern was maintained constant, while systematic variation of the imide substituents was performed. As previously mentioned in the introduction, one of the attractive features of the chemistry of the imide position is the possibility to introduce a variety of substituents, by simply using the versatile anhydride "building block". Via imidization reaction with different primary amines, several PDI derivatives can be accessed in a straightforward manner. Similarly, the possibility to synthesized an *ortho*-alkylated perylenedianhydride building block was explored.

At first direct alkylatation of perylenedianhydride (**PDA**) was screened to access the *ortho*-alkylated system **alk-PDA** (Scheme 14).
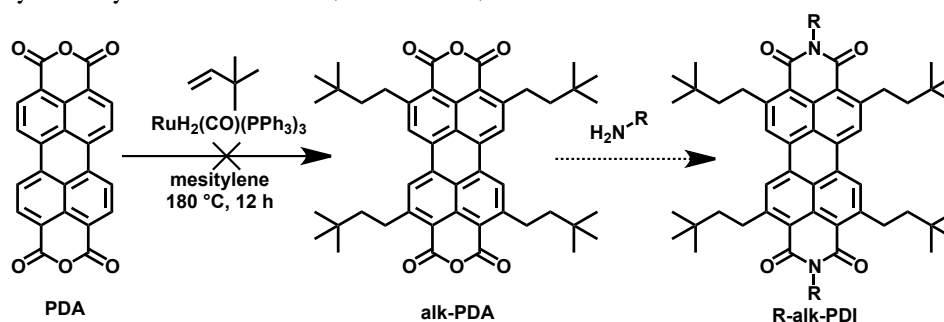
Scheme 14 Alkylation reaction of **PDA** with possible further imidization reaction.

Unfortunately the Murai alkylation protocol did not afford the desired product and the starting PDA was reobtained after reaction, without any trace of alkylated material. The absence of reactivity could be caused either by the insolubility of the PDA molecule in the solvent of the reaction or by the poisoning activity of the anhydride moiety on the Murai catalyst. To prove which of the two hypothesis was correct, the alkylation of **C2SW-PDI** was performed in presence of **PDA** (molar ratio 10:1). Applying the alkylation protocol described in the previous section, only the starting materials could be reobtained, proving the poisoning activity of the anhydride moiety on the Murai catalyst.

Having abandoned the direct alkylation of perylenedianhydride, the second synthetic route still aimed at the synthesis of **alk-PDA**, via the saponification of **C2SW-alk-PDI**. The alkylated perylenediimide could be easily synthesized in large scale, making this strategy feasible even for large scale applications. Following the standard saponification protocol used in our laboratory, **C2SW-alk-PDI** was refluxed in 2-methyl-2-butanol for 16 hours with 42 equivalents of potassium hydroxide. Surprisingly, even after several days, a consistent amount of the starting material was visible on TLC. Additionally the reaction afforded several side products. Other solvents usually applied for the reaction, such as isopropanol, toluene or mixtures in different ratios of dioxane and 2-methyl-2-butanol, did not substantially affect the outcome of the reaction.
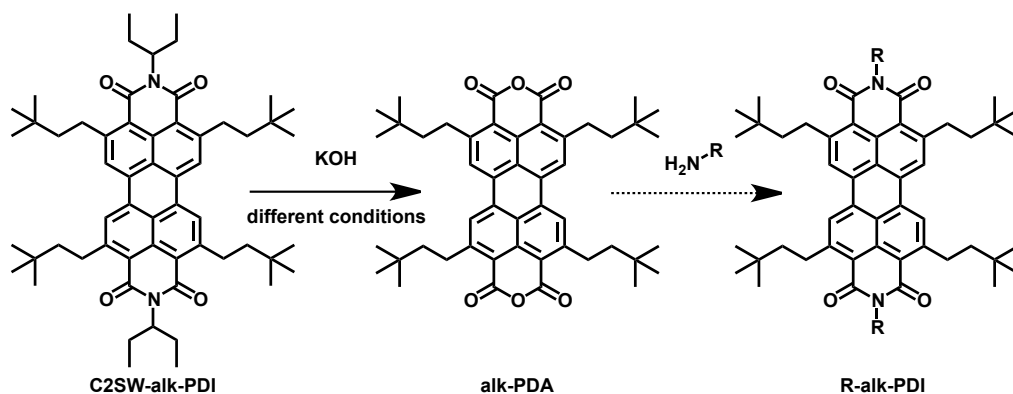
Scheme 15 Saponification of **C2SW-alk-PDI** to the desirable building block **alk-PDA** and possible further imidzation.

Nevertheless, the reaction mixture was worked up in dichloromethane and acetic acid to convert the tetracarboxylate derivative into the desired dianhydride. TLC indicated that the ring closure reaction also remained incomplete. Attempts to isolate **alk-PDA** via column chromatography with analytical purity were not successful. Due to the complications introduced by the presence of numerous side products and the low yields of the reaction (below 30 %), other strategies were considered.

Perylene tetracarboxylic esters are an alternative building block to the peryleneanhydrides. Even though they exhibit reduced chemical and photochemical stability as compared to PDIs, ester derivatives show enhanced solubility and can be readily converted into the corresponding perylene anhydrides or imides under basic or acidic conditions. Thus the Murai alkylation was tested on **4iP-PTC** (Scheme 16).
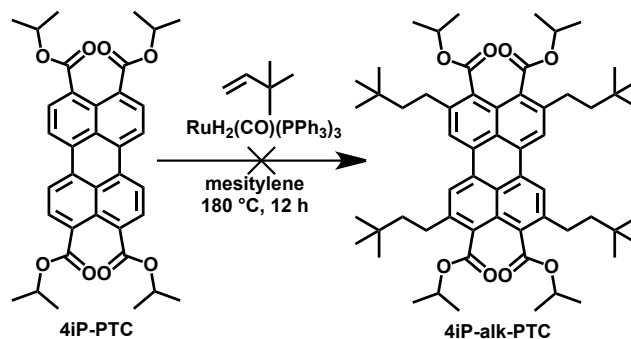
Scheme 16 Attempt of alkylation of a perylene tetraester.

Also in this case only the starting material could be obtained from the reaction. Possible reasons for the failure of the alkylation may be attributed to the impossibility of the Murai catalyst to insert into the *ortho*-positions. In fact the bulkiness of the carboxylic groups forces them to twist out of the plane of the aromatic core, providing no useful coordination site to the ruthenium catalyst. After the failure of the reaction, the synthetic strategy aiming at the creation of a common building block was set aside.

The library of *ortho*-alkylated perylenediimides was then synthesized starting from different unsubstituted PDI derivatives used to perform the *ortho*-alkylation reaction. While this strategy is time consuming, it provides the opportunity to explore the reactivity of the Murai catalyst in presence of different imide substituents, still unknown in the literature. The screened derivatives are shown in Scheme 17. **8-PDI, EH-PDI,**

HB-PDI and **C7SW-PDI** were synthesized following the conditions reported in the literature, while the industrial pigments **NH-PDI**, **Me-PDI** and **PE-PDI** were provided by BASF SE.

The reaction conditions used for **C2SW-PDI** were applied to alkylate the different derivatives, as shown in Scheme 17. For all systems undergoing the reaction, good to very good yields were obtained. In contrast, in the case of **NH-PDI**, **Me-PDI** and **PE-PDI** the reaction did not afford any alkylated product. The reason can most probably be attributed to the extreme insolubility of these materials in the solvent of the reaction even at high temperatures. Additionally the presence of impurities with poisoning effect on the Murai catalyst, such as **PDA**, cannot be completely excluded, due to the pigment nature of the materials.
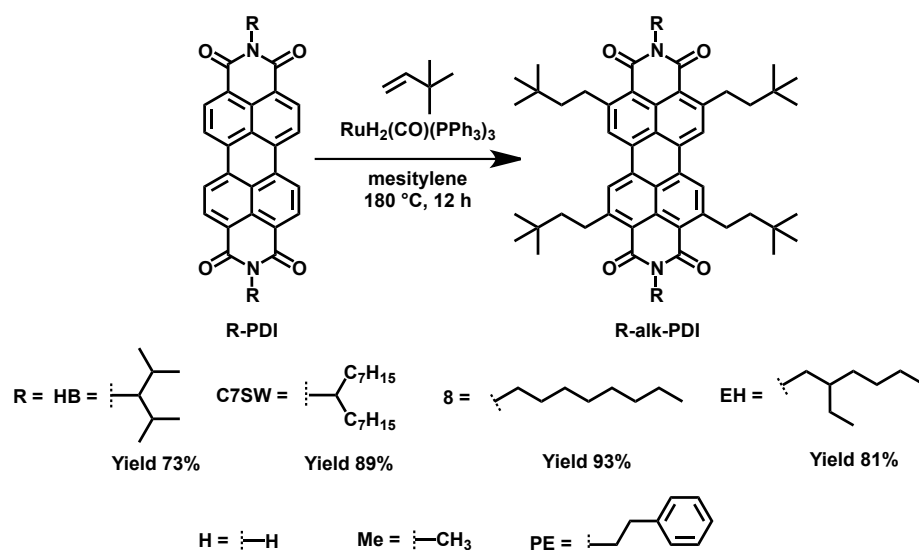
Scheme 17. Investigated perylenediimides derivatives.

According to literature reports,[44,48] *ortho*-alkylated perylenediimides should exhibit enhanced solubility compared to their unsubstituted parent compounds. This is the case for **C2SW-alk-PDI**, **8-alk-PDI** and **C7SW-alk-PDI**, for which solubilities greater than 15 mg/mL in chlorinated solvents and alkanes are observed. Surprisingly **HB-alk-PDI** and **EH-alk-PDI** are sparingly soluble in the common organic solvents at room temperature. Good solubility is observed in high boiling solvents when refluxed, suggesting interdigitation as the cause for their insolubility.

The optical properties of the series of *ortho*-alkylated-PDIs were investigated in solution and the results are summarized in Table 4.

Molecule	λ_{max} [nm]	ε [M^{-1}cm^{-1}]	λ_{em} [nm]	Φ_F (λ_{ex} [nm])	Φ_F (λ_{ex} [nm])
C2SW-alk-PDI	521	5.85 x 10^4	535	0.55 (521)	1.00 (501)
C7SW-alk-PDI	522	6.12 x 10^4	535	0.58 (522)	1.00 (503)
EH-alk-PDI	521	6.46 x 10^4	532	0.56 (521)	1.00 (501)
8-alk-PDI	521	5.92 x 10^4	535	0.58 (521)	1.00 (501)
HB-alk-PDI	521	6.04 x 10^4	532	0.56 (521)	1.00 (501)

Table 4 Optical properties of the *ortho*-alkylated PDIs measured in toluene. Φ_F measured using Rhodamine 6G as standard. **C2SW-alk-PDI** is reported for direct comparison

The variation of the imide substituents has only a marginal impact on the optical and electrochemical properties of the *ortho*-alkylated-PDIs in solution. The introduction of the *ortho*-alkyl substituents has a striking impact on the solid-state fluorescence of perylenediimides instead (Figure 13). While among the unsubstituted parent compounds only the materials bearing the most sterically demanding imide substitutens, **C7SW-PDI** and **HB-PDI**, show solid-state fluorescence, all the *ortho*-alkylated derivatives are bright solids with enhanced solid-state emission. All the 2,5,8,11-functionalized perylenediimides were used as electron acceptors in BHJ solar cells.
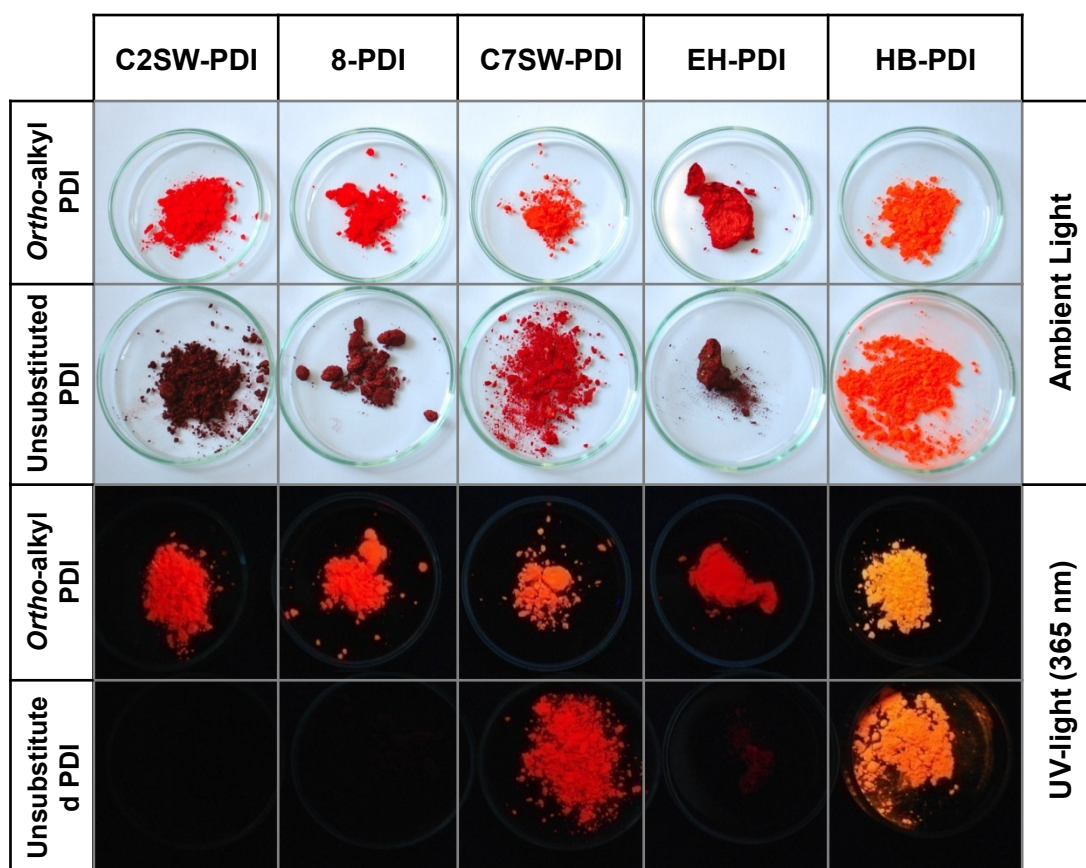
Figure 13. Direct comparison between the *ortho*-alkylated PDIs (first and third rows in the same order) and the unsubstituted parent PDI derivatives (second and fourth rows in the same order) under ambient light (upper two rows) and UV-light (lower two rows). In the columns the imide substituent remains the same.

3.5 *Ortho*-Alkylated PDIs as Electron Acceptors in Bulk Heterojunction Solar Cells

Similarly to the work presented in the previous sections, ▮▮▮▮ investigated the photovoltaic properties of the four alkylated derivatives, blended with P3HT as donor material. **C2SW-alk-PDI** was used for direct comparison. All the photovoltaic devices were built with the structure ITO/PEDOT:PSS/P3HT:PDI/Al and the P3HT used was BASF SepiolidTM P100 (rr ~ 94 %). The blends were casted tetrachloroethane. The IV-

curves measured under AM1.5 solar illumination conditions of the different devices are shown in Figure 14, while the photovoltaic parameters are reported in Table 5.
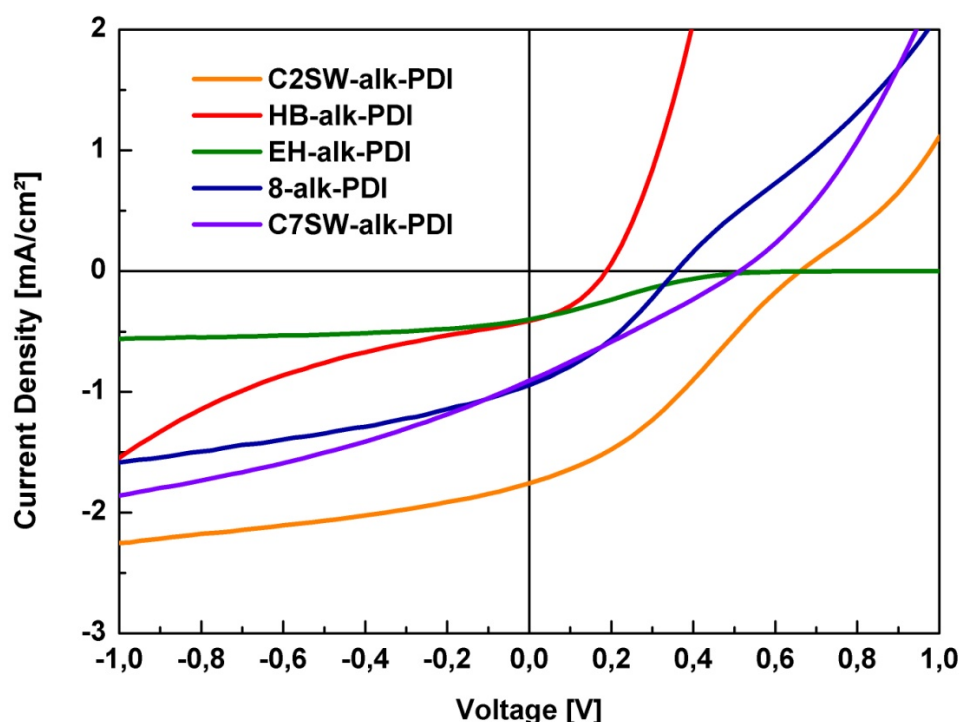
Figure 14 IV-curves of photovoltaic devices using rr-P3HT:PDI as active layers.

Sample	V_{OC}[V]	I_{SC} [A/cm^2]	FF[%]	PCE[%]
C2SW-alk-PDI	0.74	-1.7×10^{-3}	38.0	5.0×10^{-1}
HB-alk-PDI	0.28	-3.4×10^{-4}	28.1	2.9×10^{-3}
EH-alk-PDI	0.73	-4.0×10^{-4}	16.1	5.2×10^{-2}
8-alk-PDI	0.36	-9.4×10^{-4}	33.2	1.2×10^{-1}
C7SW-Alk-PDI	0.51	-9.1×10^{-4}	26.9	1.6×10^{-1}

Table 5 Comparison of the photovoltaic parameters, namely short circuit current I_{SC}, open circuit voltage V_{OC}, fill factor FF and power conversion efficiency PCE, of rr-P3HT:alk-PDI blend films.

Similarly to the results described above, the PCE of the different blends did not reach the 1 %, with **C2SW-alk-PDI** remaining the best performing material. The reason of the poor power conversion efficiencies are still be attributed to the low short circuit currents and poor fill factors, deriving most probably from the tendency of PDIs to build large crystalline domains within the polymer. This would explain the fact that the two most insoluble materials (**HB-** and **EH-alk-PDI**) exhibit the lowest PCE within the series of alkylated PDIs. Furthermore, for almost all blends, the IV-curves show an S-form, which is usually deriving from charge accumulation in the devices, due for example to unbalanced mobility of hole and electrons in the device or bad contact between the electrodes and the active layer.[60] However, studies of the blends would be required to

understand critical issues, such as morphology and phase separation. Furthermore, field effect transistors featuring the different PDI derivatives and the donor acceptor blends may give a further insight into the charge carrier ability of the materials. These measurements could also clarify if PDIs bearing extremely bulky imide substituents, such as **EH-alk-PDI,** simply do not have a favorable π-π stacking to transport electrons.

Nevertheless to further investigate the role of detrimental intramolecular charge trapping phenomena deriving from strong solid-state aggregation, the different 2,5,8,11-functionalized PDIs were blended in a polystyrene matrix with 50 % concentration in weight. Successively the absorption and emission in the solid-state were measured for all derivatives and compared with the model compound **C2SW-alk-PDI** (Figure 15).
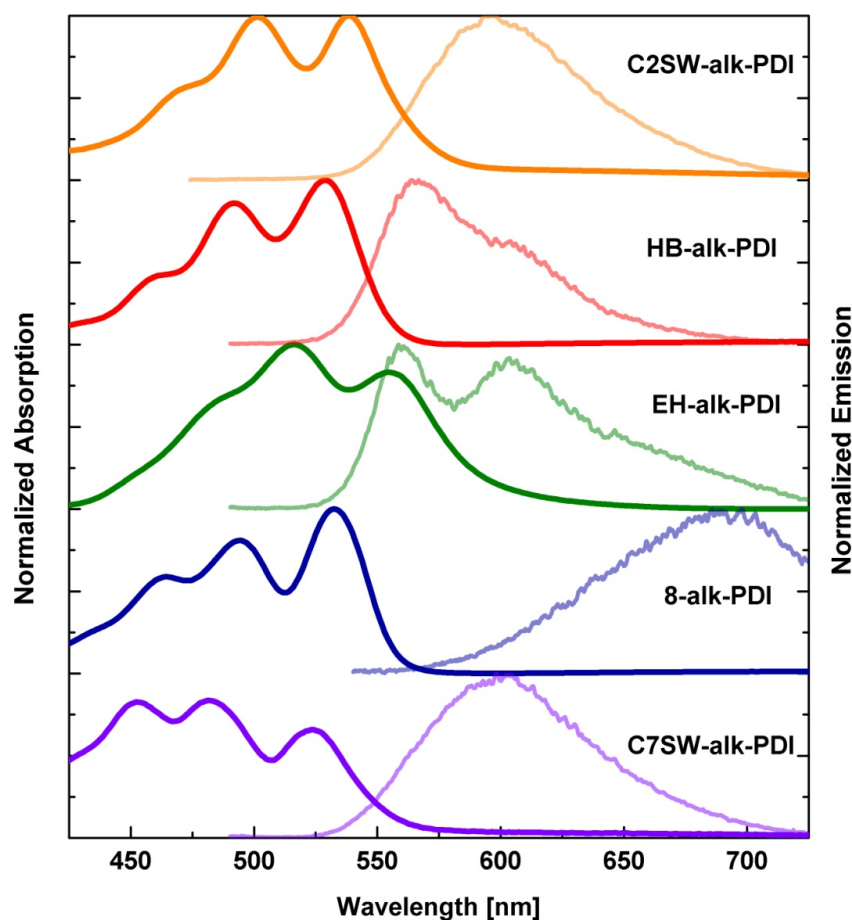
Figure 15 Normalized solid-state absorption (bright color) and emission (pale color) of the family of *ortho*-alkylated PDIs blended in a polystyrene matrix with 50 % concentration in weight.

Within the series, the optical properties are quite inhomogeneous, even though there is a common broadening of the absorption for all derivatives as compared to the data recorded in solution. This feature is a signature of the residual aggregation in the solid-state. **C2SW-alk-PDI**, **HB-alk-PDI** and **8-alk-PDI** still show a more pronounced 0-0 transition as compared to the 0-1 transition, similar to what can be observed in solution. In the case of **EH-alk-PDI** the 0-1 transition becomes the more pronounced, while for the **C7SW-alk-PDI** the absorption is dominated by the 0-2 transition, resulting in a totally reversed picture.

The solid-state emissions appears as well extremely different within the series. **C7SW-alk-PDI** shows a broad and featureless emission peaking around the 600 nm, similarly to **C2SW-alk-PDI**. For **HB-alk-PDI** and **EH-alk-PDI** the photoluminescence spectra appear to be the superposition of two different contributions: one derived from isolated PDI molecules in the polystyrene matrix, causing a peak about 30 nm red-shifted with respect to the solution state; the other originating from PDI-aggregates and having a maximum at longer wavelengths. Finally the **8-alk-PDI** derivative shows a broad, featureless and strongly bathochromically-shifted emission, most probably due to the formation of the extremely long lived intermolecular states.
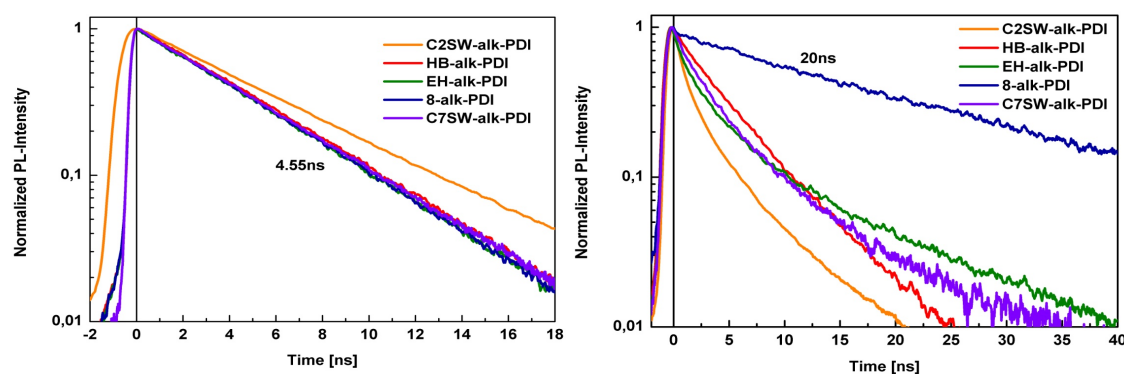
Figure 16 Fluorescent transients of the different *ortho*-alkylated PDIs in 10^{-3} M toluene solution (left) and blended in a polystyrene matrix with 50.0% concentration in weight (right).

A deeper insight could be obtained from the PL decay times measurements of the different derivatives compared to the model compound **C2SW-alk-PDI**. In a dilute toluene solution the photophysical situation was similar for all derivatives, with relaxation times of about 4.7 ns, consistent with those observed for unsubstituted perylenediimide derivatives. However in the polystyrene matrix the long lived intermolecular states of the **8-alk-PDI** already hypothesized from the fluorescence measurements appear clearly, comparable with those observed for unsubstituted PDIs. In this case a determinant role is played by the linear alkyl imide substituents, which allow strong aggregation as for the *ortho*-unsubstituted **C2SW-PDI**. For **HB-alk-PDI** and **EH-alk-PDI**, two lifetimes are present, which further support the hypothesis that PDI-domains and isolated dye-molecules may be present in the polystyrene matrix. In general, all derivatives show longer decay times than **C2SW-alk-PDI**, resulting most probably from a stronger contribution of long-lived intermolecular charge trapping states.

In conclusion the variation of the imide substituents did not improve performances compared to the first investigated system featuring **C2SW-alk-PDI** in combination with P3HT. The low power conversion efficiencies of the different derivatives can be partially explained by photophysical investigations, but, as already mentioned above, other factors must be considered to better understand the limitations of the systems described above, such as morphology of the blends and charge carrier mobilities of the materials. Further investigations about the P3HT:PDI blends of the different solar cells, have been performed by ▮▮▮▮ and can be found in his forthcoming thesis.

3.6 Conclusions and Outlook

In this chapter the Murai catalyzed alkylation of several rylene imides was explored using the olefin 3,3-dimethyl-1-butene. A deeper insight into the limitation of the synthetic protocol could be gained. While 3,3-dimethyl-1-butene underwent the ruthenium-catalyzed reaction in high yields in presence of suitable substrates, not all the investigated materials could be alkylated. *Ortho*-functionalization of perylenedianhydride failed due to the poisoning activity of the anhydride moiety on the catalyst. Alkylation of tetracarboxylic ester was unsuccessful due to the unfavorable geometry of the molecule, hindering the access of the ruthenium complex to the *ortho*-positions. Further, a strong influence of the imide functionalization on the reactivity was observed: less sterically demanding substituents afforded higher reaction yields as compared to the rigid diisopropyl substituents. However the most insoluble materials did not undergo alkylation.

Further, the saponification of the **C2SW-alk-PDI** was explored. The reaction proceeded in low yields due to the presence of several side reactions and the desired product could not be isolated in analytical purity. Nevertheless this strategy should not be excluded for future synthetic work. In fact this may be the only route to obtain derivatives bearing imide substituents that do not undergo alkylation reaction. Additionally, the saponification reaction of perylenediimides is known to be strongly dependent upon the nature of the imide substituent. Different alkyl groups, such as the linear n-octyl derivative or the branched 1-heptyloctyl, may undergo the reaction to completion in shorter reaction times, limiting the formation of side products.

The optical and electrochemical characterization of the *ortho*-alkylated ryleneimides revealed a minor impact of the substitution on the properties as compared to the unsubstituted ryleneimides. Further, all the *ortho*-alkylated PDIs show strong solid-state fluorescence, due to suppression of the aggregation. The solubility of the different materials appears to be enhanced, even though in some cases interdigitation led to extremely insoluble systems. Nevertheless, the *ortho*-alkylation appears to be a very promising method to improve solubility and processability of RIs, if the appropriate olefin is chosen. Therefore this method may further broaden the synthetic solutions to tune the aggregation of ryleneimides, based until 2009 exclusively on imide, *bay-* and *peri-*functionalization.

████████ investigated the possibility to use the alkylated PDIs as electron acceptors in bulk heterojunction solar cells in combination with P3HT. The choice of the polymer donor material was driven by its commercial availability and especially by the large number of publications featuring P3HT. All the screened materials showed low photovoltaic activity, with PCE below 1 %. However, the introduction of the bulky γ-branched alkyl chains seemed to prevent detrimental relaxation mechanisms often leading to poor photovoltaic performances. The power conversion efficiency of 0.5 % obtained using **C2SW-alk-PDI** was the highest PCE reported for P3HT:PDI solar cells at the time.

Higher power conversion efficiencies could be obtained in the future by replacement of P3HT with different donor polymers. In fact X-ray diffraction studies performed on P3HT:**C2SW-alk-PDI** solar cells demonstrated that annealing processes have no major impact on the system. While the PDI acceptor already forms crystalline domains after spin-coating, the donor polymer phase remains in a disordered state before and after annealing, probably due to the presence of the bulky *ortho*-alkyl chains hindering crystallization. However annealing processes are crucial for P3HT for the obtainment of high PCE. In fact non-annealed P3HT:PCBM devices show similar PCE to the P3HT:**C2SW-alk-PDI** devices, while after annealing efficiencies as high as 5 % can be obtained. Hence, there is potential for further improvements in the performances using donor polymers whose efficiency does not depend so strongly on postproduction annealing procedures.

While the studies reported in this chapter demonstrate that the *ortho*-alkylation may be used to limit solid-state aggregation, work has yet to be done in order to develop competitive PDI-based electron acceptors. In particular one of the main limitations of perylediimide derivatives as compared to fullerene acceptors appears to be the absence of three-dimensionality. Such limitation could be challenged by careful design of the molecular structure, as for example by linking of the PDI dyes via the imide group to rigid three-dimensional systems, which avoids conjugation with the aromatic core, preserving the desirable optical and electronic properties of the PDI acceptor. Interesting candidates could be adamantine or spiro-based materials, N-N coupled imides, periferically functionalized rigid dendrimers.
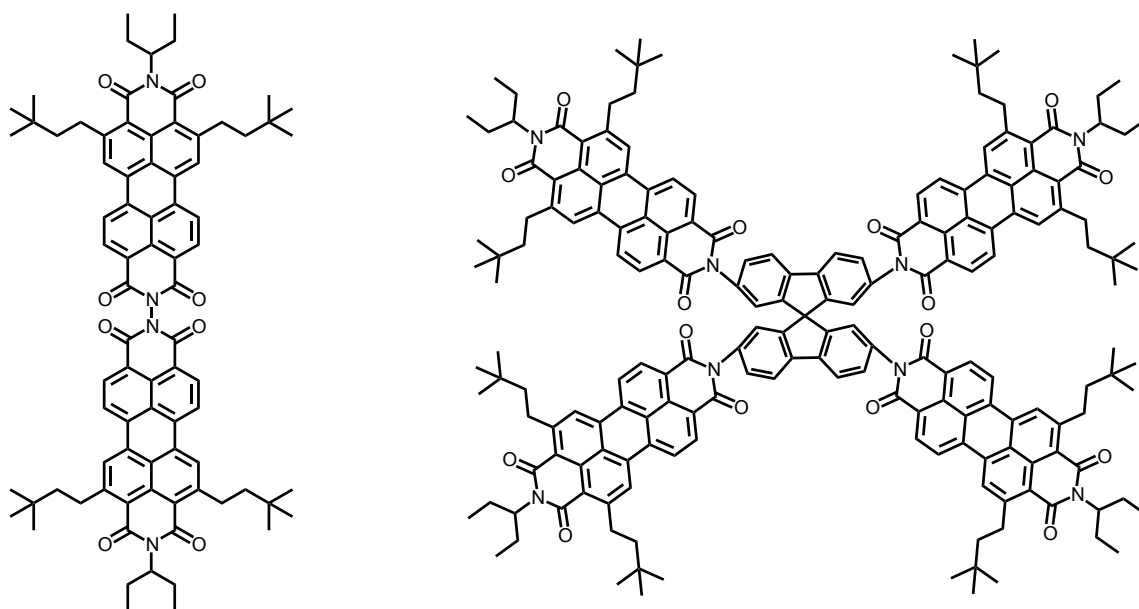
Figure 17 Threedimensional PDI derivatives.

An alternative application for the *ortho*-alkylated derivatives could be in small molecule solar cells. Via careful choice of the donor molecule, self assembly could be favored to give the formation of highly oriented materials in columnar domains. This strategy was already applied in our group[61] and via targeted simulations of the substituents, columnar

formation could be tuned in order to achieve the desired properties. The system used was a **C2SW-PDI**, known to give intermolecular aggregation leading to power conversion efficiencies still capable of improvement. In this case the alkyl substituents should be tuned in order to obtain liquid crystalline behavior. A possible strategy would be the introduction of linear substituents on the imide and on the *ortho*-positions.

HBC-based donor   **PDI-based acceptor**
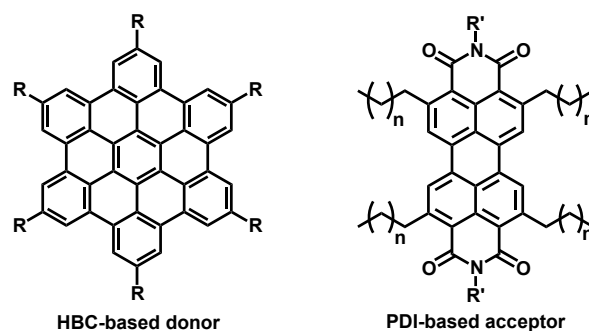
Figure 18 Possible candidates for small molecule based bulk heterojunction solar cells.

Finally the *ortho*-alkylation may prove to be useful if applied to one of the most famous perylenediimide derivatives, the *bay*-cyanated PDIs. These systems have been extensively studied as air stable n-type semiconductors in organic field effect transistor and have lead to impressive mobilities.[62] However, their application in organic bulk heterojunction solar cells gave poor results.[63] The reasons were not investigated by the reports featuring this acceptor, but also in this case intramolecular charge trapping states may be involved, which could be limited by *ortho*-alkylation.
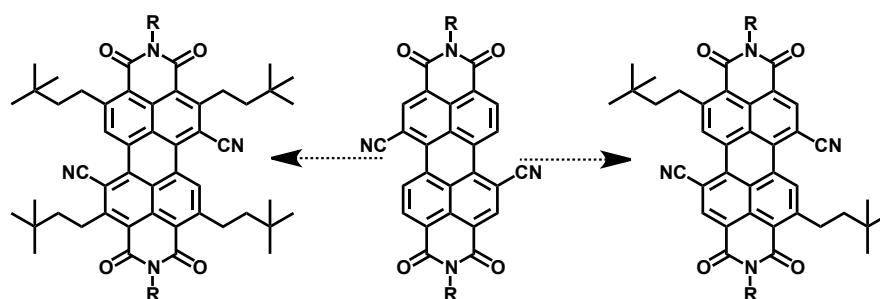
Figure 19. Possible modification of *bay*-dicyano-PDI via *ortho*-alkylation.

The use of materials with enhanced electron affinity could also allow the application of a broader library of low band gap polymers in solar cells, not possible with the more electron rich fullerene based derivatives. Electron acceptors with higher electron affinities would also provide greater stability towards air, improving the overall lifetimes of the organic based electronic devices, which still remains one of the main issues in the field of organic electronics.

3.7 References

[44] Nakazono, S., Imazaki, Y., Yoo, H., Yang, J., Sasamori, T., Tokitoh, N., et al. (2009), *Chemistry – A European Journal*, *15*(31), 7530–7533.

[45] a) Murai, S., Kakiuchi, F., Sekine, S., Tanaka, Y., Kamatani, A., Sonoda, M., & Chatani, N. (1993), *Nature*, *366*(6455), 529-531. b) Kakiuchi, F., Sekine, S., Tanaka, Y., Kamatani, A., Sonoda, M., Chatani, N., & Murai, S. (1995), *Bulletin of the Chemical Society of Japan*, *68*(1), 62-83.c) Kakiuchi, F., & Murai, S. (2002), *Accounts of chemical research*, *35*(10), 826-834.

[46] Nolde, F. (2008), Ph. D. Thesis, Johannes Gutenberg University (Mainz).

[47] Nolde, F., Pisula, W., Müller, S., Kohl, C., & Müllen, K. (2006), *Chemistry of materials*, *18*(16), 3715-3725.

[48] Bullock, J. E., Vagnini, M. T., Ramanan, C., Co, D. T., Wilson, T. M., Dicke, J. W., Marks, T. J., and Wasielewski, M. R. (2010). *The Journal of Physical Chemistry B*, *114*(5), 1794–1802. doi:10.1021/jp908679c

[49] Yu, G., Gao, J., Hummelen, J. C., Wudl, F., & Heeger, A. J. (1995), *Science*, 1789-1790.

[50] a) Brabec, C. J., Sariciftci, N. S., & Hummelen, J. C. (2001), *Advanced Functional Materials*, *11*(1), 15–26. b) Thompson, B. C., & Fréchet, J. M. (2008), *Angewandte chemie international edition*, *47*(1), 58-77. c) Günes, S., Neugebauer, H., & Sariciftci, N. S. (2007), *Chemical Reviews*, *107*(4), 1324–1338.

[51] a) Li, C., & Wonneberger, H. (2012), *Advanced Materials*, *24*(5), 613-636. b) Sonar, P., Lim, J. P. F., & Chan, K. L. (2011), *Energy & Environmental Science*, *4*(5), 1558-1574. c) Kozma, E., & Catellani, M. (2013), *Dyes and Pigments*.

[52] a) Huang, C., Barlow, S., & Marder, S. R. (2011), *The Journal of organic chemistry*, *76*(8), 2386-2407. b) Zhan, X., Facchetti, A., Barlow, S., Marks, T. J., Ratner, M. A., Wasielewski, M. R., & Marder, S. R. (2011), *Advanced Materials*, *23*(2), 268-284. c) Anthony, J. E., Facchetti, A., Heeney, M., Marder, S. R., & Zhan, X. (2010), *Advanced Materials*, *22*(34), 3876-3892.

[53] Brabec, C. J., Gowrisanker, S., Halls, J. J., Laird, D., Jia, S., & Williams, S. P. (2010), *Advanced Materials*, *22*(34), 3839-3856.

[54] Wang, H., Peng, B., & Wei, W. (2008), *Progress in Chemistry*, *20*(11), 1751-1760.

[55] Howard, I. A., Laquai, F., Keivanidis, P. E., Friend, R. H., & Greenham, N. C. (2009), *Journal of Physical Chemistry C*, *113*(50), 21225–21232.

[56] a) Langhals, H., Demmig, S., & Potrawa, T. (1991), *Journal für Praktische Chemie*, *333*(5), 733-748. b) Langhals, H., Krotz, O., Polborn, K., & Mayer, P. (2005), *Angewandte Chemie International Edition*, *44*(16), 2427-2428.

[57] Dang, M. T., Hirsch, L., & Wantz, G. (2011), *Advanced Materials*, *23*(31), 3597-3602

[58] X. Y. Guo, L. J. Bu, Y. Zhao, Z. Y. Xie, Y. H. Gengand, L. X. Wang, (2009), *Thin Solid Films*, 517, 4654.

[59] Keivanidis, P. E., Howard, I. A., & Friend, R. H. (2008), *Advanced Functional Materials*, *18*(20), 3189-3202.

[60] Qi, B., & Wang, J. (2013). *Phys. Chem. Chem. Phys.*, *15*(23), 8972-8982.

[61] Schmidt-Mende, L., Fechtenkötter, A., Müllen, K., Moons, E., Friend, R. H., & MacKenzie, J. D. (2001), *Science*, *293*(5532), 1119-1122.

[62] a) Ahrens, M. J., Fuller, M. J., & Wasielewski, M. R. (2003). *Chemistry of materials*, *5*(14), 2684-2686. b) Jones, B. A., Ahrens, M. J., Yoon, M. H., Facchetti, A., Marks, T. J., & Wasielewski, M. R. (2004), *Angewandte Chemie*, *116*(46), 6523-6526. c) Jones, B. A., Facchetti, A., Wasielewski, M. R., & Marks, T. J. (2007), *Journal of the American Chemical Society*, *129*(49), 15259-15278.

[63] Shin, W. S., Jeong, H.-H., Kim, M.-K., Jin, S.-H., Kim, M.-R., Lee, J.-K., et al. (2006), *Journal of Materials Chemistry*, *16*(4), 384–390.

4 Lactonization of a Quinoidal Perylenemonoimide as an Approach Toward Stable NIR-Absorbing Dyes

4.1 Introduction

NIR-absorbing dyes represent an extremely interesting class of materials with applications ranging from optical recording to laser filters and from medicinal applications to heat management.[64] In this field rylenes are among the most famous and investigated molecules due to their already mentioned excellent photochemical stability and versatile chemistry.[65] There are mainly three strategies to achieve NIR-absorption using RIs:
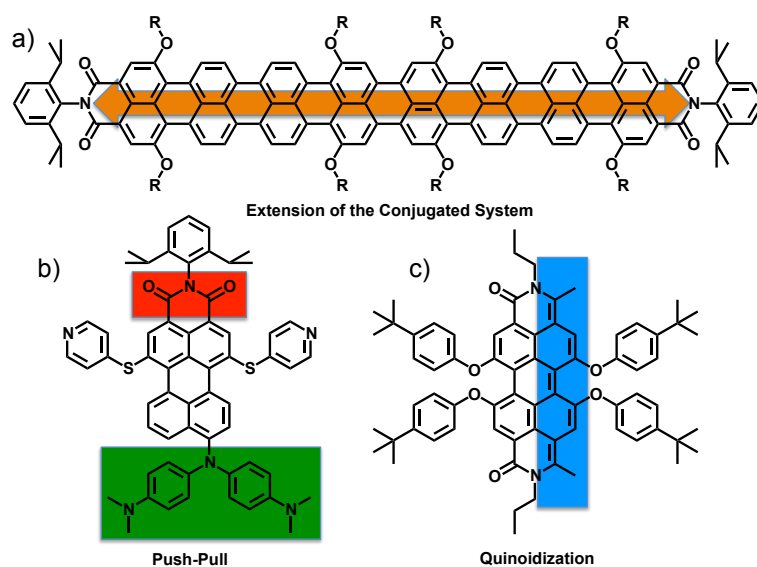
Figure 20 Approaches for the synthesis of NIR-absorbing dyes.

a) extension of the π-system: via the introduction of additional naphthalene units into the rylene aromatic core.[66] A representative example based on this concept is octarylenediimide, the longest rylenediimide known, that features an absorption maximum at 1065 nm[67];

b) creation of a push-pull system: introduction of electron-donating groups, such as amines, on the aromatic core of RIs leads to a bathochromic shift in the absorption, which can be modulated depending on the number and nature of the substituents.[68] In

the case of the perylene monoimide reported in Figure 20b, the absorption maximum reached 736 nm, 200 nm red-shifted as compared to unsubstituted PMI[69];

c) quinoidization: the transition from aromatic to quinoidal system causes a change in the absorption, as in the case of the dye reported by Quante (Figure 20c), exhibiting an 80 nm red-shift, as compared to the parent compound 1,6,7,12-tetraphenoxy PDI.[70]

In 2008 our group reported an approach combining all the above-mentioned strategies.[71] A homologous series of rylene monoimides was synthesized ranging from naphthalene to quaterrylene, bearing an amine substituent in the *peri*-position (Figure 21). Via deprotonation of the amino group, the formation of a quinoidal system was induced. A remarkable bathochromic shift and a strong increase in the absorption coefficient were associated to the transition. For example the perylenemonoimide derivative showed a maximum in the absorption shifted of almost 300 nm to longer wavelengths and a threefold increase in the extinction coefficient. In the case of the quaterryleneimide derivative the absorption maxima even reached 1186 nm. Unfortunately, the quinoidal state could be induced exclusively in a solution containing a strong base able to deprotonate the secondary amine. Removal of the solvent or neutralization of the pH caused a back-transition to the aromatic structure.
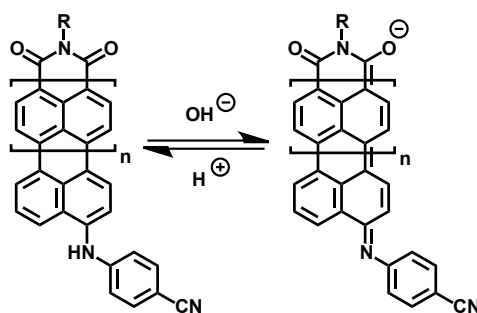
Figure 21. The reversible transition from the amino substituted ryleneimide derivate (left) to its quinoidal form (right) upon protonation or deprotonation of the amino group.

Considering the outstanding properties of the quinoidal derivatives, the stabilization of these structures would be highly desirable, leading to a new class of extraordinary NIR-absorbing dyes. In the following section, a strategy to achieve a perylene-based quinoid dye will be explored.

4.2 Synthesis of a Lactonized Perylenemonoimide

The change induced upon deprotonation of the push-pull structure described above does not only impact on the nature of the rylene core, which loses its aromaticity, but also acts on the donor and acceptor groups. As shown in Figure 22, the amino group turns into an imine acceptor, while the carbonyl forms an enolate that acts as a donor. Therefore, an attractive approach for the stabilization of the quinoidal form could be based on the covalent modification of the enolate group, which could hinder the back-transition to the aromatic state. Among the different options, it was decided to investigate the possibility to create a six-membered lactone taking advantage of a particular imide substituent, a

phenyl group bearing an *ortho*-carboxylic acid (Figure 22). This strategy could not only lead to the synthesis of the stable NIR-absorbing dye, but the lactone ring could also be eventually reopened via hydrolysis, to return to the original push-pull structure.
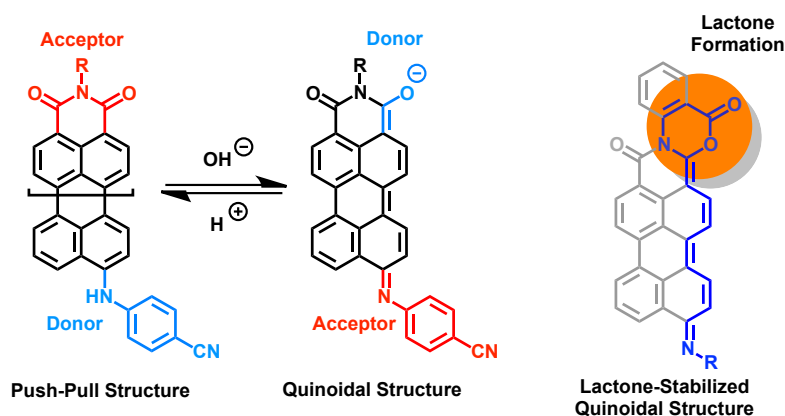
Figure 22 Reversible transition between the pusp-pull and the quinoidal structure. On the right, the lactonized quinoid investigated in this section.

Even though in the first report about the quinoidization of rylenemonoimides four different homologues were studied, in this investigation only the PMI was considered for mainly two reasons: 1) PMI offers a more straightforward synthesis as compared to the terrylene and quaterrylene derivatives; 2) this system is the first homologue in the series to exibit absorption in the NIR-region upon quinoidization (800 nm), making it more attractive than the naphthalenemonoimide derivative that absorbs only in the visible.

A careful observation of the lactone-stabilized structure (Figure 22) reveals that the formation of the six-membered ring would lead to a flat molecular structure. In fact the imide substituent would be immobilized in the plane of the perylene conjugated core, with the risk to obtain a material with a very strong tendency to aggregate. For this reason it was decided to introduce *ortho*-alkyl substituents as solubilizing groups, due to their minimal impact on the geometrical, optical and electrochemical properties of the dye. More precisely the already investigated 3,3-dimethyl-butyl chains were chosen.

The synthesis of the lactonized quinoidal derivative should proceed in a stepwise manner: first the introduction of the imide substituent, followed by the coupling of the PMI derivative with the amino group and final lactonization reaction. The alkylated perylenemonoanhydride **alk-PMA** was selected as scaffold on which the push-pull structure should be built and its synthesis was addressed at the first stage.

As discussed in the previous chapter, direct alkylation of anhydride derivatives cannot be performed, due to the poisoning effect of anhydride group on the Murai catalyst. Consequently, **alk-PMA** had to be synthesized via saponification of a 2,5-alkylated-PMI. **DiPP-alk-PMI**, already described in the previous chapter, was used as starting material. The saponification reaction was tested applying the standard reaction conditions used in our laboratory, featuring potassium hydroxide and 2-methyl-2-butanol as solvent. After heating the reaction overnight, the starting material **DiPP-alk-PMI** was reobtained. Longer reaction times and replacement of the solvent with isopropanol, toluene or

dioxane lead to the same results. The failure of the saponification was attributed to the presence of the bulky imide substituent, which may hinder saponification. Therefore the diisopropyl phenyl was replaced with a less sterically demanding group.
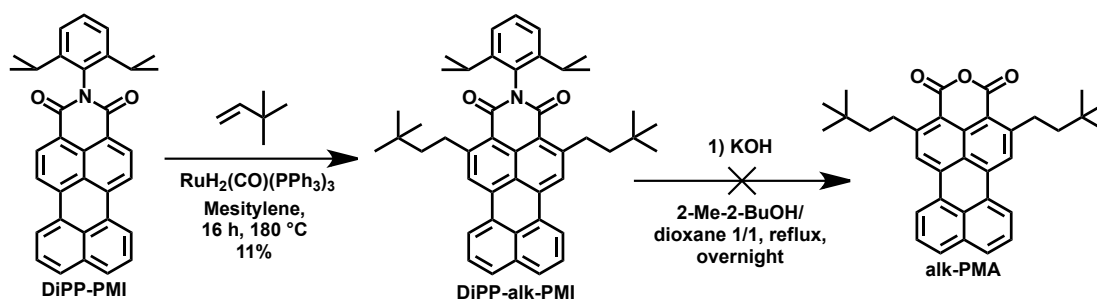
Scheme 18 Synthetic route to **alk-PMA**, starting from the **DiPP-PMI**.

The neopentyl moiety was selected as alternative imide substituent. This group allows Murai alkylation of the *ortho*-positions in high yields, as already observed in the previous chapter for **C2SW-PDI**. Additionally its less bulky nature as compared to the diisopropylphenyl group should allow saponification in good yields. To introduce the neopentyl substituent, **DiPP-PMI** was first saponified to give the monoanhydride **PMA**. The protocol was optimized to allow up-scaling by adding 1,4-dioxane to the commonly used 2-methyl-2-butanol (1:1 ratio) in order to enhance the solubility of PMI in the reaction mixture. In this way the concentration of **DiPP-PMI** could be increased from 5 g/L to 25 g/L. The pigment **PMA** was isolated after acid-catalyzed ring closure and was directly used for the next step without further purification. Imidization with 3-pentyl-amine using molten imidazole as solvent gave the desired **C2SW-PMI** after chromatographic purification, with a 78 % yield over two steps.
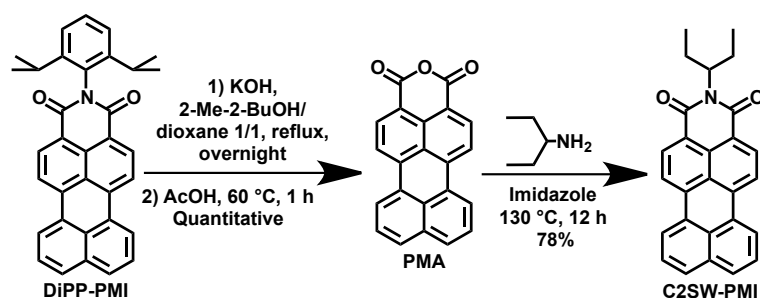
Scheme 19 Synthesis of **C2SW-PMI**.

The Murai type alkylation reaction was then applied to the perylenemonoimide and the desired compound **C2SW-alk-PMI** was isolated after crystallization from isopropanol in excellent yield (93 %). If the three steps are considered, an overall yield of 72 % was obtained using a single chromatographic purification, making this route extremely attractive for the synthesis of the alkylated perylenemonoimide scaffold.
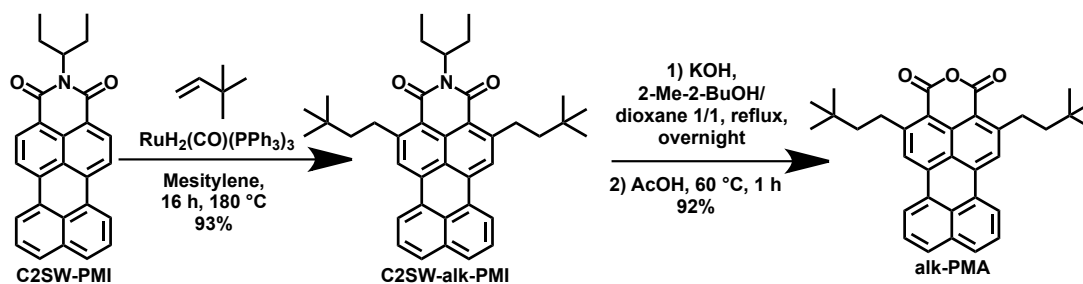
Scheme 20 Two-steps synthesis of **alk-PMA**.

C2SW-alk-PMI was then saponified using the optimized route already applied to **DiPP-PMI**, featuring the 1/1 mixture of dioxane and 2-methyl-2-butanol as solvent (Scheme 20). The reaction proceeded in almost quantitative yields and only traces of side products were observed. Purification of the desired **alk-PMA** was performed via crystallization from toluene, to give an orange crystalline solid (yield 92 %). It is worth noting that the same protocol applied to the alkylated perylenediimide **C2SW-alk-PDI** was described in the previous chapter. However in that case the reaction afforded numerous side products and unreacted starting material was always present. This difference in reactivity is surprising, considering the identical imide and *ortho*-substituents. A possible cause of the formation of the side products may be the more electron poor nature of the perylenediimide derivative as compared to the monoimide, which may activate the α-positions of the *ortho*-alkyl groups toward undesired reactions.

After obtaining the ground structure for the synthesis of the quinoidal derivative, the auxiliary imide substituent needed for the formation of the lactone cycle was introduced. Methyl-anthranilate was chosen for the imidization reaction, due to its better solubility as compared to anthranilic acid. Imidization of **Alk-PMA** in molten imidazole at 140 °C was successfully achieved (Scheme 21). However, due to the quite drastic conditions, the ester group underwent hydrolysis and also decarboxylation occurred. Nevertheless **B-alk-PMI** could be isolated after chromatographic purification in good yield (64 %). Other solvents, such as isopropanol, toluene and propionic acid were tested to improve the outcome of the reaction and limit undesired decarboxylation. However for all these alternative routes the imidization failed and only the starting anhydride was reobtained.
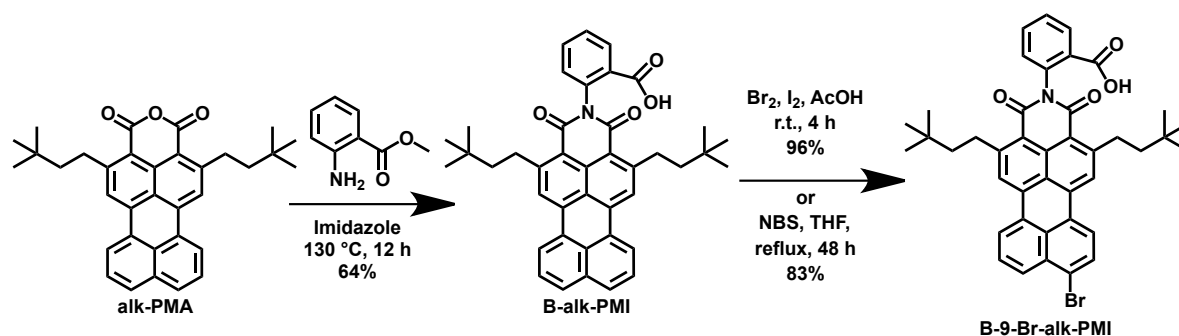
Scheme 21 Syntheses of **B-alk-PMI** and **B-9-Br-alk-PMI**.

In order to functionalize the 9-position of PMI, mono-bromination of **B-alk-PMI** was required. Two different reactions were tested: using NBS in refluxing THF and alternatively with bromine in acetic acid at room temperature (Scheme 21). Both protocols afforded the desired product in high yields. Nevertheless the route featuring bromine in acetic acid is to prefer dur to the shorter reaction times, lower temperature and better reaction yield (96 %).

Finally **B-9-Br-alk-PMI** was converted into the push-pull molecule **B-9-amino-alk-PMI** via Buchwald-Hartwig coupling with 4-amino-benzonitrile (Scheme 22). This amino substituent was already reported in the preliminary work from our group about quinoidal ryleneimides and was chosen due to the larger bathochromic shift achieved upon quinoidization as compared to octylamine, also investigated. The reason of such a shift can be assigned to the stronger electron withdrawing nature of the imine bearing the benzonitrile substituent, that increases the donor acceptor character of the molecule.
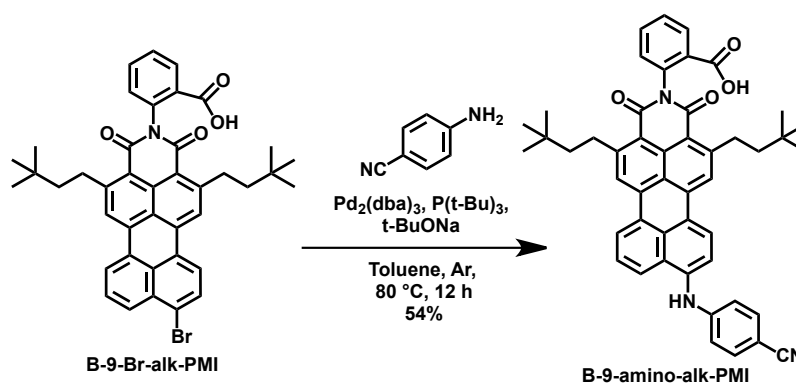
Scheme 22 Synthesis of the donor acceptor system **B-9-amino-alk-PMI**.

After amination, the desired **B-9-amino-alk-PMI** could be isolated via column chromatography (yield 54 %) from the debrominated perylenemonoimide **B-alk-PMI,** also obtained as a side product. The introduction of the donor moiety caused a strong change in the optical properties of the PMI system. In fact, while **B-9-Br-alk-PMI** exhibits a bright orange color as solid and in solution, **B-9-amino-alk-PMI** appears as a dark violet material.

Before approaching the lactonization reaction, the transition from the push-pull structure to the open quinoid form **Na-B-9-amino-alk-PMI** was investigated (Scheme 23). Such transition would be necessary in order to achieve the target lactonized material and the presence of a different imide group and of the *ortho*-alkyl substituents may influence the behavior of the system.
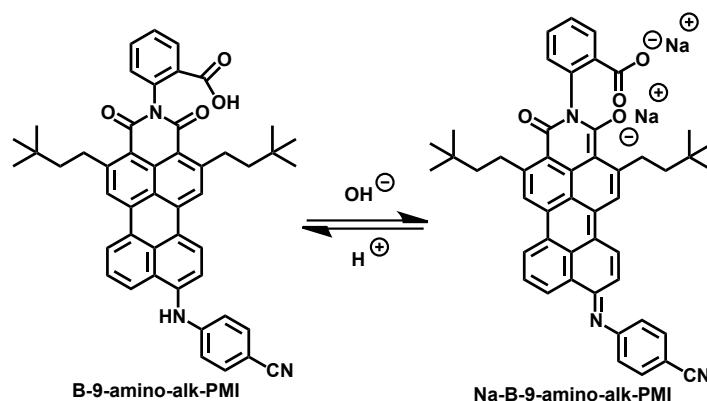
Scheme 23 Transition from the push-pull stracture (**B-9-amino-alk-PMI**) to the quinoidal form (**Na-B-9-amino-alk-PMI**).

A THF solution of **B-9-amino-alk-PMI** was prepared and the absorption spectra recorded in presence and absence of sodium tert-butylate. Before deprotonation **B-9-amino-alk-PMI** showed a broad featureless absorption, typical for push-pull conjugated molecules, with a maximum at 515 nm (Figure 23). After addition of sodium tert-butylate to the solution, a drastic color change occurred, with an immediate transition from the violet to the yellow. While the color of **Na-B-9-amino-alk-PMI** derives from the residual absorption between 400 and 500 nm, the extinction coefficient reaches its maximum at 800 nm, in the NIR region. This is in agreement with what was previously observed from our group, proving that the quinoidization of **B-9-amino-alk-PMI** can be successfully induced despite the presence of the new substituents. Also in this case, upon neutralization of the pH of the solution or removal of the solvent the back-transformation to the original push-pull structure was observed.
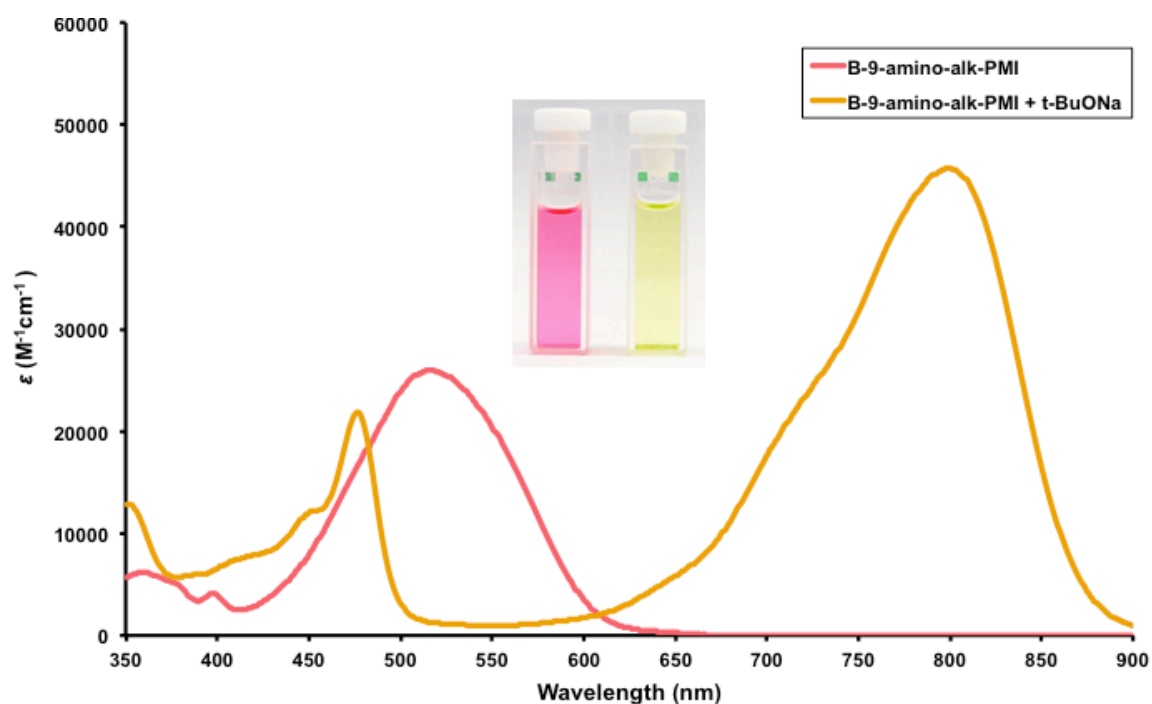
Figure 23 Image and absorption spectra of **B-9-amino-alk-PMI**, before and after addition of sodium tert-butylate.

The transition of **B-9-amino-alk-PMI** from donor-acceptor to its quinoidal form was further investigated via ^{1}H-NMR in deuterated THF, before and after addition of sodium tert-butylate. In the aromatic region depicted in Figure 24 a dramatic upfield shift of the signals of the protons on the side of the quinoid structure (i, j and k) is observed. This is due to the increased electron density on the carbon atoms after deprotonation, deriving from the delocalization of negative charge of the nitrogen atom. Additionally, a downfield shift of the signal of the proton in the free *peri*-position (h proton in Figure 24) occurs, due to the vicinity of the newly formed imine double bond. This behavior is also in agreement with the previous report from our group about ryleneimide quinoidal derivatives.[71]
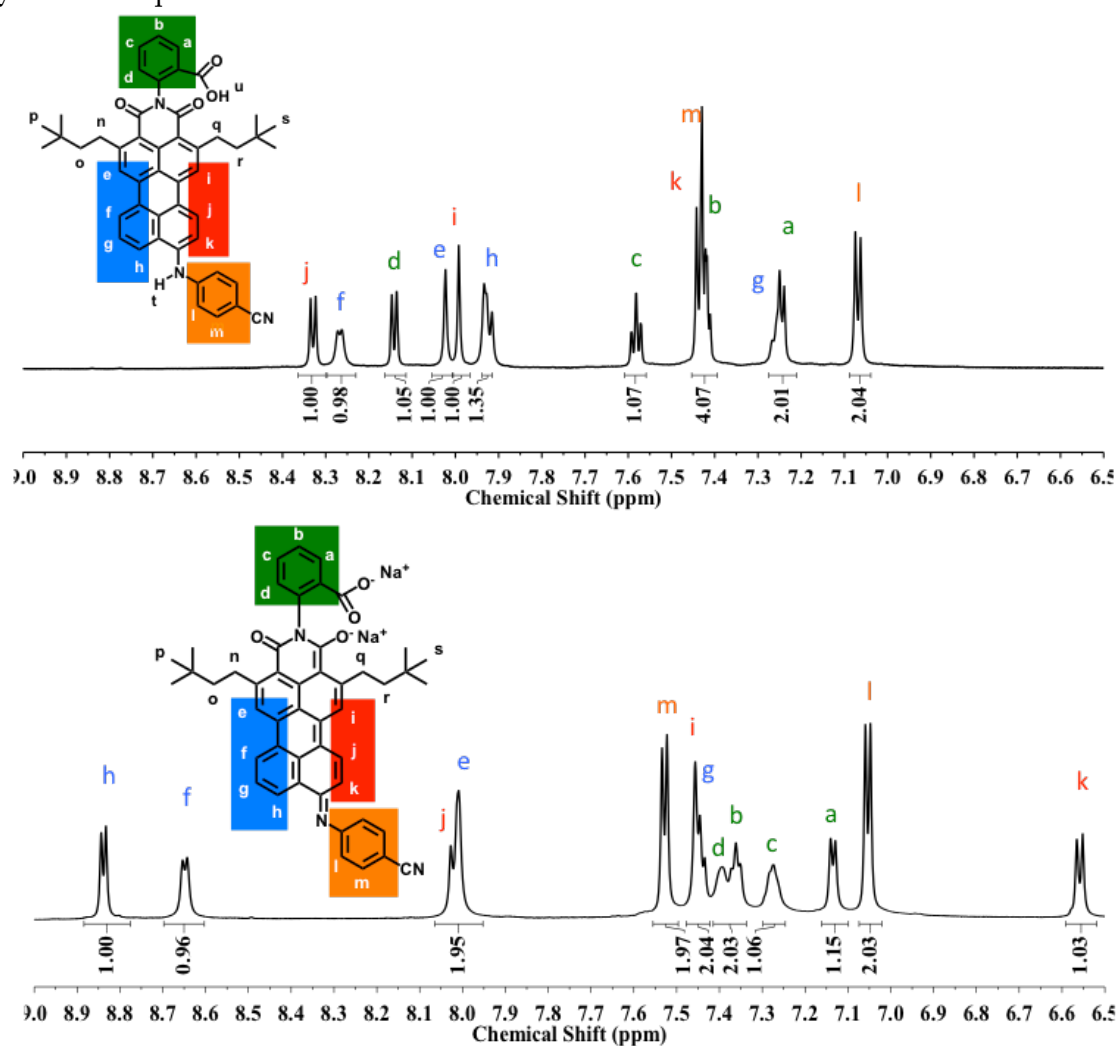
Figure 24 Aromatic region of the ^{1}H-NMR in deuterated THF of **B-9-amino-alk-PMI**, before and after addition of sodium tert-butylate (top and bottom, respectively).

After proving the possibility to induce the quinoidization of **B-9-amino-alk-PMI**, the cyclization reaction was addressed (Scheme 24). In order to achieve the formation of the six-membered lactone ring, first the carboxylic acid was converted into its acyl chloride, refluxing **B-9-amino-alk-PMI** in thionyl chloride for two hours. As soon as $SOCl_2$ was added, the color of the material changed from violet to dark red, due to the protonation of the amino group. After removal of the solvent, the solid was dissolved in anhydrous

THF and the solution was slowly added to a sodium hydride suspension in THF at 0 °C under argon atmosphere. NaH was chosen due to its non-nucleophilic character, able to deprotonate the amine group without attacking the acyl chloride derivative. Fivefold excess of base was used in order to neutralize residual traces of thionyl chloride. After each addition, the droplet initially red turned to violet and then immediately to yellow. These color changes could be assigned to the initial transition from ammonium salt to amine, followed by the deprotonation of the secondary amine, to finally form the quinoid derivative.
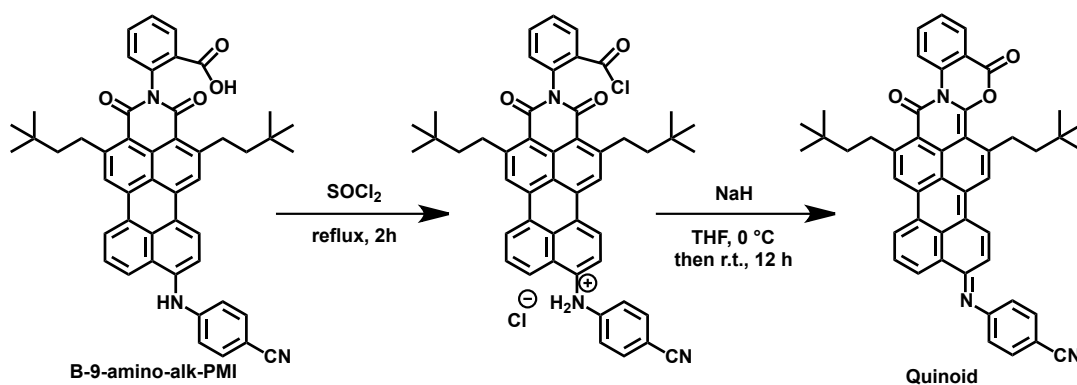
Scheme 24 Synthesis of the **Quinoid** derivative.

After destroying the excess of base by slowly adding methanol to the solution at 0 °C in air, an unexpected new color transition to the red was observed in concomitance with the formation of a precipitate. The red solid was isolated by filtration, washed with water and dried in vacuum before characterization.

Initially a determination of the mass was attempted via FD-MS, MALDI-TOF and high-resolution mass spectrometry, however in all cases no ionized species could be detected. Similarly, no clear ^{1}H-NMR spectrum could be measured. Several deuterated solvents were screened, such as THF, acetone, MeOH and TFA at room temperature and DMSO, DMF at 298 K. Even though the material was appearantly dissolved, no defined splitting pattern could be observed in the aromatic region, most probably due to strong intermolecular aggregation. The only distinguishable signals were two singlets at about 1 ppm, most probably deriving from the terminal methyl groups of the *ortho*-substituents. The strong tendency of the system to aggregate could be a consequence of the planarization of the system that could be assigned to the desired formation of the six-membered lactone ring.

Further investigations were performed by UV-visible absorption spectroscopy to confirm the formation of the desired lactonized quinoid system (Figure 25). Surprisingly the absorption of a THF solution of the material was located exclusively in the visible region between 400 nm and 600 nm, in disagreement with the formation of the target **Quinoid** molecule that shoul absorb in the NIR. However the features of the absorption spectra are also different from those of the push-pull precursor **B-9-amino-alk-PMI,** confirming the formation of a new species after the cyclization reaction.

To better understand the nature of the compound, two different THF solutions of **Quinoid** were prepared containing acetic acid and sodium hydride. Under acidic

conditions, no major change in the shape of the absorption spectra occurred. On the contrary, the solution containing sodium hydride showed a color change from orange to green. An increase in the absorption at 800 nm could be also recorded, comparable to the one observed after deprotonation of the push-pull system, featuring two maxima, one in the visible region and one in the NIR. However, similarly to the non-lactonized quinoidal structures, upon removal of the solvent or neutralization of the pH, the color shifted back to the red.
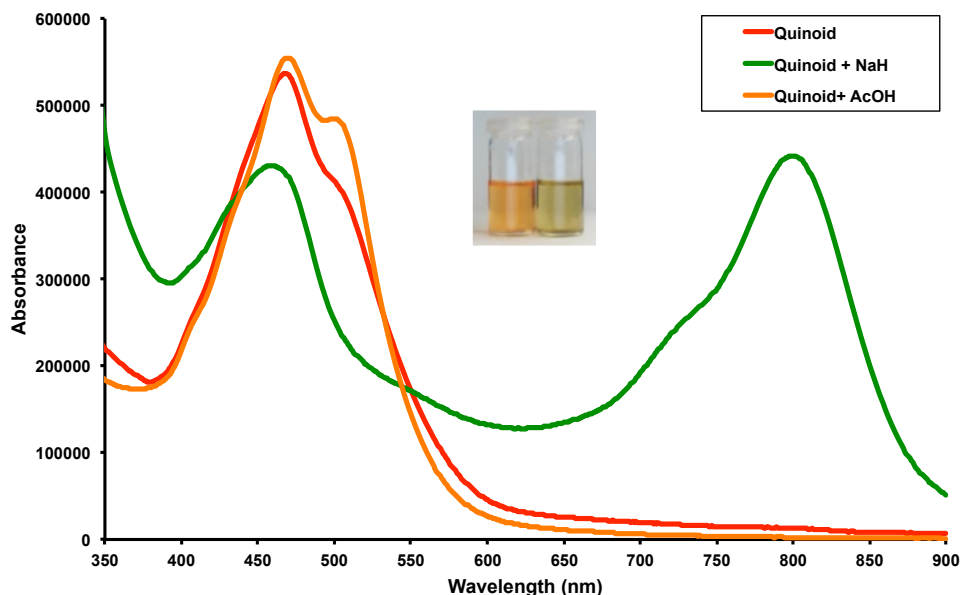
Figure 25 Absorption spectra of of the supposed **Quinoid** derivative in a neat THF solution and in presence of acid and base. In the image, the neutral and basic solution (left and right, respectively).

This unexpected behavior could be explained by assuming the successful cyclization reaction and at the same time a strong basicity of the imine of the **Quinoid** molecule, which coul lead to the formation of the protonated species at neutral pH.
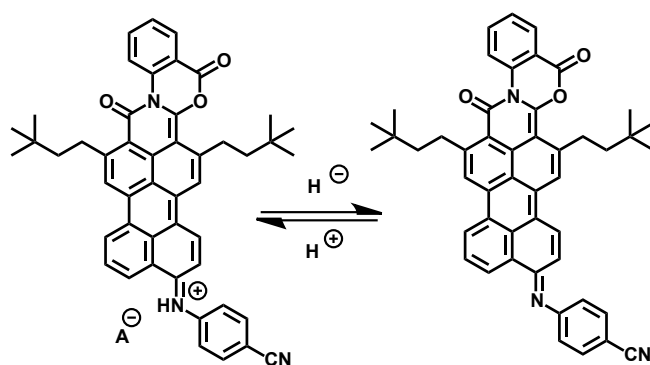
Scheme 25 Protonation of **Quinoid**.

This hypothesis would be further supported by the ATR-FTIR-spectrum of the compound (Figure 26). While the signals deriving from the formation of the lactone cannot be assigned unambiguously, due to the overlapping of several peaks, a distinctive signal can be observed at 2370 cm^{-1}, which may correspond to the presence of an iminium salt.

In the attempt to further confirm this hyphotesis, NMR spectra of the red material in presence of sodium hydride were measured in deuterated THF and acetone. Unfortunately also in this case only the signals deriving from the terminal methyl groups of the *ortho*-substituents could be observed, while only a broad and featureless peak was detected in the aromatic region.

To further strenghten the above described hypothesis, a final attempt was done. Considering the chemistry of lactones, by heating the material in presence of sodium hydroxide, the six-membered ring should be hydrolyzed, affording the push-pull molecule **B-9-amino-alk-PMI**. Therefore the red material was dissolved in methanol and sodium hydroxide added. The reaction was refluxed for several hours, however no change in the color occurred, even after several days. This behavior could be deriving from a very high stability of the planar quinoidal derivative, making the hydrolysis extremely difficult.
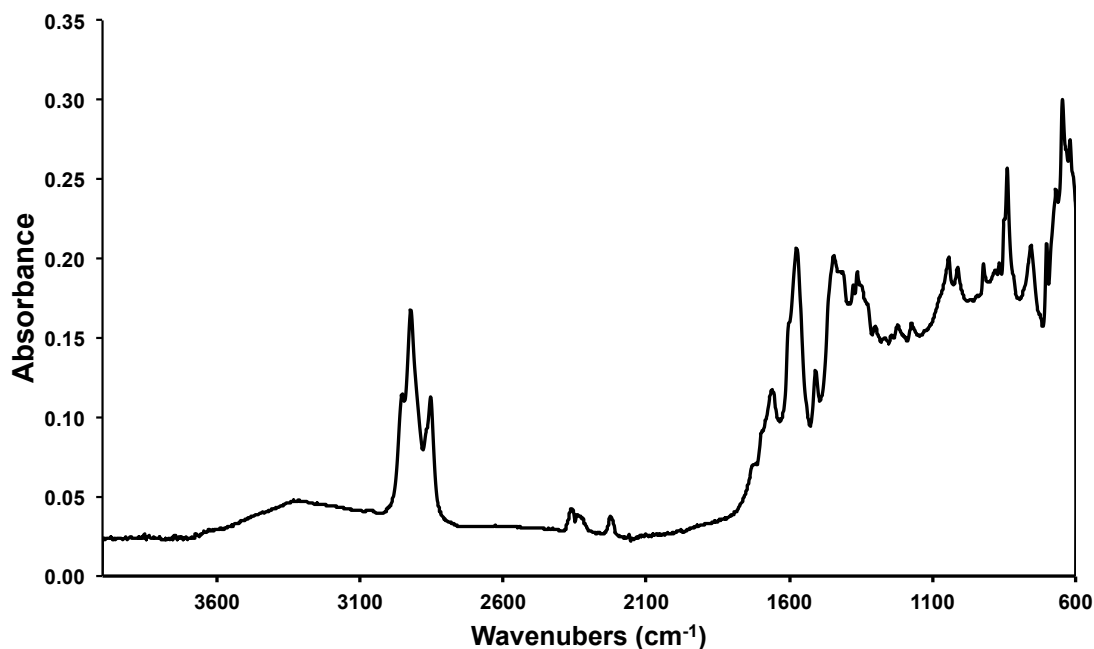
Figure 26 ATR-FTIR spectrum of **Quinoid**.

4.3 Conclusions and Outlook

In this chapter an interesting strategy for the creation of a stable quinoidized perylenemonoimide was explored. The seven-step synthesis of the push-pull molecule **B-9-amino-alk-PMI**, precursor of the quinoidized PMI, was accomplished and in the process, a more cost effective procedure for the up-scaling of the saponification of **DiPP-PMI** was developed. Furthermore, saponification of **C2SW-alk-PMI** was achieved, demonstrating for the first time the applicability of such reaction to *ortho*-alkylated ryleneimides.

The possibility to induce quinoidization of **B-9-amino-alk-PMI** was demonstrated via UV-visible spectroscopy and ¹H-NMR, and the lactone formation reaction afforded a

new material. The change in color and reduced solubility could be interpreted as signs of successful ring formation. However, the isolated compound may be the protonated form of the target **Quinoid** molecule. This fact could explain the optical behavior of the compound that in neutral solution absorbs exclusively in the visible region, while, after addition of base, the maximum is shifted to the NIR-region (800 nm), as observed for the other quinoidal derivatives of PMI. Quaternarization of the nitrogen at the imine group could also be expected considering the basic character of the imine group and ATR-FTIR-spectroscopy could support this hyphothesis. However a clear structural evidence could not be obtained.

In this chapter the alkylation of the *ortho*-positions was chosen as solubilizing strategy due to its minimum impact on the geometrical and optical properties of the system. Indeed the presence of the *ortho*-alkyl chains did not influence substantially the molecular features and guaranteed solubility throughout the multistep synthesis, even after the supposed formation of the lactone. However, the 3,3-dimethyl-butyl substituents could not completely prevent aggregation. Therefore for future investigations, groups with better solubilizing ability should be considered, for example bearing bulkier terminal substituents. An alternative could also be the introduction of α-branched alkyl chains via the use of internal double bonds in the Murai coupling.

The investigation here reported could not provide a clear proof of the applicability of the lactonization strategy to achieve stable quinoidal rylene derivatives. Nevertheless this approach remains extremely promising and should be further studied. In particular, besides the creation of a more soluble system, interesting alternative dyes could be achieved via the replacement of the imine with a less basic functional group, such as a ketone, to give a quinoid (Figure 27, left). Further, following the work recently reported by ▮▮▮▮▮▮[72] about the introduction of two donors at the *peri*-positions of PMI, a double lactonization could be considered, to obtain a fully quinoidized molecule (Figure 27, right).
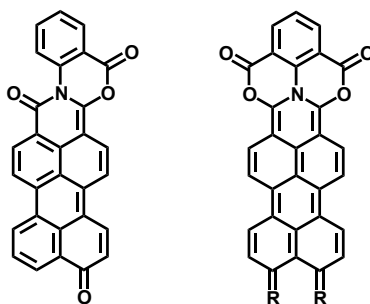
Figure 27 Alternative quinoidal PMI derivatives that could be achieved via the lactonization strategy.

4.4 References

[64] a) Daehne, S., Resch-Genger, U., & Wolfbeis, O. S. (1998). *Near-infrared dyes for high technology applications* (Vol. 52). Kluwer Academic Pub. b) Fabian, J., Nakazumi, H., & Matsuoka, M. (1992). *Chemical reviews*, *92*(6), 1197-1226. c) Luo, S., Zhang, E., Su, Y., Cheng, T., & Shi, C. (2011). *Biomaterials*, *32*(29), 7127-7138. d) Qian, G., & Wang, Z. Y. (2010). *Chemistry, an Asian journal*, *5*(5), 1006–1029.

[65] a) Avlasevich, Y., Li, C., & Müllen, K. (2010). *Journal of Materials Chemistry*, *20*(19), 3814-3826. b) Herrmann, A., & Mullen, K. (2006). *Chemistry Letters*, *35*(9), 978-985. c) Yao, J. H., Chi, C., Wu, J., & Loh, K. P. (2009). *Chemistry-a European Journal*, *15*(37), 9299-9302. d) Liu, Z., Li, C., Wagner, M., Avlasevich, Y., Herrmann, A., & Müllen, K. (2008). *Synfacts*, *2009*(01), 0040-0040.

[66] a) Pschirer, N. G., Kohl, C., Nolde, F., Qu, J., & Müllen, K. (2006). *Angewandte Chemie International Edition*, *45*(9), 1401-1404. b) Avlasevich, Y., & Müllen, K. (2007). *The Journal of Organic Chemistry*, *72*(26), 10243-10246.

[67] Qu, J., Pschirer, N. G., Koenemann, M., Muellen, K., & Avlasevic, Y. (2011). *U.S. Patent No. 8,052,899*. Washington, DC: U.S. Patent and Trademark Office.

[68] Li, C. (2008), Ph. D. Thesis, Johannes Gutenberg University (Mainz).

[69] Li, C., Schöneboom, J., Liu, Z., Pschirer, N. G., Erk, P., Herrmann, A., & Müllen, K. (2009). *Chemistry – A European Journal*, *15*(4), 878–884.

[70] Quante, H. (1994), Ph. D. Thesis, Johannes Gutenberg University (Mainz)

[71] Liu, Z., Li, C., Wagner, M., Avlasevich, Y., Herrmann, A., & Müllen, K. (2008). *Chemical communications (Cambridge, England)*, (40), 5028–5030.

[72] Zagranyarski, Y., Chen, L., Zhao, Y., Wonneberger, H., Li, C., & Müllen, K. (2012), *Organic letters*, *14*(21), 5444-5447.

5 *Ortho*-Alkylation of Perylenediimides for the Synthesis of Water-Soluble Fluorescent Probes

5.1 Introduction[c]

The possibility to distinguish individual phenomena from ensemble averages has made of single molecule spectroscopy (SMS)[73] a very popular and powerful method for the study of biological processes[74]. In order to monitor the desired information, a key role is played by the fluorescent probes, which are normally organic compounds. Such molecules should ideally possess high molar absorption coefficients, fluorescence quantum yields close to unity, and good photostability; requirements that are usually fulfilled by perylenediimides (PDIs) in common organic solvents.[75] Unfortunately, in polar environments, e.g. water, PDI dyes tend to strongly aggregate due to their relatively large conjugated core. Direct consequence is the loss of their desirable optical features, i.e. good fluorescence. For this reason the development of successful strategies to confer water-solubility and preserve their high fluorescence quantum yields in aqueous solution is of fundamental importance.
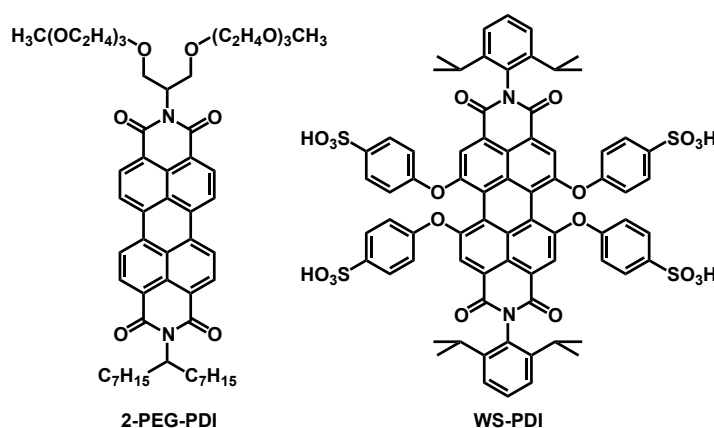
Figure 28 Chemical structure of **2-PEG-PDI** and **WS-PDI**.

Fluorescent probes for biological applications can be successfully synthesized via the introduction of hydrophilic moieties. As already mentioned in the introduction, there are

two approaches that are mainly investigated. The first relies on the introduction of suitable water-solubilizing substituents on the imidic nitrogens. Promising results were achieved via functionalization with polyacrylates or alpha-branched glycol chains, as in the case of **2-PEG-PDI** (Figure 28)[76]. Ultrahigh quantum yields could be obtained, but the absence of sites available for bioconjugation limits their use in biological applications. [77]

The second strategy is based on the functionalization of the *bay*-region (1,6,7,12-positions) of the perylene core. Among *bay*-functionalized PDIs, a special role is occupied by derivatives of **WS-PDI** (Figure 28), a tetra-phenoxy substituted derivative carrying four sulfonic acid moieties, which was synthesized and widely investigated in our group.[78] With its superior photostability, good water-solubility and the possibility to introduce anchors at the N-imide positions, these *bay*-functionalized water-soluble PDIs can be bioconjugated and outperform most of the commercially available chromophores in the bioimaging fields[79]. Unfortunately, absorptivities and emissions in water are much lower as compared to those of PDIs in organic solvents.

The introduction of alkyl substituents in the *ortho*-positions of ryleneimides may represent an alternative strategy to imide and *bay*-functionalization to achieve water-solubility. As already demonstrated in the previous chapter, *ortho*-alkylation of PDIs successfully reduces aggregation, while preserving the attractive electro-optical properties of the unsubstituted dye.[80] Hence, the functionalization of the 2,5,8,11-positions of PDIs with an olefin conferring water-solubility could lead to the synthesis of fluorescent probes for bioimaging applications. Unfortunately, one of the major drawbacks of the Murai-alkylation is the limited number of alkenes that can be used. The reason is to find in the ruthenium complex reactivity.[81] Nevertheless an extensive study about the groups not tolerated in the reaction is still missing, leaving open the possibility to find a suitable double bond able to undergo the reaction and afford the desired hydrophilic fluorescent probe. This is what will be explored in this chapter.

5.2 Synthesis of a Fluorescent Probe via Murai Type Alkylation

To develop a competitive functionalization method, a cheap and commercially available olefin should be used. This alkene should react in high yields with perylendiimides and readily provide effective water-solubilizing groups. An additional requisite is the absence, or alternatively a limited number, of allylic hydrogens to avoid undesired parasitic isomerisation reactions, which are usually lowering the yields of the alkylation procedure.[82]

After a screening the commercially available products, a few suitable olefins were selected (see Scheme 26). None of these materials was known in the literature to undergo Murai alkylation. Among the investigated systems were alkenes bearing epoxydes, glycol groups,

amine, hydroxide, sulfonates, acetals and phosphonates. Acrylates were excluded since the ruthenium complex would catalyze a polymerization reaction.[83]
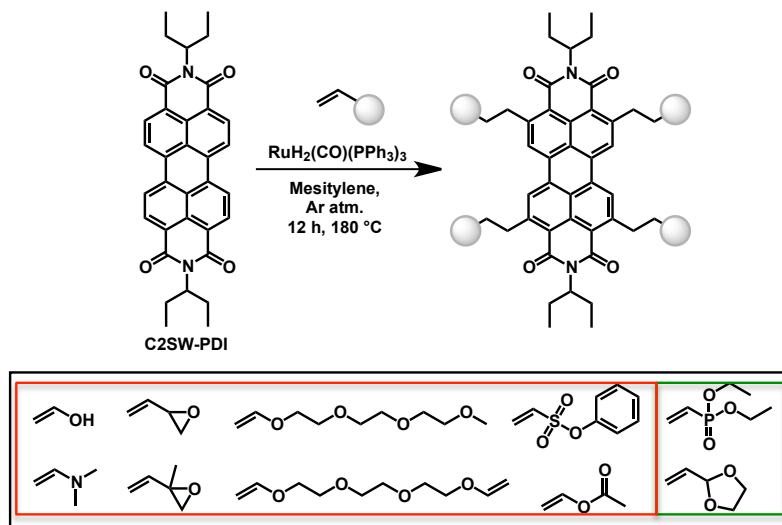
Scheme 26 Screening of commercially available olefins, which may confer aqueous solubility, reported in the box at the bottom. In green are highlighted the olefins undergoing Murai alkylation.

Standard alkylation conditions were used for all the selected olefins to test the applicability of the reaction. All the reactions were monitored via FD-MS and TLC analysis. Among the olefins selected, only two underwent Murai alkylation: acrolein and diethyl vinylphosphonate. The FD-MS spectra of the two reaction mixtures are reported in Figure 29.

As it can be seen from the FD-MS spectra, acrolein underwent the reaction, but a mixture of the starting material, as well as the mono-, di-, tri- and tetra-substituted derivatives was obtained. This result was confirmed by TLC. Vinylphosphonate gave instead more promising results. After reaction TLC and FD-MS showed exclusively the presence of the tetrasubstituted product.

Due to the better yields of the reactions obtained using diethyl vinylphosphonate and the apparently quantitative formation of the desired product, the further work focused exclusively on the synthesis of tetraphohphonate-PDI and its conversion into a water-soluble fluorescent probe. For this scope phosphonic acids, easily obtained via hydrolysis of the phosphonate precursor are quite promising candidates.[84] Such functional groups are capable of carrying two negative charges at some biologically relevant pH values, giving the possibility to obtain water-soluble labels with enhanced resistance to aggregation and fluorescence quenching.[85]

```
File:ACETAL Ident:1_12 SMO(1,7) Acq:25-OCT-2010 18:16:49 +3:42 Cal:FD_100-4000
ZAB-SEFPD FD+ Magnet BpI:9019914 TIC:6987657728
File Text:batt
```

C2SW-PDI — 531.7

Monoalkylated-PDI — 631.6

Bisalkylated-PDI — 732.0

Trialkylated-PDI — 831.8

Tetraalkylated-PDI — 932.8

279.1

1147.3

```
File:PHOSPHONATE Ident:1_11 SMO(1,7) Acq:12-AUG-2010 13:01:18 +3:25 Cal:FD_100-4000
ZAB-SEFPD FD+ Magnet BpI:15831357 TIC:4822320640
File Text:batt
```

Tetralkylated-PDI — 1189.4

Dimer of the tetralkylated-PDI — 2375.9

Dication of the tetralkylated-PDI — 595.7

Trimer of the tetralkylated-PDI — 3557.4

Figure 29. FD-MS spectra of the ruthenium-catalyzed alkylation reaction of **C2SW-PDI** with acrolein (top) and diethyl vinylphosphonate (bottom). While the spectrum above shows the different degree of substitution on the PDI core, the tetraphosphonate is the only derivative observed.

The alkylation reaction using diethyl vinylphosphonate and **C2SW-PDI** was repeated using 500 mg of the perylenediimide derivative. Once again, after 12 hours TLC and FD-MS analysis showed exclusively the presence of the desired compound **C2SW-4PO(OEt)$_2$-PDI**. After removing the solvent the desired compound was obtained in 95 % yield via simple precipitation from methanol in water.
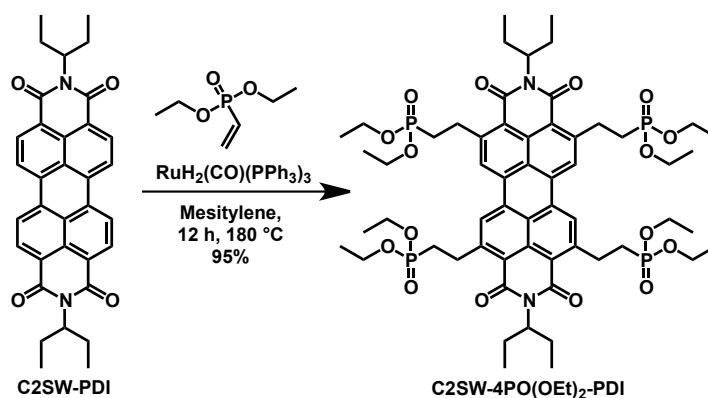
Scheme 27 Synthesis of C2SW-4PO(OEt)₂-PDI.

C2SW-4PO(OEt)₂ appears as a dark red waxy solid. The introduction of four phosphonates makes the PDI derivative extremely soluble (more than 25 mg/mL) in practically all organic solvents, ranging from pentane to methanol. Unfortunately the desired solubility in water was not observed.

The ^{1}H-NMR spectrum of C2SW-4PO(OEt)₂ in CD₂Cl₂ is shown in Figure 30. The high symmetry of the system is reflected in the only singlet in the aromatic region. As for C2SW-alk-PDI, splitting of the signals of the b-protons occurs.
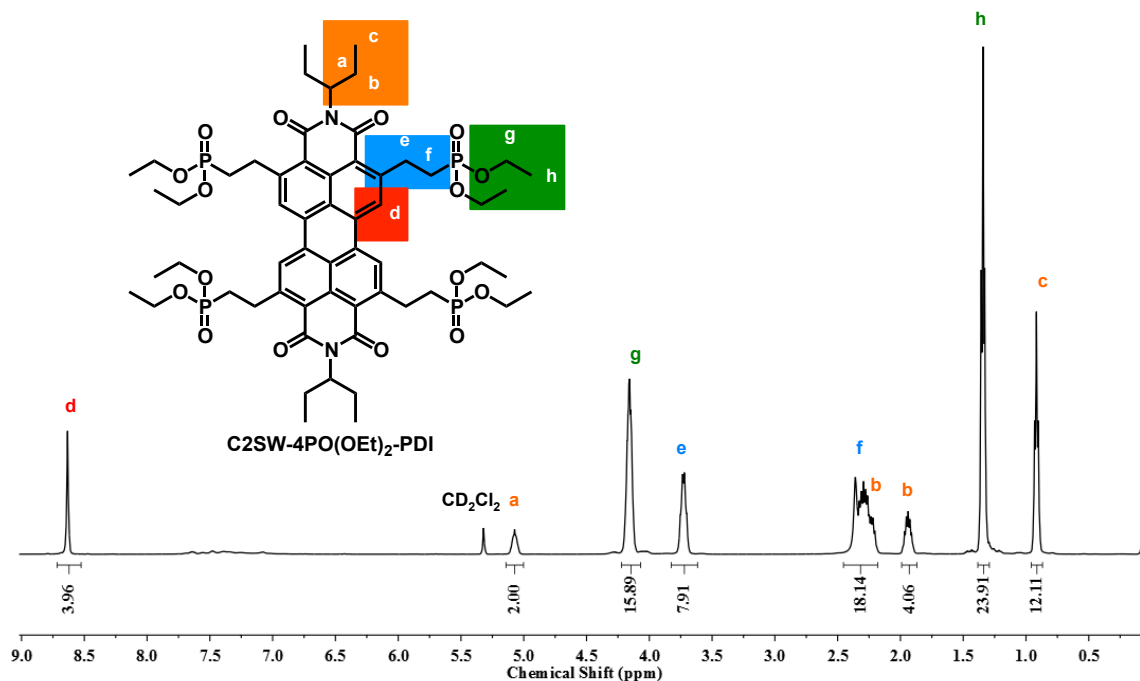
Figure 30 ^{1}H-NMR in CD₂Cl₂ of C2SW-4PO(OEt)₂-PDI.

C2SW-4PO(OEt)₂ was successively hydrolyzed to C2SW-4PO(OH)₂ via reaction with trimethylsilylbromide in dichloromethane, followed by treatment with methanol. This standard procedure afforded the desired tetraphosphonic acid in good yields. A substantial change in the solubility was observed. In contrast with C2SW-4PO(OEt)₂,

C2SW-4PO(OH)₂ appears to be soluble exclusively in water and DMSO. Solubility up to 5 mg/mL in water could be achieved, even though some time was needed for the complete dissolution of the material at higher concentrations. This was the first report about a water-soluble-PDI derivative obtained via *ortho*-alkylation reaction.
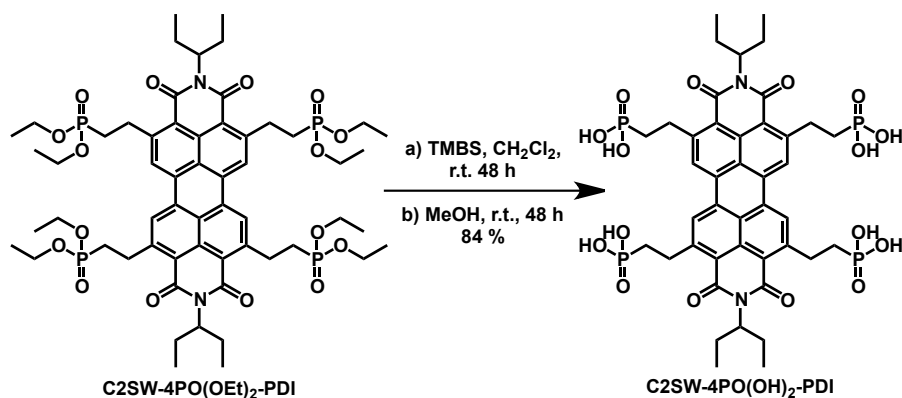
Scheme 28 Synthesis of **C2SW-4PO(OH)₂-PDI**.

The successful hydrolysis of the phophonate groups to phosphonic acids was confirmed by the ¹H-NMR spectrum of **C2SW-4PO(OH)₂** (Figure 31). While the splitting pattern of the common molecular skeleton remained substantially the same, the signals deriving from the ethoxy groups disappeared.
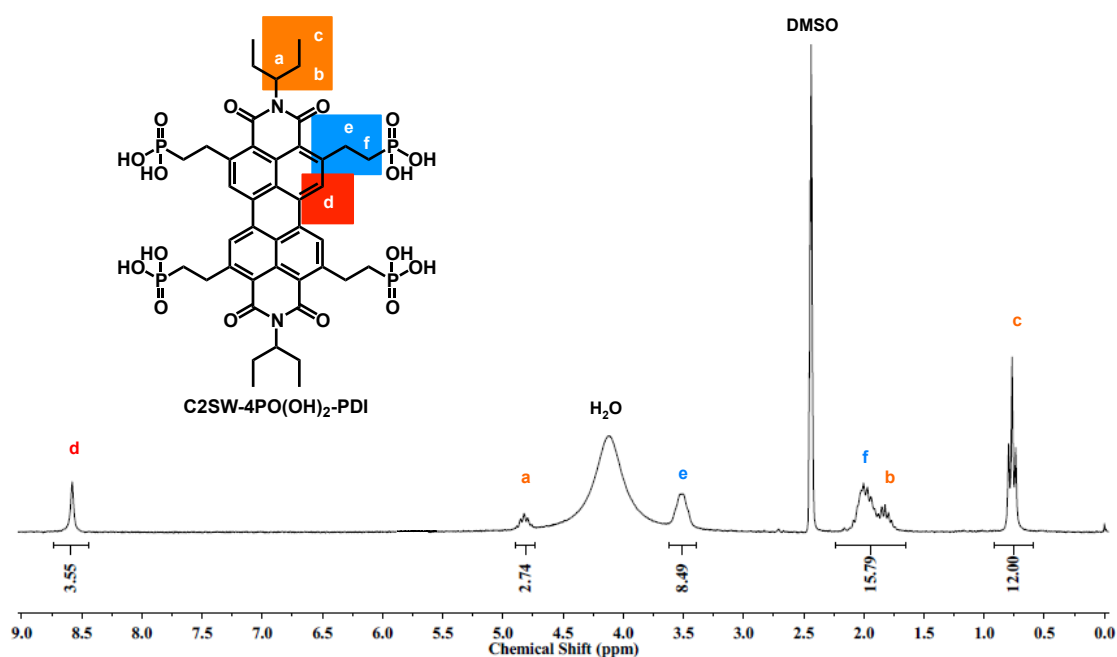
Figure 31 ¹H-NMR in DMSO of **C2SW-4PO(OEt)₂-PDI**.

Having achieved the desired water-solubility, the optical properties of **C2SW-4PO(OH)₂** in water were investigated. The measured values are summarized in Table 6, where for comparison also the results obtained for **C2SW-PDI** and the phosphonate precursor **C2SW-4PO(OEt)₂-PDI** in dichloromethane are reported.

Table 6 Optical properties in solution of **C2SW-4PO(OEt)₂-PDI**, **C2SW-4PO(OH)₂-PDI** and **C2SW-PDI** as comparison.

Molecule	λ_{max} [nm]	ε [M⁻¹cm⁻¹][c]	λ_{em} [nm][d]	$\Phi_f (\lambda_{ex})$[e]
C2SW-PDI[a]	526	8.43 X 10⁴	538	0.99 (526)
C2SW-4PO(OEt)₂-PDI[a]	524	5.70 X 10⁴	532	0.88 (524)
C2SW-4PO(OH)₂-PDI[b]	531	5.45 X 10⁴	548	0.76 (535)

[a]Measured in dichloromethane. [b]Measured in water. [c]Calculated at λ_{max} [d] Excited at λ_{max} [e]Measured using Rhodamine 6G as standard.

It is possible to notice the marginal effect of the *ortho*-alkylation on the optical properties of the system as compared to the parent unsubstituted compound. While the major features are preserved (Figure 32), only a minor bathochromic shift in the absorption (5 nm) and emission maxima (10 nm) occurs. But more importantly for the application as fluorescent probe, the absorption coefficient and fluorescence quantum yield remain as high as 54000 M⁻¹cm⁻¹ and 0.77 respectively. Such properties make this dye an ideal candidate for investigation in single molecule spectroscopy and biolabeling experiments.
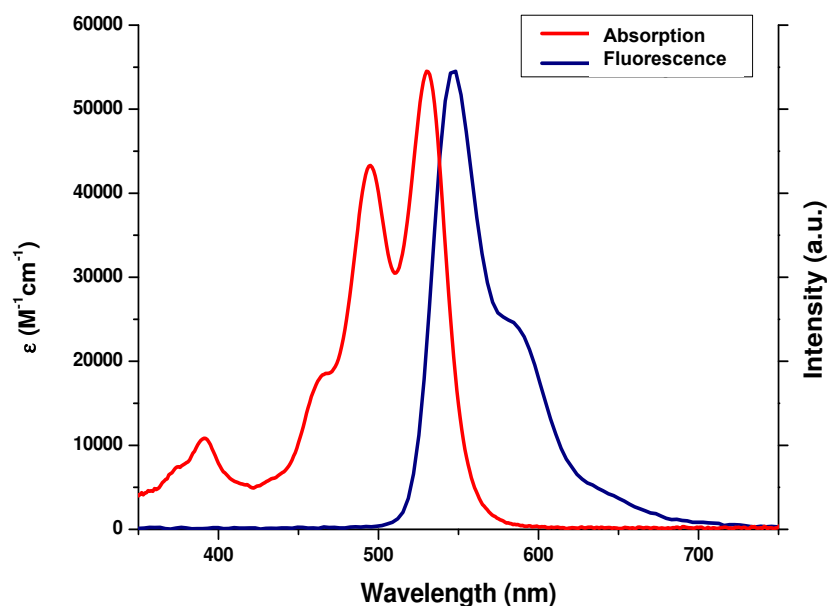
Figure 32 Absorption and fluorescence spectra (red and blue respectively) of **C2SW-4PO(OH)₂-PDI in** water (λ_{ex} = 531 nm).

5.3 Single Molecule Spectroscopy and Bioimaging

The single molecule spectroscopy and bioimaging experiments were performed by ███████████ in the group of ████████████ at the ████████████ ████████████████ of ██████████████ .

To investigate the photostability of **C2SW-4PO(OH)$_2$-PDI**, the dye was dissolved in a highly diluted solution of polyvinyl alcohol (PVA). Thin polymer films (thickness 100-200 nm) were spin-coated onto a substrate in polymer solutions at a concentration of 10-10 mol/L (1 min at 3000 rpm, 2 wt %/wt PVA in water). In this way the molecules were separately immobilized, so that on average only one molecule was in the confocal spot of the laser beam. For direct comparison the photostability of **2-PEG-PDI** was also investigated as a reference. All dyes were excited with a Nd-YAG laser (532 nm). By scanning the laser beam across the sample, single molecules were detected by their fluorescence. The number of totally emitted photons (TEP, area under the function as integral over time corrected by detection efficiency of the setup; see Experimental Section) and the survival time (ST, time to the irreversible photobleaching) could then be extracted. These two parameters are representative for the fluorescence capability and the photostability of a fluorescent dye.

In the single molecule studies the fluorescence intensity trajectories of at least 30 single molecules for each dye were observed. Molski developed a formalism to calculate the TEP and ST from the resulting distributions and showed that they are well approximated by either mono- or multiexponential distributions.[86] A mono- or biexponential function was successfully fitted to the data. The corresponding averaged TEP and ST for the dyes embedded in PVA together with some data from the literature are summarized in Table 7. It should be mentioned that the photobleaching mechanisms and the multiexponential decays are not fully understood on a molecular level so far.[87] However, mulitexponential decays typically are observed when more than one mechanism is present.

Table 7 Averaged TEP and ST parameters of the different dyes in spin-coated PVA.

Molecule	TEP in PVA	ST [s] in PVA
WS-PDI[a]	$(7.8 \pm 0.4) \times 10^6$	14.7 ± 0.3
2-PEG-PDI	$(4.3 \pm 0.8) \times 10^6$	3.8 ± 0.2
C2SW-4PO(OH)$_2$-PDI	$(8.3 \pm 0.5) \times 10^4$	2.7 ± 0.8
[a] Data taken from Reference 87		

The average TEP for **C2SW-4PO(OH)$_2$-PDI** in PVA was calculated to be $(0.83 \pm 0.05) \times 10^5$, and the average ST gives 2.7 ± 0.8 s. These results could be directly compared with **2-PEG-PDI**, which was studied under the same experimental conditions and **WS-PDI** (data taken from Reference 87). The comparison of TEP and ST of the three PDI derivatives show that **C2SW-4PO(OH)$_2$** has a approximately 100 times lower TEP but its ST is similar to that of **2-PEG-PDI**. For single molecule experiments the TEP value is more important, since it counts the number of emitted photons whereas ST includes breaks due to blinking. The blinking activity is higher for charged dyes than for uncharged dyes. This explains the fact that **C2SW-4PO(OH)$_2$** has a similar ST to **2-**

PEG-PDI although its TEP value is much lower. In summary, the data show that the phosphonic acid functionalized PDI is a worse fluorescent dye than the other investigated probes regarding the number of totally emitted photons.

Due to the good water-solubility of **C2SW-4PO(OH)₂-PDI**, the potential to use the dye for labeling HeLa cells was investigated. [88] After 4 h of incubation with a dye concentration of 2 μM, **C2SW-4PO(OH)₂-PDI** was taken up by the cells and was present in the cytosol, presumably in endosomes (Figure 33, green). An increased fluorescence intensity around the perinuclear region (Figure 33, green) could be observed as well as the lack of green fluorescence in the cell membrane. For imaging of the cell membrane, the cells were labelled with Deep Red (Figure 33, red). The corresponding transmission image is depicted in Figure 33b. The cells seem to be healthy according to their morphology, successfully proving the possibility to use **C2SW-4PO(OH)₂-PDI** as fluorescent probe.
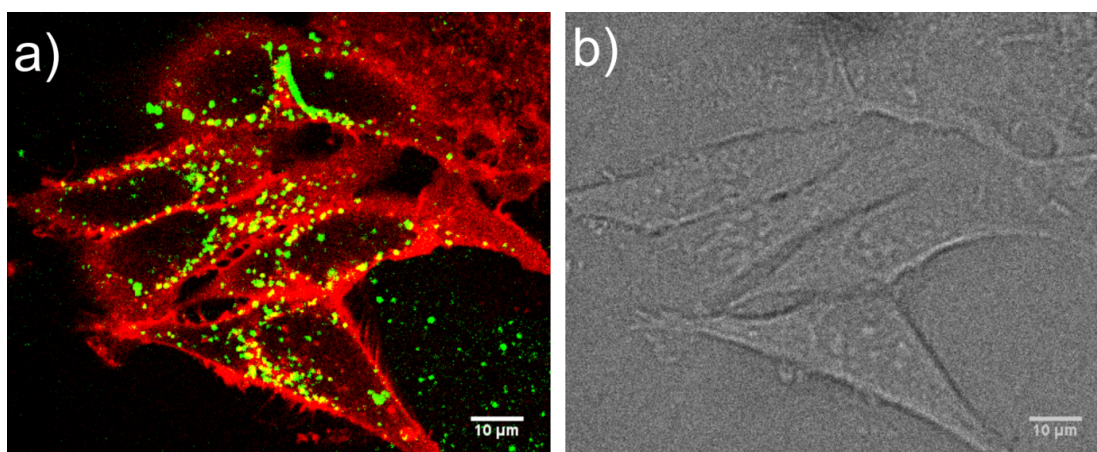
Figure 33 a) Confocal fluorescence image of HeLa cells excited with 488nm and 639nm laser light. The cell membrane was labelled with Deep Red (red). Uptake of **C2SW-4PO(OH)₂** (green) by the HeLa cells is clearly visible as well as an increased dye concentration around the perinuclear region. b) Transmission image of the Hela cells after laser excitation.

5.4 Conclusion and Outlook

In this chapter the synthesis of the first *ortho*-alkylated water-soluble PDI was reported. The new fluorescent probe was developed with an efficient two-step synthetic protocol, affording the target molecule in excellent yields. The extinction coefficient and quantum yield of **C2SW-4PO(OH)₂-PDI** are much higher than of most commonly used PDI derivatives for bioapplications. This result confirms the high potential that *ortho*-alkylation has for improving solubility and processability of ryleneimide dyes, without affecting their attractive electro-optical properties. Therefore this solubilizing strategy can be considered as a valid alternative to the established methods based on imide and *bay*-functionalization.

The fluorescence capability and the photostability of **C2SW-4PO(OH)$_2$-PDI** were investigated by TEP and ST experiments. Lower lifetimes were observed as compared to other standard water-soluble fluorescent probes, but the decreased stability may be attributed to the presence of ionic substituents and not necessarily to the functionalization pattern. HeLa cells were successfully impregnated with a solution containing **C2SW-4PO(OH)$_2$-PDI**, proving the suitability of the dye as fluorescent probe for application in bioimaging.

The synthetic protocol here presented describes the use of phosphonate derivatives in a Murai type alkylation reaction. No previous report was known in the literature about this functionalization and this work provides an additional candidate to the limited number of olefins undergoing the reaction. Considering that phosphonic acids find application not only in biorelated applications, but also in fields such as surface chemistry and fuel cells, this new synthetic protocol may provide an additional instrument for the development of innovative materials.

Despite the successful discovery of the new functionalization, the screening of the different olefins highlighted the limitations of the Murai alkylation method for the modification of the *ortho*-positions of RIs. In the next chapter, a new approach able to overcome such limitations will be described.

5.5 References

[73] a) Plakhotnik, T., Donley, E. A., & Wild, U. P. (1997), *Annual review of physical chemistry*, *48*(1), 181-212. b) Moerner, W. E. (2002), *The Journal of Physical Chemistry B*, *106*(5), 910-927. c) Barkai, E., Jung, Y., & Silbey, R. (2004), *Annu. Rev. Phys. Chem.*, *55*, 457-507.

[74] Weiss, S. (1999), *Science*, *283*(5408), 1676-1683.

[75] Weil, T., Vosch, T., Hofkens, J., Peneva, K., & Müllen, K. (2010), *Angewandte Chemie International Edition*, *49*(48), 9068–9093.

[76] a) Gao, B., Li, H., Liu, H., Zhang, L., Bai, Q., & Ba, X. (2011), *Chemical Communications*, *47*(13), 3894-3896. b) Davies, M., Jung, C., Wallis, P., Schnitzler, T., Li, C., Müllen, K., & Bräuchle, C. (2011), *ChemPhysChem*, *12*(8), 1588-1595.

[77] Heek, T., Fasting, C., Rest, C., Zhang, X., Würthner, F., & Haag, R. (2010), *Chemical Communications*, *46*(11), 1884-1886.

[78] a) Qu, J., Kohl, C., Pottek, M., & Müllen, K. (2004), *Angewandte Chemie*, *116*(12), 1554-1557. b) T. Cordes, J. Vogelsang, M. Anaya, C. Spagnuolo, A. Gietl, W. Summerer, A. Herrmann, K. Müllen, P. Tinnefeld, (2010), *Journal of the American Chemical Society*, *132*(7), 2404-2409.

[79] Peneva, K., Mihov, G., Nolde, F., Rocha, S., Hotta, J. I., Braeckmans, K., J. Hofkens, H. Uji-i, A. Herrmann, & Müllen, K. (2008), *Angewandte Chemie*, *120*(18), 3420-3423.

[80] a) Nakazono, S., Imazaki, Y., Yoo, H., Yang, J., Sasamori, T., Tokitoh, N., ... & Osuka, A. (2009). *Chemistry–A European Journal*, *15*(31), 7530-7533. b) Bullock, J. E., Vagnini, M. T., Ramanan, C., Co, D. T., Wilson, T. M., Dicke, J. W., Marks, T.J. & Wasielewski, M. R. (2010). *The Journal of Physical Chemistry B*, *114*(5), 1794-1802.

[81] Murai, S., Kakiuchi, F., Sekine, S., Tanaka, Y., Kamatani, A., Sonoda, M., & Chatani, N. (1994), 66(7), 1527-1534.

[82] Kakiuchi, F., & Chatani, N. (2003). *Advanced Synthesis & Catalysis*, 345(9‐10), 1077-1101.

[83] Kakiuchi, F., & Murai, S. (1999). Activation of CH bonds: catalytic reactions. In *Activation of Unreactive Bonds and Organic Synthesis* (pp. 47-79). Springer Berlin Heidelberg.

[84] McKenna, C. E., & Schmidhuser, J. (1979). *Journal of the Chemical Society, Chemical Communications*, (17), 739-739.

[85] a) Borbas, K. E., Mroz, P., Hamblin, M. R., & Lindsey, J. S. (2006), *Bioconjugate chemistry*, *17*(3), 638-653. b) Reddington, M. V. (2007), *Bioconjugate Chemistry*, *18*(6), 2178-2190.

[86] Molski, A. (2001), *The Journal of Chemical Physics*, *114*, 1142.

[87] Jung, C., Müller, B. K., Lamb, D. C., Nolde, F., Müllen, K., & Bräuchle, C. (2006), *Journal of the American Chemical Society*, *128*(15), 5283-5291.

[88] Jung, C., Ruthardt, N., Lewis, R., Michaelis, J., Sodeik, B., Nolde, F., Peneva, K., Müllen, K., & Bräuchle, C. (2009), *ChemPhysChem*, *10*(1), 180-190.

6 Creating a Versatile Building Block for the *Ortho*-Position Chemistry

6.1 Introduction[d]

The pioneering work about the alkylation and arylation of the 2,5,8,11-positions of perylenediimides showed the possibility to selectively address the *ortho*-positions via metal-catalyzed reaction.[89] However, these synthetic protocols are rather limited synthetic instruments for the functionalization of ryleneimides. Several factors are affecting these methods, as already mentioned in the previous chapters. For both functionalization methods the number of terminal alkenes and aryl boronates, which can be used remains limited, as also proved by the restricted number of reports in the literature. Olefins with allylic hydrogens undergo rapid isomerization affording lower reaction yields,[90] while the arylation procedure works in high yields with aryl neopentylglycol boronates, but not as efficiently with different boronates.[91] Additionally boronates of aromatic heterocycles do not undergo the reaction.

Further limitations are due to the reactivity of the ruthenium complex. In fact the Murai catalyst is involved in several other catalytic reactions, such as the rearrangment of oximes into amides, the conversion of nitroarenes into tertiary amines,[92] transfer hydrogenation processes[93] and many others;[94] thus a considerable number of functional groups, such as for example the already cited nitroarenes, internal triple bonds, alcohols and enones must be avoided to prevent side reactions. Additionally only the possibility to form C-C bonds was demonstrated, limiting the number of materials which could be developed.
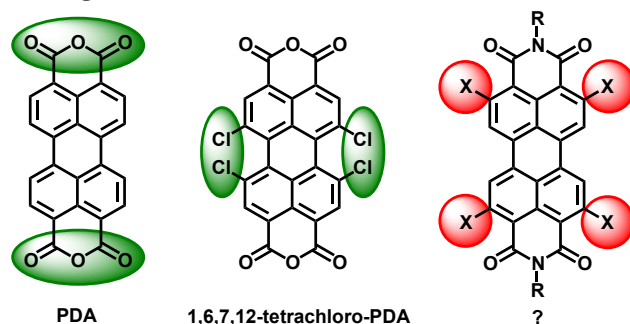
Figure 34 The building blocks in the perylenediimide chemistry.

This shows clearly the need for an alternative strategy that may provide more flexibility. If the chemistry of the *ortho*-positions is compared to the established imide and *bay-*

functionalizations, one major difference can be noticed: the absence of a building block (Figure 34). The perylenedianhydride for example provides a universal platform for the introduction of various substituents on the imide via a simple imidization reaction.[95] The 1,6,7,12-tetrachloro perylenedianhydride gives access to a large number of possible *bay*-functionalizationss via nucleophilic substitution or metal-catalyzed coupling reactions.[96] But an analogue general building block for the 2,5,8,11-positions of perylenediimides is still unknown.

In this chapter, the development of a synthetic route to obtain such a building block will be described. While the first part will focus exclusively on perylenediimides, other ryleneimides will be considered later on. Finally, the building block concept and its importance for the *ortho*-functionalization will be demonstrated through the introduction of various substituents, which cannot be obtained via other synthetic protocols.

6.2 *Ortho*-Borylation of Perylenediimides

An efficient building block for the chemistry of the *ortho*-positions should satisfy mainly two requisites: first, it should be synthesized in a straightforward manner and second, should bear on these molecular sites functional groups enabling the introduction of a broad range of substituents. Up to date, the *ortho*-positions of ryleneimides have been selectively addressed exclusively via metal-catalyzed reactions, as in the case of the Murai alkylation.[89] Consequently for the synthesis of the desired building block, the introduction of the functional groups should be assisted as well by a metal catalyst. Once this requirement is recognized, the choice of the functional group appears to be clear: a boronic ester. Over the last years, boronates have gained more and more importance. Their ability to be synthesized via several metal-catalyzed reactions has enabled the selective functionalization of positions inaccessible via the more classical halogenation reactions.[97] Additionally they can be replaced by other substituents using straightforward reactions, such as the Suzuki Miyaura cross coupling.[98] Furthermore, recent work from different research groups has shown the possibility to convert boronates into halogens, amines, ethers and many other functional groups in high yields.[97] This synthetic effort has been further supported by the constantly growing availability of boronates from commercial suppliers, owing also to their low toxicity.

Keeping in mind the former considerations, different synthetic protocols were considered. Unfortunately, at the time of these investigations, the routes reported in the literature for the *ortho*-borylation of aromatic carbonyls use alkanes as solvent for the reaction,[99] which are usually not suitable for ryleneimide derivatives. Therefore a completely new protocol for the borylation of the *ortho*-positions was required.

Among the catalysts known in literature to give the desired selectivity, $RuH_2(CO)(PPh_3)_3$ was chosen. The ruthenium complex is able to activate the *ortho*-positions of ryleneimides as already shown in the previous chapters and is known to react with boronic ester derivatives, for example in the arylation reaction applied also by the Shinokubo group

(Scheme 29).[100] In this reaction an aryl-boronate is typically mixed with an aromatic ketone in presence of the Murai catalyst to give an *ortho*-arylated ketone. But what would happen if the aryl-boronate is replaced with a bis-boronate derivative? Could this synthetic protocol lead to the missing building block for the *ortho*-functionalization of ryleneimides?
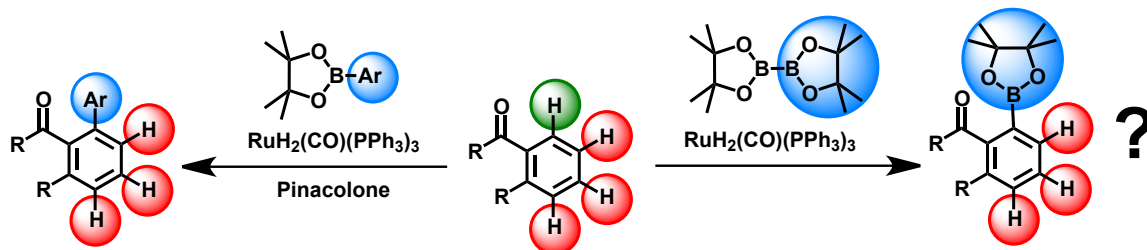
Scheme 29. Ruthenium-catalyzed reaction for the *ortho*-arylation of benzoate and possible modification of the reaction to achieve *ortho*-borylation.

A preliminary test reaction was performed using bis(pinacolato)diboron. **C2SW-PDI** was suspended in anhydrous mesitylene together with 4 equivalents of bis(pinacolato)diboron and the Murai catalyst (5 % molar, Scheme 30). The reaction was performed in a sealed tube under microwave heating for one hour in argon atmosphere. Right after the reaction a sample was extracted from the mixture to perform preliminary characterizations. The formation of new products was observed on TLC, while FD-MS analysis showed the presence of two new products with mass corresponding to the mono and bisborylated perylenediimides. Encouraged by this promising result, different reaction conditions were screened to synthesize the desired tetraboronate-derivative, varying concentration of the chemicals, solvent, amount of catalyst and reaction times.
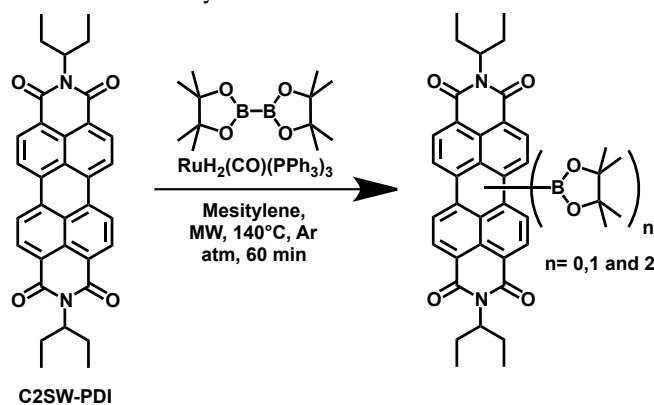
Scheme 30 Explorative borylation of **C2SW-PDI** using the Murai catalyst.

In the arylation of aromatic ketones the aliphatic ketone plays a fundamental role. In fact this species acts as a scavenger for the H-B species evolving from the reaction, regenerating the ruthenium catalyst and avoiding the undesired reduction of the keto group.[100] Considering the similarity of the borylation protocol with the *ortho*-arylation method, pinacolone was added to the mixture. This modification gave a major breakthrough. For the first time the formation of the tetraboronate derivative could be observed via FD-MS analysis. Due to the cheaper price and larger availability, acetone

was also screened as sacrificial ketone. Since equivalent results could be obtained, pinacolone was replaced.

Surprisingly, if the ketone was used as solvent for the reaction, the yields decreased, rather than improve. This is a major difference with the arylation protocol from which the new borylation reaction is inspired. Instead of the desired tetraboronate, a violet side product is obtained exclusively, not observed in absence of the ketone. According to the studies performed, the formation of such side product is not possible to be hindered, even using the optimized reaction conditions. Attempts to isolate the undesired species were unsuccessful. Most probably the reaction affords a series of side products, due to the presence of four reactive sites on each perylenediimide molecule.

The other major adjustments leading to the final optimized conditions were the use of 8 equivalents of bis(pinacolato) diboron and the increase of the amount of catalyst to 50 mol %. The exclusive formation of the desired tetraboronate and the disappearance of the lower substituted derivatives were observed in FD-MS analysis and confirmed by thin-layer chromatography. Unfortunately TLC also shows the persistent formation of the undesired violet side product, which was not detected in FD-MS or MALDI-TOF measurement. The undesired side reaction is most probably responsible for the low turnover numbers associated with the borylation using the Murai catalyst. In comparison, for the *ortho*-alkylation and arylation of perylenediimides respectively 6 mol % and 20 mol % of $RuH_2(CO)(PPh_3)_3$ are used.[89]
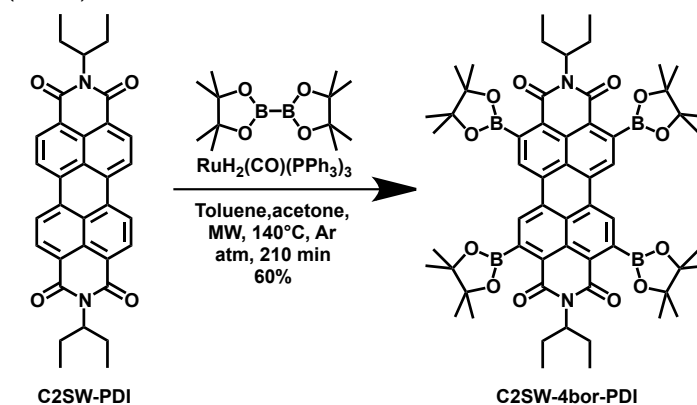
Scheme 31 Optimized conditions for the obtainment of **C2SW-4bor-PDI**

The final optimized conditions for the borylation reaction are shown in Scheme 31. Mesitylene was initially used as solvent for the reaction, but was replaced with toluene in order to reduce costs and facilitate the removal after reaction via simple rotary evaporation. The best results were achieved using 10 mL of toluene and 0.8 mL of acetone for 500 mg of **C2SW-PDI**, performing the reaction in a sealed vial using microwave heating. In this way the reaction was completed after 210 minutes at 140 °C. Longer reaction times did not improve the yields. Increased reaction temperatures favored side reactions, while lower temperatures were not sufficient to activate the reaction. The role of the reaction pressure, monitored via the microwave oven sensor, is not clear: after an increase to 3 bar in the initial minutes, then dropped to 1 bar.

The reaction was also tested in a round bottom flask, using a condenser and the higher boiling mesitylene and pinacolone. Under these conditions the desired product could also be obtained, but longer times were needed (about 17 hours) and lower substituted derivatives were still present in the reaction mixture, decreasing yields and making purification more difficult. The use of sealed pressure vials afforded better results, even though the reaction times remained of about 16 hours. It is not clear though whether the reaction is favored by an increased pressure or simply by the fact that the lower boiling aliphatic ketone does not evaporate from the reaction.

Due to the strong interaction of the boronate groups with silica and alumina, an alternative purification method to column chromatography was applied to obtain the compound without major losses. **C2SW-4bor-PDI** could be isolated from the reaction mixture after removal of the solvent, addition of methanol and filtration. In the methanol solution only the violet side products could be found. Successive reprecipitations from dichloromethane in methanol afforded the tetraboronate perylenediimide with analytical purity (60 % yield).
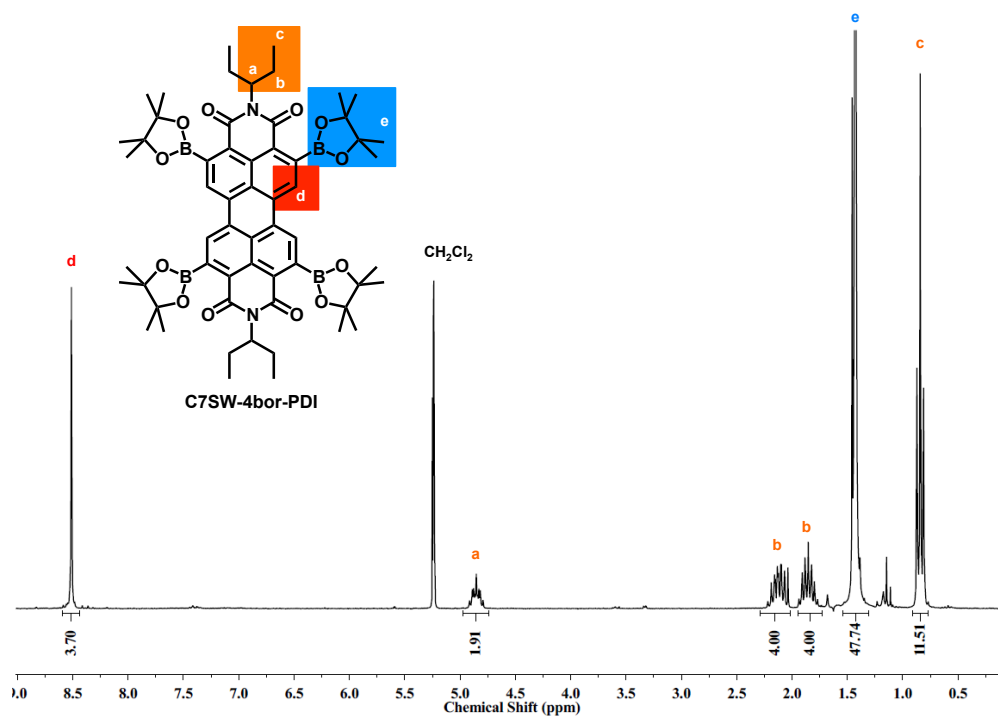
Figure 35 ^{1}H-NMR of **C2SW-4bor-PDI** in CD$_2$Cl$_2$

The ^{1}H-NMR of **C2SW-4bor-PDI** is displayed in Figure 35. The only singlet present in the aromatic region at about 8.5 ppm is a first evidence of the symmetric substitution pattern. Nevertheless this ^{1}H-NMR spectrum does not prove in a unambiguous way that the borylation took place at the *ortho*-position and not in the *bay*-region, even though this second possibility is not known in literature and would be rather sterically hindered.

In order to fully prove the 2,5,8,11-substitution pattern of the tetraboronate PDI, crystals of **C2SW-4bor-PDI** were grown from a chloroform/hexane mixture and characterized by X-ray analysis (Figure 36). The molecular structure confirmed shows two main important features: 1) the borylation reaction occurs selectively and exclusively at the *ortho*-positions;

2) the core maintains its planarity, even in presence of the sterically demanding boronyl moieties, as in the case of previously reported *ortho*-functionalized perylenediimides. The boronates are instead twisted almost orthogonally to the plane of the perylene core.
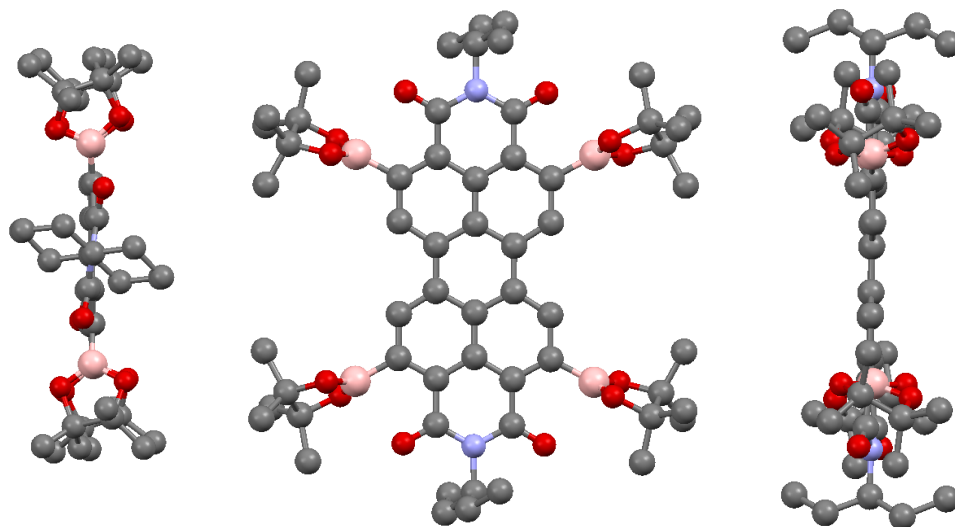
Figure 36 Top view (middle) and side views (left and right) of the X-ray crystal structure of compound **C2SW-4bor-PDI**. Hydrogen atoms and solvent molecules are omitted for clarity.

The selective substitution at the 2,5,8,11-positions proves once again the activating effect of the Murai catalyst on the *ortho*-positions to the carbonyl groups. In Scheme 32 the suggested reaction mechanism is presented, which is similar to the one reported for the ruthenium-catalyzed arylation of aromatic ketones.[100]
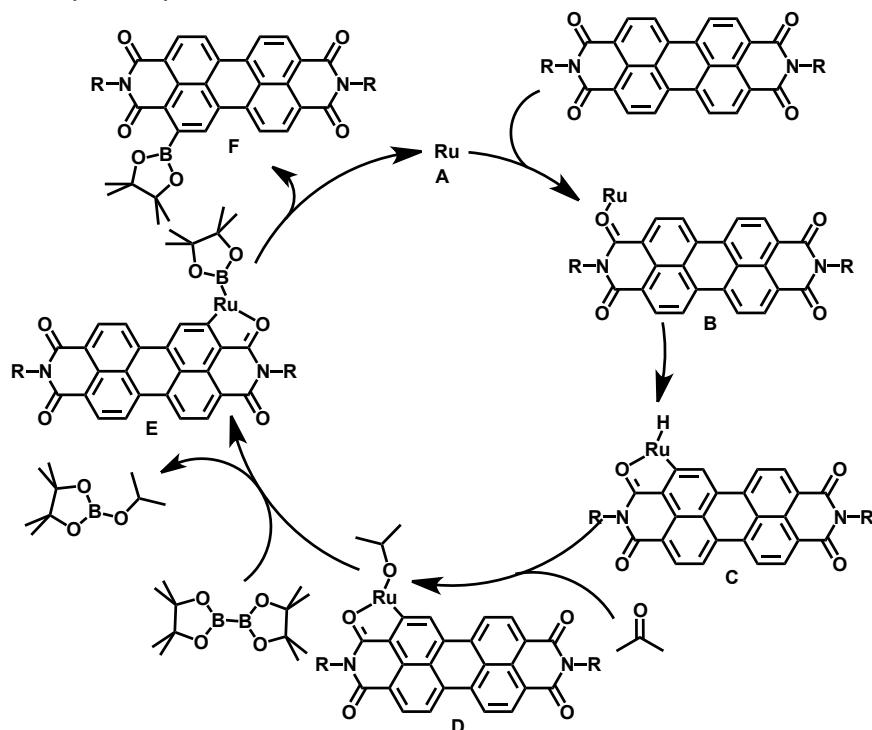
Scheme 32. Proposed reaction pathway.

As already mentioned, acetone acts as a scavenger of the H-B species generated during the reaction and prevents the undesired reduction of the imide group. The reaction starts

with the coordination of the carbonyl by the ruthenium(0) complex **A** to give intermediate **B**, followed by the formation of the *ortho*-metalated intermediate **C**, after cleavage of the C-H bond. Addition of the Ru-H to the carbonyl group of acetone leads to the production of the (alkoxy)-ruthenium intermediate **D**. Transmetalation between the bis(pinacolato)diboron and the intermediate **D** results in the formation of a trialkoxyborane and the aryl-boryl-ruthenium complex **E**. Reductive elimination leading to C-B bond formation provides the borylated product **F** and regenerates the active catalyst species **A**.

Further evidence for the plausibility of this mechanism is the fact that in none of the reaction conditions screened during the optimization process fivefold substitution could be observed, neither by FD-MS spectroscopy nor by TLC.

According to the ruthenium-catalyzed protocol for the *ortho*-arylation, the perylenediimide boronate **F** would also be able to react with another PDI molecule to form a PDI-dimer. Surprisingly such a coupling reaction was not observed. A possible explanation may be the rather bulky nature of the PDI boronate **F**. But other factors, such as a deactivating effect of the imide on the reactivity of the boronic ester cannot be excluded.

After confirming the *ortho*-selectivity of the reaction and the possibility to obtain a tetraboronate derivative, two other PDI substrates were considered for the reaction: **C7SW-PDI** and **DiPP-PDI**.
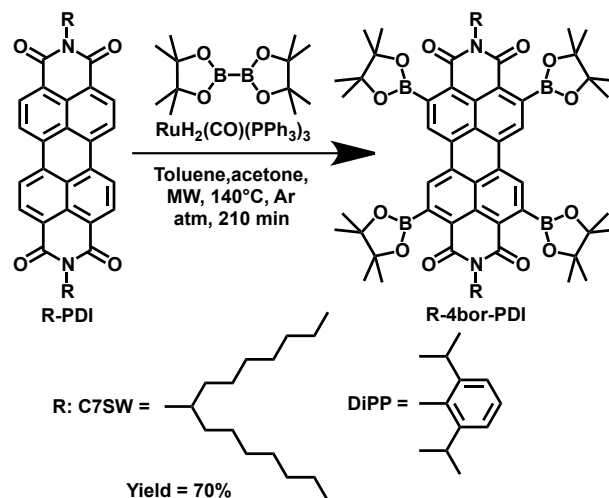
Scheme 33 *Ortho*-borylation reaction of **C7SW-PDI** and **DiPP-PDI**.

The borylation conditions optimized for **C2SW-PDI** were applied to both perylenediimides. In the case of **C7SW-PDI** the desired tetraboronate was obtained in good yields. Due to the good solubility deriving from the α-branched alkyl chains on the imide the concentration of the reaction could be increased, allowing the synthesis of **C7SW-4bor-PDI** on a gram scale within a day. Also in this case the formation of the undesired violet side product occurred. But similarly to **C2SW-4bor-PDI**, the tetraboronate could be isolated with analytical purity as an orange crystalline solid via simple reprecipitations from dichloromethane in methanol.

Different results were achieved using **DiPP-PDI** as substrate. The desired tetraboronate could be formed, but the reaction mixture also gave mono-, bi- and tri-substituted PDIs. TLC and FD-MS measurement showed also the presence of unreacted starting material. Attempts to isolate the desired **DiPP-4bor-PDI** from the reaction mixture via reprecipitations failed, due to the large amount of lower substituted perylenediimides. The difference in reactivity between **DiPP-PDI**, **C7SW-PDI** and **C2SW-PDI** can be explained by the presence of bulky and rigid diisopropylphenyl imide substituents, hindering the fundamental coordination of the ruthenium to the carbonyl group. A similar behavior was observed for the *ortho*-alkylation reaction in Chapter 1 and in other literature reports. An additional issue is the decreased solubility of **DiPP-PDI** in the solvent of the reaction as compared to **C7SW-PDI** and **C2SW-PDI**, which may require additional optimization of the conditions in order to afford the desired product in better yields.

The effect of the *ortho*-borylation on the optical and electrochemical properties of perylenediimides was investigated by UV-visible optical absorption spectroscopy, photoluminescence spectroscopy and cyclic voltammetry. Only the curves measured for **C2SW-4bor-PDI** in toluene are reported here, since the two spectra look virtually identical for C2 or C7 swallow-tail alkyl chains (Figure 37). The spectra show that the *ortho*-borylation has only a minor impact on the absorption and emission of the PDI. All the typical features of the curves are maintained, but shifted of about 10 nm to the longer wavelengths as compared to the unsubstituted derivative. The measured values are summarized in Table 8, where the negligible effect of the variation of the imide substituents on the optical and electronic properties of the systems can be seen.
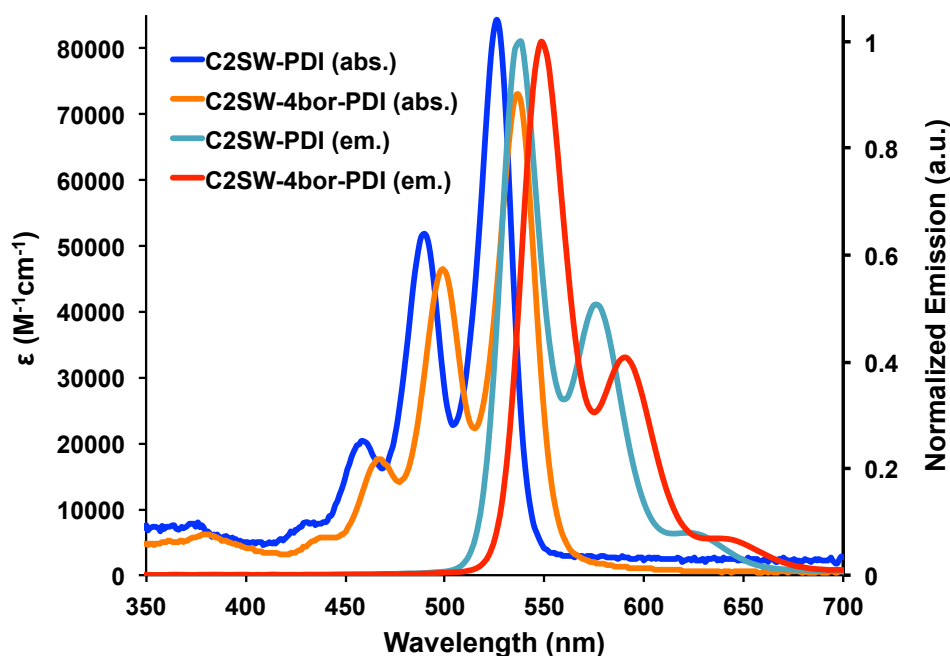
Figure 37 UV-visible absorption spectra and fluorescence spectra of **C2SW-PDI** and **C2SW-4bor-PDI** in toluene (λ_{exc} =538 nm).

The LUMO energy levels of the tetraboronate derivatives were estimated using cyclic voltammetry. The LUMO energies of the perylenediimides remain practically unaffected

upon substitution as compared to the parent unsubstituted materials (Table 8). Therefore the bathochromic shift in the absorption and fluorescence spectra is due to the HOMO energies, resulting from the slightly electron donating effect of the boronate groups.[97b]

Table 8 Electro-optical properties of tetraboronate-PDIs and of their unsubstituted parent compounds as comparison.

PDI[a]	ε [M⁻¹cm⁻¹][b]	λ_{max} [nm]	λ_{em} [nm][c]	φ_f[d]	E_{red1} [V][e]	LUMO [eV][f]	HOMO [eV][g]
C2SW-PDI	84300	526	538	0,99	-0,95	-3,85	-6,13
C2SW-4bor-PDI	73000	538	548	0,89	-0,96	-3,84	-6,07
C7SW-PDI	83300	526	538	0,97	-0,95	-3,85	-6,13
C7SW-4bor-PDI	72100	538	548	0,83	-0,97	-3,83	-6,06

[a]Optical properties measured in toluene. [b]Measured at λ_{max}. [c]Excited at λ_{max}. [d]Determined using Rhodamine 6G as standard. [e]Determined by cyclic voltammetric measurement in 0,1 M solution of Bu₄NPF₆ in CH₂Cl₂: vs Fc/Fc⁺. [f]Estimated vs. vacuum level from E_{LUMO} = 4.80 eV - E_{red1}. [g]Estimated from HOMO = LUMO - E_g, where E_g = optical gap, calculated from the optical absorption/emission data.

With the successful development of the new borylation protocol, the possibility to obtain 2,5,8,11-tetraboronate-PDIs was proved. Even though perylenediimides constitute the most investigated structures in the ryleneimide family, the extension of the new synthetic strategy to other RIs could confirm the validity and importance of the borylation procedure and provide an entire set of building blocks for the functionalization of the *ortho*-positions.

6.3 *Ortho*-Borylation of Ryleneimides

In order to demonstrate the general applicability of the *ortho*-borylation procedure, the reaction was tested on two model compounds of the class of rylenemonoimides and higher rylenediimides: perylenemonoimide and terrylenediimide, respectively. Perylenemonoimides exhibit two free *peri*-positins (9,10-positions) that exhibit a different reactivity as compared to the bay-positions.[101] TDIs exhibit instead a more elongated conjugated core responsible for a higher tendency to aggregation, making purification more challenging. Further these two molecules play a key role in applications such organic solar cells[96b] and bioimaging [102] and additional functionalizations may broaden the synthetic instruments to tune their electro-optical properties.

To exclude any difference in reactivity derived exclusively from the imide substituents, RIs bearing the α-branched alkyl chains used in the previous section were chosen. More precisely **C2SW-PMI** and **C7SW-TDI** were selected, which also exhibit good solubility in the solvents of the reaction.

The borylation was first tested on the perylenemonoimide derivative (Scheme 34) and was performed in a pressure vial heated in an oil bad. A longer reaction time was required for the completion of the reaction as compared to the experiments performed in a microwave oven. Nevertheless the desired product **C2SW-2,5-bor-PMI** could be obtained in good yields (76 %). The reaction mixture exhibits a violet color, and similarly

to the perylenediimide case the target compound could be separated from the undesired side products by multiple repreciptations from dichloromethane in methanol.
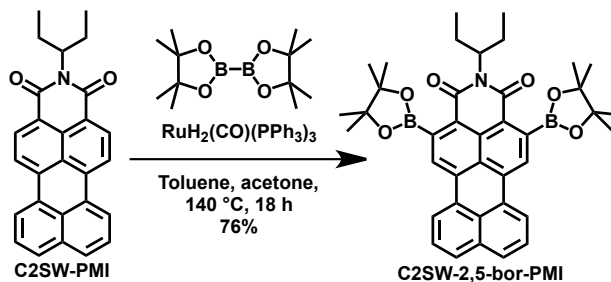
Scheme 34 *Ortho*-borylation of **C2SW-PMI**.

It must be noted that as compared to the perylenediimide derivative, the yield of the reaction is higher. The side reaction that usually occurred during the synthesis of the 2,5,8,11-tetraboronate-PDIs appeared to be less significant for **C2SW-PMI**, due to the lower number of active sites.

The application of the borylation reaction to terrylendediimide-derivatives required slight modifications of the synthetic protocol. The more extended core of the TDI lowers the solubility of the system, as compared to the perylene derivatives. The microwave assisted reaction afforded a mixture of various borylated derivatives ranging from the mono-substituted TDI to the desired product **C7SW-4bor-TDI**. A consistent amount of starting material was also present, indicating that most probably **C7SW-TDI** was not completely dissolved in the reaction mixture. Consequently the concentration of the TDI molecule in solution needed to be lowered. In order to monitor the complete dissolution of the starting material during the reaction and at the same time scale up the quantities, the borylation was performed in a transparent glass pressure vial.
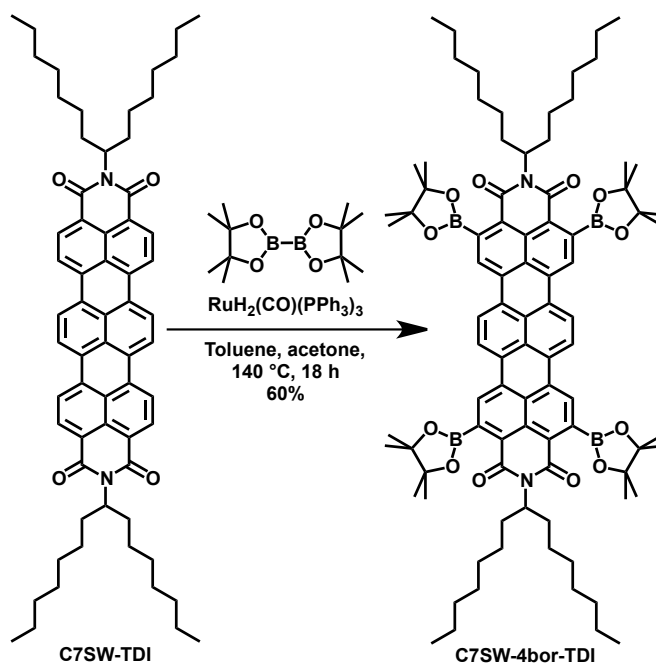
Scheme 35 *Ortho*-borylation of **C7SW-TDI**.

The desired product was obtained, even though traces of not fully substituted materials were still visible on TLC and in FD-MS. The reaction mixture had a green color deriving from the presence of side products. For the borylations applied to the perylene derivatives, the desired borylated products could be isolated via successive reprecipitations from dichloromethane in methanol. In the case of **C7SW-4bor-TDI** a partial removal of the side products was possible with this method, but further purification was required to achieve analytical purity. In fact the more extended conjugated core reduces the difference in solubility between the desired product and the impurities. Using gel permeation chromatography **C7SW-4bor-TDI** was obtained in good yield (60 %).
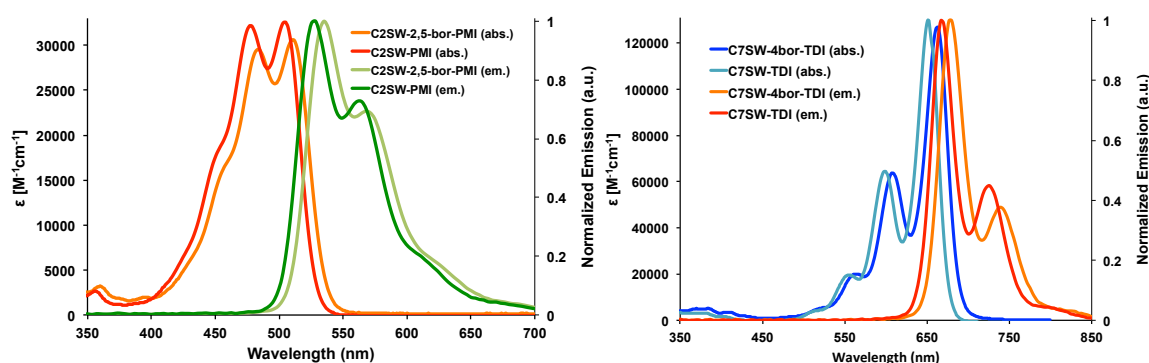
Figure 38 Absorption and fluorescence spectra of **C2SW-2,5-bor-PMI** and **C2SW-PMI** in toluene (left) and of **C7SW-4bor-TDI** and **C7SW-TDI** in chloroform.

The optical properties of **C2SW-2,5-bor-PMI** and **C7SW-4bor-TDI** were investigated by means of UV-visible absorption and fluorescence spectroscopy. The recorded spectra of the two derivatives are presented in Figure 38, while the extinction coefficients and the wavelength of the absorption and fluorescence maxima of the borylated PMI and TDI are summarized in Table 9.

Table 9 Optical properties of the *ortho*-borylated PMI and TDI and of their unsubstituted parent compounds as comparison.

RI	$\varepsilon \, [\text{M}^{-1}\text{cm}^{-1}]^{d}$	$\lambda_{max}\,[\text{nm}]$	$\lambda_{em}\,[\text{nm}]$	φ_f
C2SW-PMI[a]	3.06×10^{4}	504	529[e]	0.86 (504)[g]
C2SW-2,5-bor-PMI[a]	3.26×10^{4}	511	535[e]	0.78 (511)[g]
C7SW-TDI[b]	1.27×10^{5}	651	538	–
C7SW-4bor-TDI[c]	1.30×10^{5}	663	680[f]	1.00(632)[h]

[a]Measured in toluene. [b]Data from reference XXX. [c] Measured in chloroform. [d]Measured at λ_{max}. [e]Excited at λ_{max}. [f]Excited at λ= 632 nm. [g]Determined using Rhodamine 6G as fluorescent standard in ethanol. . [h]Determined using Cresyl Violet as fluorescent standard in methanol.

Similarly to what is observed for PDI derivatives, the borylation of the *ortho*-positions has only a minor impact on the optical properties of the molecules. The absorption and emission curves of both derivatives are slightly shifted to longer wavelengths as compared to the unsubstituted materials, while the characteristic spectral features are preserved.

6.4 Proving the Building Block Concept[e]

To prove that the newly developed boronates are effective building blocks for the chemistry of the *ortho*-positions, their use in different reactions was envisioned. The focus was concentrated on the synthesis of derivatives that cannot be obtained via the ruthenium-catalyzed reactions reported by the Shinokubo group. These reactions include aryl-aryl hetero-coupling via Suzuki type reaction and the introduction of a series of heteroatoms. For the proof of principle, the work described in the following pages was focused on perylenediimide tetraboronates.

6.4.1   Suzuki Coupling

The Suzuki coupling is probably the most important and established reaction in which aryl boronates are involved. This synthetic method was honored by the 2010 Nobel Prize in Chemistry, which was awarded in part to Suzuki for discovering it.[103] Using a palladium(0) catalyst in the presence of a base, the boronate can be coupled with aryl- or vinyl-halides or triflates, leading to the formation of a C-C bond.[98] The reaction tolerates a large number of functional groups and the chemicals involved have reduced toxicity as compared to other widespread coupling reactions, involving the use of nickel or stannyl derivatives.

Due to the key role that Suzuki coupling plays in organic chemistry, the possibility to apply this protocol to the *ortho*-borylated ryleneimides would be crucial. Two systems were tested as substrates, **C2SW-4bor-PDI** and **C7SW-4bor-PDI**.
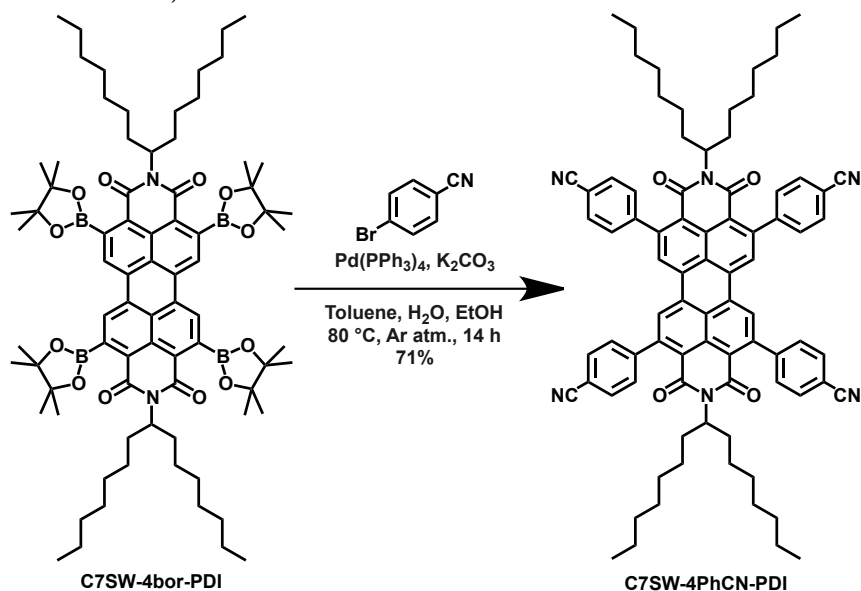
Scheme 36 Synthesis of **C7SW-4PhCN-PDI** via Suzuki coupling reaction.

Methyl 4-bromobenzoate and 4-bromo-benzonitrile were investigated as partners in the coupling reactions. Benzonitriles and benzoates belong to the substituents that cannot be introduced using the Murai arylation protocol. In fact these molecules feature a carbonyl and a boronate, which in the presence of the ruthenium catalyst would react with themselves, leading to the formation of undesired products.[104] Hence, the synthesis of tetrabenzoate and tetrabenzonitrile PDI would not only overcome the limitations of the already known *ortho*-functionalization method, but also successfully demonstrate the usefulness of *ortho*-boronates as building blocks.

The same conditions were applied for the coupling of **C7SW-4bor-PDI** with 4-bromo-benzonitrile and for **C2SW-4bor-PDI** with methyl 4-bromobenzoate (Scheme 36 and Scheme 37, respectively.) The reactions were monitored via TLC and FD-MS. In both cases the desired product could be obtained. While the reaction affording **C7SW-4PhCN-PDI** was completed after 16 hours, for **C2SW-4PhCOOMe-PDI** much longer reaction times were required. In both reactions lower substituted products were formed, due to deborylation. The side products could be easily separated from the target compounds either by column chromatography or via size exclusion chromatography.
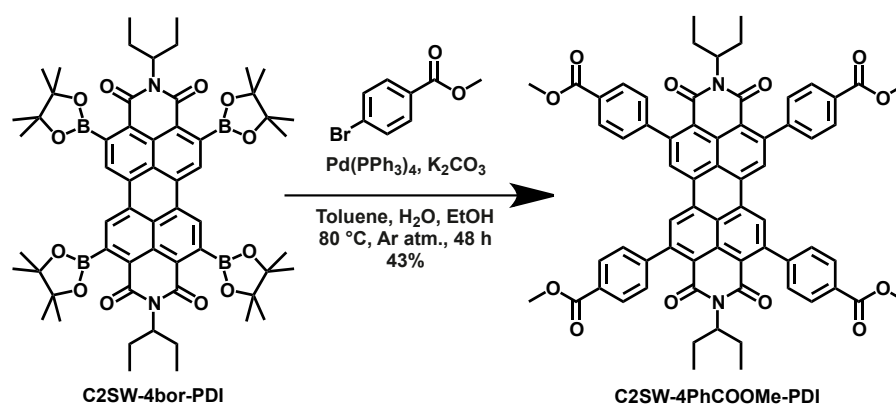
Scheme 37 Synthesis of **C2SW-4bor-PDI** via Suzuki coupling reaction.

Even though the reaction conditions were not optimized, the desired products could be obtained in good yields. The lower yields of **C2SW-4PhCOOMe-PDI** was most probably caused by the longer reaction times, which favor the deborylation reaction, as well as the progressive change in solubility upon substitution during the reaction. In fact **C2SW-4bor-PDI** is better soluble in the solvent of the reaction as compared to the final tetrabenzoate product. Therefore partial precipitation after the introduction of the first aryl groups in the *ortho*-positions may be responsible for deborylation. In the case of **C7SW-4PhCN-PDI**, the long branched imide substituents guaranteed good solubility throughout the entire reaction, leading to a better yield.
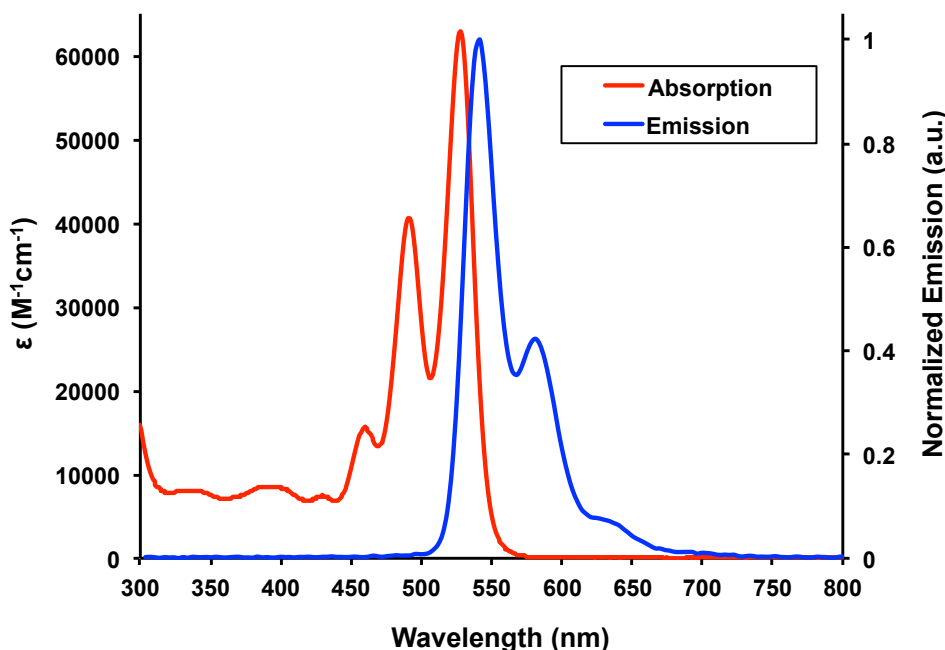
Figure 39 Absorption and fluorescence spectra of **C7SW-4PhCN-PDI** in dichloromethane.

UV-visible absorption and fluorescence spectroscopy revealed that the introduction of the four aryl groups has only a marginal impact on the optical properties as compared to the unsubstituted derivatives (Table 10). This is a consequence of the twisting of the *ortho*-phenyl substituents out of the plane of the perylene core, interrupting the conjugation. Consequently the perylenediimide optical properties are preserved and only a slight increase of the absorption in the region between 300 and 400 nm is observed (Figure 39).

Table 10 Optical properties of the *ortho*-tetraarylated PDI derivatives synthesized via Suzuki coupling. Their parent unsubstituted compounds are reported as comparison.

PDI[a]	ε [M^{-1}cm^{-1}][b]	λ_{max} [nm]	λ_{em} [nm][c]	φ_f[d]
C2SW-PDI	84300	526	538	0.99
C7SW-PDI	83300	526	538	0.97
C7SW-4PhCN-PDI	62900	528	542	0.69
C2SW-4PhCOOMe-PDI	70200	528	542	0.43

[a]Optical properties measured in toluene for compound **C2SW-PDI** and **C7SW-PDI**, in dichloromethane for compound **C7SW-4PhCN-PDI** and **C2SW-4PhCOOMe-PDI** [b]Measured at λmax. [c]Excited at λmax. [d]Determined using Rhodamine 6G in ethanol as standard.

6.4.2 Introduction of Heteroatoms

After successfully demonstrating the possibility to use the 2,5,8,11-tetraboronate-PDIs in the Suzuki coupling, further reactions were considered to prove the versatility of *ortho*-boronic esters as building blocks. The introduction of halogens and amino substituents was envisioned, still unknown in the literature focusing on perylenediimides at the time of these investigations. The synthesis of *ortho*-halogenated perylenediimides was selected not only to demonstrate the versatility of the tetraboronate as starting material, but also to provide additional building blocks for the chemistry of the *ortho*-positions.

In the exploration of the Suzuki coupling reaction, complications derived from the change in solubility occurring during the reaction featuring **C2SW-4bor-PDI**. In order to limit this factor, the introduction of heteroatoms was exclusively explored on the **C7SW**-derivative, which exhibits better solubility in organic solvents and facilitates purification.

First the introduction of bromine and chlorine was explored. The synthetic protocol is very similar for both systems. The copper(II) salt of the desired halogen is used, and by simply mixing the two reagents and heating, substitution is achieved.[105] Unfortunately the general method uses polar solvents to dissolve the inorganic salt, which is feasible for most of the boronates of small molecules, but unfortunately not for perylenediimides.
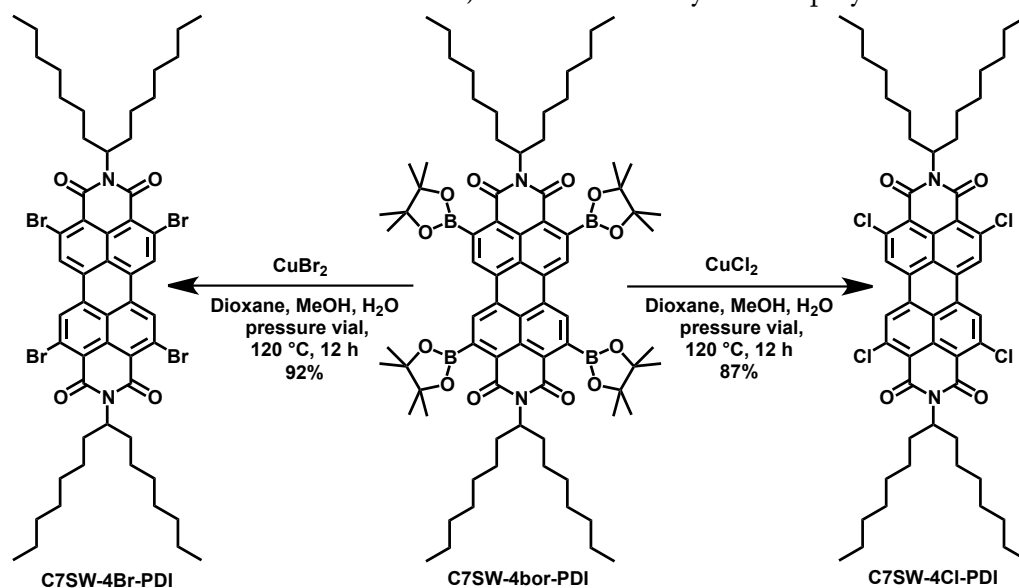
Scheme 38 Copper-catalyzed halodeboronation reactions for the conversion of **C7SW-4bor-PDI** into **C7SW-4Br-PDI** and **C7SW-4Br-PDI**.

Exchange was observed using a mixture of methanol and water, but mainly the undesired hydrodeborylation occurred, leading only to the lower substituted derivatives. The change of solubility of the system during the reaction was most probably the cause. In fact at first a clear homogeneous solution was obtained upon heating, but the replacement of the first and second boronate groups with an halogen lead to a consistent decrease in solubility and successive precipitation of the perylene derivative, preventing the full conversion to the product. This side reaction could be successfully limited by changing the solvent mixture. In particular the addition of 1,4-dioxane lead to the most appreciable improvement. Its complete miscibility with water and methanol prevents the formation of biphasic mixtures, while its boiling point (101 °C) permits to reach higher reaction temperatures as compared to THF (boiling point at 66 °C). More precisely the best results could be obtained using a mixture of dioxane, methanol and water in a 5/2/1 volume ratio, applying the conditions described in Scheme 38.

The optimized solvent mixture afforded **C7SW-4Br-PDI** and **C7SW-4Cl-PDI** in good yields (92 and 87 % respectively). Already after cooling the reaction to room temperature the desired products precipitated from the reaction mixture as crystalline solids. The small

amounts of only three times halogenated perylenediimide still present in the solid could be easily removed via column chromatography. No traces of singly or doubly halogenated materials or unsubstituted PDI were observed.

The introduction of iodine atoms required a different synthetic route. The only protocol described in the literature for the halodeboronation reaction is based on the use of chloramine-T and sodium iodide in a 1:1 THF/water mixture at room temperature in exclusion of light.[106] While this synthesis is known to work in short reaction times and good yields on electron rich aromatic systems, it appears to be less suited for electronpoor systems, such as perylenediimides. Longer reaction times are required and in some cases the desired aryl iodide cannot be isolated. Nevertheless the protocol was tested on **C7SW-4bor-PDI**.
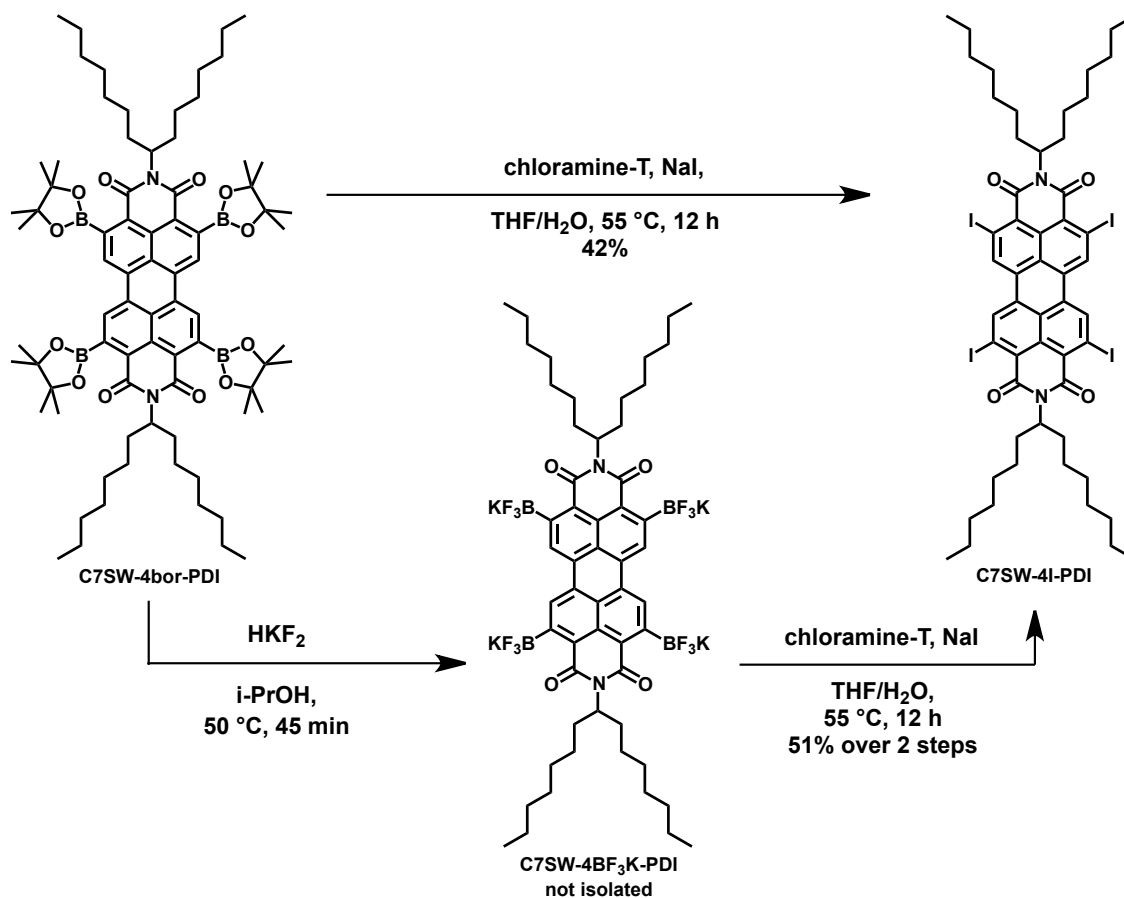
Scheme 39 Synthetis of **C7SW-4I-PDI**.

Also in this case the outcome of the conversion was strongly driven by the poor solubility of the system in the solvent of the reaction. Applying the exact conditions reported in literature, a mixture of iodinated products could be obtained, with only traces of **C7SW-4I-PDI**. By careful observation of the reaction, the initially homogeneous solution became a suspension after a few hours, due to the change in solubility associated to the replacement of the first boronate groups with iodine. As in the case of **C7SW-4Br-PDI** and **C7SW-4Cl-PDI**, the boronic ester groups are easily cleaved if the perylene molecule is not completely dissolved in the reaction. In order to limit deboronation more diluted conditions were used and the reaction was performed at 55 °C to improve the solubility

throughout the entire duration (Scheme 39). Even though deborylation could not be completely suppressed, the desired **C7SW-4I-PDI** was finally obtained in moderate yield (42 %) as a dark red solid after column purification. Further attempts to improve the reaction yields by modifying the temperature or the solvent mixture were not successful. **C7SW-4I-PDI** represents the first iodo-substituted perylenediimide reported in the literature.

Slightly higher yields were achieved by modifying the synthetic route, converting the tetraboronate derivative into its potassium trifluoroborate salt. Potassium trifluoroborates undergo the same iodination reaction with chloramine-T and sodium iodide, providing the advantage of better solubility in polar environments. [107] **C7SW-4bor-PDI** was converted into its potassium trifluoroborate salt by using a water solution of potassium hydrogen difluoride in isopropanol. By heating the reaction mixture at 55 °C for one hour, a color darkening occurred and no traces of residual boronate were observed on TLC. **C7SW-4BF$_3$K-PDI** was not isolated, but directly used for the halogenation reaction. **C7SW-4I-PDI** was obtained after column chromatography with improved yields (51 % over two steps) as compared to the direct halodeboronation reported above (40 % yield).

After successful substitution of the *ortho*-boronates of perylenediimides with iodine, bromine and chlorine, the introduction of fluorine was investigated. A recently reported protocol was followed featuring sodium hydroxide, silver triflate and 1-chloromethyl-4-fluoro-1,4-diazoniabicyclo[2.2.2]octane bis(tetrafluoroborate) (also known as Selectfluor® or F-TEDA-BF$_4$). [108] Direct application of the reaction conditions described in the literature (Scheme 40) lead indeed to the formation of one and two times fluorinated perylenediimides, observed in FD-MS analysis. Unfortunately TLC indicated also the presence of a large variety of side products. No major improvements could be achieved by replacing the solvent of the reaction with dioxane, THF, isopropanol or water or mixture of those.
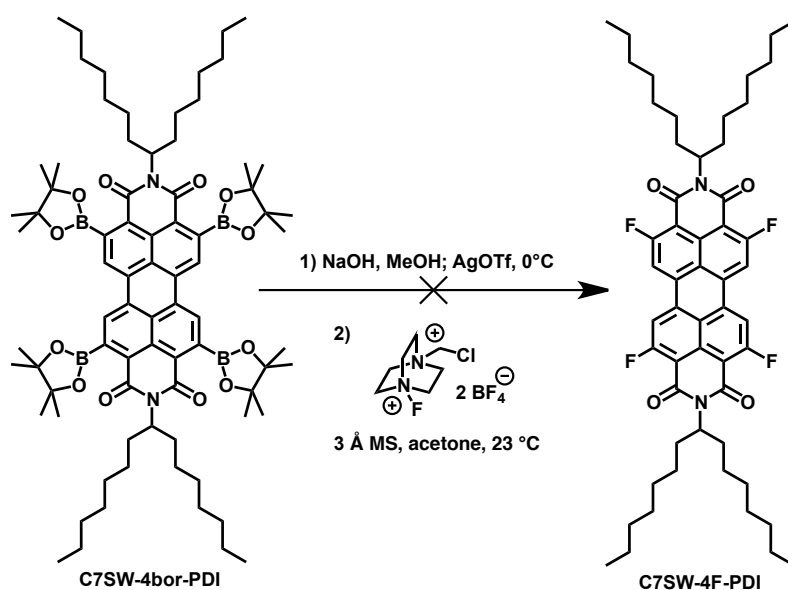
Scheme 40 Attempted synthesis of **C7SW-4F-PDI.**

Besides the solubility problems, the major obstacle may be the difficulty to form the tetrametalated perylenediimide. The synthetic protocol envisages the replacement of the boronyl moieties in the *ortho*-positions with silver atoms, to activate the aromatic system for the successive insertion of the fluoride ion. While the activation of one of the positions can proceed without affecting the properties of the system too much, simultaneous metalation at multiple sites may be difficult to achieve and radically change the reactivity of the system, allowing also less probable side reactions.

Without the possibility to directly perform a halodeboronation reaction to obtain the desired **C7SW-4F-PDI**, alternative routes were considered. While in the case of boronic acid derivatives the number of applicable reactions is still limited, the well-established chemistry of aryl halides gives a large variety of additional synthetic possibilities. Consequently, the *ortho*-halogenated perylenediimides obtained above represent building blocks themselves, providing to further extend the chemistry of the *ortho*-positions. Thus, the desired product was targeted using **C7SW-4Cl-PDI** in a halogen exchange (halex) reaction.

Several conditions were considered to synthesize **C7SW-4F-PDI**. Considering the poor solubility of **C7SW-4Cl-PDI**, the first attempt was performed using tetrabutylammonium fluoride (TBAF) in organic solvents.[109] According to literature this protocol is particularly appropriate for electron poor aromatic systems, such as perylenediimide. Unfortunately the reaction did not work for **C7SW-4Cl-PDI**. Upon addition of TBAF to a solution of the perylenediimde, the color turned from yellow into dark blue. Similar behavior was observed also in the case of **C7SW-4Br-PDI** and for **C7SW-PDI**. This color change can most probably be attributed to the strong interaction between the fluoride ion and the π-system of the perylenediimide. This adduct changes the electronic nature of the core system, making it less capable to undergo nucleophilic substitution.
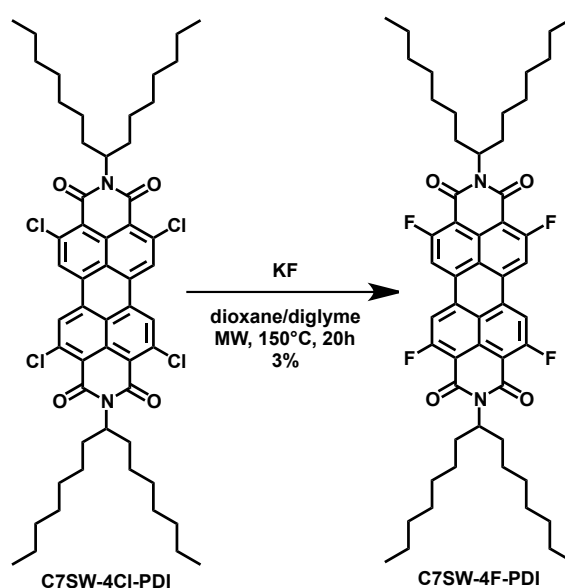
Scheme 41 Synthesis of **C7SW-4F-PDI** via halogen exchange reaction.

As an alternative, other halex protocols were explored using potassium and cesium fluoride. Complete decomposition of **C7SW-4Cl-PDI** was observed using KF, 18-crown-6-ether and sulfolane as solvent at 160 °C in a microwave oven.[110] More encouraging results could be obtained with a mixture of anhydrous dioxane and diglyme in a closed vessel, with **C7SW-4Cl-PDI** and potassium fluoride (Scheme 41). While initially a clean substitution of the first chlorine atoms with fluorine was achieved, more and more dark red-colored side products were formed with the time. This may most probably be attributed to the substitution of the halogen atoms with alcohols derived from the decomposition of the dioxane or diglyme. Nevertheless small amounts of **C7SW-4F-PDI** could be obtained after 20 hours. Several successive column chromatographic purifications were required to purify the target compound from the side products of the reaction and only 3 mg could finally be obtained. This small amount was not sufficient for complete characterization of the material.

Finally the introduction of nitrogen atoms to the *ortho*-positions was explored. Once again direct conversion of the tetraboronate perylenediimide was envisioned using Chan Lam amination reaction.[111] This was tested, using copper(II) acetate, potassium fluoride and octyl amine in dioxane. After heating the reaction at 80 °C, no traces of aminated product could be observed. Similar results were obtained for the different conditions explored and lead to the decision to abandon this route.

As an alternative, halogenated perylenediimides were once again used as starting materials. Direct nucleophilic substitution on **C7SW-4Br-PDI** and **C7SW-4I-PDI** was tested. Suspension of the starting material in octylamine and successive heating at 130 °C under argon atmosphere afforded **C7SW-4N-PDI** as a dark red solid, in both cases quantitatively. Despite the presence of the long alkyl chains in the *ortho*-position and imide-nitrogens, **C7SW-4N-PDI** was found to be highly insoluble in most of the organic solvents, except toluene.
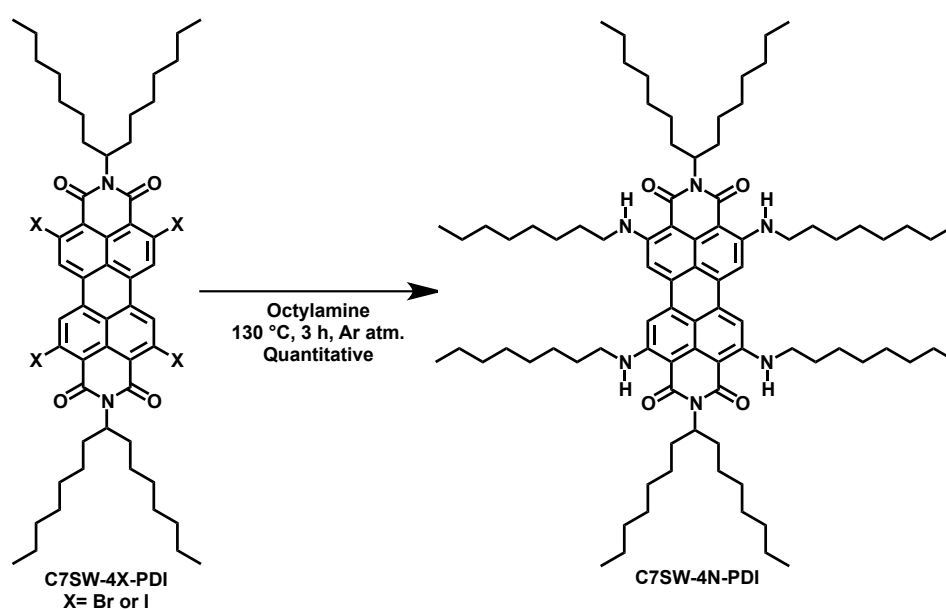
Scheme 42 Synthesis of **C7SW-4N-PDI** via nucleophilic substitution.

The influence of the introduction of halogens and amino groups in the *ortho*-positions on the optical properties of the system was investigated via UV-vis absorption and fluorescence spectroscopy. The results for the derivatives bearing the different heteroatoms are shortly summarized in Table 11. The properties of parent unsubstituted compound **C7SW-PDI** are also reported for direct comparison.

Table 11 Electro-optical properties of *ortho*-tetrahalogenated and tetramino perylenediimides.

PDI[a]	ε [M^{-1}cm^{-1}][b]	λ_{max}[nm]	λ_{em}[nm][c]	φ_f[d]	E_{red1} [V][e]	LUMO [eV][f]	HOMO [eV][g]
C7SW-PDI	83300	526	538	0,97	–0,95	–3,85	–6,13
C7SW-4F-PDI[h]	-	500	509	-	-	-	-
C7SW-4Cl-PDI	57000	505	515	0.47	–0.83	–3.97	–6.33
C7SW-4Br-PDI	79000	509	519	0.21	–0.90	–3.90	–6.26
C7SW-4I-PDI	72300	518	-	-	–0.89	–3.91	–6.21
C7SW-4N-PDI	54200	512	608	0.05	–1.59	–3.21	–5.61[h]

[a]Optical properties measured in toluene for compound **C7SW-PDI**, in dichloromethane for all the other compounds. [b]Measured at λ_{max}. [c]Excited at λ_{max}. [d]Determined using Rhodamine 6G in ethanol as standard. [e]Half-wave potentials, determined by cyclic voltammetric measurement in 0.1 M solution of Bu$_4$NPF$_6$ in CH$_2$Cl$_2$: vs Fc/Fc$^+$. [f]Estimated vs. vacuum level from E_{LUMO} = -4.80 eV - E_{red1}. [g]Estimated from HOMO = LUMO - E_g, where E_g = optical gap, calculated from the optical absorption/emission data. [h]Estimated vs. vacuum level from E_{LUMO} = -4.80 eV + E_{ox1}. [h]Only partial characterization was possible, due to the small amounts of material.

In all cases the *ortho*-substitution leads to a hypsochromic shift in the absorption maximum. Within the series of halogens, the fluorinated derivative shows the most blue-shifted absorption followed by the chlorinated, brominated and iodinated PDIs (Figure 40). The same trend is observed for the fluorescence emission, where the quantum yield decreases within the series, to reach the complete quenching in the case of **C7SW-4I-PDI**, due to the heavy atom effect.

A similar trend is known in literature for tetra-*bay*-halogenated perylenediimides.[112] The only major difference is represented by the fact that the *bay*-tetrabromo-derivatives exhibit a more bathochromic absorption as compared to the unsubstituted PDIs, consequence of the strong twisting of the aromatic core.
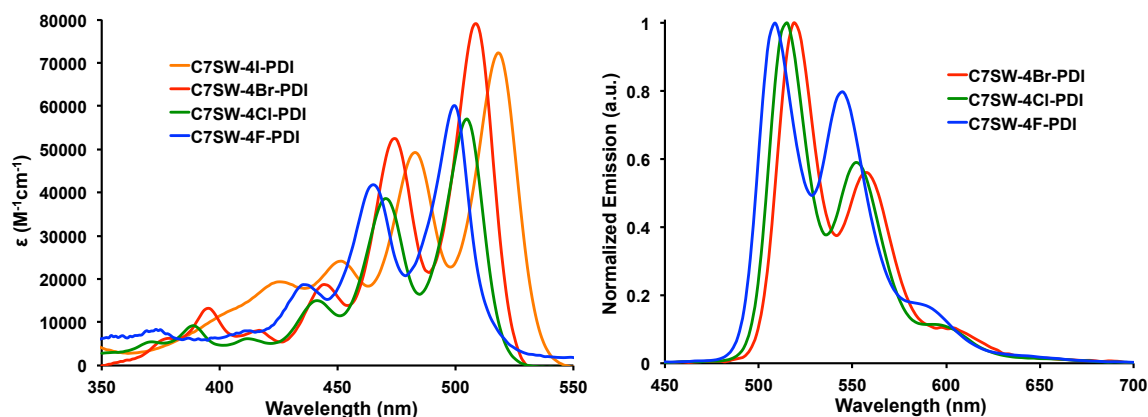
Figure 40 Absorption (left) and fluorescence spectra (right) of the seiries of *ortho*-tetrahalogenated perylenediimides with general formula **C7SW-4X-PDI**, where X=F, Cl, Br, I in dichloromathane. (λ_{exc} = λ_{max}). The extinction coefficient of **C7SW-4F-PDI** is arbitrarly set to 60000 M^{-1}cm^{-1}.

Quite unexpected optical properties are instead observed for **C7SW-4N-PDI**. In contrast to *bay*-amination of PDIs[113] or tetramination of naphthalenediimides,[114] the *ortho*-substitution does not cause a strong color change. A broadening of the absorption curve is observed, combined with a hypsochromic shift in the absoption maximum of about 14 nm.
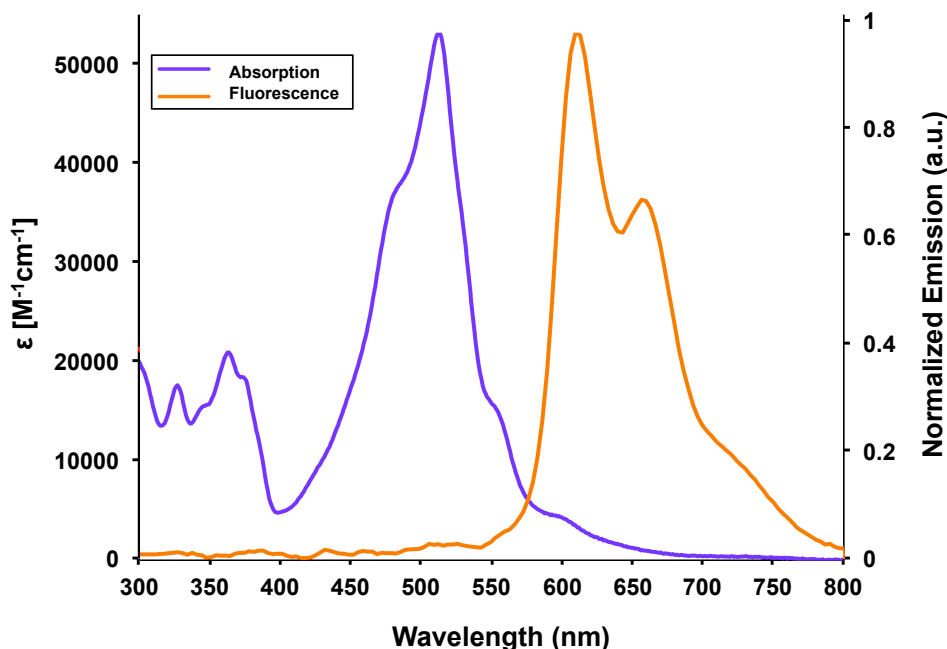
Figure 41 Absorption and fluorescence spectra of C7SW-4N-PDI in toluene. (λ_{exc} = λ_{max}).

These unexpected results are confirmed by the electrochemical data. The introduction of alkylamine moieties leads to a consistent lifting of the HOMO and LUMO levels of 0.64 eV and 0.52 eV respectively. The almost identical effect on the two frontier molecular orbitals renders the molecule easier to be oxidized, without substantially altering the HOMO-LUMO gap.

Cyclic voltammetry was also performed on the tetraiodo, tetrabromo and tetrachloro perylenediimide. As it can be seen from Table 11, the fourfold introduction of halogens, makes the perylenediimide slightly easier to be reduced as compared to **C7SW-PDI**.

6.5 Conclusions and Outlook

In this chapter the possibility to overcome the limitations of the *ortho*-functionalization of ryleneimides via the synthesis of a common building block was investigated. An unprecedented protocol for the borylation of the *ortho*-positions could be successfully developed using the Murai catalyst $RuH_2(CO)(PPh_3)_3$ and bis(pinacolato) diboron. Optimization of the reaction conditions lead to the 2,5,8,11-tetraboronate-perylenediimide directly from the unsubstituted PDI via a one step reaction in good yields. Ths synthetic protocol does not only work on perylenediimides bearing different imide substituents, but can also be applied with comparable results to other ryleneimides, such as terrylenediimide and perylenemonoimide. X-ray structure determination of

C2SW-4bor-PDI demonstrated the selectivity of the reaction on the *ortho*-position and the retention of planarity of the aromatic core, even upon introduction of sterically demanding substituents.

The potential of *ortho*-borylated ryleneimides as versatile building block was demonstrated using 2,5,8,11-tetraboronate-PDIs as model compounds not only in Suzuki coupling, but also for the introduction of halogens and amino substituents. A limitation of *ortho*-boronic esters as building blocks is their tendency to undergo deborylation, especially when the compound is not completely dissolved in the reaction mixture. This phenomenon is well known in the chemistry of aryl-boronates and becomes an issue for the tetraboronates of perylenediimide, since the replacement of one or two boronic esters with other substituents can already drastically change the solubility of the system. Nevertheless, by careful observation of the reaction and fine tuning of the concentration and solvent mixture, tetraboronates could be converted with high yields, as in the case of the Suzuki coupling or fourfold introduction of chlorine and bromine atoms.

Further, the possibility to use *ortho*-tetrahalogenated PDIs as building blocks was also demonstrated. These tetrahalogenated materials represent a useful alternative to the boronic ester derivatives, especially due to their established chemistry, which provides a broader range of opportunities for further functionalization. Additionally, aryl halides can be purified using chromatography over silica or alumina without major losses of material caused by side reactions with the stationary phase. These possibilities strengthen the fundamental role of *ortho*-boronates for the development of the chemistry of the *ortho*-positions, filling the vacant places in the library of general building blocks in the field of ryleneimides, alongside with ryleneanhydrides and *bay*-halogenated ryleneimides.
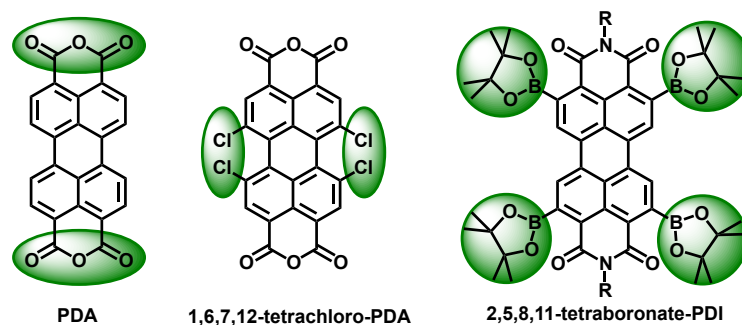
Figure 42 The building blocks in the perylenediimide chemistry.

The importance of the development of a building-block for the chemistry of the *ortho*-positions is further confirmed by a report of the Shinokubo group, which in parallel to the work performed in our laboratory, published an alternative synthesis of 2,5,8,11-tetraboronate-PDIs. In their report, the tetraboronic ester of perylenediimide could be obtained using an iridium-catalyzed reaction, following the work of the Miyaura group,. In their case aryl heterocycles, alkoxy and hydroxyl groups were introduced starting from the boronate derivatives.

The borylation of the *ortho*-positions also opens a variety of other possibilities if combined with the well established chemistry of the imide and *bay*-positions. Combining

the advantages of the different functionalizations could lead to very innovative materials. An example is presented in Scheme 43. In this case the famous electron acceptor 1,7-dicyano-PDI is used as starting material for the borylation reaction of the *ortho*-positions. Selective functionalization of the less sterically hindered positions might be achieved, providing an extremely interesting electron acceptor to incorporate of low band-gap conjugated polymers.
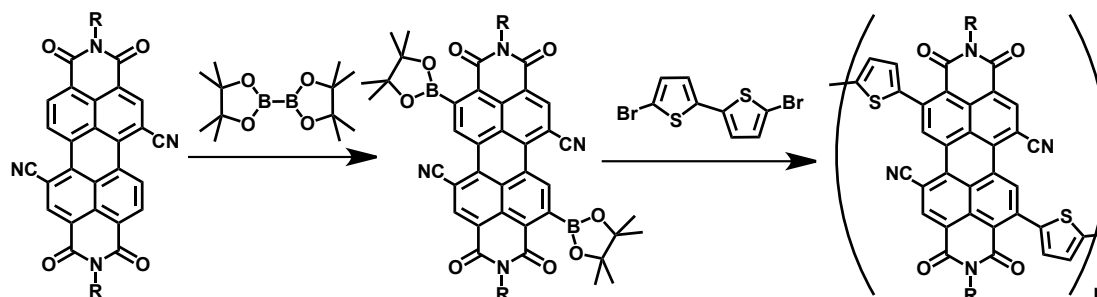
Scheme 43

In this chapter also the consequences of *ortho*-substitution for the optical and electrochemical properties were investigated. The introduction of boronic esters does not substantially change the characteristics of the ryleneimide. This conservation of property appears to be of high interest for example for the development of covalent organic frameworks.[115] Rylenediimides could be condensed with molecules bearing two vicinal hydroxyl groups, to create 2D and 3D frameworks. Via careful choice of the second component, highly ordered donor-acceptors arrays could be synthesized, as shown in Figure 43, with possible applications in the field of organic solar cells.
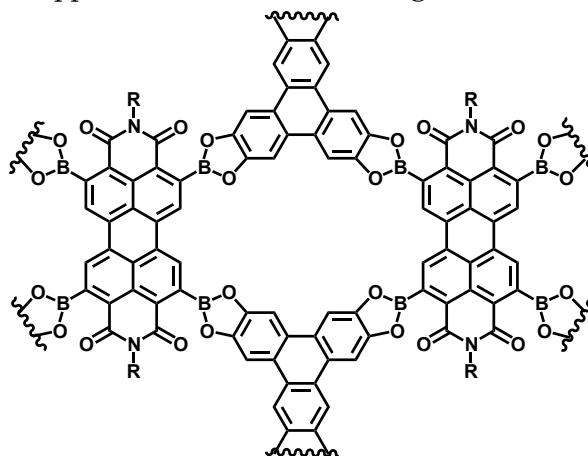
Figure 43 Example of possible covalent organic framework including *ortho*-tetraboronate-PDIs.

The fourfold introduction of *para*-benzonitriles and benzocarboxylates units in the 2,5,8,11-positions of PDIs also has a negligible impact on the optical and electrochemical properties of perylenediimide. The decoupling effect caused by the twisting of the substituents limits the possibility to tune the optical and electrochemical properties of the system, but may be a desirable property for the construction of light harvesting systems[116] or highly decoupled donor acceptor structures for fundamental photophysical investigations.[117]

C7SW-4PhCN-PDI and **C2SW-4PhCOOMe-PDI** can also be seen as interesting building blocks for the synthesis of metal organic frameworks (MOFs).[118] For these materials the stability and optical and electrochemical properties of PDI could be combined with the properties of the metaloxide coordinating sites in a defined geometrical disposition, with interesting applications in the field of gas adsorption, sensing, catalysis and semiconducting materials.[119]

Finally, the introduction of halogens and aminooctyl substituents resulted in a hypsochromic shift of the absorption maxima. This was quite surprising in the case of **C7SW-4N-PDI**, since amino substituted naphthalenes (fourfold substitution on the aromatic core) and perylenediimides (twofold substitution in the *bay*-positions) already reported in the literature exhibit a remarkable bathochromic shift instead. But in the case of the *ortho*-tetrasubstituted PDI, the donating effect of the amino groups seems to have an equally strong influence on the HOMO and LUMO energies, retaining the difference in energy. This observation was confirmed with electrochemical measurements and calculations.

The introduction of halogen substituents in the *ortho*-positions appears instead to have a relatively small impact on the frontier molecular orbitals of the derivatives investigated. Only a moderate increase of the electron affinities and ionization potentials could be obtained. However a more consistent lowering of the energy of the LUMO levels would be of high interest for the application of these materials in n-type organic field effect transistors.[120] Attempts to reach this goal via *ortho*-substitution will be presented in the next chapter.

6.6 References

[89] a) Nakazono, S.; Imazaki, Y.; Yoo, H.; Yang, J.; Sasamori, T.; Tokitoh, N.; Cédric, T.; Kageyama, H.; Kim, D.; Shinokubo, H.; Osuka, 2009). *Chemistry-A European Journal*, *15*(31), 7530-7533. (b) Nakazono, S., Easwaramoorthi, S., Kim, D., Shinokubo, H., & Osuka, A. (2009), *Organic letters*, *11*(23), 5426-5429.

[90] Kakiuchi, F., & Chatani, N. (2003), *Advanced Synthesis & Catalysis*, *345*(9-10), 1077-1101.

[91] Kakiuchi, F., Matsuura, Y., Kan, S., & Chatani, N. (2005), *Journal of the American Chemical Society*, *127*(16), 5936-5945.

[92] Feng, C., Liu, Y., Peng, S., Shuai, Q., Deng, G., & Li, C. J. (2010), *Organic Letters*, *12*(21), 4888-4891.

[93] Maytum, H. C., Tavassoli, B., & Williams, J. M. (2007), *Organic letters*, *9*(21), 4387-4389.

[94] a) Blacker, A. J., Farah, M. M., Hall, M. I., Marsden, S. P., Saidi, O., & Williams, J. M. (2009), *Organic letters*, *11*(9), 2039-2042. b) Anand, N., Owston, N. A., Parker, A. J., Slatford, P. A., & Williams, J. M. (2007), *Tetrahedron Letters*, *48*(44), 7761-7763. c) Hall, M. I., Pridmore, S. J., & Williams, J. M. (2008), *Advanced Synthesis & Catalysis*, *350*(13), 1975-1978. d) Han, H., & Krische, M. J. (2010), *Organic letters*, *12*(12), 2844-2846. e) Pridmore, S. J., Slatford, P. A., Daniel, A., Whittlesey, M. K., & Williams, J. M. (2007), *Tetrahedron letters*, *48*(29), 5115-5120. f) Shibahara, F., Bower, J. F., & Krische, M. J. (2008), *Journal of the American Chemical Society*, *130*(20), 6338-6339. g) Ueno, S., Mizushima, E., Chatani, N., & Kakiuchi, F. (2006), *Journal of the American Chemical Society*, *128*(51), 16516-16517.

[95] a) Herrmann, A., & Mullen, K. (2006), *Chemistry Letters*, *35*(9), 978-985.
b) Herbst, W., & Hunger, K. (2006). *Industrial organic pigments*. Wiley-VCH.

[96] a) Huang, C., Barlow, S., & Marder, S. R. (2011), *The Journal of Organic Chemistry*, *76*(8), 2386–2407. b) Li, C., & Wonneberger, H. (2012), *Advanced Materials*, *24*(5), 613–636.

[97] a) Mkhalid, I. A. I., Barnard, J. H., Marder, T. B., Murphy, J. M., & Hartwig, J. F. (2010), *Chemical Reviews*, *110*(2), 890–931. b) Hall, D. G. (Ed.). (2012). *Boronic acids* (Vol. 2). Wiley-VCH. c) Hartwig, J. F. (2011), *Chemical Society Reviews*, *40*(4), 1992–2002.

[98] Miyaura, N., & Suzuki, A. (1995), *Chemical reviews*, *95*(7), 2457-2483.

[99] a) Kawamorita, S., Ohmiya, H., Hara, K., Fukuoka, A., & Sawamura, M. (2009), *Journal of the American Chemical Society*, *131*(14), 5058–5059. b) Ishiyama, T., Isou, H., Kikuchi, T., & Miyaura, N. (2010), *Chemical Communications*, *46*(1), 159–161.

[100] Kakiuchi, F., Kan, S., Igi, K., Chatani, N., & Murai, S. (2003), *Journal of the American Chemical Society*, *125*(7), 1698–1699.

[101] Li, C., Schöneboom, J., Liu, Z., Pschirer, N. G., Erk, P., Herrmann, A., & Müllen, K. (2009), *Chemistry-A European Journal*, *15*(4), 878-884. b) Zagranyarski, Y., Chen, L., Zhao, Y., Wonneberger, H., Li, C., & Müllen, K. (2012), *Organic letters*, *14*(21), 5444-5447.

[102] Weil, T., Vosch, T., Hofkens, J., Peneva, K., & Müllen, K. (2010), *Angewandte Chemie International Edition*, *49*(48), 9068–9093.

[103] www.nobelprize.org

[104] Ackermann, L., Vicente, R., & Kapdi, A. (2009), *Angewandte Chemie International Edition*, *48*(52), 9792–9826.

[105] Murphy, J. M., Liao, X., & Hartwig, J. F. (2007), *Journal of the American Chemical Society*, *129*(50), 15434-15435.

[106] Kabalka, G. W., Akula, M. R., & Zhang, J. (2002), *Nuclear medicine and biology*, *29*(8), 841-843.

[107] Kabalka, G. W., & Mereddy, A. R. (2004), *Tetrahedron Letters*, *45*(2), 343–345.

[108] Furuya, T., & Ritter, T. (2009), *Organic letters*, *11*(13), 2860-2863.

[109] Hu, Y. F., Luo, J., & Lü, C. X. (2010), *Chinese Chemical Letters*, *21*(2), 151-154.

[110] Würthner, F., Osswald, P., Schmidt, R., Kaiser, T. E., Mansikkamäki, H., & Könemann, M. (2006), *Organic Letters*, *8*(17), 3765–3768.

[111] a) Antilla, J. C., & Buchwald, S. L. (2001), *Organic Letters*, *3*(13), 2077–2079. b) Quach, T. D., & Batey, R. A. (2003), *Organic letters*, *5*(23), 4397-4400.

[112] Schmidt, R., Oh, J. H., Sun, Y.-S., Deppisch, M., Krause, A.-M., Radacki, K., et al. (2009), *Journal of the American Chemical Society*, *131*(17), 6215–6228.

[113] Zhao, Y., & Wasielewski, M. R. (1999), *Tetrahedron letters*, *40*(39), 7047-7050.

[114] Fin, A., Petkova, I., Doval, D. A., Sakai, N., Vauthey, E., & Matile, S. (2011), *Organic & Biomolecular Chemistry*, *9*(24), 8246–8252.

[115] Feng, X., Ding, X., & Jiang, D. (2012), *Chemical Society Reviews*, *41*(18), 6010-6022.

[116] a) Weil, T., Reuther, E., & Müllen, K. (2002), *Angewandte Chemie International Edition*, *41*(11), 1900-1904. b) Dichtel, W. R., Hecht, S., & Fréchet, J. M. (2005), *Organic Letters*, *7*(20), 4451-4454. c) Balzani, V., Ceroni, P., Maestri, M., & Vicinelli, V. (2003), *Current opinion in chemical biology*, *7*(6), 657-665.

[117] Schlichting, P., Duchscherer, B., Seisenberger, G., Basché, T., Bräuchle, C., & Müllen, K. (1999), *Chemistry-A European Journal*, *5*(8), 2388-2395.

[118] a) James, S. L. (2003), *Chemical Society Reviews*, *32*(5), 276-288. b) Long, J. R., & Yaghi, O. M. (2009), *Chemical Society Reviews*, *38*(5), 1213-1214.

[119] MacGillivray, L. R. (Ed.). (2010). *Metal-organic frameworks: design and application*. Wiley.

[120] Jones, B. A., Facchetti, A., Wasielewski, M. R., & Marks, T. J. (2007), *Journal of the American Chemical Society*, 129(49), 15259–15278.

7 Tetracyanation of Rylenediimides

7.1 Introduction[f]

Perylenediimides are without any doubt among the most promising and investigated materials for the development of n-type semiconductors. [121] In fact, as previously mentioned, PDIs do not only possess outstanding thermal and chemical stability, but they also offer the possibility to tune selectively solid-state packing or the energy of their molecular orbitals via functionalization of the imide positions or of the conjugated core, respectively. Nevertheless further effort is needed to improve the performances of PDIs in n-type field effect transistors and in particular their air-stability under operating conditions. [122] In fact the initial performances are quite often not stable in time due to the degradation of the active layer, caused by side reactions with impurities such as water and oxygen.

One of the approaches to improve air-stability is based on lowering the energy of the LUMOs.[123] Core functionalization has already demonstrated the possibility to decrease the energy of molecular orbitals of PDIs.[124] Enhanced electron affinities and improved air stability in operating devices have been achieved via introduction of electron withdrawing halo or cyano substituents.[125] LUMO values as low as -4.5 eV could be reached in the case of *bay*-dicyano-PDIs bearing perfluorinated alkyl chains at the imide nitrogens.[126]

Typically, the introduction of electron-withdrawing substituents is performed at the 1,6,7,12-positions (or *bay*-positions). However, the functionalization of these molecular sites presents some limitations. Due to steric reasons, the replacement of *bay*-hydrogens with other functional groups induces a deviation of the perylene core from planarity.[127] The degree of bending depends upon the nature and number of substituents, but non-planarity is sometimes undesirable for solid-state packing. Additional limitation of the *bay*-functionalization is the impossibility to introduce four sterically demanding substituents, such as for example cyano groups.

Ortho-functionalization provides an attractive alternative to *bay*-substitution for the synthesis of unique PDI-based semiconductors. In the previous chapter it was demonstrated that fourfold *ortho*-substitution can be achieved even in the case of bulky groups, such as boronic esters. Additionally the planarity of the perylene core is preserved upon functionalization. More importantly, the *ortho*-borylated and halogenated PDIs described in the previous chapter provide for the first time the possibility to take

---

advantage of this functionalization pattern for the synthesis of PDI-based semiconductors.

In this chapter, the lowering of the LUMO levels of rylenediimides will be investigated using *ortho*-cyano substituents. The first section will be focusing on the development of a synthetic strategy for tetracyanation of perylenediimides. In the second part tetracyanation will be extended to the higher homologue terrylenediimides. Finally the synthesis of NH-tetracyano rylenediimides derivatives will be envisioned as possible strategy to achieve n-type semiconducting pigments.

7.2 *Ortho*-Tetracyanation of Perylenediimides

A major limitation of *bay*-functionalization is the impossibility to introduce more than two cyano substituents due to steric reasons. *Ortho*-cyanation would allow instead fourfold substitution while preserving the planarity of the molecule, as predicted from calculations (Figure 44). Stronger electron acceptors than *bay*-cyano perylenediimides should be obtained. However the planar target tetracyano-PDI should exhibit a strong tendency to aggregate and reduced solubility. Therefore PDIs bearing α-branched alkyl chains as imide substituents were chosen for the explorative synthetic work. More precisely **C2SW-4bor-PDI** and **C7SW-4bor-PDI** were selected as starting materials.

R-4CN-PDI   **Calculated geometries of Me-4CN-PDI**   **R-2CN-PDI**
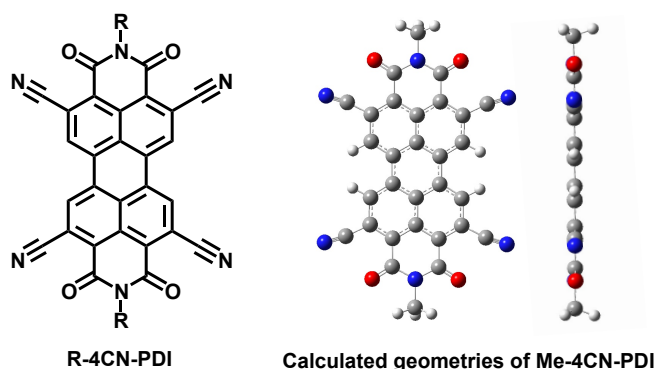
Figure 44 *Ortho*-tetracyano-PDI (left) and the geometry of N,N'-methyl-2,5,8,11-tetracyano-PDI obtained from DFT calculations (right).

In order to compete with the synthesis of *bay*-cyanated materials, *ortho*-tetracyano-PDIs should be obtained in maximum three steps from the unsubstituted derivative with a good overall yield. Therefore the possibility to directly convert the *ortho*-tetraboronate to the desired tetracyano-PDI was considered. In 2010 Hartwig and coworkers published a synthetic protocol allowing the direct conversion of aryl boronates into nitriles.[128] The reaction features zinc cyanide as cyanating agent in combination with caesium fluoride and copper(II) nitrate in a water/methanol mixture at 80 °C. This reaction was initially tested on **C2SW-4bor-PDI**.

Direct application of the literature reaction conditions afforded **C2SW-PDI** as main product of the reaction, with traces of one and two-times cyanated perylenediimides and several other unidentified side products. In the previous chapter deborylation reaction was observed when the perylenediimide boronates were not completely dissolved in the

reaction mixture. Therefore to improve the solubility, a mixture of dioxane and methanol was screened. This modification gave **C2SW-4CN-PDI** as main product of the reaction. Unfortunately deborylation was only prevented to some extent, as well as the formation of unidentified side products. Further optimization work was performed to improve the outcome of the reaction. Even though the reaction was found to proceed already at room temperature overnight, the best yields were reached with microwave heating. The reaction was completed after 5 minutes at 80 °C and the desired **C2SW-4CN-PDI** could be obtained as a brown solid after chromatographic purification (30 % yield). Similar results were achieved applying the reaction to **C7SW-4bor-PDI** (39 % yield). The rather moderate yields for the fourfold substitution are higher than those reported in the literature, where monosubstitution typically proceeds in 60 % yields.
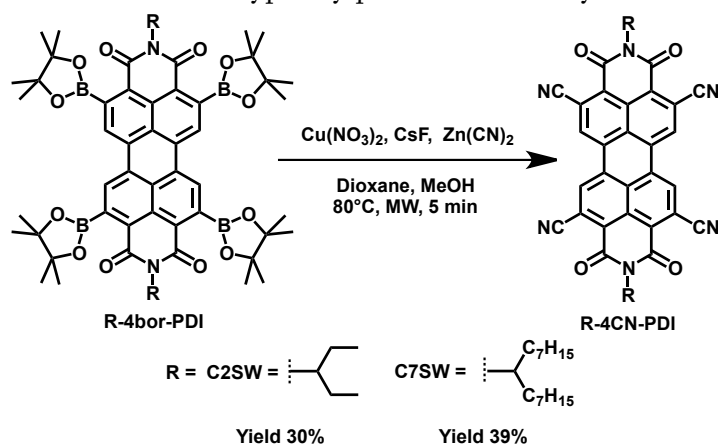
Scheme 44 Direct conversion of **R-4bor-PDI** into **R-4CN-PDI** .

Despite the presence of the solubilizing imide substituents, the two tetracyano derivatives exhibit reduced solubility. **C7SW-4CN-PDI** is soluble exclusively in chlorinated solvents, while the shorter chains of **C2SW-4CN-PDI** are only partially preventing aggregation. Solubility lower than 0.5 mg/mL in chloroform and dichloromethane was observed, allowing only partial characterization of the material.
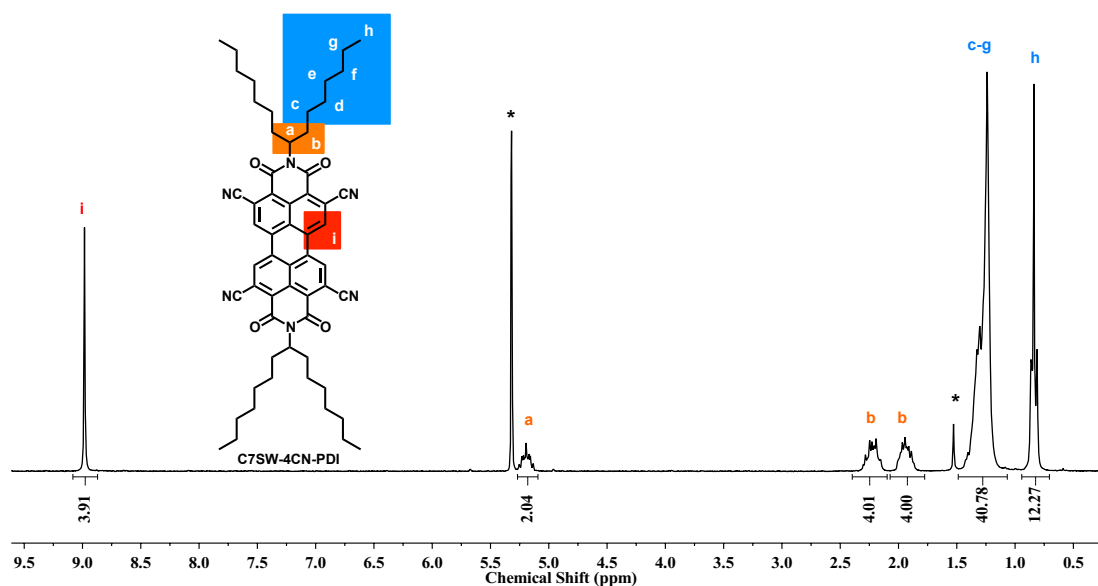
Figure 45 ^{1}H-NMR of **C7SW-4CN-PDI** in CD$_2$Cl$_2$

The ^{1}H-NMR of **C7SW-4CN-PDI** (Figure 45) exhibits one singlet in the aromatic region (H^i around 9 ppm), proving the symmetric substitution of the *ortho*-positions. The remarkable downfield shift of the signal assigned to the *bay*-hydrogens is a consequence of the strong electron withdrawing character of the nitriles.

The one-step conversion of boronates into nitriles is very appealing due to the short reaction times and the reduced number of steps. However the reaction yields are rather low due to the formation of numerous side products. Hence the isolation of the target molecule requires several chromatographic purifications. Therefore this synthetic protocol would definitely not be suitable for up-scaling or for the synthesis of derivatives bearing less solubilizing imide substituents not allowing column chromatography.

Since at the time of these investigations, no other synthetic routes were known for the direct conversion of boronates into nitriles, a different approach was considered, starting from an alternative building block: the *ortho*-tetrabromo PDI. As already demonstrated in the previous chapter, *ortho*-tetrabromo PDIs can be readily obtained in high yields from the boronates and used as starting materials. Their established chemistry of aryl bromides provides the advantage of a larger number of synthetic possibilities as compared to boronates, especially for the introduction of cyano substituents. For these reasons the tetrabromo **C7SW-4Br-PDI** was screened as alternative starting material. The **C2SW-PDI** based materials were not tested due to the reduced solubility of the final product.

C7SW-4Br-PDI allows the application of cyanation procedures already optimized for *bay*-bromo substituted PDIs, providing also a comparison of the reactivity of the two positions. The protocol featuring copper(I) cyanide in DMF reported by the Wasielewski group was tested due to its expectedly high yields (Scheme 45).[126] Direct application of the literature conditions gave the desired product **C7SW-4CN-PDI** (yield 82 %). Triply cyanated PDI and traces of dimethyl amino substituted perylenediimides were obtained as side products, but could be easily removed via column chromatography.
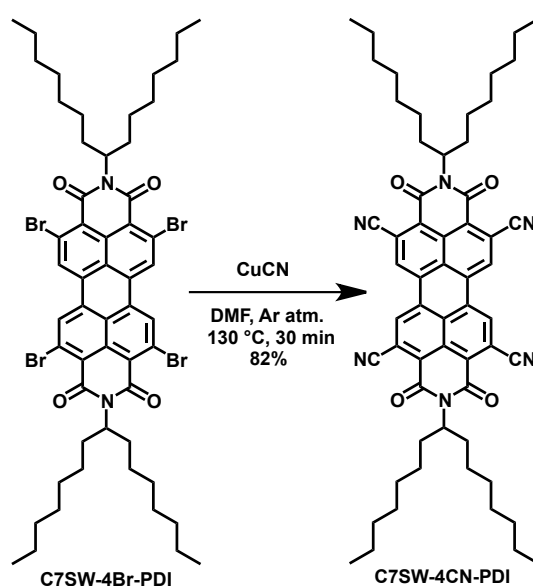
Scheme 45 Cyanation of **C7SW-4Br-PDI**

Compared to the conditions applied for *bay*-cyanation of perylenediimides, **C7SW-4Br-PDI** reacts at lower temperatures in shorter time (130 ℃ for 30 minutes for *ortho*–cyanation and 150 ℃ for 5 hours for *bay*-cyanation), which indicates a more activated nature of these positions towards nucleophilic substitution.

The up-scaling of the reaction was also explored starting from the unsubstituted **C7SW-PDI**. An overall yield of 56 % over three steps could be obtained, with a single chromatographic purification after the final cyanation reaction. In this way, the tetracyano derivative could be synthesized on a gram scale within a week.

The effect of *ortho*-tetracyanation on the optical and electrochemical properties of perylenediimide was investigated via UV-visible optical absorption spectroscopy, photoluminescence spectroscopy and cyclic voltammetry.
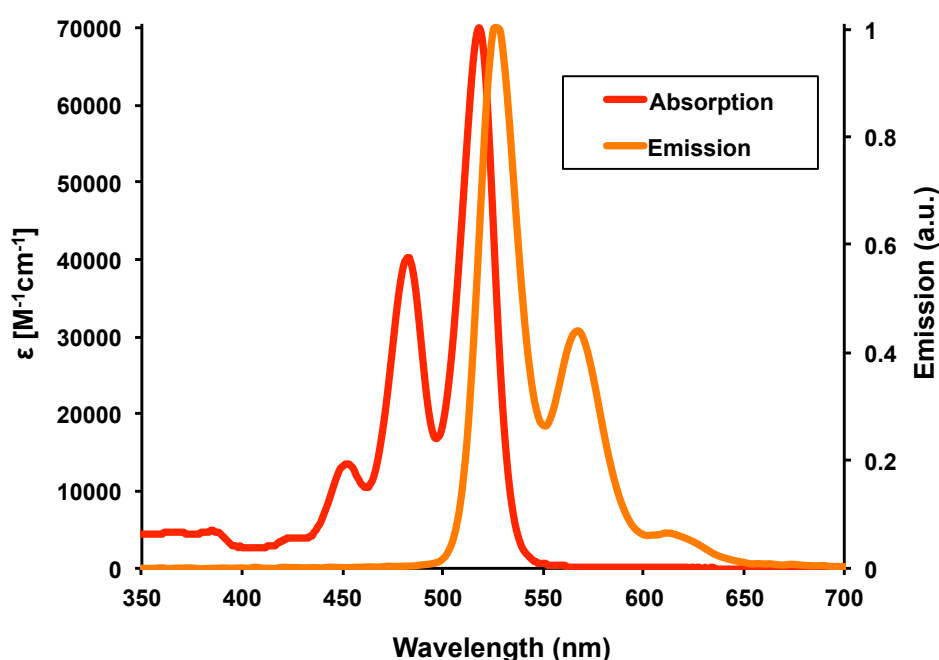
Figure 46 Absorption and fluorescence spectra of **C7SW-4CN-PDI** in dichloromethane ($\lambda_{exc} = \lambda_{max}$).

PDI[a]	ε [M⁻¹cm⁻¹][b]	λ_{max} [nm]	λ_{em} [nm][c]	φ_f[d]
C2SW-PDI	84300	526	538	0,99
C2SW-4CN-PDI	73100	517	525	0,52
C7SW-PDI	81000	526	538	0,97
C7SW-4CN-PDI	70000	518	528	0,55

[a]Optical properties measured in dichloromethane. [b]Measured at λ_{max}. [c]Excited at λ_{max}. [d]Determined using Rhodamine 6G as standard.

Table 12 Optical properties of **C2SW-4CN-PDI**, **C7SW-4CN-PDI** and their parent unsubstituted compounds **C2SW-PDI** and **C7SW-PDI** for direct comparison.

A hypsochromic shift in the absorption and emission and a substantial decrease in the fluorescence quantum yields are observed for **C7SW-4CN-PDI** as compared to **C7SW-PDI** (Figure 46, Table 1). This trend is actually opposite to what is reported in the literature for *bay*-dicyano-perylenediimide, where the introduction of cyano substituents

causes a slight bathochromic shift in both absorption and emission. Furthermore, the introduction of cyano-substituents should actually extend the conjugation length of the system, decreasing the HOMO-LUMO gap and leading to absorption at longer wavelengths as compared to unsubstituted material. One possible explanation may be the formation of strong H-aggregates in solution, due to the strong interaction between the electronpoor molecular cores.

Cyclic voltammetric analysis shows two reversible reduction waves corresponding to the formation of the radical anions and dianions (Figure 47). No oxidation is observed in the potential window investigated. The halfwave potentials, together with the extracted HOMO and LUMO values are reported in Table 2.
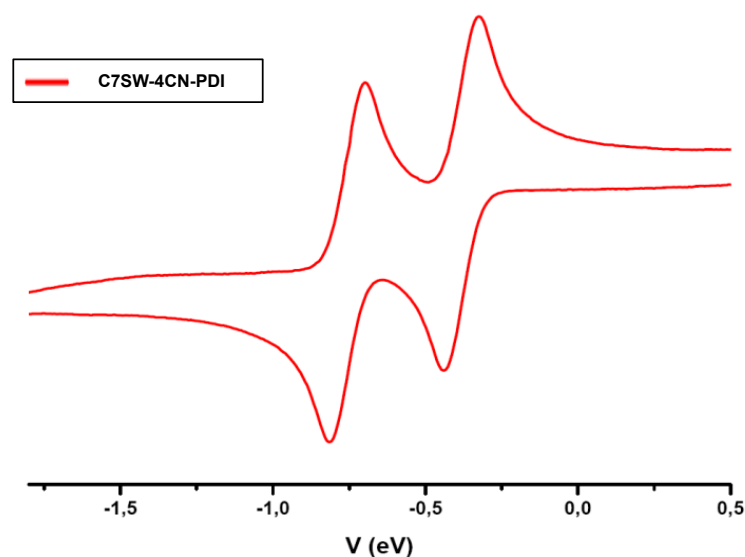
Figure 47 Cyclic voltammetry of **C7SW-4CN-PDI** in dichloromethane.

PDI	E_{red1} [V][a]	E_{red2} [V][a]	LUMO [eV][b]	HOMO [eV][c]
C7SW-PDI	-0,98	-1,21	-3,82	-6,13
C7SW-4CN-PDI	-0,38	-0,75	-4,42	-6,73

[a]Determined by cyclic voltammetric measurement in 0,1 M solution of Bu_4NPF_6 in CH_2Cl_2: vs Fc/Fc$^+$.
[b]Estimated vs. vacuum level from $E_{LUMO} = 4.80$ eV - E_{red1}. [c]Estimated from HOMO = LUMO - E_g, where E_g = optical gap, calculated from the optical absorption data.

Table 13 Electrochemical properties and estimated HOMO and LUMO levels of *ortho*-tetracyanated PDIs and their parent unsubstituted compounds.

A substantial enhancement of the electron affinity as compared to the unsubstituted PDIs is achieved. The estimated LUMO value of -4.4 eV is the lowest reported in the literature for N,N'-alkyl-substituted perylenediimides. Lower values are known only for a *bay*-cyanated-PDI bearing a perfluorinated alkyl chains on the imide, as shown in Figure 48
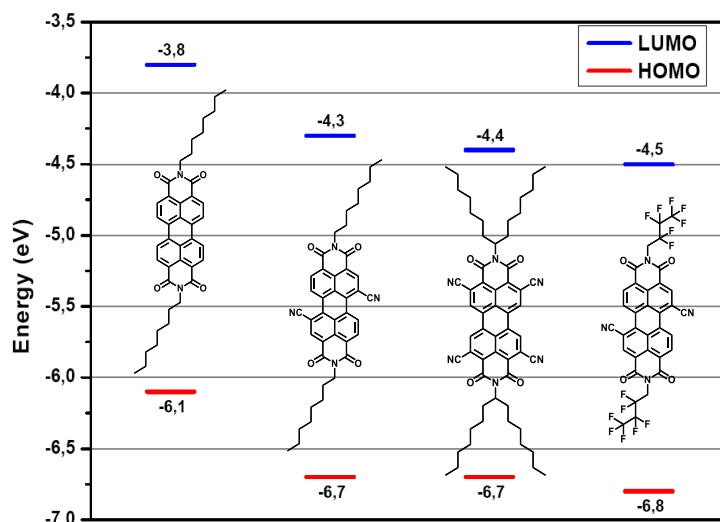
Figure 48 HOMO and LUMO levels of **C7SW-4CN-PDI** compared with those of the best PDI-based n-type semiconductors.

The possibility to use **C2SW-4CN-PDI** and **C7SW-4CN-PDI** as n-type semiconducting materials was explored. Bottom-gate bottom-contact field effect transitors were fabricated by ▮▮▮▮▮▮▮▮ using the two perylenediimides as channel materials. The experimental details are reported in the caption of Table 14. For **C2SW-4CN-PDI** no field effect mobilities could be measured in devices fabricated via drop-casting or vapor-deposition.

Table 14 Extracted performance data for **C7SW-4CN-PDI**.

	μ_{sat} (cm^{2}V^{-1}s^{-1})	I_{ON}/I_{OFF}	V_{SO} (V)
C7SW-4CN-PDI	1.5 ($\pm$ 1.2) x 10^{-6}	1.6 ($\pm$ 0.4) x 10^2	61.3 ($\pm$ 2.0)

For the devices fabricated and studied, highly doped silicon was used as the gate electrode, while the dielectric was a 200 nm thick thermally grown SiO$_2$ film. The substrates were silanized using HMDS by vapor deposition (resulting in contact angles of 93.2 $\pm$ 1.3). A series of bottom contact FETs (10/40 nm Ta/Au electrodes with channel length of 5-100 μ m and width of 0.35 to 7.0 mm, W/L = 70) was prepared by drop-casting 10 gL^{-1} chloroform solutions. Solution processing and electrical characterization by using a Keithley 4200 machine were performed inside a nitrogen filled glovebox (O2: 0.1 ppm, H2O: 0.0 ppm, p: 1120 Pa, T: 17 °C). The transistor performance data of the active layers made of C7SW-4CN-PDI are listed in table. Herein the average values and the 90 % confidence interval (in parentheses) are specified.

C7SW-4CN-PDI showed instead rather poor charge carrier properties, with a n-type mobility not exceeding 10^{-6} cm^{2}V^{-1}s^{-1} and on/off ratios in the order of 10^2. These performances may be caused by the presence of the α−branched imide substituents that due to their bulkiness usually lead to an unfavorable solid-state packing for good charge carrier mobilities. Furthermore grazing incidence wide-angle X-ray scattering (GIWAXS) performed by ▮▮▮▮▮▮▮▮ showed that **C7SW-4CN-PDI** has an amorphous phase in the thin films, which would explain the low mobilities. The reason of this amorphicity is not clear, since all the other *ortho*-substituted C7SW-PDI derivatives presented in this thesis showed high crystallinity.

7.3 Tuning of the Imide Substituents for the Application in Organic Field Effect Transistors

In the previous section the possibility was demonstrated to obtain two different *ortho*-tetracyano-PDIs. As expected, the fourfold cyanation has lead to stronger electron acceptors, as compared to the *bay*-dicyano-PDIs. However extremely low n-type mobilities could be measured in field effect transistors. To really demonstrate the advantages and disadvantages of *ortho*-substitution over *bay*-functionalization for the synthesis of n-type semiconductors, derivatives bearing the same imide substituents should be compared. In fact the imide functionalization strongly influences the solid-state packing of the molecule. Therefore the same imide substituents of some of the best performing *bay*-dicyano materials should be used.[129]

The derivatives investigated are shown in Scheme 46. **C4F7-PDI** was selected as first candidate. The *bay*-substituted dicyano-PDI bearing this imide substituent exhibits outstanding charge carrier mobilities and good stability in air. Unfortunately application of the borylation protocol did not show any trace of substituted perylenediimide. It is not clear if the reason is a poisoning activity of the fluorine atoms on the Murai catalyst or the high insolubility of **C4F7-PDI**.
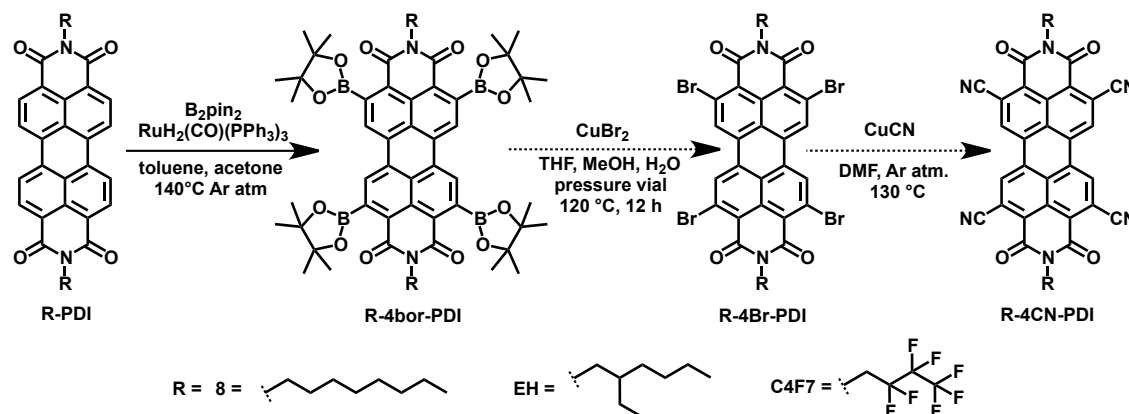
Scheme 46 Explored route for the synthesis of tetracyano-PDIs.

8-PDI and **EH-PDI** were also investigated. These two materials were already used in Chapter 3 for the Murai alkylation reaction and the tetraalkylated derivatives could be synthesized in excellent yields (93 % and 80 % for **8-PDI** and **EH-PDI**, respectively). After applying the borylation protocol to the unsubstituted PDIs, the presence of the desired fourfold substituted product could be detected in FD-MS. However TLC of the reaction mixture showed the presence of only small amounts, together with the violet side product of the reaction and large amounts of unreacted perylenediimide. More diluted environment lead only to marginal improvements. Even though the unreacted materials could be removed by simple filtration due to their reduced solubility, the tetraboronate derivative could not be isolated. The contaminated material was still used for the synthesis of the *ortho*-tetrabromo-PDI, but for **8-PDI** and **EH-PDI** the change in

solubility was so drastic during the reaction, that mainly deborylation occurred (even with concentrations in the order of 1 mg/mL). Even higher dilution may be required for the borylation and halodeboronation reaction (in the order of 0,1 mg/mL), but these conditions make the reaction extremely inefficient in terms of costs. For this reason the synthesis of tetracyano-PDIs was not investigated further.

7.4 Tetracyanation of Terrylenediimides: *Ortho* vs. *Bay*

In the previous section *ortho*-substitution was introduced as a means to lower the energy of the frontier molecular orbitals of perylenediimides. The fourfold introduction of cyano substituents can be used to synthesize strong electron acceptors for potential application in n-type organic field effect transistors. Nevertheless the preliminary work presented above did not lead to materials with good charge carrier mobilities due to presence of imide substituents that hinder favorable solid-state packing. Additionally low solubility limited the possibility to synthesize *ortho*-tetracyano PDIs bearing more suitable imide substituents to be tested in operating devices. Consequently the potentially beneficial effect of *ortho*-cyanation could not be demonstrated.

To directly compare the different effects of *bay*- and *ortho*-substitution, the attention was turned to terrylenediimides. TDIs feature one more naphthalene unit in their conjugated core than PDIs. This structural difference allows tetra-substitution not only in the *ortho*-positions, but also in the *bay*-region, even in the case of sterically demanding substituents. Consequently two tetracyano derivatives could be synthesized via selectively addressing the *ortho*- and *bay*-position, providing a direct comparison for a deeper insight into the effects of the different functionalization geographies on the properties of the system.

Even though less easily accessible than perylenediimides from a synthetic point of view, terrylenediimides are a very interesting platform for the creation of n-type semiconductors. In fact TDIs possess high thermal and chemical stability, low-lying LUMO values and a planar extended conjugated core. Also, the more elongated aromatic system as compared to PDIs favors π-π stacking in the solid-state, fundamental to achieve high charge carrier mobilities. Nevertheless only two publications feature unsubstituted terrylenediimides as organic semiconductor.[130]

C7SW-TDI
Mobility = 1.1 x 10^{-2} cm^{2}V^{-1}s^{-1} (n-type)
= 2.2 x 10^{-3} cm^{2}V^{-1}s^{-1} (p-type)

5-TDI
Mobility = 7.24 x 10^{-2} cm^{2}V^{-1}s^{-1} (n-type)
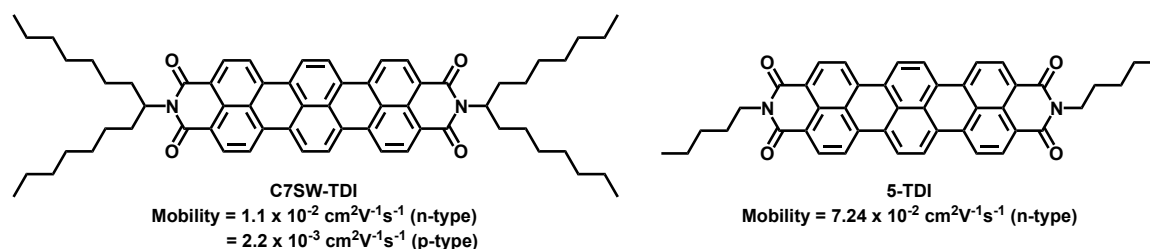
Figure 49 TDIs showing semiconducting properties reported in the literature.

Despite the interesting mobilities no other reports are known about further optimization of this material. In this section the synthesis of two tetracyano terrylenediimides and their application in field effect transistors will be described.

7.4.1 Tetracyanation of Terrylenediimides

The synthesis of the two derivatives started from the common derivative **C7SW-TDI**. This material was chosen as platform for the introduction of the cyano-substituents due to the presence of the long α-branched alkyl chains on the imide. These groups provide enough solubility, enabling the use of standard purification methods. Additionally **C7SW-TDI** is known to show good charge carrier mobilities and even ambipolar behavior, despite the presence of the sterically demanding α-branched imide substituents. In order to achieve selective functionalization of the *ortho*-positions, the ruthenium-catalyzed borylation was applied to obtain **C7SW-4bor-TDI**, as already described in the previous chapter. Further conversion into *o*-**C7SW-4Br-TDI** was achieved using copper(II) bromide and the product was isolated in good yields (82 %). This synthetic route was preferred to the direct conversion of boronates into nitriles due to the higher reaction yields and the easier purification.
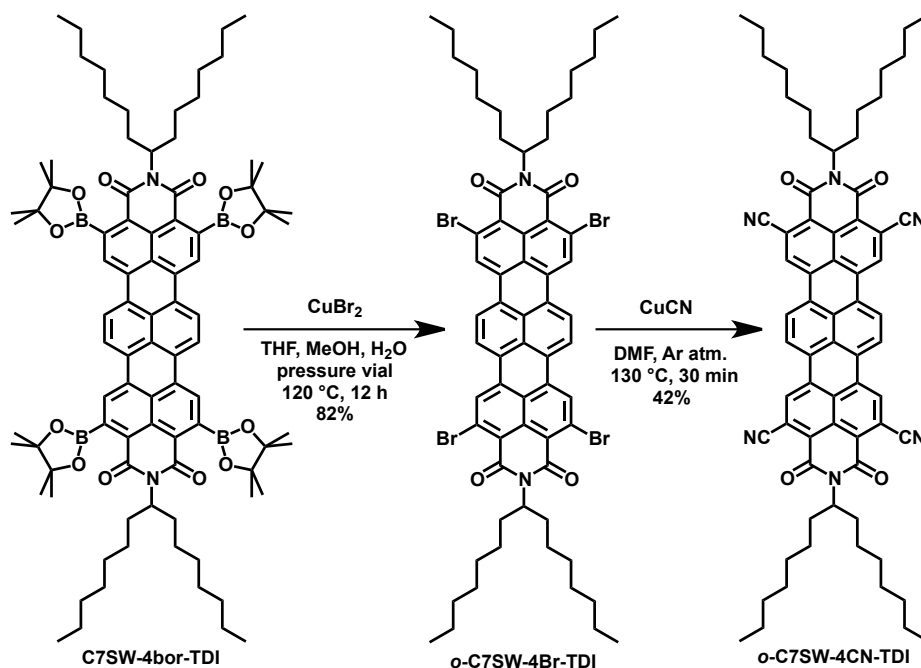
Scheme 47 Synthesis of **o-C7SW-4CN-TDI**.

Dilution was required due to the stronger tendency of TDI to aggregate as compared to PDI, making the deborylation reaction more significant. The final target molecule *o*-**C7SW-4CN-TDI** was achieved via cyanation using copper(I) cyanide in DMF. The moderate reaction yields (42 %) do not properly describe the reactivity of the system. While after reaction *o*-**C7SW-4CN-TDI** was obtained almost quantitatively, removal of

the traces of tri-cyanated side product lead to major losses of the material due to the extreme insolubility of the molecule.

Selective functionalization of the *bay*-positions was achieved via nucleophilic bromination reaction. The tetrabromo derivative *b*-**C7SW-4Br-TDI** was obtained in good yields by bromination using bromine in chloroform. Traces of tribrominated product could be removed from the desired product by successive reprecipitations from dichloromethane in a petrol ether/methanol mixture. The thus obtained tetrabromo derivative was reacted with copper(I) cyanide in anhydrous DMF at 150 °C for 6 hours. In this case the reaction required longer time and higher temperature than the *ortho*-derivatives, revealing a less activated nature of the *bay*-positions toward substitution. The more drastic conditions lead to debromination and substitution with dimethylamine, which is formed from the decomposition of DMF.
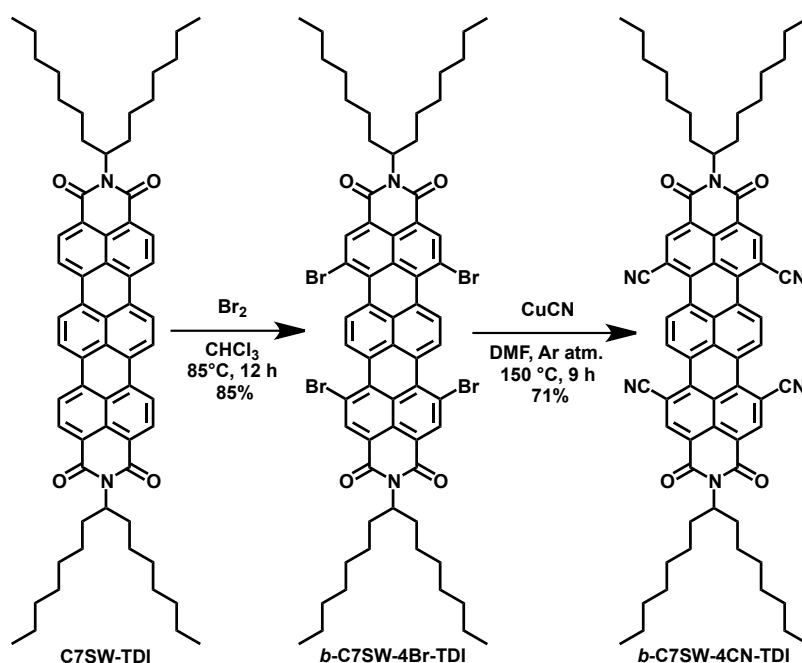
Scheme 48 Synthesis of *b*-**C7SW-4CN-TDI**.

Compared to the unsubstituted starting material **C7SW-TDI,** the fourfold cyanated terrylenediimides exhibit an increased tendency to aggregation. But the functionalization pattern is responsible for the substantial difference in solubility between the two isomers. The *ortho*-substituted derivative *o*-**C7SW-4CN-TDI** exhibits poor solubility at room temperature (lower than 1 mg/mL) even in chloroform and o-dichlorobenzene, in which the twisted *b*-**C7SW-4CN-TDI** appears fairly soluble (7 mg/mL). This behavior can be understood if the calculated geometries of the two systems are compared (Figure 50): while *o*-**C7SW-4CN-TDI** appears to be completely planar, favoring strong π-π interaction, *b*-**C7SW-4CN-TDI** possess a twisted core, with each naphthalene unit being distorted of an angle of about 15° in respect to the neighboring unit.
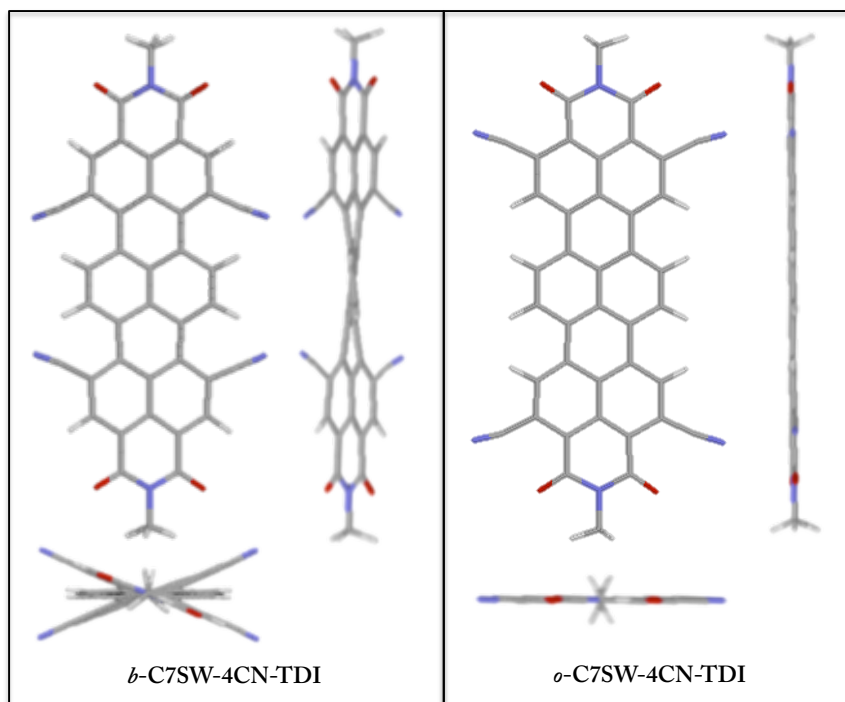
Figure 50 Calculated geometries of N-methyl substituted *ortho-* and *bay-*tetracyano TDIs.

The optical and electrochemical properties of the *ortho-* and *bay-*tetrabromo and tetracyano TDIs were characterized via UV-visible optical absorption spectroscopy, photoluminescence spectroscopy and cyclic voltammetry. The absorption and emission properties are summarized in Table 15 and compared to the unsubstituted **C7SW-TDI**. Both tetracyano-derivatives exhibit a bathochromic shift of about 10 nm in the absorption and emission as compared to the unsubstituted terrylenediimide. The effect of *ortho-*cyanation on the optical properties appears of TDI is different from that of PDI. On the smaller homologue a hypsochromic shift in the absorption is observed compared to the unsubstituted material, while *o-***C7SW-4CN-TDI** absorbs at longer wavelengths instead. All the reported terrylenediimides possess comparable absorptivities, while the quantum yield of fluorescence are slightly lower for the tetrabrominated derivatives, as expected for the heavy atom effect.

Figure 51. Direct comparison of the absorption and fluorescence spectra (left and right, respectively) of *o-***C7SW-4CN-TDI** and *b-***C7SW-4CN-TDI** in chloroform (λ_{ex} = 632 nm for both compounds).

Table 15 Optical properties of *ortho*- and *bay*-tetrasubstituted TDIs.

TDI[a]	ε [M^{-1}cm^{-1}][b]	λ_{max} [nm]	λ_{em} [nm][c]	φ_f^d (λ_{ex})
C7SW-TDI[e]	1.27 X 10^5	651	669	–
o-**C7SW-4Br-TDI**	1.52 X 10^5	640	654	0.89 (632)
b-**C7SW-4Br-TDI**	8.75 X 10^4	651	683	0.79 (632)
o-**C7SW-4CN-TDI**	1.48 X 10^5	661	680	1.00 (632)
b-**C7SW-4CN-TDI**	1.12 X 10^5	657	673	1.00 (632)

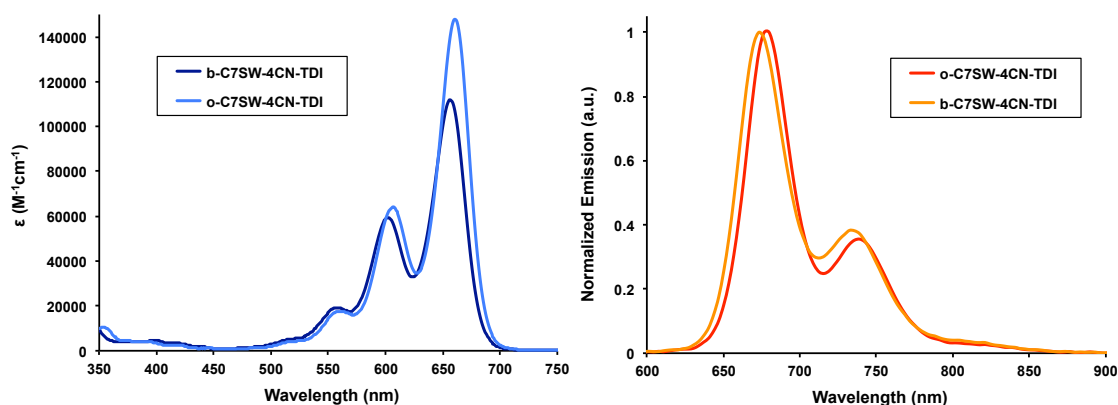[a]Optical properties measured in chloroform. [b]Measured at λ_{max}. [c]Excited at λ_{max}. [d]Determined using Cresyl Violet in methanol as standard. [e]Data from the PhD thesis of Fabian Nolde, Mainz University, 2008.

The electrochemical properties of the tetrabromo and tetracyano derivatives were investigated via cyclovoltammetric measurements, as shown in Table 16. The halfwave oxidation and reduction potentials and extrapolated HOMO and LUMO values are reported. While unsubstituted TDI-derivatives undergo a double electrochemical reduction at the same potential, the two cyanated derivatives show instead two distinct reduction peaks. This behavior must be connected with the fourfold introduction of cyano substituents, since it is not observed for the two tetrabromo terrylenediimides reported here. Interestingly **o-C7SW-4CN-TDI** appears to undergo a third reduction at -2.01 V.
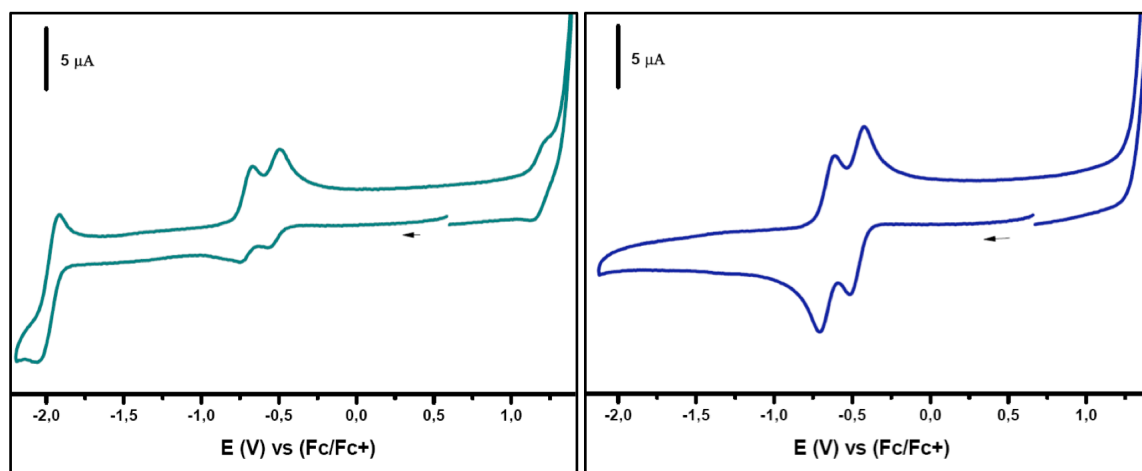
Figure 52 Cyclic voltammetric measurement for *o*-**C7SW-4CN-TDI** (left), and *b*-**C7SW-4CN-TDI** (right).

The LUMO and HOMO levels of the two tetracyano isomers, estimated from the electrochemical measurements and the optical bandgap respectively, appear substantially lowered in energy as compared to the parent unsubstituted **TDI** (having LUMO located at about -3.6 eV and HOMO at -5.3 eV).[130a] The *bay*-substituted derivative shows a slightly larger electron affinity as compared to the *ortho*-isomer. Nevertheless the different functionalization pattern does not appear to cause major differences on the optical and electrochemical properties of the two tetracyano isomers.

Table 16 Electrochemical properties of the reported terrylenediimides determined by cyclic voltammetric measurement.

Compound	Δ_{abs}[a]	E_{ox}	E_{red1}	E_{red2}	E_{red3}	HOMO[b]	LUMO[c]
b-C7SW-4Br-TDI	1.79	0.94	-0.97	-	-	-5.74	-3.83
o-C7SW-4Br-TDI	1.86	0.96	-0.99	-	-	-5.76	-3.81
b-C7SW-4CN-TDI	1.81	-	-0.47	-0.66	-	-6.14	-4.33
o-C7SW-4CN-TDI	1.80	-	-0.54	-0.73	-2.01	-6.06	-4.26

Measured in 0,1 M solution of Bu_4NPF_6 in CH_2Cl_2: vs Fc/Fc$^+$. The values reported are referred to half wave potentials. [a]Optical bandgap. [b]Estimated vs. vacuum level from $E_{HOMO} = 4.80$ eV $+ E_{ox1}$. [c]Estimated vs. vacuum level from $E_{LUMO} = 4.80$ eV $- E_{red1}$.

The remarkable lowering of LUMO energies of the two tetracyano derivatives makes these molecules suitable for their application as n-type semiconductors in field effect transistors. In the next section the device fabrication and thin film characterization will be presented.

7.4.2 OFET Fabrication and Morphological Characterization

The charge carrier transport properties of *o*-C7SW-4CN-TDI and *b*-C7SW-4CN-TDI were investigated by ▮▮▮▮▮▮▮▮▮▮ using bottom-gate, bottom-contact FETs with a hexamethyldisilazane (HMDS) SiO_2 dielectric. In the first step, both TDIs were deposited by drop-casting a 5 mg/mL chlorobenzene solution on FET substrates heated at 100 °C in nitrogen atmosphere, followed by annealing at 250 °C for 1 h.

As previously mentioned, while *b*-C7SW-4CN-TDI is fairly soluble, the planar *o*-C7SW-4CN-TDI exhibits a strong tendency to aggregate. Consequently thermal treatment was necessary to dissolve *o*-C7SW-4CN-TDI at the concentration used for the device fabrication. The devices prepared from drop-casting of a chlorobenzene solution of the material showed no field-effect response under nitrogen atmosphere. Since this result was most probably influenced due to the poor solubility, a different processing method was tested.
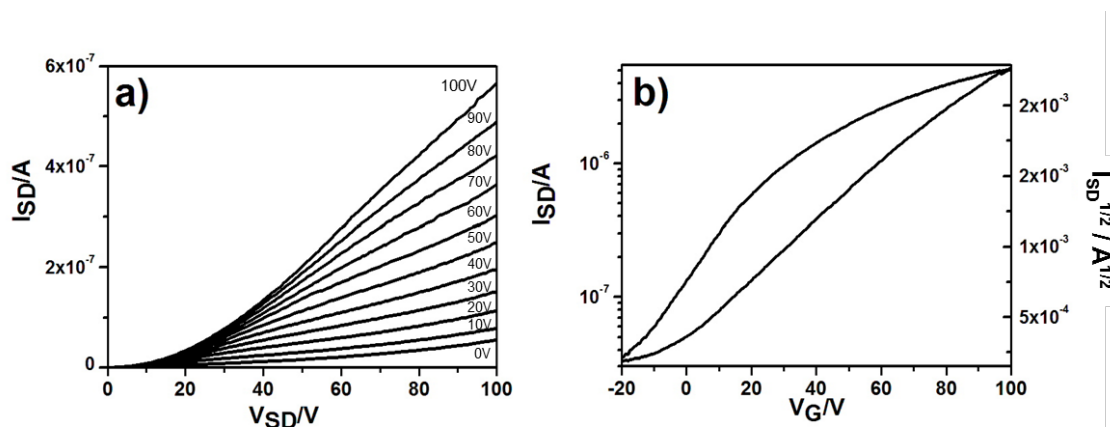

Figure 53 Field-effect transistor performance of **o-C7SW-4CN-TDI** drop-cast from a 5 mg/mL chloroform solution: a) output characteristics at various gate biases V_G and b) transfer curve at a source drain bias of $V_{SD} = 100$ V.

A diluted chloroform solution of *o*-**C7SW-4CN-TDI** was prepared. The amount of solvent was then reduced by controlled evaporation, until a higher concentration was reached for immediate drop casting in air. For these films a field-effect could be measured. However only moderate maximum n-type performance of 10^{-3} cm^{2}V^{-1}s^{-1} and 1×10^2 on/off ratio were measured (Figure 53). The low on/off ratio and the incomplete saturation in the output FET curves may be due to partial doping of the material due to the presence of impurities deriving from the processing in air or vicinity of the dielectric interface.[131] Contributions deriving from other impurities present in the material can be excluded due to the extremely highi purity, achieved via column chromatography and reprecipitation processes and confirmed by analytical characterizations. Further thermal treatment of the devices or solvent annealing did not lead to any improvement in the performances. Additionally, processing from alternative solvents could not be performed due to the high insolubility of the material, causing precipitation already before the deposition of the film.

In the case of *b*-**C7SW-4CN-TDI**, the devices fabricated from drop-casting of the chlorobenzene solution showed instead electron mobilities up to 0.18 cm^2/Vs with on/off ratio of 5×10^3 (Figure 54). The performances here described for *b*-**C7SW-4CN-TDI** are comparable to those of *bay*-dicyanoperylenediimide measured for solution processed OFET (0.15 cm^2/Vs with on/off ratio of 10^3 under inert atmosphere), previously reported in the literature.[132]
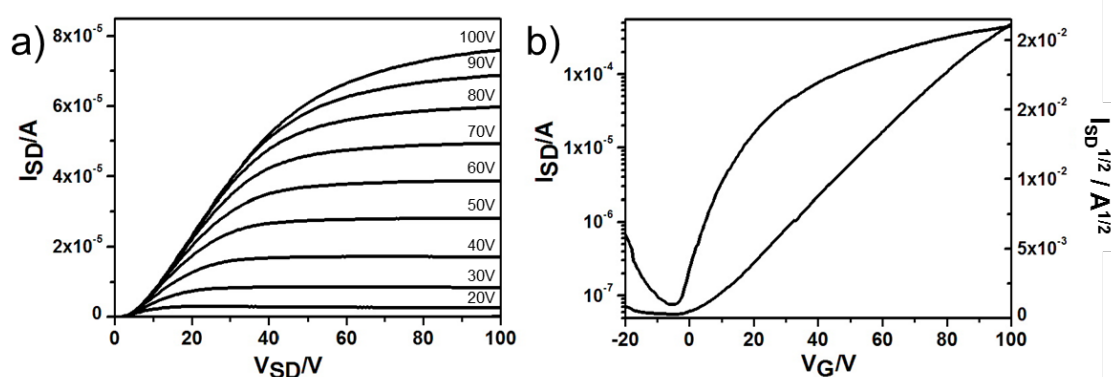
Figure 54 Field-effect transistor performance of *b*-**C7SW-4CN-TDI** drop-cast from a 5 mg/mL chlorobenzene solution a) output characteristics at various gate biases V_G and b) transfer curves at a source-drain bias of V_{SD} = 100 V.

The deep LUMO level of *b*-**C7SW-4CN-TDI** is supposed to favor electron injection from the Au electrode as suggested by the low threshold voltage of around 0 V. However, the nonlinear rise of the current at low source-drain voltage in the output curves is a sign for trapping at the dielectric interface, doping due to the presence of impurities (to be excluded due to the extremely high purity of the material) or/and high contact resistance. To rule out interfacial problems, top-gate devices were fabricated by spin-coating *b*-**C7SW-4CN-TDI** and a subsequent PMMA dielectric on top of the active layer. An electron mobility of only 6×10^{-3} cm^2/Vs was determined, most probably due to the fast solvent evaporation leading to molecular disorder. More importantly, a similar nonlinear trend of the source-drain current was measured as in the case of the bottom-gate transistor. This outcome points towards a charge injection barrier at the electrodes, which

may be related to molecular disorder (see below the structural investigation by GIWAXS).

To understand the substantial difference in performances between *o*-**C7SW-4CN-TDI** and *b*-**C7SW-4CN-TDI**, the supramolecular organization in the films was investigated via grazing incidence wide-angle X-ray scattering (GIWAXS). Surprisingly, despite the low solubility after casting from both solvents chlorobenzene and chloroform, *o*-**C7SW-4CN-TDI** reveals a pattern with well defined, intensive reflections which are characteristic for highly ordered molecules on the surface (Figure 55a). Based on these results ▮▮▮▮▮▮▮▮ derived a model for the organization. Reflections on the meridional plane of the pattern (along q_z at $q_{x,y} = 0$ Å^{-1}) are related to layers which are arranged parallel to the substrate. The main reflection and its higher order ones (*h00*) are related to an interlayer distance of 2.02 nm, which is in agreement with the size of tilted TDI towards the surface. Scattering intensities on the equatorial and off-equatorial planes of the pattern are ascribed to the molecular packing within the layers. The off-equatorial reflections correspond to a tilting towards the layer axis, which is typical for crystalline disc-shaped molecules.[133] A π-stacking distance of 0.34 nm and a tilting angle of 50° in respect to the surface are determined from the off-equatorial reflection with the highest intensity. The arrangement of *o*-**C7SW-4CN-TDI** on the surface is illustrated in Figure 55b. This organization is in agreement with the bulk organization as found by two-dimensional wide-angle X-ray scattering (2DWAXS) on extruded, macroscopically aligned fibers. The 2D pattern indicates also highly crystalline layer structure in which the TDI molecules are tilted. Interestingly, *o*-**C7SW-4CN-TDI** is not packed in a helical manner as other TDI derivatives,[130a,134] but the cores seem to be shifted at least along the long molecular axis. In the earlier cases, the molecules were rotated towards each other in order to overcome the steric hindrance of the side chains.
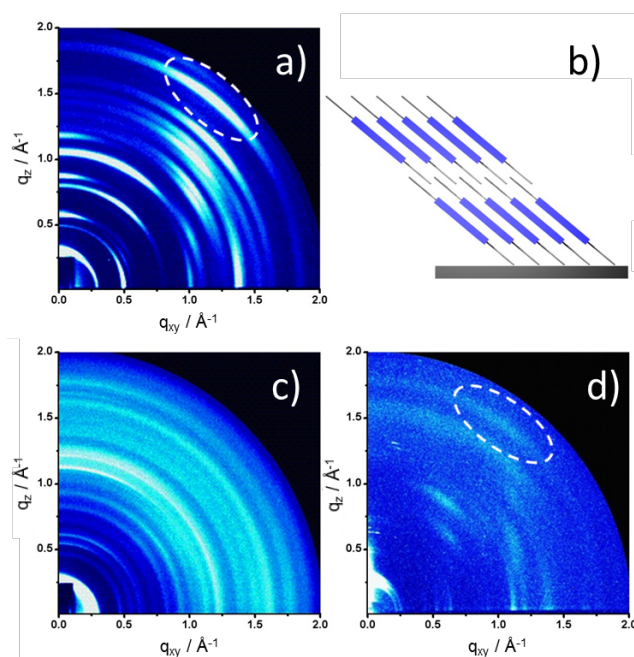
Figure 55 GIWAXS of a) *o*-**C7SW-4CN-TDI** (drop-cast from chlorobenzene), b) schematic illustration of the surface arrangement of *o*-**C7SW-4CN-TDI** after drop-cast from chlorobenzene; c) *b*-**C7SW-4CN-TDI** (drop-cast from chlorobenzene), d) SVD processed *b*- **C7SW-4CN-TDI**. Dashed circule indicates the π-stacking reflection.

In strong contrast to the pronounced surface order of *o*-**C7SW-4CN-TDI**, the GIWAXS pattern of *b*-**C7SW-4CN-TDI** shows a high number of quite isotropic reflections implying crystallinity, but low degree of preferential orientation of crystallites with respect to the substrate (Figure 2c). This means that the molecules are packed in domains, which are oriented relatively randomly towards the surface. Due to this lack of preference for a specific orientation and pronounced long-range disalignment a detailed structure analysis was not possible. The first main scattering intensity related to the interlayer spacing is located at an identical position as for *o*-**C7SW-4CN-TDI**. Additionally, it is possible to identify a reflection, which corresponds to the π-stacking of 0.35 nm. To conclude the GIWAXS analysis, both compounds are crystalline, but *o*-**C7SW-4CN-TDI** organizes on the surface in more defined way than *b*-**C7SW-4CN-TDI**. This is surprising since an enhanced charge carrier transport should be expected for the derivative exhibiting long-range organization. In this case it is instead observed for the highly misaligned *b*-**C7SW-4CN-TDI**, that due to the molecular disorder should feature a higher number of defects, responsible for increased charge trapping and low device performance. Therefore the difference in behavior should derive from the different morphologies of the film.

Indeed a better understanding of the different FET performances of the two materials could be gained by confocal surface measurement system. *b*-**C7SW-4CN-TDI** and *o*-**C7SW-4CN-TDI** both processed from chlorobenzene were inspected (Figure 56). The microstructure of the films of compound *o*-**C7SW-4CN-TDI** shows a significantly higher surface roughness consisting of large aggregates in comparison to the relatively smooth film of *b*-**C7SW-4CN-TDI**. This difference is directly connected to the variation in solubility between both TDI derivatives. The highly insoluble *o*-**C7SW-4CN-TDI** probably aggregates already in solution and precipitates on the surface during casting. Therefore the *o*-**C7SW-4CN-TDI** molecules are well organized as indicated by the above discussed GIWAXS data, but the numerous grain boundaries between the aggregates act as serious trapping sites for charge carriers and lead finally to a lack of any field-effect response. In the case of *b*-**C7SW-4CN-TDI**, the disordered, but larger domains guarantee instead good charge carrier transport throughout the film.

Furthermore the investigations about the morphology of the film could explain the behavior of the two materials after exposure to air. In the case of the *b*-**C7SW-4CN-TDI** the mobility slightly decreased from 0.16 cm^2/Vs to 0.11 cm^2/Vs, maintaining the same on/off ratio, to further decrease after prolonged exposure. Similarly *o*-**C7SW-4CN-TDI** showed a reduction of the mobilities, which could not be exactly quantified due to the low reproducibility of the results. Nevertheless, according to previous reports correlating LUMO level energies and stability in air, both TDI derivatives should exhibit air-stability under operating conditions, thanks to their low-lying LUMO level.[126] However, the packing of the materials also plays a crucial role and the large number of grain boundaries present in the *o*-**C7SW-4CN-TDI** and the disordered domains of *b*-**C7SW-4CN-TDI** may provide preferential pathways to water and oxygen to penetrate into the active layer, decreasing the performances of the materials. This behavior may be due to the formation

of a metastable complex between the n-type semiconductors and oxygen, since the performances rose again after taking the devices back into the glovebox. Nevertheless, also in this case the behavior could not be exactly quantified due to the lack of reproducibility of the results.
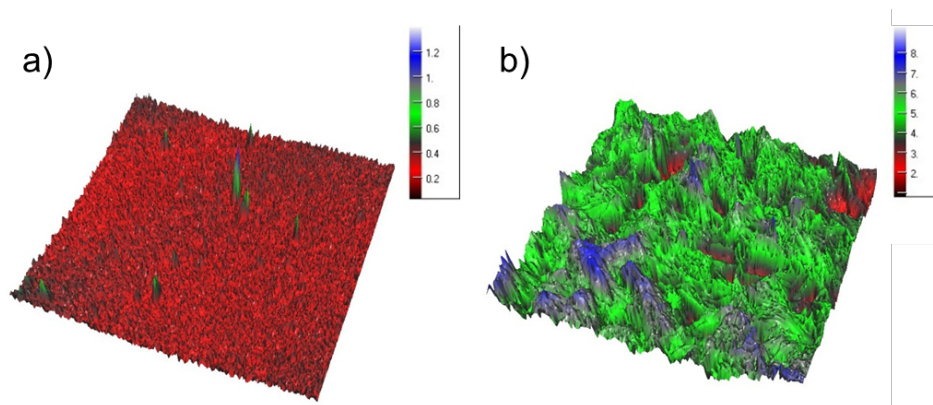

Figure 56 Confocal 3D topographic images of a) *b*-**C7SW-4CN-TDI** and b) *o*-**C7SW-4CN-TDI** after drop-casting from 5 mg/mL chlorobenzene.

Finally, considering the good performances obtained using *b*-**C7SW-4CN-TDI** despite the fairly misaligned crystalline domains, experiments to further improve the mobilities of this molecule in device were attempted. To induce molecular order, solvent vapor diffusion (SVD) was applied on the film of *b*-**C7SW-4CN-TDI** in bottom-gate, bottom-contact HMDS modified devices. This processing method permits to control the self-assembly of the molecules on the surface during solvent evaporation.[135] Thereby, a drop of a dichlorobenzene solution was exposed to saturated dichlorobenzene of the same solvent in an airtight container. After the solvent was evaporated, long-range aligned, continuous films were obtained with improved saturated electron mobility up to 0.65 cm²/Vs and on/off ratio of 2.5×10^4 under nitrogen conditions. The increase in mobility can be attributed as one factor to the fiber alignment along the transistor channel, which is considered to be beneficial to the charge carrier transport. The second reason is the higher molecular order as evident from the GIWAXS pattern for the SVD obtained film (Figure 55d). In fact the shape of the reflections changes from isotropic for the drop cast layer to more distinct for the SVD film. The analysis of the pattern indicates an identical organization of *b*-**C7SW-4CN-TDI** as determined for the drop-cast *o*-**C7SW-4CN-TDI**. Thereby, the molecules are also assembled into layers and are tilted by ca 55° towards the surface. The π-stacking of 0.35 nm remains unchanged in comparison to the drop-cast layer. However, the crystallinity of SVD processed *b*-**C7SW-4CN-TDI** remains significantly lower than *o*-**C7SW-4CN-TDI** as highlighted by the lack of higher order scattering intensities and larger FWHM (full width at half maximum) of the reflections. These results confirm the high potential of terrylenediimides as scaffolds for the synthesis of small molecule n-type semiconducting materials for solution processed OFET and at the same time leave open the possibility to further enhance the

performances of tetracyano terrylenediimides by targeted modification of the imide substituents.

7.5 Synthesis of N-H Rylenediimides

In 2001, the Bao group demonstrated the possibility to improve the field effect performances of a quaterrylenediimide derivative via thermal cleavage of its imide substituents.[136] The reaction was described for two different derivatives bearing on the imide α-branched alkyl substituents, which after thermal treatment in vacuum afforded the clean N-H substituted quaterrylenediimide (Scheme 49). The only side product of the reaction was the alkene, obtained from the cleaved substituent, that could be easily removed under reduced pressure. This method provides a clean and effective synthetic route for the synthesis of N-H rylenediimide pigments, often difficult to be synthesized due to their insolubility.
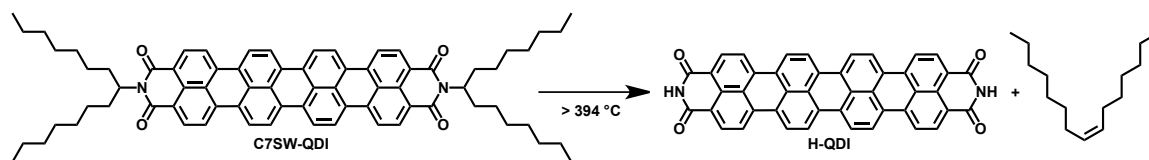
Scheme 49 Synthesis of NH-quaterrylenediimide via thermal cleavage of the imide substituents.[136]

This class of pigments is not only of interest due to their high thermal stability, but also as semiconducting materials. The absence of imide substituents favors a more dense packing of the molecules, which prevents penetration of oxygen and water, improving the stability of the operating devices. Additionally NH derivatives favor the formation of larger grain size and closer π-π interaction due to the possibility to form hydrogen bonds, as already demonstrated in the case of octachloro PDI and *bay*-tetrachloro perylenediimide.[137] Consequently the synthesis of NH-tetracyano-rylenediimides could provide a very interesting class of semiconducting materials.

The tetracyano-PDIs and TDIs described in this chapter feature α-branched alkyl substituents on their imide. Therefore they would be suitable systems to undergo thermal cleavage reaction to give NH-unsbstituted derivatives with high purity. To explore the reaction, the first investigations were performed on the parent unsubstituted compounds **C7SW-PDI**, **C2SW-PDI** and **C7SW-TDI**. Preliminary thermal gravimetric analysis (TGA) of these derivatives showed a first pronounced mass loss at about 350 °C followed by a range in which the molecules appear to remain stable before undergoing the next decomposition reaction (Figure 57). The data obtained from TGA are summarized in Table 17. The calculated retained mass after thermal cleavage of the imide substituents is also reported. As it can be seen, experimental and calculated values are in good agreement with what is expected for the cleavage reaction, except in the case of **C2SW-PDI**, which undergoes a more pronounced mass loss. A higher thermal stability is observed in the case of the **NH-TDI** derivative as compared to **NH-PDI**. Thus, the reaction was tested on

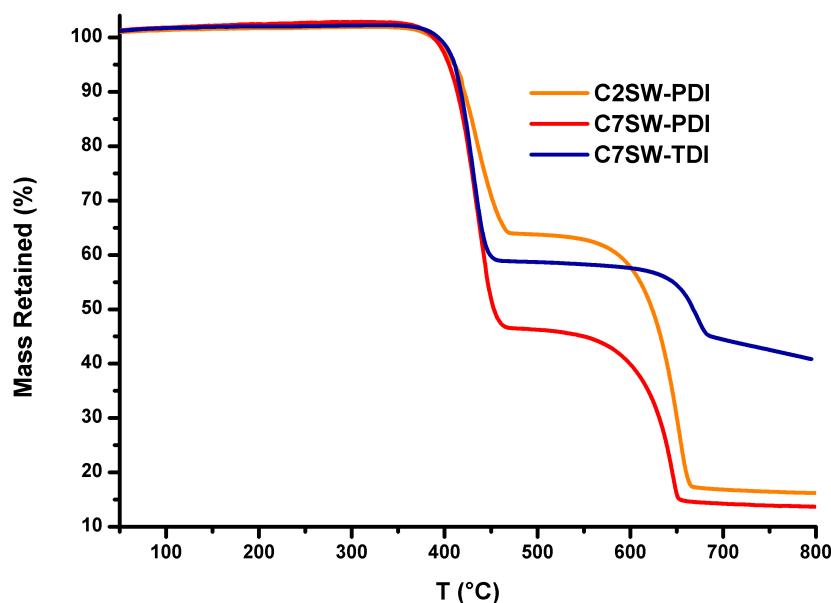the three investigated unsubstituted derivatives (reports the reaction of **C7SW-TDI** is depicted in Scheme 50).

Figure 57 Thermal gravimetric analyses of **C2SW-PDI**, **C7SW-PDI** and **C7SW-TDI**.

Molecule	Decomposition Temperature 1 [°C]	End Decomposition Temperature [°C]	Decomposition Temperature 2 [°C]	Retained Mass [%] (Measured)	Retained Mass [%] (Calculated)
C2SW-PDI	386	475	506	64	73
C7SW-PDI	387	478	505	46	48
C7SW-TDI	391	468	546	59	55

Table 17 Extrapolated values from the TGA of **C2SW-PDI**, **C7SW-PDI** and **C7SW-TDI**, compared with the theoretical values associated to the thermal cleavage of the imide substituents.

In all three cases the rylenediimide was sealed under vacuum in a glass ampoule and successively heated in an oven, following a temperature gradient over 90 minute to reach the desired reaction temperature. Successively the temperature was maintained constant for 90 minutes and finally the system was cooled down to the initial temperature over 90 minutes. After reaction the materials showed a substantial change in color and morphology. The two perylene derivatives had a dark purple color, typical of the NH substituted materials, well known in the field of organic pigments. A dark solid with metallic reflections was obtained in the case of the terrylene derivative. Colorless drops were also present in the ampoules in the case of **C7SW-PDI** and **C7SW-TDI**, most probably the pentadecene formed during the reaction.
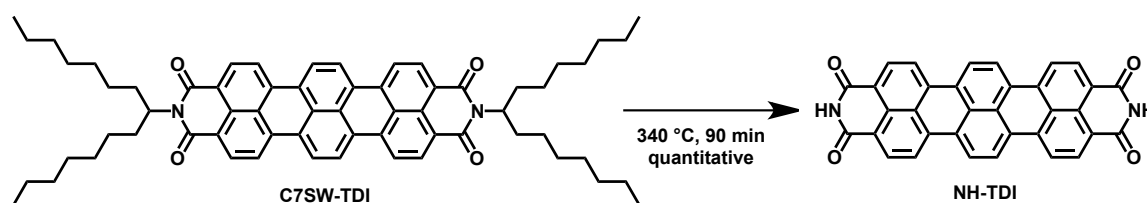
Scheme 50 Thermal cleavage of the alkyl chains of **C7SW-TDI**.

The three target molecules were recovered after opening the ampoules and dried in vacuum oven to remove the side products of the reaction. The desired **NH-PDI** and **NH-TDI** were obtained in quantitative yields. The ^{1}H-NMR of **NH-TDI** in deuterated sulfuric acid is shown in Figure 58. Minor traces of the alkyl chains can be still detected in the aliphatic region, but it is worthwhile noting that no side product is observed in the aromatic region.
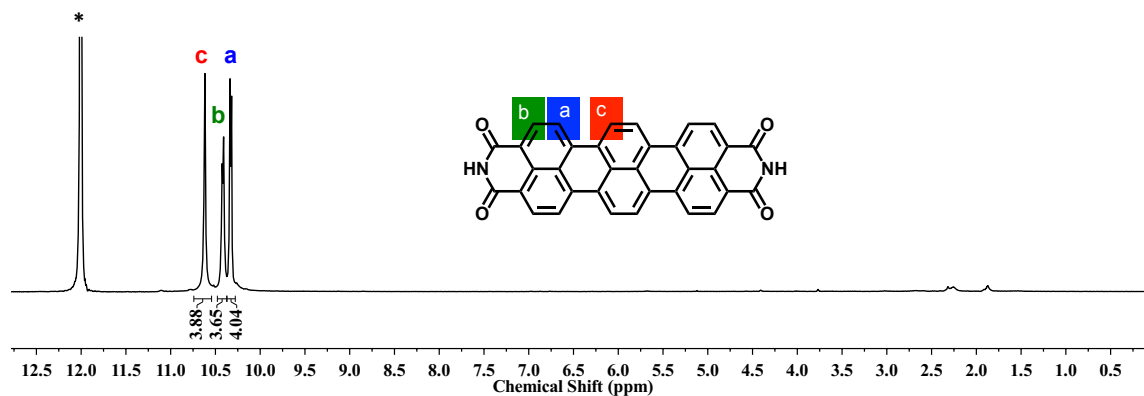
Figure 58 ^{1}H-NMR spectra of **NH-TDI** in D$_2$SO$_4$.

The results obtained from the preliminary screening proved the effectiveness of this synthetic strategy, in particular in the case of **NH-TDI**. Several routes were previously tested in our group for the synthesis of this material, but the pure material could never be obtained due to the pronounced tendency of the molecule to aggregate, hindering the purification.

The focus was then moved to the tetracyano-rylenediimides. Thermal-gravimetric analysis was performed for **C7SW-4CN-PDI**, *o*-**C7SW-4CN-TDI** and *b*-**C7SW-4CN-TDI**.

Figure 59 Thermal gravimetric analyses of **C7SW-4CN-PDI**, *o*-**C7SW-4CN-TDI** and *b*-**C7SW-4CN-TDI**.

Similar to the unsubstituted compounds, the cyanated derivatives undergo a first mass loss at about 320 °C, followed by a range of temperatures where no modification occ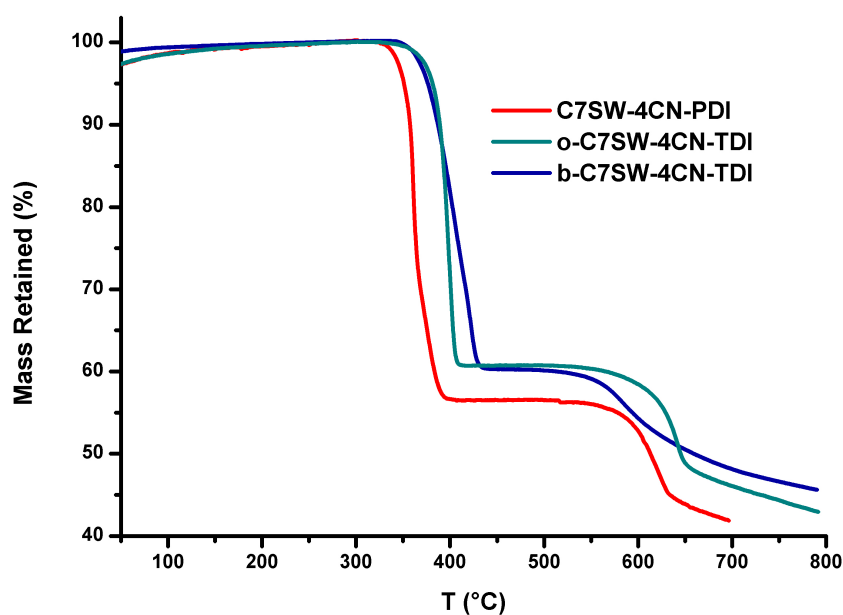urred (Figure 59). The mass percentage retained (Table 18) confirms the selective cleavage of the alkyl chains in the temperature range between 320 °C and 340 °C. **C7SW-4CN-PDI** is the compound undergoing the reaction at lower temperatures (320 °C). In general the presence of cyano groups lowers the temperatures at which the dealkylation occurs, as compared to the parent unsubstituted compounds, but also reduces the range in which the alkylated precursors are stable.

Molecule	Decomposition Temperature 1 [°C]	End Decomposition Temperature [°C]	Decomposition Temperature 2 [°C]	Retained Mass [%] (Measured)	Retained Mass [%] (Calculated)
C7SW-4CN-PDI	320	408	492	57	54
o-**C7SW-4CN-TDI**	330	418	520	61	59
b-**C7SW-4CN-TDI**	342	444	503	60	59

Table 18 Extrapolated values from the TGA of **C7SW-4CN-PDI**, *o*-**C7SW-4CN-TDI** and *b*-**C7SW-4CN-TDI**, compared with the theoretical values associated to the thermal cleavage of the imide substituents.

Due to the good availability of the material, the dealkylation reaction was investigated on **C7SW-4CN-PDI**. The thermal treatment was performed heating the material up to 380 °C. Similarly to the previously studied reactions, a striking change in color from red to black was observed, as well as the presence of pentadecene evolving from the cleavage of the alkyl substituents. The material could be extracted from the ampoule and dried in vacuum to remove the side product of the reaction. In the case of **NH-4CN-PDI** the planar molecule appeared to have a higher tendency to aggregate as compared to **NH-PDI**. In fact after the reaction the unsubstituted PDI could be extracted from the ampoule by simple sonication in dichloromethane and formed finely dispersed small aggregates. **NH-4CN-PDI** remained instead as a solid and had to be manually extracted and separated from the glass of the reaction vial.

Characterization of **NH-4CN-PDI** was attempted. However no mass proof could be obtained from MALDI spectroscopy and the elemental analysis always deviated from the expected values, probably due incomplete combustion of the material. Further, ^{1}H-NMR in deuterated sulfuric acid did not show any definite splitting pattern, but only broad and weak signals. Solid-state ^{1}H-NMR was also investigated, but the bulk material after reaction appears to be highly disordered, therefore leading to undefined signals. Furthermore, due to the strong aggregation no further processing was possible to induce intermolecular order and even sublimation failed with the machines present in house. Therefore the synthetic route was set aside and not extended to the tetracyano terrylenediimide derivatives.

7.6 Conclusion and Outlook

In this chapter the synthesis of the first tetracyano perylenediimide was presented. Two different synthetic protocols were described leading to the target compound. The first one enabled the direct conversion of boronates into nitriles. Yields and purification issues limited the applicability of the method for large scale reaction. The second route, proceeding through the intermediate *ortho*-tetrabromo PDI, afforded instead the desired **C7SW-4CN-PDI** in high yields, allowing even gram scale synthesis. Both protocols emphasized once again the importance of the *ortho*-tetraboronates and tetrahalogenated derivatives presented in the previous chapter as building blocks to achieve novel 2,5,8,11-substituted PDIs.

The preliminary work on the more soluble derivatives **C2SW-4CN-PDI** and **C7SW-4CN-PDI** could demonstrate the effectiveness of *ortho*-tetracyanation in lowering the energy of the LUMO levels of PDI. The lowest reported value for N,N'-alkyl-substituted perylenediimides could be achieved. However only poor n-type mobilities were mesured for **C7SW-4CN-PDI**, due to its amorphous solid phase. The tetracyanation protocol could not be extended to perylenediimides bearing less steric demanding imide substituents, such as linear or β-branched alkyl chains, due to their low solubility. Nevertheless these derivatives would exhibit a closer and more favorable π-π stacking, necessary to achieve high charge carrier mobilities.

The major problems in the synthesis of *ortho*-tetracyano-PDIs arise from the poor solubility of these materials at any temperature in the borylation and successive halodeboronation reaction mixtures. A possible solution could be the introduction of longer alkyl substituents on the imide groups. Explorative experiments were performed using N,N'-octadecyl-PDI. The long linear alkyl imide substituents provided good solubility in hot toluene, xylene, tetrachloroethane and DMF. The tetraborylation reaction afforded the desired product, which could be further converted using the non-purified material into the tetrabromo and tetracyano derivative. No major undesired deborylation or debromination was observed. However the purification and characterization of the materials could not be concluded during the final period of this thesis work. Optimization of the reaction conditions and of the purifications methods combined with a targeted tuning of the lengths of the chains may afford the desired semiconducting materials. Further, the long alkyl substituents would lead to lower melting points as compared to the derivatives bearing shorter alkyl substituents. This would allow thermal annealing processes, which plays a key role to improve solid-state packing and charge carrier mobilities, as already reported for unsubstituted PDIs.[138]

A deeper insight on the major difference between *ortho* and *bay* substitution on the properties of the system could be obtained by directly comparing two different tetracyano TDIs: *o*-**C7SW-4CN-TDI** and *b*-**C7SW-4CN-TDI**. The synthetic protocol optimized for **C7SW-4CN-PDI** enabled the synthesis of *o*-**C7SW-4CN-TDI** in good yields, while *b*-**C7SW-4CN-TDI** was successfully synthesized via bromination and cyanation reaction in high yields. The two tetracyano-TDI isomers show only minor differences in the

optical and electrochemical properties. The absorption and emission of both compounds is bathochromic shifted as compared to the unsubstituted **C7SW-TDI**, while the LUMO values are consistently lowered. *b*-**C7SW-4CN-TDI** exhibits the lowest LUMO value of the two (-4.3 eV). These results further confirm the effectiveness of core tetracyanation in increasing the electron affinities of rylenediimides.

The different substitution patterns of the two teteracyano TDIs strongly influence their solubility, solid-state packing and charge carrier performances as direct consequence of their molecular geometry. The planar conjugated core of the *ortho*-substituted *o*-**C7SW-4CN-TDI** favors strong π-π aggregation and low solubility despite the presence of the bulky imide substituents. Highly oriented films can be obtained from solution, but the strong aggregation upon processing leads to fast precipitation, with the formation of numerous crystalline domains and grain boundaries. This morphology has a direct impact on the performances of the device exhibiting moderate charge carrier mobilities, despite the high molecular order. A quite different situation was observed for *b*-**C7SW-4CN-TDI**. Its twisted conjugated core hinders strong aggregation and makes the material soluble in chlorinated solvents. Solution processing lead to high n-type mobilities in OFET for TDI-based materials (0.18 $cm^2V^{-1} s^{-1}$ under nitrogen, 0.11 $cm^2V^{-1} s^{-1}$ in air). This result could be further improved by solvent vapor diffusion process. Mobilities as high as 0.65 $cm^2V^{-1} s^{-1}$ were obtained in inert atmosphere. However morphology studies revealed less ordered packing in the case of the better performing *b*-**C7SW-4CN-TDI**. The high n-type mobilities derive instead from the larger domains.

The work here reported has demonstrated the high potential of terrylenediimide based materials as n-type semiconductors. However in the future higher electron mobilities may be achieved via targeted replacement of the imide substituents. Considering the low solubility and highly ordered solid-state packing of the *ortho*-tetracyano-TDI, longer α-branched alkyl chains could be used, such as for example decyl-undecyl groups. This may improve processability and favor the formation of bigger crystalline domains. In the case of the more soluble *bay*-tetracyano-TDI, shifting of the branching of the alkyl chains to the β-position may favor a more ordered solid-state packing

Finally the possibility to thermally cleave the alkyl imide substituents of rylenediimides was explored. This method afforded the NH derivatives for core unsubstituted perylene and terrylenediimides in quantitative yields and with analytical purity. The possibility to extend this method to tetracyano rylenediimides was also explored. Unfortunately, the preliminary work performed on **C7SW-4CN-PDI** afforded a material that did not allow structural characterization, most probably due to strong solid-state aggregation.

7.7 References

[121] a) Zhan, X., Facchetti, A., Barlow, S., Marks, T. J., Ratner, M. A., Wasielewski, M. R., & Marder, S. R. (2011), *Advanced Materials*, *23*(2), 268–284. b) Huang, C., Barlow, S., & Marder, S. R. (2011), *The Journal of Organic Chemistry*, *76*(8), 2386–2407. Li, C., & Wonneberger, H. (2012), *Advanced Materials*, *24*(5), 613–636.

[122] Anthony, J. E., Facchetti, A., Heeney, M., Marder, S. R., & Zhan, X. (2010), *Advanced Materials*, *22*(34), 3876-3892. b) Würthner, F., & Stolte, M. (2011), *Chemical Communications*, *47*(18), 5109-5115.

[123] a) Newman, C. R., Frisbie, C. D., da Silva Filho, D. A., Brédas, J. L., Ewbank, P. C., & Mann, K. R. (2004), *Chemistry of materials*, *16*(23), 4436-4451. b) Chang, Y. C., Kuo, M. Y., Chen, C. P., Lu, H. F., & Chao, I. (2010), *The Journal of Physical Chemistry C*, *114*(26), 11595-11601.

[124] Li, Y., Tan, L., Wang, Z., Qian, H., Shi, Y., & Hu, W. (2008), *Organic letters*, *10*(4), 529-532.

[125] a) Ahrens, M. J., Fuller, M. J., & Wasielewski, M. R. (2003), *Chemistry of materials*, *15*(14), 2684-2686. b) Jones, B. A., Ahrens, M. J., Yoon, M. H., Facchetti, A., Marks, T. J., & Wasielewski, M. R. (2004), *Angewandte Chemie*, *116*(46), 6523-6526. c) Gsänger, M.; Oh, J. H.; Könemann, M.; Höffken, H. W.; Krause, A.-M.; Bao, Z.; Würthner, F., (2010) *Angewandte Chemie.–Int. Edit.*, *49*, 740. d) Tang, M. L., & Bao, Z. (2010) *Chemistry of Materials*, *23*(3), 446-455.

[126] Jones, B. A., Facchetti, A., Wasielewski, M. R., & Marks, T. J. (2007), *Journal of the American Chemical Society*, *129*(49), 15259-15278.

[127] a) Osswald, P., & Würthner, F. (2007), *Journal of the American Chemical Society*, *129*(46), 14319-14326. b) Würthner, F. (2006), *Pure and applied chemistry*, *78*(12), 2341-2349.

[128] Liskey, C. W., Liao, X., & Hartwig, J. F. (2010), *Journal of the American Chemical Society*, *132*(33), 11389–11391.

[129] Wang, C., Dong, H., Hu, W., Liu, Y., & Zhu, D. (2012), *Chemical Reviews*, 112(4), 2208–2267.

[130] a) Liu, C., Liu, Z., Lemke, H. T., Tsao, H. N., Naber, R. C. G., Li, Y., et al. (2010), *Chemistry of Materials*, *22*(6), 2120–2124. b) Petit, M., Hayakawa, R., Shirai, Y., Wakayama, Y., Hill, J. P., Ariga, K., & Chikyow, T. (2008), *Applied Physics Letters*, *92*(16), 163301.

[131] Jones, B. A., Facchetti, A., Marks, T. J., & Wasielewski, M. R. (2007), *Chemistry of materials*, 19(11), 2703-2705.

[132] Piliego, C., Jarzab, D., Gigli, G., Chen, Z., Facchetti, A., & Loi, M. A. (2009), *Advanced Materials*, *21*(16), 1573-1576.

[133] Pisula, W., Feng, X., & Müllen, K. (2010), *Advanced Materials*, *22*(33), 3634-3649.

[134] Nolde, F., Pisula, W., Müller, S., Kohl, C., & Müllen, K. (2006), *Chemistry of materials*, *18*(16), 3715-3725.

[135] Wang, S., Dössel, L., Mavrinskiy, A., Gao, P., Feng, X., Pisula, W., & Müllen, K. (2011), *Small*, *7*(20), 2841-2846.

[136] Oh, J. H., Lee, W.-Y., Noe, T., Chen, W.-C., Könemann, M., & Bao, Z. (2011), *Journal of the American Chemical Society*, *133*(12), 4204–4207.

[137] a) Gsänger, M., Oh, J. H., Könemann, M., Höffken, H. W., Krause, A.-M., Bao, Z., & Würthner, F. (2009), *Angewandte Chemie International Edition*, *49*(4), 740–743. b) Ling, M. M., Erk, P., Gomez, M., Koenemann, M., Locklin, J., & Bao, Z. (2007), *Advanced Materials*, *19*(8), 1123-1127.

[138] Tatemichi, S., Ichikawa, M., Koyama, T., & Taniguchi, Y. (2006), *Applied physics letters*, *89*(11), 112108-112108.

8 *Edge*-Functionalization of Perylenemonoimides

8.1 Introduction

The functionalization of the *ortho*-positions had a striking impact on the chemistry of ryleneimides for mainly two reasons: 1) provided additional powerful tools to tailor the properties of RIs, which could be combined or used as alternative to the imide and *bay*-substitution; 2) demonstrated the possibility to address any available site of the rylenediimide structures. If this is true for diimide derivatives, rylenemonoimides still feature two unexplored molecular sites. These sites are located between the *peri*- and the *bay*-positions of the unsubstituted terminal naphthalene unit and, as already mentioned in the introduction, will be defined as *edge*-positions. For perylenemonoimide, the only rylenemonoimide that will be investigated in this chapter, the *edge*-sites correspond to the 8,11-positions (Figure 60).
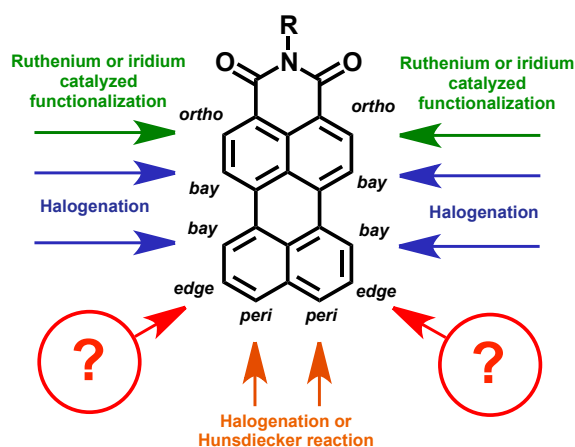

Figure 60 Unsubstituted aromatic core of perylenemonoimide and synthetic methods for their selective functionalization.

The functionalization of the *edge*-positions poses new synthetic challenges, as compared to the imide, *peri*-, *bay*- and *ortho*-modification. In fact the *edge*-sites are not addressable via halogenation or following multistep synthesis. Further, the absence of substituents on the adjacent positions excludes the possibility to use directing groups to coordinate metal catalysts to achieve selectivity.

Despite the synthetic challenges, this new functionalization pattern would be of high interest for several reasons. First of all, perylenemonoimides are ideal scaffolds for the creation of light absorbers for dye sensitized solar cells (DSSC).[139] Their absorption and energy levels can be tuned according to needs via the introduction of substituents on the aromatic core, as demonstrated by ▮ and ▮▮▮▮▮.[140] Therefore the modification of

the *edge*-positions could provide further synthetic solutions for the tuning of the optical and electrochemical properties of PMIs. Additionally the difunctionalization could enable the creation of a push-pull system bearing two donors, interesting alternative to the double *peri*-functionalized perylenemonoimide investigated for long time in our group and only recently reported by ▓▓▓▓▓▓▓▓.[141] Double *edge*-functionalization might also provide a unit to incorporate in conjugated polymers, where the introduction of perylene-based structures may have a beneficial impact on the π-π stacking ability of the materials.[142] Last but not least, the 8,11-positions of PMIs may be addressed to extend the aromatic core of the rylenemonoimide. Aromatic moieties bearing *ortho*-substituents may be introduced and further reacted on the adjacent free *peri-* or *bay*-positions to achieve annulation.

8.2 The Creation of the Building Blocks

A suitable strategy to access the *edge*-positions should ideally satisfy three requirements: selectivity, straightforwardness and versatility. The first two conditions are necessary to make *edge*-functionalization competitive and appealing from a synthetic point of view. A one-step reaction should already provide the desired functionalization pattern. Therefore strategies based on the introduction of cleavable directing groups in the *bay-* or *peri*-positions should be excluded. The third requirement should be satisfied to be able to extend the synthetic protocol to the entire class of rylenemonoimides. Furthermore, versatility should be guaranteed in terms of number of substituents that can be introduced. In order to meet all the above mentioned requirements, the work was oriented toward the development of a synthetic protocol affording one or more building blocks.

Since the *edge*-positions cannot be accessed via halogenation, metal-catalyzed reactions were considered, as in the work presented in Chapter 6. Once again a borylation protocol offered the synthetic solution. In fact, a careful observation of the PMI structure reveals a unique feature of the *edge*-positions: these are the only sites on the molecular skeleton having both *ortho*-positions unsubstituted. This situation already provides the basic conditions to achieve selective functionalization. In fact in 2001 the groups of Miyaura and Hartwig reported an iridium-catalyzed borylation of arenes influenced exclusively by steric factors.[143] More precisely, functionalization occurs selectively at those sites having two unsubstituted *ortho*-positions, as shown in Scheme 51. The factor influencing the reactivity is the rather bulky coordinating sphere of the iridium catalyst, which does not permit the activation of the more congested aromatic positions.
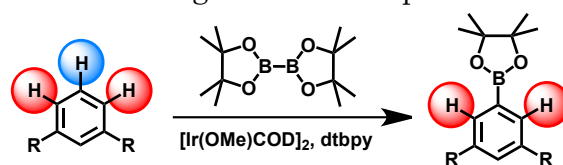
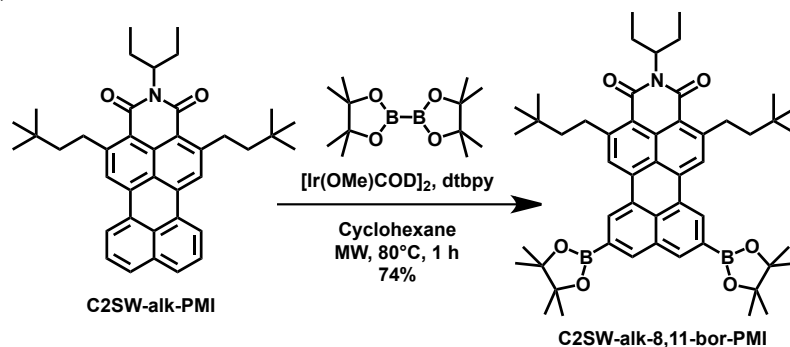**Scheme 51** The iridium-catalyzed borylation of arenes reported by Miyaura and Hartwing in 2001.

This synthetic method has become very popular since it is possible via a one-step reaction to access, in a very selective way, positions that are quite often deactivated and therefore difficult to be functionalized. A large variety of substituents are tolerated, such as carbonyl groups, nitriles, halogens, amines and ethers. Additionally, the precatalyst [IrCl(cod)]$_2$, the ligand 4,4'-di-tert-butyl-2,2'-bipyridine (dtbpy) and bis(pinacolato) diboron are commercially available air-stable compounds.[144] Alkanes are typical solvents for the reaction, while aromatic molecules exhibiting positions able to undergo borylation, such as benzene, toluene or xylene, must be avoided.[143] The protocol can also be combined in several one-pot reactions. [145]

In 2005 the Marder group applied this functionalization method to unsubstituted naphthalene, pyrene and perylene molecules. In the latter case, selective borylation of the 2,5,8,11-positions was achieved to give the perylene tetraboronate shown in Scheme 52.[146]
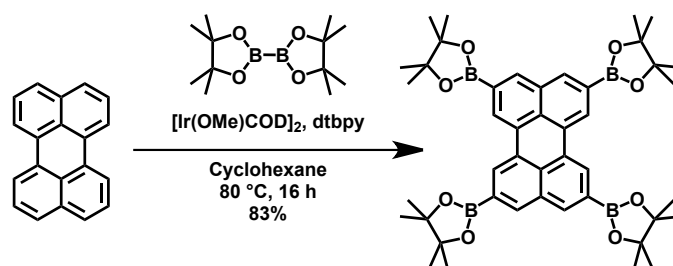
Scheme 52 Iridium-catalyzed tetraborylation of the 2,5,8,11-positions of perylene.

Due to the high yields, good selectivity and straightforwardness of the method, the reaction was tested on a perylenemonoimide derivative. The *ortho*-alkylated **C2SW-alk-PMI** was chosen for the preliminary exploration due to its good solubility in cyclohexane and the reduced number of aromatic protons that could simplify the interpretation of the proton NMR of the product. The reaction was performed in microwave oven to reduce the heating times.[147] The progress was monitored via TLC and FD-MS analysis and the formation of a new species was observed, with a mass corresponding to the desired **C2SW-alk-8,11-bor-PDI**.

Scheme 53 Iridium-catalyzed borylation of the 8,11-positions of **C2SW-alk-PMI**.

After solvent evaporation and a fast filtration over silica to remove small impurities, the desired product could be isolated as a bright orange solid in high yield (74 %).

The ¹H-NMR of the compound clearly shows that the functionalization took place selectively at the 8,11-positions (Figure 61). Only three singlets are observed in the aromatic region, corresponding to the *peri-* and *bay-*protons of the perylene core. In the aliphatic region the signal deriving from the methyl groups of the pinacol ester is well visible, instead.
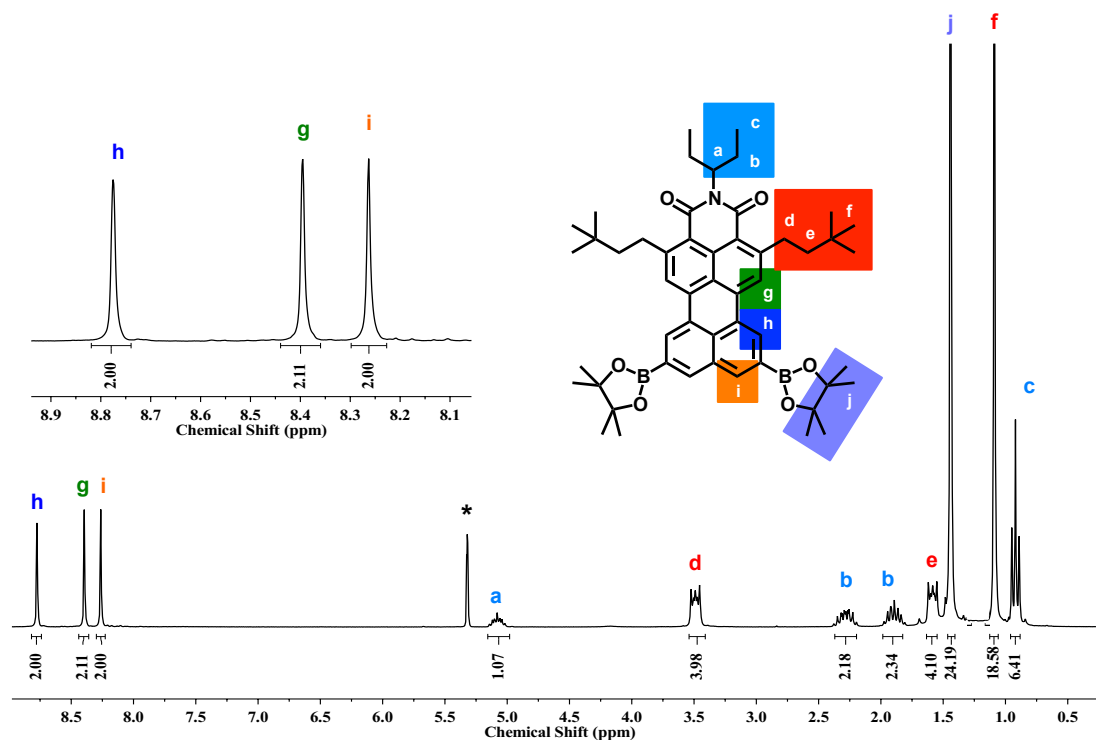

Figure 61 ¹H-NMR of **C2SW-alk-8,11-bor-PDI** in CD₂Cl₂. Assignation of the aromatic proton has been done according to the simulated spectra obtained from the software ChemDraw.

After demonstrating the applicability of the reaction, the extension of the synthetic protocol to other PMI derivatives was considered. THF was chosen as alternative solvent for the reaction, being suitable for a larger number of perylenemonoimides as compared to cyclohexane. Literature reports described slightly lower reaction yields when more polar solvents are used, due to a decreased activity of the iridium catalyst.[143] Nevertheless THF offers the advantage to allow higher concentrations of the perylenemonoimide in the reaction mixture, with a consistent saving on the amount of solvents used. Additionally lower temperatures are needed, which may limit the thermally activated formation of undesired side products.

The first derivative that was considered is **DiPP-PMI**, molecule that plays a key role in the perylenemonoimide chemistry as starting material. In fact **DiPP-PMI** can be readily synthesized starting from perylenedianhydride and diisopropylphenyl amine via an imidization-decarboxylation reaction on the gram scale in high yields. Unfortunately the harsh conditions of the synthetic route limit the number of amines that can be used. Therefore in most cases PMIs bearing other imide substituents must be synthesized starting from **DiPP-PMI** via saponification and imidization. Hence direct borylation of **DiPP-PMI** to obtain the 8,11-functionalized derivative would be highly desirable.

The reaction was explored using THF as solvent and heating at 60 °C for 12 hours under argon atmosphere (Scheme 54). Indeed the reaction afforded borylated perylenemonoimides. Unfortunately the 4-position of the diisopropylphenyl group also satisfies the requirements to undergo the iridium–catalyzed borylation. FD-MS analysis showed the formation of the tris–borylated product, together with the lower substituted derivatives.

Scheme 54 Iridium-catalyzed borylation of **DiPP-PMI** and suggested structure of the tris-borylated product.

Attempts to separate the different compounds via chromatography were unsuccessful and the reaction was set aside. Nevertheless conditions may be tuned to obtain the trisborylated product, but the possibility was not explored, not being in the focus of the investigation.

To avoid undesired side borylation of imide substituents, **C2SW-PMI** and **C7SW-PMI** were chosen. The same protocol applied to **DiPP-PMI** for the *edge*-borylation was used (Scheme 55). The bisborylated **C2SW-8,11-bor-PMI** and **C7SW-8,11-bor-PMI** were obtained in good yields. After the reaction traces of monoborylated derivatives were observed on TLC and FD-MS analysis. The *edge*-functionalized products could be isolated after gel permeation chromatograpy, as well as the mono-borylated and unsubstituted perylenemonoimide.

Scheme 55 *Edge*-borylation of **C2SW-PMI** and **C7SW-PMI**.

The reaction times could be in principle prolonged in order to reduce the amount of mono-functionalized derivatives. However longer reaction times and increased amounts of bis(pinacolato) diboron seemed to favor borylation of less favored sites of the aromatic core, leading to traces of three times borylated PMIs, detected by FD-MS. Since the third borylation may occur in a very unselective way affording several isomers, it was preferable to stop the reaction in presence of small amounts of the monosubstituted derivative, easily removable via gel permeation chromatography. The ^{1}H-NMR of the **C7SW-8,11-bor-PMI** is displayed in Figure 62.
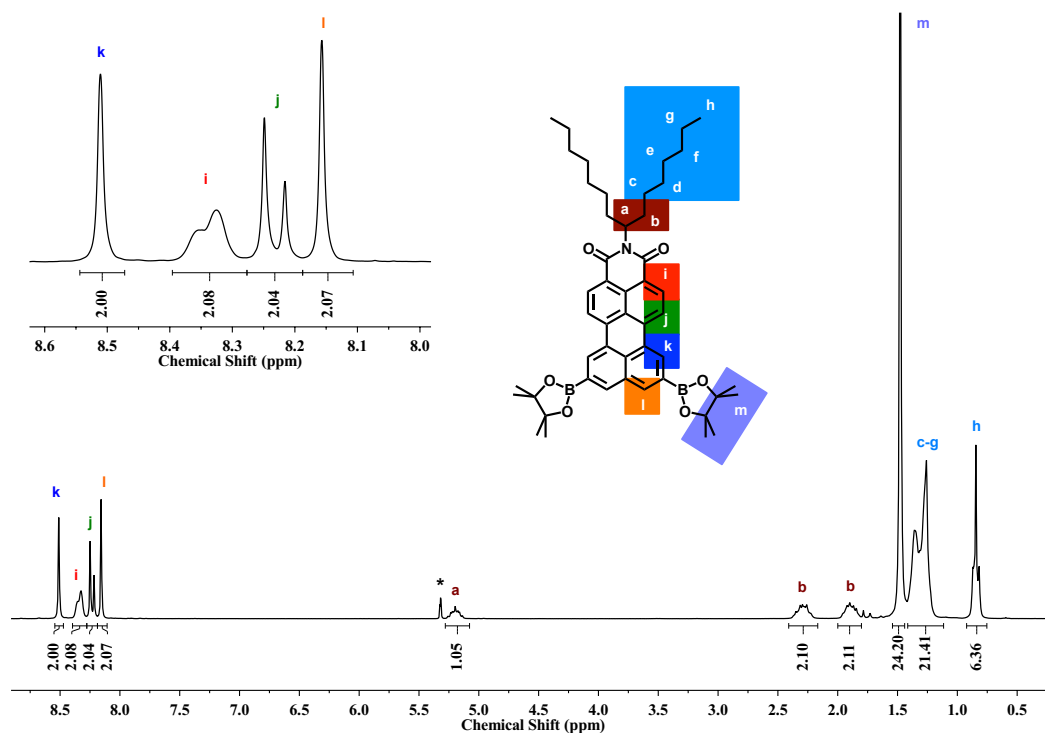
Figure 62 ^{1}H-NMR of **C7SW-8,11-bor-PDI** in CD_2Cl_2.

While the reaction afforded mainly the desired 8,11-functionalized materials and the 8-mono-borylated PMI, TLC revealed also the presence of two minor side products with polarity similar to the *edge*-functionalized molecules. These materials could be removed from the target compound by simple successive reprecipitations in methanol from dichloromethane. Unfortunately separation from the *edge*-functionalized materials was not possible neither by column chromatography nor by gel permeation chromatography. Therefore no structural informations could be obtained. However, since FD-MS only showed the molecular masses of the mono and bis-borylated products, the impurities were identified as isomers of the *edge*-functionalized materials and more precisely as the 8,10-diboronate and the 9-boronate PMIs (Figure 63). To further proof this hypothesis, the borylation reaction mixture of **C7SW-PMI** was compared on TLC with **C7SW-9-bor-PMI**, already available in our laboratory. The results would confirm the presence of the 9-functionalized PMI.
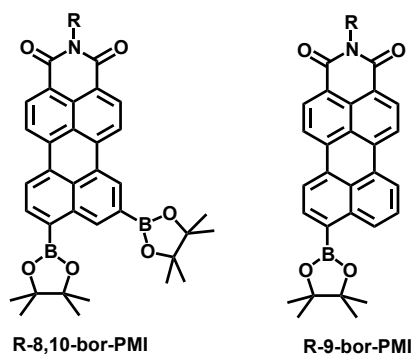
Figure 63 Suggested structures of the side products obtained from the *edge*-borylation reaction. The presence of isomers was not mentioned in the literature report describing the synthesis of 2,5,8,11-tetraboronate perylene.

The work described above demonstrated the possibility to successfully access the last unexplored positions of the perylenemonoimide core. More importantly, boronate derivatives are precious building blocks that allow the access to a broad range of functionalizations, as it was already demonstrated in Chapter 6. To prove the potential of these derivatives, their conversion into the halogenated derivatives was explored. In this case the investigations were limited to the introduction of chlorine and bromine atoms, that afforded the best results in the work described in the previous chapters. More importantly, the *edge*-dibromo and dichloro derivatives were chosen to further extend the number of building blocks available and to broaden the functionalization possibilities. For example, standard reaction conditions used for *bay-* and *peri*-halogenated PMIs could be directly applied, such as for example Buchwald-Hartwig and Suzuki-coupling reactions. As a result, straightforward introduction of known substituents, such as secondary amines, could readily provide donor acceptor dyes to test in dye sensitized organic solar cells.

The preliminary screening was performed using **C2SW-8,11-bor-PMI** and applying the conditions optimized for the synthesis of **C7SW-4Cl-PDI** and **C7SW-4Br-PDI** (Scheme 56). Quite surprisingly, the introduction of the halogen atoms in the *edge*-positions induced an increased tendency to aggregation. Direct consequence was the precipitation of the perylenemonoimide during the reaction and the occurrence of undesired deborylation, affording significant amounts of **C2SW-PMI** and monohalogenated products. Therefore the desired products could be isolated, but only in moderate yields (48-54 %). Decreasing the concentration of the diborylated-PMI in the reaction mixture may lead to higher yields, but this possibility was not explored. **C2SW-8,11-Cl-PMI** and **C2SW-8,11-Br-PMI** exhibited some solubility only in toluene, xylene and mesitylene (lower than 1 mg/mL), therefore NMR-characterization was performed in deuterated sulfuric acid.
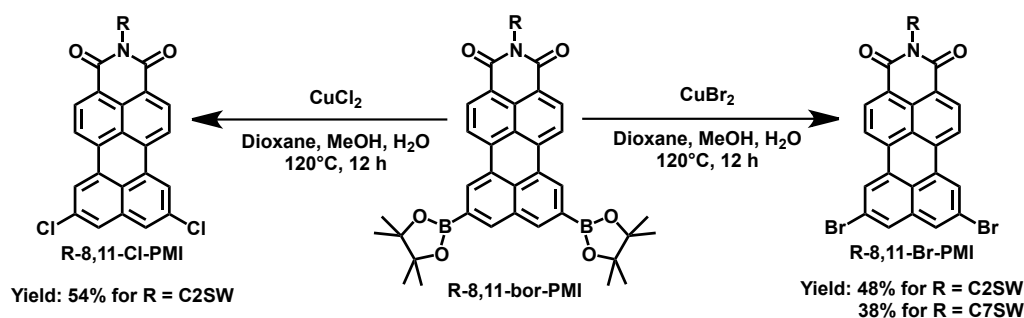
Scheme 56 Halodeboronation reactions of **C2SW-8,11-bor-PMI**, using copper(II) salts.

A different reactivity was observed for **C7SW-8,11-bor-PMI**. While the long alkyl imide substituents guaranteed enough solubility throughout the reaction, use of a 1:12 molar ratio of PMI:CuBr$_2$ (instead of 1:20) afforded only traces of the desired **C7SW-8,11-Br-PMI**. Similar results were achieved also in test reactions using copper(II) chloride. In both cases the reaction conditions seemed to favor the formation of a polymer. It must be noted that the same protocol was successfully applied for the synthesis of the *ortho*-tetrahalogenated PDIs, for which almost quantitative yields were obtained. However boronic acid derivatives are known in the literature to give homo-coupling reactions in the presence of copper salts, particularly favored in the case of electron poor aryl systems.[148] While in the case of the *ortho*-substituted PDIs, polymerization was hindered most probably by steric factors, the *edge*-boronates offered an easily accessible position for homocoupling reactions. Nevertheless the side reaction could be limited increasing the molar ration of PMI:CuBr$_2$ to 1:20 and the desired **C7SW-8,11-Br-PMI** was isolated after column chromatography (38 %).

As previously mentioned, one of the attractive features of the iridium-catalyzed borylation is the possibility to be applied in one-pot reactions. These synthetic protocols are extremely useful to reduce purification steps, proceeding directly to further conversion of the products. Therefore direct synthesis of the *edge*-halogenated-PMIs from the unsubstituted **C2SW-PMI** was explored and similar yields were obtained as compared to the two-step protocol.

The effect of *edge*-functionalization on the optical properties of the different derivatives was investigated via absorption and fluorescence spectroscopy and the results are briefly summarized in Table 19. All the *edge*-functionalized perylenemonoimides exhibit comparable extinction coefficients and slightly lower fluorescence quantum yields, as compared to their unsubstituted derivatives. Similarly to what was observed for the *ortho* substituted PDIs, the introduction of boronic esters induces a bathochromic shift in the onset of the absorption and the emission, while halogenation leads to the opposite hypsochromic shift. The boronates and halogens have also a different impact on the profile of the optical absorption. The chloro and bromo substituted derivatives exhibit curves similar to the PDI derivatives, with the S_0-S_1 transition being the most intense one, while the *edge*-boronates have a slightly stronger contribution of the $S_0 \rightarrow S_2$ transition.
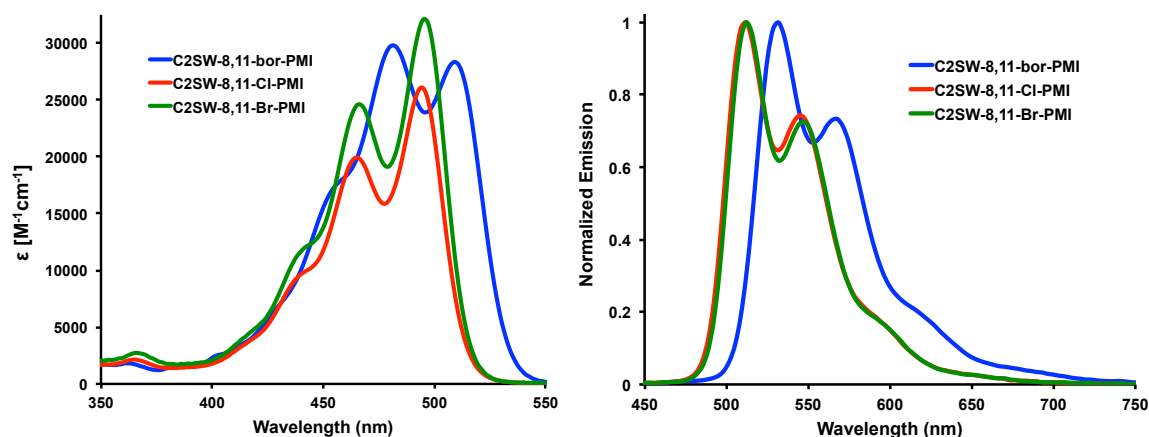
138

Figure 64 Absorption (left) and fluorescence spectra (right) of **C2SW-8,11-bor-PMI**, **C2SW-8,11-Cl-PMI** and **C2SW-8,11-Br-PMI** in toluene. ($\lambda_{em} = \lambda_{max}$).

Table 19. Optical properties of *edge*-functionalized PMIs.

PMI[a]	ε [M^{-1}cm^{-1}][b]	λ_{max} [nm]	λ_{em} [nm][c]	φ_f[d]
C2SW-PMI	3.06 X 10^4	504	529	0.86 (504)
C2SW-8,11-bor-PMI	2.98 X 10^4	481	532	0.51 (481)
C7SW-8,11-bor-PMI	3.24 X 10^4	482	532	0.53 (482)
C2SW-8,11-Cl-PMI	2.61 X 10^4	494	512	0.64 (494)
C2SW-8,11-Br-PMI	3.21 X 10^4	495	512	0.63 (495)
C7SW-8,11-Br-PMI	3.68 X 10^4	496	512	0.65 (496)

[a]Optical properties measured in toluene. [b]Measured at λ_{max}. [c]Excited at λ_{max}. [d]Determined using Rhodamine 6G as standard.

Summarizing, in this section it was successfully demonstrated the possibility to selectively access the 8,11-positions of perylenediimides. Derivatives bearing boronates, chlorine and bromine atoms were synthesized, isolated and characterized. These molecules represent promising starting materials for the functionalization of the *edge*-positions of PMIs, which were used by ▮▮▮▮▮▮ for the synthesis of donor acceptor structures for application in dye sensitized solar cells.

8.3 Palladium-Catalyzed Coupling Reactions: the Migration Issue

As previously mentioned, perylenemonoimides represent extremely interesting systems for the synthesis of light absorbers for dye-sensitized solar cells. Extensive work has been done in the ▮▮▮▮ group using this leitmotif for the creation of push-pull structure. While the imide or anhydride group was used as acceptor, the donor groups have been systematically varied as well as their number and position on the aromatic core. Among the different possibilities ▮▮▮▮▮▮ investigated the synthesis of double donor systems starting from the *edge*-derivatives described in the previous section. Two approaches were envisioned: Buchwald amination using *edge*-dihalogenated PMIs and Suzuki coupling followed by Cadogan reaction. The desired double *edge*-functionalized

materials could be obtained in most of the cases. However Buchwald and Suzuki coupling reactions unexpectedly afforded also 8,10-subtituted materials in small amounts.

The first formation of an 8,10-derivative occurred in a Buchwald coupling reaction between **C2SW-8,11-Cl-PMI** and bis(4-(2,4,4-trimethylpentan-2-yl)phenyl)amine (Scheme 57).

C2SW-8,11-Cl-PMI

Pd₂(dba)₃, BINAP, Cs₂CO₃

Toluene, Ar, 100 °C, 16 h

C2SW-8,10-diamino-PMI

C2SW-8,11-diamino-PMI
Not isolated
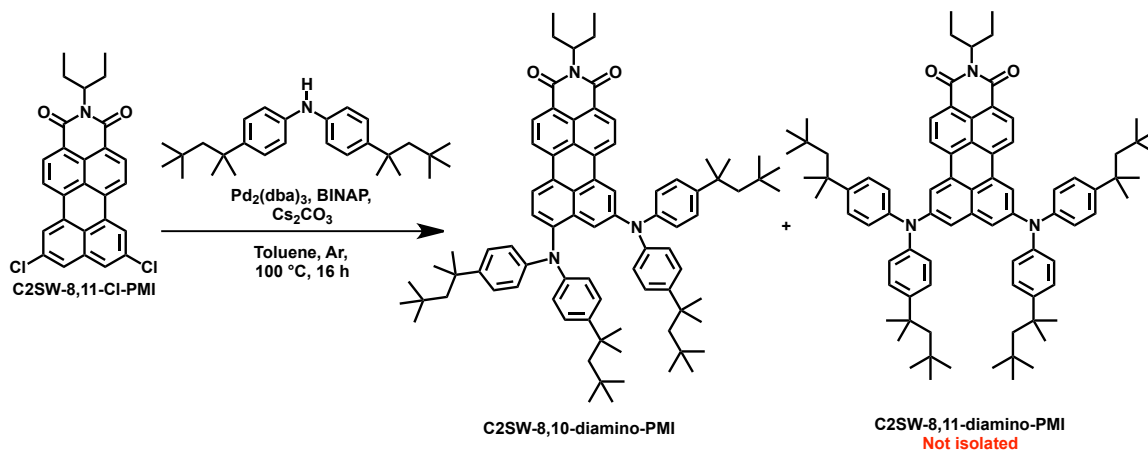
Scheme 57 Buchwald-Hartwig coupling reaction using **C2SW-8,11-Cl-PMI** reported by ▮▮▮▮▮▮▮

The dichloro-PMI derivative was synthesized from a one-pot procedure in which **C2SW-PMI** was borylated and successively subjected to halodeboronation and column purification. During the Buchwald coupling consistent dehalogenation occurred due to the poor solubility of **C2SW-8,11-Cl-PMI**. Additionally the reaction afforded a mixture of several products, with different colors, ranging from the orange, to the dark red, blue and green. Due to its desirable absorption, the green derivative was isolated and characterized. Surprisingly instead of the 8,11-functionalized system, the 8,10-diamino derivative was obtained.

To try to explain this surprising result, the starting material **C2SW-8,11-Cl-PMI** was again characterized and even though the dye showed reduced solubility in organic solvents, no major traces of impurities could be detected in ¹H-NMR. Similarly, due to the strong aggregation, the presence of isomers was not observed on TLC or during the chromatographic purification of the *edge*-halogenated materials of **C2SW-PMI**. Further, **C7SW-8,10-diamino-PMI** was isolated with yield lower than 5 %.

Similarly, 8,10 functionalization occurred also during Suzuki coupling of **C7SW-8,11-bor-PMI** with 1-bromo-2-nitrobenzene. Also in this case a one-pot reaction was applied: after iridium-catalyzed borylation, the solvent was removed and the material used directly for the coupling. From the reaction a mixture of isomers was obtained, the 8,10- and the 8,11-functionalized derivative.

The unexpected isolation of 8,10 functionalized materials lead to the postulation of a migration mechanism occurring during base and palladium-catalyzed reactions. It must be specified that the experiments were performed during the initial stage of the development of the synthetic protocol for the *edge*-functionalization. At the time the presence of small amounts of isomers was not known yet and in ¹H-NMR such impurities were not detecded. Even though this hypothesis appears less likely than the

simple presence of isomers, the migration could not be excluded *a priori*. Therefore, new experiments clarifying the situations were required to have a better understanding and allow further work on the *edge*-functionalization.

To deeper investigate the migration issue and eventually prove the possibility to selectively obtain 8,11-diamino perylenemonoimides, the Buchwald-Hartwig coupling reaction was repeated using bis(4-(2,4,4-trimethylpentan-2-yl)phenyl)amine
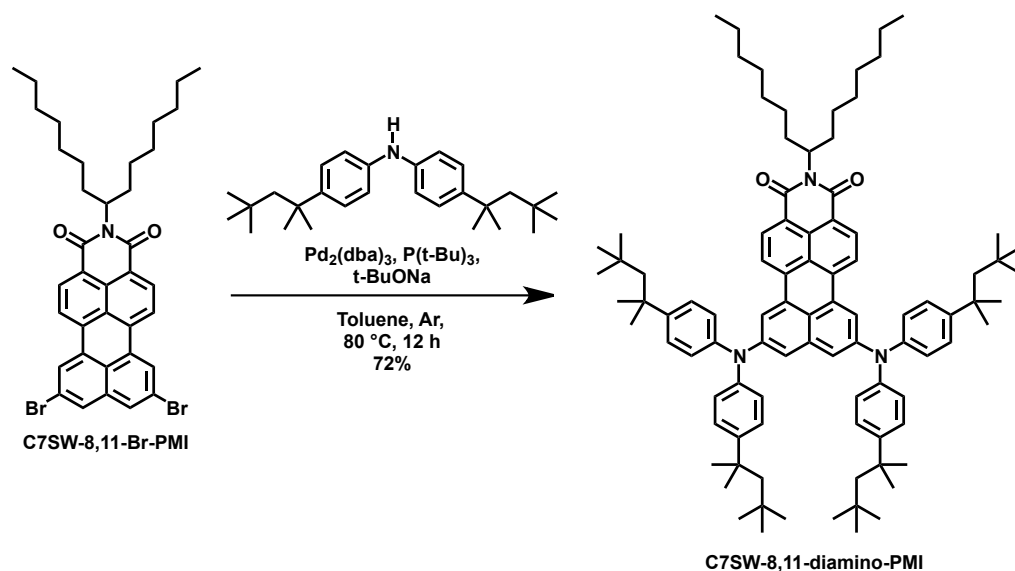
Scheme 58 Buchwald coupling reaction between **C7SW-8,11-Br-PMI** and bis(4-(2,4,4-trimethylpentan-2-yl)phenyl)amine.

. In this case the more soluble **C7SW-8,11-Br-PMI** was selected. Particular attention was paid to the complete removal of any trace of the 8,10-functionalized PMI after the borylation reaction: several reprecipitation were performed until complete disappearance of the undesired isomer from TLC (Scheme 58).

Since the *peri*-functionalized systems (9- and 8,10-functionalized perylenemonoimides) can be easily identified on TLC due to their distinctive color ranging from the blue to the green, the reaction was constantly monitored. Only a main red product and two orange side products were formed. The absence of the *peri*-functionalized systems could be further confirmed after purification of the reaction mixture via gel permeation chromatography. The double *edge*-functionalized material **C7SW-8,11-diamino-PMI** was formed as major product, with traces of 8-mono-substituted and unsubstituted PMI. In Figure 65 is depicted the NMR-spectra of the 8,11-derivative: only four distinct sets of signals are present in the aromatic region. In the case of the isomer 8,10-diamino PMI ten signals have been described.
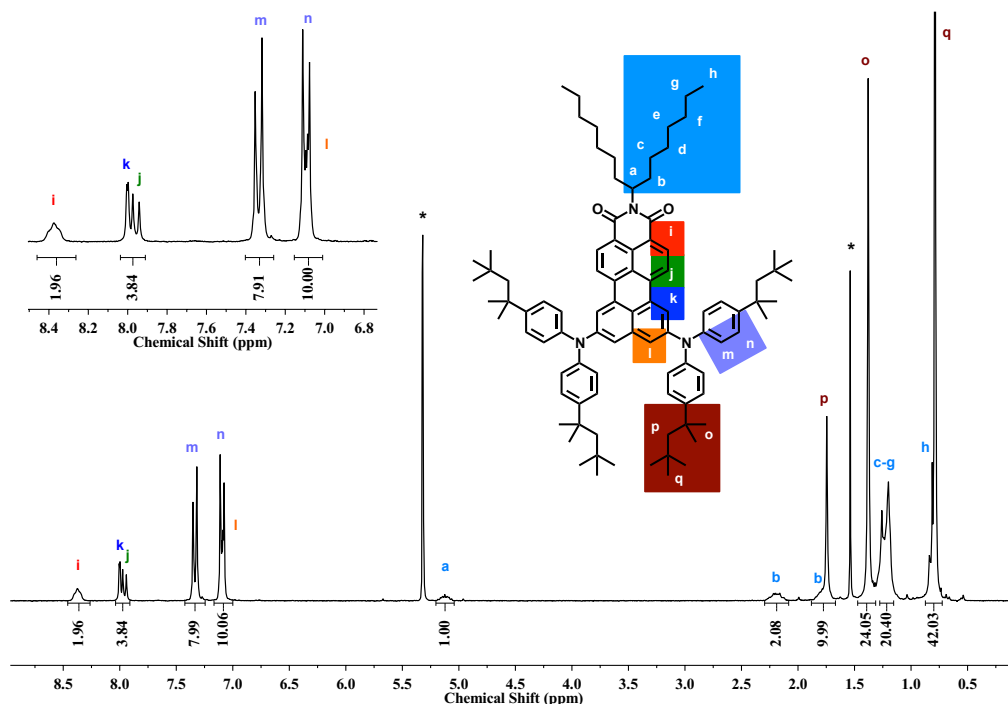
Figure 65 ¹H-NMR of **C7SW-8,11-diamino-PMI** in CD₂Cl₂.

Similarly, the Suzuki coupling was investigated. To simplify the interpretation of the results and the purification in case of migration, a model system bearing only one boronate moiety was synthesized, **C7SW-8-bor-PMI** (Scheme 59). The 8-position of **C7SW-PMI** was borylated by halving the amount of catalyst and bis(pinacolato) diboron. The reaction afforded the desired **C7SW-8-bor-PMI** with consistent amounts of unreacted PMI and difunctionalized derivative. The 9-functionalized PMIs were removed from the mixture by successive reprecipitations and the product purified via size exclusion chromatography. Then Suzuki coupling was performed using **C7SW-8-bor-PMI** and 4-bromobenzonitrile. The choice of *para*-benzonitrile was driven by the need of a molecular fragment having a symmetrical structure, possessing distinctive ¹H-NMR-signals and facilitating the interpretation of the results.
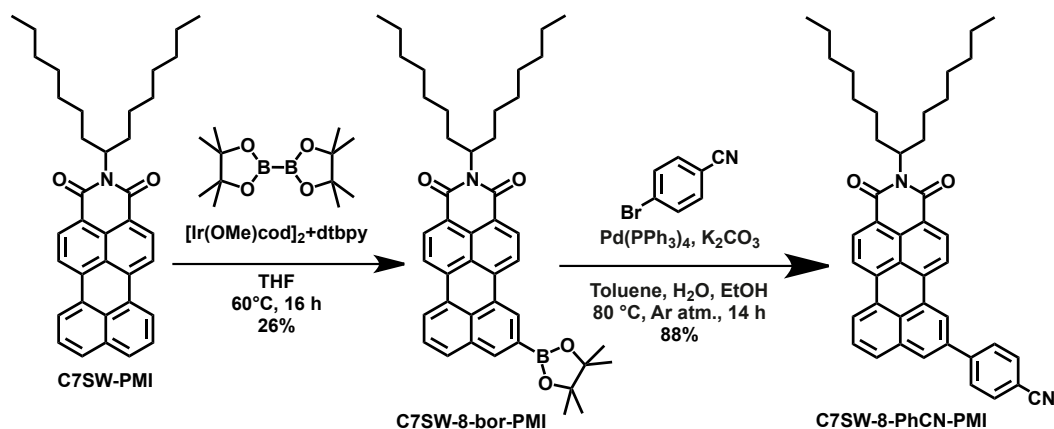
Scheme 59 Synthesis of 8-functionalized perylenemonoimides.

The reaction conditions used for the coupling were maintained equal to those used by ▮▮▮▮▮▮▮▮ for the introduction of the nitro-phenyl groups. The monoarylated **C7SW-8-PhCN-PMI** was isolated in high yields after purification via column chromatography. The only side product formed during the reaction was **C7SW-PMI**. The selective functionalization of the 8-position could be proven via ^{1}H-NMR (Figure 66).
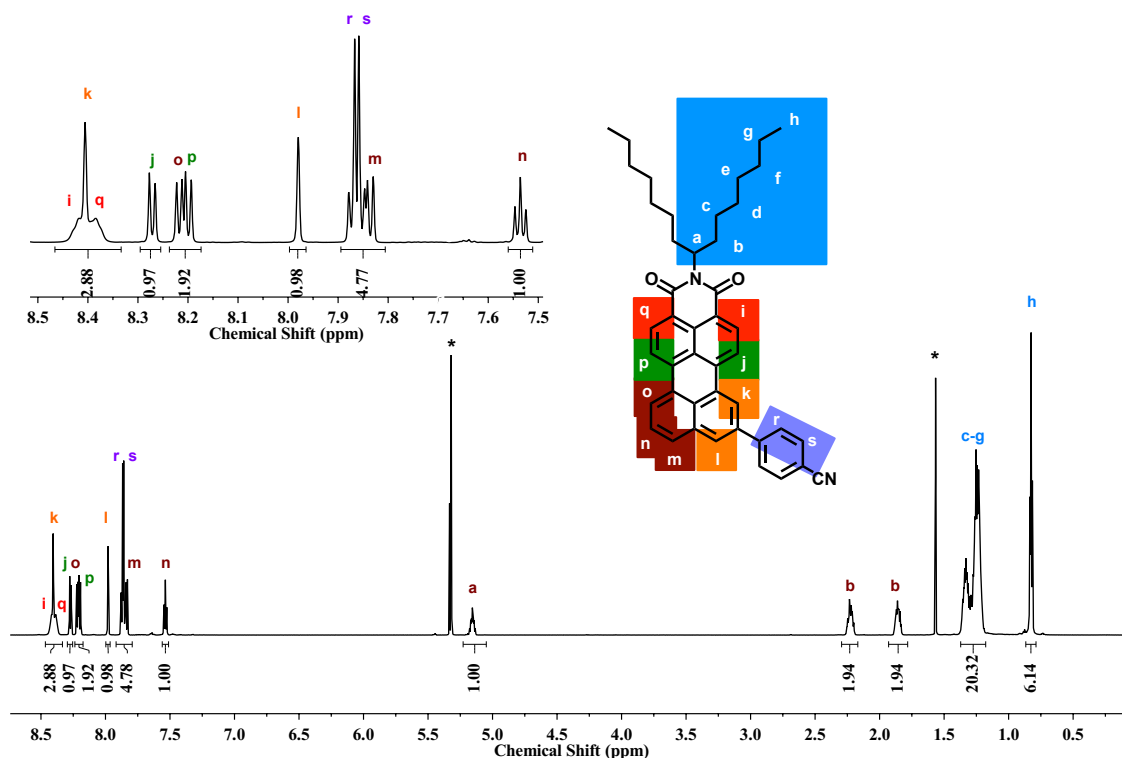
Figure 66 ^{1}H-NMR of **C7SW-8-PhCN-PMI** in CD_2Cl_2. ^{1}H, ^{1}H-COSY, not reported here, was used for the assegnation of the signals.

Encouraged by the positive results, the Suzuki coupling between 1-bromo-2-nitrobenzene and the well soluble **C7SW-8,11-bor-PMI** was repeated. The reaction afforded **C7SW-8,11-PhNO2-PMI** in good yields after purification. All the side products of the reaction were isolated, but no trace of the 8,10 functionalized system could be found.
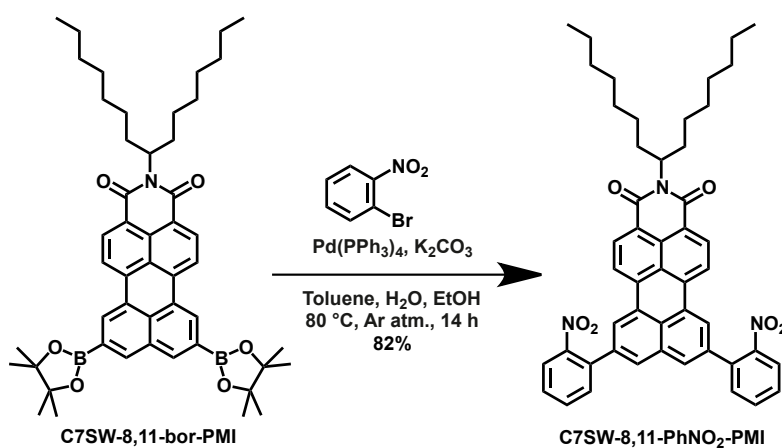
Scheme 60 Synthesis of **C7SW-8,11-PhNO2-PMI.**

In summary, these results demonstrate that in the case of the Suzuki coupling, the 8,10-functionalization observed by ████████ has most probably to be assigned to the presence of isomers originated during the borylation reaction. A similar conclusion could also be drawn for the Buchwald coupling, for which the highly insoluble halogenated PMIs probably hided the traces of impurities.

8.4 Conclusions and Outlook

In this final chapter, the last missing synthetic tool for the functionalization of ryleneimides was described. The first route to the selective addressing of the 8,11-positions of perylenemonoimides was described. The iridium-catalyzed borylation published by Hartwig and Miyaura could be applied to various perylenemonoimides to obtain the desired 8,11-diboronate derivatives. Such derivatives could not only be isolated and characterized, but also further converted into *edge*-dichloro and dibromo-PMIs. Borylated, chlorinated and brominated perylenemonoimides constitute a powerful set of building blocks, first steps toward the synthesis of *edge*-functionalized materials.
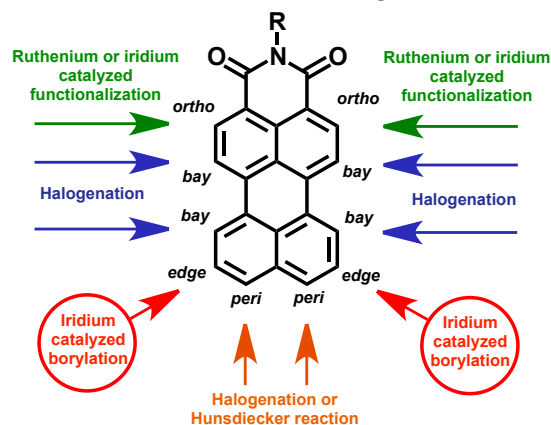
Figure 67 Synthetic routes for the functionlization of perylenemonoimides.

The purely steric factors affecting the reactivity of the iridium catalyst make possible the application of this method not only to the here described perylenemonoimides, but also to higher rylenemonoimides. More importantly the investigation here reported demonstrates that via halogenation or metal-catalyzed reactions, any available position of the aromatic core of ryleneimides can be successfully targeted, providing a complete set of tools for the creation of innovative materials.

While the iridium-catalyzed borylation affords mainly the 8,11-functionalization of perylenemonoimides, formation of *peri*-functionalized materials was also observed. Initially these molecules were considered as the result of a palladium-catalyzed arine type migration mechanism. More detailed investigations reported here confirmed instead the presence of isomers generated during the borylation reaction, which would exclude the migration hypothesis.

If the unexpected isolation of 8,10-functionalized perylenemonoimides complicated purification processes and the interpretation of the results, their serendipitous discovery

led to double-donor dyes with outstandingly broad absorption, extremely promising for their application in dye sensitized organic solar cells. Consequently a new synthetic route was designed for their synthesis, taking advantage of the tools developed in this chapter (Scheme 61). The optimized reaction conditions applied for the functionalization of the *edge*-positions could be used in a series of reactions, starting from the iridium-catalyzed borylation, followed by bromodeboronation and Buchwald coupling. Chromatogaphic purification was performed after the introduction of the second donor group, since at each step, the only side product obtained was the starting donor acceptor molecule. Further, the modiefied push-pull dye bearing either a boronic ester group or a bromine substituent provide a ground structure, on which several substituents can be introduced, allowing fine tuning of the electro-optical properties of the molecule via a quasi-combinatorial approach.
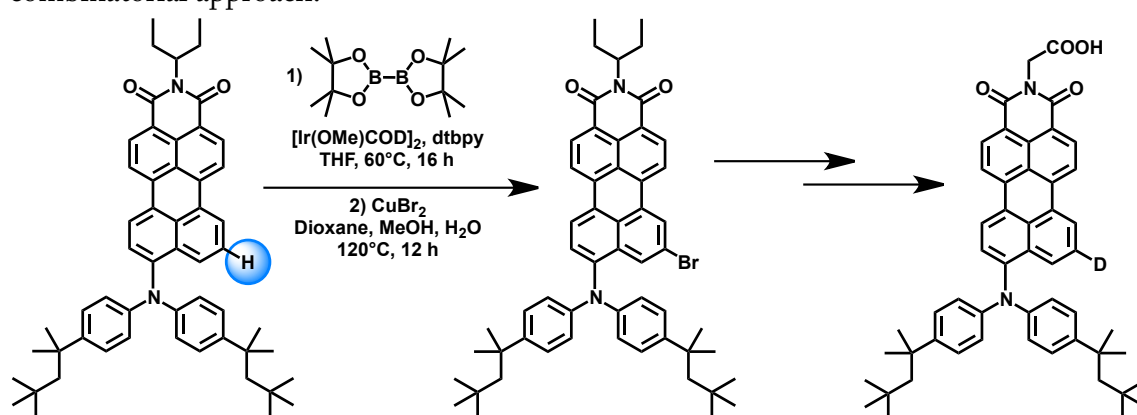
Scheme 61 Synthetic protocol for the introduction of the second donor group on a PMI donor-acceptor molecule.

The iridium-catalyzed borylation here reported does not only represent a powerful method for the *edge*-functionalization of PMIs, but may be also used for the post-modification of rylenediimides. In fact, careful choice of the imide and core substituents may provide accessible positions to be functionalized via the synthetic protocol affording useful building blocks. An example is the diisopropylphenyl group, used as standard imide substituent. Boronate groups may be easily introduced and eventually be converted into their chloro or bromo-derivatives affording interesting units to be incorporated in more extended molecular structures, such as for example rylene-based donor acceptor combinations. These systems have been reported in the literature by our group and they are usually obtained via tedious multistep synthesis. [149] By simple application of the borylation reaction (Scheme 62), the rylene arrays could be synthesized starting from readily available materials within a few steps.
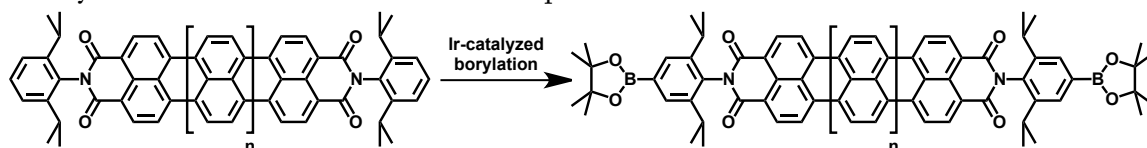
Scheme 62 Iridium-catalyzed borylation of rylenediimides, providing within one step a bifunctional building block.

The investigation reported in the final part of the chapter has proved the applicability of Suzuki and Buchwald coupling for the functionalization of the *edge*-positions. As a

consequence, projects that were first set aside due to the challenges posed by migration issues may now be reconsidered. One of the most promising is the double Cadogan reaction, explored by ███████████ in her thesis. This route was explored for the synthesis of the *peri*-double donor systems depicted in Scheme 63. The absorption of these moleculeis already peaks at 600 nm, but this may be further tuned via deprotonation of the nitrogens and insertion of cations or BF_2 groups for the synthesis of NIR-absorbing dyes.

R-8,11-PhNO$_2$-PMI
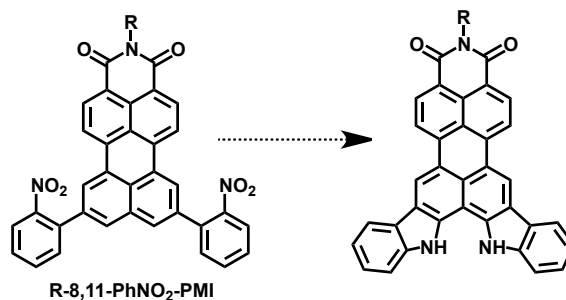
Scheme 63 Double Cadogan reaction.

Finally double *edge*-functionalized perylenemonoimide could be incorporated in conjugated polymers and macrocyles (Scheme 64). Poly-*edge*-perylenemonomides could assume either a linear or coiled conformation, which may lead to different opto-electrochemical properties. In their coiled form they may incorporate guest systems, such as fullerenes, carbon nanotubes or other conjugated polymers, while in their linear conformation they may be applied as solubilizing agent for grapheme fragments.
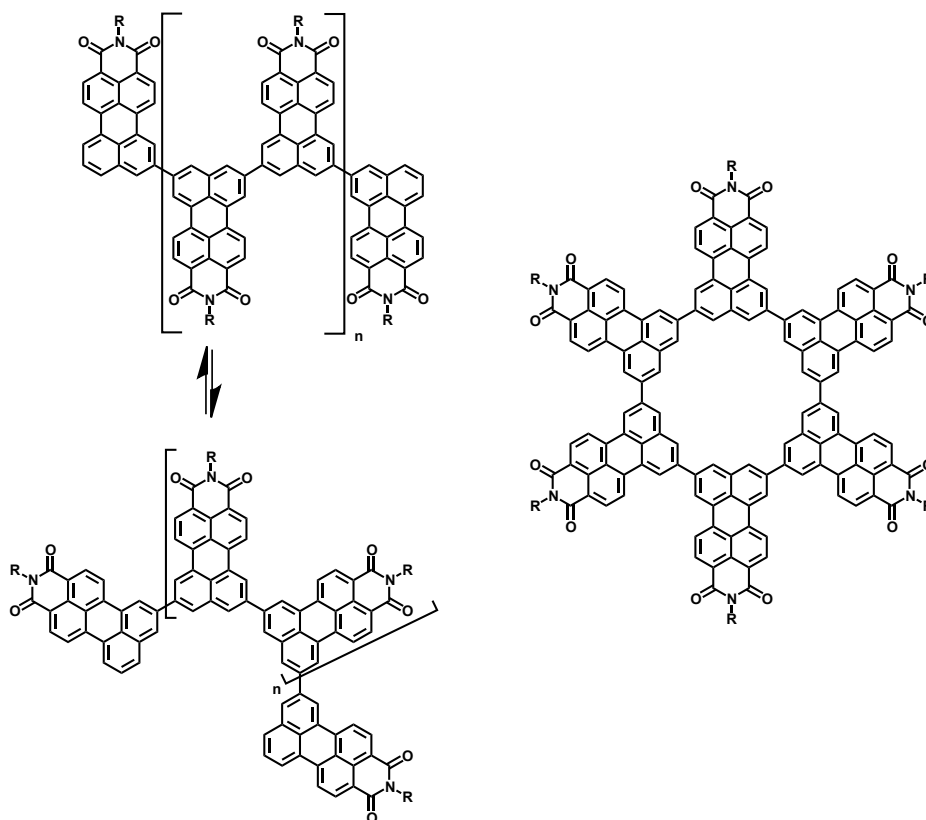
Scheme 64 Poly-*edge*-perylenemonomides.

8.5 References

[139] Li, C., & Wonneberger, H. (2012), *Advanced Materials*, *24*(5), 613–636.

[140] a) Li, C. (2008), Ph. D. Thesis, Johannes Gutenberg University (Mainz). b) Wonneberger, H. (2012), Ph. D. Thesis, Johannes Gutenberg University (Mainz).

[141] Zagranyarski, Y., Chen, L., Zhao, Y., Wonneberger, H., Li, C., & Müllen, K. (2012), *Organic letters*, *14*(21), 5444-5447.

[142] Facchetti, A. (2010), *Chemistry of Materials*, *23*(3), 733-758.

[143] Ishiyama, T., Takagi, J., Hartwig, J. F., & Miyaura, N. (2002), *Angewandte Chemie International Edition*, 41(16), 3056–3058.

[144] Boller, T. M., Murphy, J. M., Hapke, M., Ishiyama, T., Miyaura, N., & Hartwig, J. F. (2005), *Journal of the American Chemical Society*, 127(41), 14263–14278.

[145] Murphy, J. M., Liao, X., & Hartwig, J. F. (2007) *Journal of the American Chemical Society*, *129*(50), 15434–15435.

[146] Coventry, D. N., Batsanov, A. S., Goeta, A. E., Howard, J. A. K., Marder, T. B., & Perutz, R. N. (2005), *Chemical communications (Cambridge, England)*, (16), 2172–2174.

[147] Harrisson, P., Morris, J., Marder, T. B., & Steel, P. G. (2009), *Organic letters*, *11*(16), 3586-3589.

[148] Kirai, N., & Yamamoto, Y. (2009), *European Journal of Organic Chemistry*, *2009*(12), 1864-1867.

[149] Schlichting, P., Duchscherer, B., Seisenberger, G., Basché, T., Bräuchle, C., & Müllen, K. (1999), *Chemistry-A European Journal*, *5*(8), 2388-2395.

9 Conclusions

The central objective of this thesis was the development of new functionalization of the *ortho–* and *edge*-positions of ryleneimides, and in particular of the compounds perylenediimide, terrylenediimide and perylenemonoimide. Major motivation was the access to these "unconventional" molecular sites to further broaden the chemistry of ryleneimides, providing new instruments for the creation of innovative RI-based materials.

The synthetic work started with the study of the alkylation of the *ortho*-positions of ryleneimides in Chapter 3. Deeper understanding could be gained on the ruthenium-catalyzed protocol using the olefin 3,3-dimethyl-butene. A strong dependence of the reactivity on the imide substituents was observed and not all the substrates could be successfully alkylated. Nevertheless optical and electrochemical characterizations demonstrated that the introduction of *ortho*-alkyl chains maintains the ground properties of ryleneimides almost unmodified: therefore this functionalization may be applied as alternative approach to imide and *bay*-modification to improve solubility and reduce solid-state aggregation. Further, *ortho*-alkylated PDIs were screened as electron acceptors in bulk heterojunction solar cells. Low power conversion efficiencies were achieved in combination with P3HT. However, the work presented here demonstrated that optimization of the PDI-molecular structure may be useful to control aggregation and π-π stacking to improve the performances of BHJ solar cells.

In Chapter 4 a strategy for the synthesis of a stable lactonized quinoidal PMI derivative was explored. The synthesis of a push-pull perylenemonoimide bearing a phenyl imide substituent with an *ortho*-carboxylic acid was achieved via a multistep synthesis. In this case the *ortho*-alkyl substituents were selected to provide solubility to the dye. The quinoidization of such a structure could be induced. Nevertheless the final lactonization reaction afforded a material, which could not be characterized, most probably due to the strong aggregation, deriving from the planar extended conjugated system. Via optical characterization a hypothesis about the nature of the final compound could be formulated, however no structural proof could support this supposition.

The potential of *ortho*-alkylation as solubilizing strategy was further investigated in Chapter 5. The screening of a variety of different olefins allowed the identification of a new double bond undergoing Murai type coupling: diethyl vinylphosphonate. This discovery provides not only an additional functionalization possibility, but also allowed the synthesis of a water-soluble perylenediimide, bearing four phosphonic acid moieties. The target compound was obtained in two steps, both with excellent yields, making this approach very competitive for the synthesis of PDI-based fluorescent probes. Thanks to the little impact of the *ortho*-alkyl substitution on the optical properties of

perylenediimide, a high extinction coefficient and quantum yield in water were achieved, higher than most of the commonly used PDI derivatives for bioapplications.

The real turning point in the chemistry of the *ortho*-position was reached in Chapter 6. A protocol for the borylation of these molecular sites was discovered and developed using the Murai catalyst. The synthetic method could be extended to all the ryleneimides investigated, affording the desired boronates. The introduction of boronic ester groups provides precious building blocks, which allow a completely different and more versatile approach to the modification of the *ortho*-positions. In fact a large variety of functional groups can be introduced, without being limited by the reactivity and tolerance of the Murai catalyst. This could be proved by the substitution of the boronates with a variety of groups, such as arenes and halogens. *Ortho*-halogenated ryleneimides could be used as additional building blocks, offering valid synthetic alternatives where the chemistry of boronates failed.

The importance of *ortho*-boronates and *ortho*-halogenated ryleneimides was further proved in Chapter 7. Starting from these building blocks, strong electron acceptors could be created via the fourfold introduction of cyano-substituents. *Ortho*-tetracyano perylenediimides with remarkably high electron affinities were synthesized and characterized. Similarly, *ortho*-tetracyano TDI could be obtained as well as its isomer derivative *bay*-tetracyano TDI. These two molecules allowed a direct comparison of the features of the different substitution patterns. *Ortho*- and *bay*-tetracyanation have similar impact on the electro-optical properties. However, major difference in solubility and solid-state packing derive from the different functionalization, consequence of the different geometry of the two molecules. Both materials exhibit n-type semiconducting behavior and the highest electron mobilities were achieved with the *bay*-tetracyano derivative. This investigation focused simply on the comparison of the two functionalizations and in the future improved n-type semiconducting materials based on TDI may be synthesized by careful tuning of the molecular structure.

Finally, in Chapter 8 a synthetic method to functionalize the *edge*-positions of perylenemonoimides was presented. Novel building blocks were synthesized, via the straightforward introduction of boronate substituents via iridium-catalyzed reaction and halodeboronation. Such building blocks could be used by ████████ for the synthesis of innovative light absorbers for dye-sensitized solar cells, via the introduction of amino and aryl substituents by palladium-catalyzed reactions. Further in this chapter light was shed on the migration issue that was hypothesized during the initial work on these derivatives, demonstrating that the origin of the unexpected 8,10 substitution pattern was simply caused by the presence of traces of unidentified isomers.

Concluding the major goal of this thesis was indeed reached. The chemistry of the investigated molecules could be enriched through innovative functionalization reactions. Additionally understanding of the structure-property relation of the *ortho*- and *edge*-functionalized materials was gained. This work provides the synthetic instruments to allow the selective targeting of the "unconventional" positions of ryleneimides, filling the existing gaps in their chemistry. However the challenge for the future will be the

combination of imide, *bay-*, *ortho-* and *edge*-functionalizations for the synthesis of innovative ryleneimide-based materials.

10 Experimental Part

10.1 Measurements and Methods

10.1.1 Chemicals and Solvents

Unless otherwise noted, all reagents were obtained from commercial suppliers (e.g. Acros, Aldrich, Fluka, Strem). N-(2,6-Diisopropylphenyl)-perylene-3,4-dicarboximide was kindly supplied by BASF SE.

10.1.2 Chromatography

Preparative column chromatography was performed on silica gel 60 (0.063-0.2 mm/70-230 mesh ASTM) from Machery Nagel. For analytical thin layer chromatography (TLC) aluminum plates with 0.2 mm silica-gel coating with fluorescent indicator (ALUGRAM® SIL G/UV$_{254}$ from Machery Nagel) were used. Preparative gel permeation chromatography was carried out on Bio-Beads™ S-X1 Beads (200-400 Mesh) from BIO-RAD.

10.1.3 NMR Spectroscopy

^{1}H-NMR and ^{13}C-NMR as well as the ^{1}H,^{1}H-COSY spectra were recorded with a Bruker DPX-250, Bruker AMX-300, Bruker DRX-500 or Bruker DPX-700 spectrometer by using the residual proton resonance of the solvent or the carbon signal of the deuterated solvent as the internal standard. Chemical shifts are reported in parts per million.

10.1.4 Mass Spectrometry

FD mass spectra were recorded with a VG Instruments ZAB 2-SE-FPD, Maldi-TOF mass spectra on a Bruker Reflex II-TOF spectrometer using a 337 nm nitrogen laser. High resolution mass spectra (ESI) were measured as a service of the Institute of Organic Chemistry, Johannes-Gutenberg-Universität, Mainz. High-resolution MALDI spectra (ESI) were measured at the ETH, Zürich.

10.1.5 IR Spectroscopy

Infrared spectra were recorded on a Nicolet FT-IR 730 with an ATR unit (Zn-Se crystal).

10.1.6 UV-Vis and Fluorescence Spectroscopy

UV-Vis spectra in solution were recorded on a Perkin-Elmer Lambda 40 and Perkin-Elmer Lambda 9 spectrometers. Fluorescence emission spectra were recorded on a J & M Tidas spectrometer.

10.1.7 Elemental Analysis

Elemental analysis of solid samples was carried out on a Foss Heraeus Vario EL as a service of the Institute for Organic Chemistry, Johannes-Gutenberg-Universität, Mainz.

10.1.8 Electrochemical Characterisation

Cyclic voltammetry for spectroelectrochemistry experiments were carried out with an EG&G Princeton Applied Research potentiostat, model 273. The working electrode consisted of an palladium-carbon electrode (1.5 mm diameter) that was polished on a felt pad with 0.05 μm alumina and washed with milli-Q water before each experiment. A platinum wire was used as the counter electrode and an Ag wire as the reference electrode. The measurements were calibrated with ferrocene/ferrocenium (Fc/Fc_+). The CV measurements were carried out in a solution of Bu_4NPF_6 (0.1 M) in dry dichloromethanewith a scan rate of 50 mVs^{-1} at room temperature under argon.

10.1.9 Crystal Diffraction

Crystal diffraction data were recorded using a Bruker AXS KCCD diffractometer with Mo K α radiation at 120 K.

10.1.10 Thermal Gravimetric Analysis

The thermal characterizations were performed using a thermobalance TG 50 of Mettler Toledo.

10.1.11   Confocal Microscopy[g]

To investigate the photostability on a single molecule level, the dyes were fixed in a polymer matrix (polyvinyl alcohol, PVA). Thin polymer films (thickness 100-200 nm) were prepared by spin-coating fluorophores in polymer solutions at a concentration of 10-10 mol/L (1 min at 3000 rpm, 2 wt %/wt PVA in water). In addition to the photostability of the new PDI dye (GB2-26), the photostability of 2-PEG-PDI was also investigated as a reference. All dyes were excited with aNd-YAG laser (532 nm). A modified scanning confocal microscope (ZEISS LSM 410) was used to visualize fluorescence of the individual dye molecules. High spatial resolution and detection efficiency were achieved with a high-numerical aperture oil-immersion objective (ZEISS 40 x 1.3 NA oil). Using circular polarized excitation light, all in-plane molecular absorption dipoles are excited with the same probability. The fluorescence emission of the dyes were separated from the excitation laser beam using a combination of emission filters (LP 532 and LP 540, AHF Analysentechnik). The fluorescence signal was detected by an avalanche photodiode (APD, EG&G SPCM-AQ 141). The excitation power at the entrance of the objective was set to 20 µW. With the confocal setup, the laser beam could be positioned over individual molecules, and their fluorescence intensities were recorded with time. Two photostability parameters could be automatically extracted from the fluorescence time trajectories of individual molecules by a custom-written LabView program: the number of detected photons before photobleaching as the integral over a time trace and the survival time, which is the total duration of the time trace until photobleaching. The total detection efficiency of our experimental setup is estimated to be 2.5% and was used to calculate the total number of emitted photons.

10.1.12   Data Analysis[g]

The analysis of the photostability parameters was based on calculating the probability distributions of the number of total emitted photons (TEP) before photobleaching and of the survival times (ST). Analyzing probability distributions instead of histograms allows a more precise analysis, avoiding the loss of information due to binning of the histogram. Also mono- and biexponential decays can be better distinguished. The distributions in TEP and ST are well approximated by a multiexponential function, S(t), which is defined by characteristic decay parameters (see equation below)

$$S(t) = \sum_{i=0}^{n} A_i \exp\left(-\frac{t}{\tau_i}\right)$$

where τ_i is the decay time and A_i is the amplitude of the individual components. The number of exponential components was determined by the decrease in the reduced χ^2 of the fit function. A minimum 2-fold decrease in the reduced χ^2 of the fit was required to justify an additional exponential decay in the model function. For all results presented in this article, it is indicated which function was found to give the best fit for the TEP and the ST. For comparison of the photobleachingbehavior between the different dyes, an average TEP or ST, represented by < τ >, was defined as (see equation below):

$$\langle \tau \rangle = \sum_{i=0}^{n} A_i \tau_i$$

10.1.13 Live-Cell Measurements[g]

HeLa cells (HeLa ACC57, DSMZ, Braunschweig, Germany) were grown in Dulbecco's modified Eagle's medium (DMEM) supplemented with 10% fetal calf serum at 37 ℃ in 5% CO2 humidified atmosphere. Cell culture, fetal calf serum, and PBS buffer were purchased from Invitrogen GmbH (Karlsruhe, Germany). Dye-uptake experiments were conducted in HeLa cells at 37 ℃. Solutions of **C2SW-4PO(OH)₂-PDI** (c ≈ 5 mg/mL) were added to the cells adherent on the surface of a cover glass. After an incubation time of about 8h, the solution of **C2SW-4PO(OH)₂-PDI** were washed 3 times with PBS buffer to remove the excess of dye. The fluorescence signal from labeledHeLa cells was monitored by a homebuild wide-field microscope based on a Nikon Eclipse Ti microscope corpus. The dye was excited with 488 nm. The excitation power was set to 88 µW at the entrance of the microscope. The laser beam was expanded and focused onto the back-focal plane of a microscope objective (Nikon Plan Apo TIRF 60x/1.45 NA oil immersion). Fluorescence was collected by the same objective, separated from backscattered laser light with a combination of filters (dichroic mirror 565 DCXR, Chroma and band-pass BP575/76 AHF), and imaged onto a back-illuminated EMCCD detector (Andor, iXon+). Movies were recorded with a resolution of 123 nm per pixel and an integration time of 400 ms per frame for the measurements with HeLa cells.

10.1.14 Photovoltaic device preparation[h]

Commercial indium tin oxide (ITO) substrates (PGO CEC020S) were wet-etched to obtain a stripe-shaped anode area. The substrates were successively cleaned with acetone, isopropanol and ethanol in an ultrasonic bath and dried under a flow of dry nitrogen. Prior to the deposition of the organic layers the substrates were cleaned in argon plasma for 10 min. A PEDOT:PSS (Clevios P VP AI 4083, H.C. Stark) solution was then spin-

---

[h] These experiments were performed by ██████ ██████████████ in the group of Dr. ████████████████ at the Max Planck Institute for Polymer Research in Mainz.

coated at 2500 rpm for 5 s and 5000 rpm for 30 s onto the cleaned ITO substrates resulting in a thickness of approximately 20 nm as determined with a Dektak surface profilometer. The PEDOT:PSS layer was annealed for 30 min at 120 °C in a nitrogen-filled glove box.

For preparation of the active layer P3HT (BASF SE Sepiolid™ P100) and PDI were separately dissolved in chlorobenzene at a concentration of 20 mg/ml and stirred for 14 h at a temperature of 70 °C on a hot plate. The solutions were then mixed and further stirred for 1 h at 70 °C. In case of chloroform an initial concentration of 10 mg/ml was used the solutions were stirred for 14 h, mixed and further stirred for 1 h at room temperature. Prior to deposition of the active layer the mixed solution of P3HT:PDI was filtered through a PTFE syringe filter (0.45 µm pore size). The active layer was then spin-coated on top of the PEDOT:PSS film at 1000 rpm (chlorobenzene) or 1200 rpm (chloroform) for 1 min resulting in a film thickness of ~100 nm. Aluminum counter electrodes were evaporated through a shadow mask on top of the active layer with a thickness of ~100 nm. The films were annealed at 120 °C for 20 min on a hot plate in the glove box. The active area of the pixels as defined by the overlap of anode and cathode area was 14 mm^2. The photovoltaic performance was determined under simulated sunlight using a commercial solar simulator (K.H. Steuernagel Lichttechnik GmbH, Germany) at an area power density of 99,6 mW/cm^2.

10.1.15 Fluorescence lifetime measurements[h]

For fluorescence lifetime measurements a Streak Camera System (Hamamatsu C4742) was used. The samples were housed in a home-built sample holder under a dynamic vacuum of 10^{-5} mbar and excited at 520 nm by the output of an OPA (Coherent OPerA Solo) itself pumped by the output of a femtosecond amplifier (Coherent LIBRA HE) operating at a repetition rate of 1 kHz. The pulse length was determined to 100 fs with an autocorrelator setup (APE Berlin).

10.1.16 Field-Effect Transistors[i]

Bottom-gate, bottom-contact FETs were fabricated using substrates with a 200 nm thick SiO$_2$ dielectric covering highly doped Si acting as the gate electrode. The SiO$_2$ surface was functionalized with hexamethyldisilazane (HMDS) to minimize interfacial trapping sites. The channel lengths and widths are 20 and 1400 µm, respectively. All the electrical measurements are performed using Keithley 4200 SCS in a glovebox under nitrogen atmosphere and also in air.

---

[i] **Work performed by** ▮▮▮▮▮▮▮▮▮▮▮▮▮▮ **in the group of Professor** ▮▮▮▮ **at the Max Planck Institute for Polymer Research in Mainz.**

156

Top-gate transistors were prepard also on Si/SiO$_2$ substrate with thermal evaporation of 25 nm Au bottom contact and 5 nm Cr adhesion layer (shadow mask with channel dimensions of W=1000 μm and L=30 μm). The substrates were cleaned before film deposition. The active layer of *b*-**C7SW-4CN-TDI** was prepared under glovebox conditions by spin-coating from 5mg mL^{-1} chlorobenzene solution at 2krpm and annealed at 250°C for 2 h. Top-gate (Sigma-Aldrich, M$_w$=225000) PMMA dielectric was spin-coated from 50 mg mL^{-1} Butyl Acetate solution at 2k rpm (thickness 320 nm) and annealed at 150 °C for 3 h. Finally 90 nm thick Au gate electrode was deposited by thermal evaporation.

10.1.17 Grazing Incidence Wide Angle X-ray Scattering[j]

GIWAXS measurements were performed using a custom setup consisting of rotating anode X-ray source (Rigaku Micromax, operated at 42 kV and 20 mA), Osmic confocal MaxFlux optics and a three pin-hole collimation system (JJ X-ray). Samples on the top of approx. 1×1 cm silicon platelets were irradiated at the incident angle (αi) of 0.20°. Diffraction patterns were recorded on a MAR345 image plate detector.

10.1.18 Three-dimensional confocal surface measurements[k]

The three-dimensional (3D) topography images were obtained by using a confocal surface measurement system from NanoFocus μSurf C.

10.1.19 Two-Dimensional Wide Angle X-ray Scattering.[l]

2D-WAXS measurements were performed using a custom setup consisting of the Siemens Kristalloflex X-ray source (copper anode X-ray tube, operated at 35 kV/20 mA), Osmic confocal MaxFlux optics, two collimating pinholes (1.0 and 0.5 mm – Owis, Germany) and an antiscattering pinhole (0.7 mm – Owis, Germany). The patterns were recorded on a MAR345 image plate detector (Marresearch, Germany). The samples were prepared by filament extrusion using a custom-built mini-extruder.

---

[j] Work performed by ▮▮▮▮▮ ▮▮▮▮▮▮▮▮▮▮▮▮ and ▮▮▮▮▮▮▮▮▮ in the group of Professor ▮▮▮▮ at the Max Planck Institute for Polymer Research in Mainz.

[k] Work performed by ▮▮▮▮▮▮▮▮▮▮▮▮▮▮ in the group of Professor ▮▮▮▮ at the Max Planck Institute for Polymer Research in Mainz.

[l] Work performed by ▮▮▮▮ ▮▮▮▮ ▮▮▮▮ ▮▮▮▮ and ▮▮▮▮ ▮▮▮▮ ▮▮▮▮ in the group of Professor ▮▮▮ at the Max Planck Institute for Polymer Research in Mainz.

10.1.20 Solvent Vapor Diffusion[m]

A 25 mL *b*-**C7SW-4CN-TDI** dichlorobenzene solution (concentration 3mg/mL) was drop-cast on a HMDS modified SiO2 dielectric surface and exposed to an airtight container (50mL) that was saturated with dichlorobenzene solvent vapor (with 5mL dichlorobenzene in the container) at room temperature.

---

[m] **Work performed by** ▮▮▮▮▮▮▮▮▮ **in the group of Professor** ▮▮▮▮ **at the Max Planck Institute for Polymer Research in Mainz.**

10.2 Material Synthesis

10.2.1 *N,N'*-Bis(1-ethylpropyl)-2,5,8,11-tetrakis[3,3-dimethylbutyl]perylene-3,4:9,10-tetracarboxylic acid diimide (C2SW-alk-PDI)
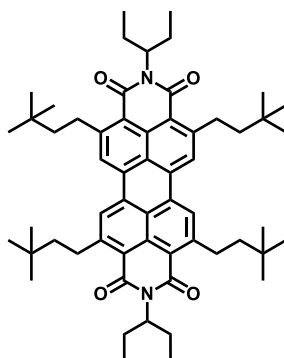
N,N'-Bis(1-ethylpropyl) perylene-3,4:9,10-tetracarboxylic acid diimide (1.50 g, 2.82 mmol), and 3,3-dimethyl-1-butene (4.76 g, 56.5 mmol) were mixed in 30 mL of dry mesitylene in an oven dried round bottom flask. Argon was bubbled through the solution for 30 minutes, and successively $RuH_2(CO)(PPh_3)_3$ (0.13 g, 0.14 mmol) was added. The reaction was stirred under argon at 185 °C (bath temperature) for 10 hours. After removal of the solvent, the crude product was purified by column chromatography (silicagel CH_2Cl_2/petroleum ether 1:2), to give the desired compound (87 % yield, 2.13 g, 2.46 mmol) as a bright orange solid.

¹H-NMR (300 MHz, CD_2Cl_2): δ (ppm): 8.35 (s, 4H), 5.06 (m, 2H), 3.58–3.44 (m, 8H), 2.39–2.15 (m, 4H), 2.01–1.82 (m, 4H), 1.67–1.56 (m, 8H), 1.09 (s, 36H), 0.92 (t, *J* = 7.5 Hz, 12H).

¹³C-NMR (63 MHz, CD_2Cl_2): δ (ppm): 164.8, 151.7, 133.2, 132.2, 127.2, 124.4, 121.0, 57.7, 46.2, 32.9, 31.4, 29.7, 25.7, 11.8.

FD Mass Spectrum (8kV): m/z= 866.5 (100 %) [M+].

IR spectrum (ATR): ν_{max} [cm^{-1}]= 2954; 2872; 1688; 1652; 1601; 1545; 1459; 1429; 1399; 1363; 1324; 1246; 1219; 1151; 1093; 877; 773; 751; 629.

UV-Vis (in toluene): $\lambda_{max}(\varepsilon)$: 455 nm (1.58 x 10^4 M^{-1}cm^{-1}), 485 nm (3.98 x 10^4 M^{-1}cm^{-1}), 521 nm (5.85 x 10^4 M^{-1}cm^{-1}).

Fluorescence (in toluene) λ_{max}: (λ_{ex}=521 nm) 535 nm, 571 nm. φ_F: 0.55.
(λ_{ex}=501 nm): 535 nm, 571 nm. φ_F: 1.00.

Elemental Analysis: calculated (%): C, 80.33; H, 9.07; N, 3.23;
experimental (%) C, 80.45; H, 9.32; N, 3.16.

10.2.2 N-(2,6-Diisopropylphenyl)-2,5-bis[3,3-dimethylbutyl]-perylene-3,4-dicarboxylic acid imide (DiPP-alk-PMI)
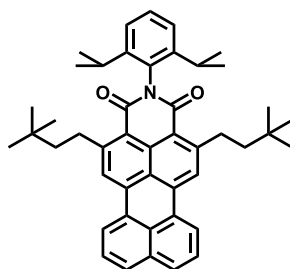
N-(2,6-Diisopropylphenyl)-perylene-3,4-dicarboxylic acid imide (5.00 g, 10.4 mmol), and 3,3-dimethyl-1-butene (8.74 g, 0.10 mol) were mixed in 100 mL of dry mesitylene in an oven dried round bottom flask. Argon was bubbled through the solution for 30 minutes, and successively $RuH_2(CO)(PPh_3)_3$ (0.23 g, 2.50 mmol) was added. The reaction was stirred under argon at 185 °C (bath temperature) for 72 hours. After removal of the solvent, the crude product was purified by column chromatography (silicagel CH_2Cl_2/petroleum ether 1:2), to give the target compound (16 % yield, 1.11 g, 1.69 mmol) as a bright orange solid.

^{1}H-NMR (250 MHz, CD_2Cl_2): δ (ppm): 8.37 (d, J = 7.5 Hz, 2H), 8.13 (s, 2H), 7.83 (d, J = 8.0 Hz, 2H), 7.63–7.45 (m, 3H), 7.37 (d, J = 7.4 Hz, 2H), 3.56–3.35 (m, 4H), 2.81 (hept, J = 6.6 Hz, 2H), 1.70–1.54 (m, 4H), 1.20 (d, J = 6.9 Hz, 12H), 1.03 (s, 18H).

^{13}C-NMR (63 MHz, CD_2Cl_2): δ (ppm): 164.4, 152.9, 148.2, 146.6, 136.2, 134.6, 133.8, 133.3, 130.9, 129.4, 128.2, 127.3, 125.2, 125.1, 124.5, 123.9, 118.5, 46.2, 33.1, 31.3, 30.3, 29.7, 24.4.

FD Mass Spectrum (8kV): m/z= 646.2 (100 %) [M+].

IR spectrum (ATR): ν_{max} [cm^{-1}]= 2956; 2866; 1689; 1654; 1596; 1543; 1465; 1407; 1361; 1339; 1289; 1258; 1224; 1157; 912; 891; 878; 837; 822; 800; 771; 757; 737; 687; 677; 608; 595; 560.

UV-Vis (in toluene): λ_{max} (ε): 473 nm (3.37 x 10^4 M^{-1}cm^{-1}), 501 nm (3.16 x 10^4 M^{-1}cm^{-1}).

Fluorescence (in toluene): λ_{max} (λ_{ex}=473 nm): 525 nm, 558 nm. φ_F: 0.49.

Elemental Analysis: calculated (%): C, 85.01; H, 7.91; N, 2.16;
experimental (%): C, 84.67; H, 7.84; N, 2.14.

10.2.3 *N*-(1-Heptyloctyl)-4-bromo-naphthalene-1,8-dicarboxylic acid monoimide (C7SW-4-Br-NMI)
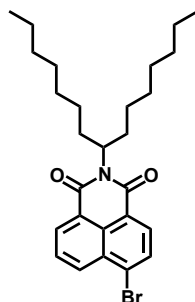
4-Bromo-1,8-naphthalic anhydride (15.0 g, 54,1 mmol) and 1-(heptyl)-octylamine (14.8 g, 65.0 mmol) were added to 30 g of imidazole. The reaction was heated to 130 ˚C stirred under argon atmosphere for 18 hours. After cooling to room temperature, the mixture was treated with 500 mL hydrochloric acid (1 N) to remove the imidazole and was extracted with dichloromethane (3 x 200 mL). The combined organic extracts were dried over sodium sulfate and the solvent removed under reduced pressure to give a brown oil. The desired product was purified by column chromatography (petroleum ether/dichloromethane 3:1) and obtained as a yellow oil with a 66 % yield (17.3 g, 35.5 mmol).

10.2.4 *N*-(1-Heptyloctyl)-perylene-3,4-dicarboxylic acid monoimide (C7SW-PMI)
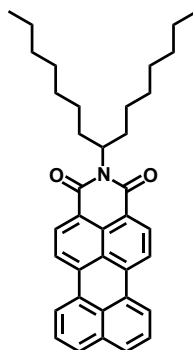
Perylene-3,4-dicarboxylic acid anhydride (10.0 g, 31.0 mmol) and (1-heptyl)-octylamine (8.47 g, 37.2 mmol) were added to 30 g of imidazole. The reaction mixture was heated to 130 °C under argon atmosphere overnight. The mixture was cooled down to room temperature. The so obtained solid was crushed into small pieces and suspended and sonicated in hydrochlic acid (1 N). The remaining material was filtered and washed with water and methanol. The raw product was dried under vacuum and purified by column chromatography (petroleum ether/dichloromethane 1:1) to give the desired product as a dark-red solid in 60 % yield (9.89 g, 18.6 mmol).

10.2.5 *N*-(1-Heptyloctyl)-9-bromo-perylene-3,4-dicarboxylic acid monoimide (C7SW-Br-PMI)
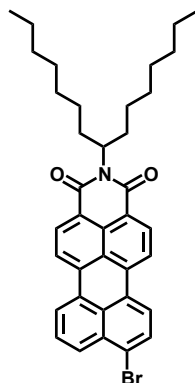
N-(1-Heptyloctyl)-perylene-3,4-dicarboxylic acid monoimide (5.83 g, 10.9 mmol) was suspended in 110 mL of acetic acid in presence of iodine (109 mg, 0.84 mmol). Bromine (2.33 mL, 7.32 g, 90.5 mmol) was added dropwise and the reaction was then left at room temperature for 7 hours under exclusion of light and vigorous stirring (monitored by TLC using toluene as eluent). After completion, the reaction was quenched by adding methanol (100 mL) and stirred overnight. The precipitate was filtered, washed with methanol and dried to give the target compound as a shiny orange solid in 96 % yield (6.40 g, 10.5 mmol).

10.2.6 *N*-(1-Heptyloctyl)-9-[4,4,5,5-tetramethyl-1,3,2-dioxaborolan-2-yl]-perylene-3,4-dicarboxylic acid monoimide (C7SW-9-bor-PMI)
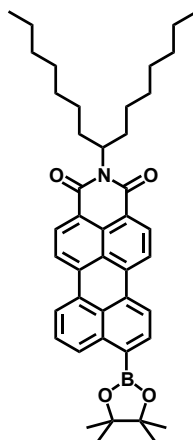
N-(1-Heptyloctyl)-9-bromo-perylene-3,4-dicarboxylic acid monoimide (4.51 g, 7.39 mmol) was dissolved in 75 mL of 1,4-dioxane. Bis(pinacolato) diboron (2.07 g, 8.15 mmol) and potassium acetate (2.07 g, 21.1 mmol) were added to the solution. Argon was bubbled through the reaction mixture for 30 minutes before [1,1-bis(diphenylphosphino)ferrocene]dichloro-palladium(II) (160 mg, 0.22 mmol) was added. The flask was evacuated and flushed with argon three times before heating at 70 °C for 20 hours. The reaction was monitored by mass spectroscopy and TLC. After completion the solvent was removed under reduced pressure and the remaining solid was dissolved in dichloromethane. The solution was extracted with water and a saturated NaCl-solution. The organic extract dried over sodium sulfate. The solvent was removed under reduced pressure and the raw product was precipitated from dichloromethane in methanol to give a dark-red solid used for the next step without further purification (4.60 g).

10.2.7 *N*-(1-Heptyloctyl)-9-(4-N-(1-heptyloctyl)-naphthalen-1,8-dicarboxylic acid monoimide)-perylene- 3,4-dicarboxylic acid monoimide (C7SW-9-(C7SW-NMI)-PMI)
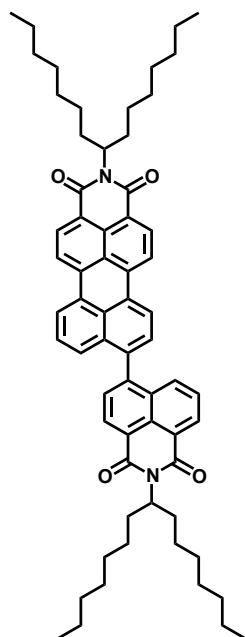
N-(1-Heptyloctyl)-9-[4,4,5,5-tetramethyl-1,3,2-dioxaborolan-2-y]-perylene-3,4-dicarboxylic acid monoimide (3.08 g, 4.68 mmol) and *N*-(1-heptyloctyl)-4-bromo-naphthalene-1,8-dicarboxylic acid monoimide (2.28 g, 4.68 mmol) were dissolved in 235 mL of toluene. Successively ethanol (15 mL) and an aqueous solution of Na_2CO_3 (1 M, 195 mL) were added to the mixture. Argon was bubbled through the solution for 30 minutes before adding tetrakis(triphenylphosphine)palladium(0) (246 mg, 0.21 mmol). The mixture was stirred under argon atmosphere at 80 ˚C for 18 hours. The reaction was monitored by TLC using petroleum ether/dichloromethane 1:1 as eluent. After cooling to room temperature, the organic solvent was removed. The aqueous phase was washed three times with 50 mL of toluene. The collected organic extracts were dried over magnesium sulfate. The solvent was removed under reduced pressure to give a brown solid. The raw product was precipitated from dichloromethane in methanol to give a red solid. The product was isolated after column chromatography (silica, petroleum ether/dichloromethane 1:1) as a red solid in 67 % yield (2.96 g, 3.17 mmol).

10.2.8 *N,N'*-Bis(1-heptyloctyl)-2,5,10,13-tetrakis[3,3-dimethylbutyl]terrylene-3,4:11,12-tetracarboxylic acid diimide (C7SW-TDI)
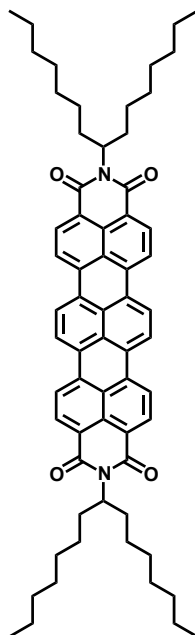
N-(1-heptyloctyl)-9-(4-N-(1-heptyloctyl)-naphthalene-1,8-dicarboxylic imide)-perylene-3,4-dicarboxylic imide (0.92 g, 0.98 mmol) was dissolved in 18 mL ethanolamine. Potassium carbonate (6.55 g, 47.40 mmol) was added to the solution which then was stirred under argon atmosphere for 3 hours at 160 °C. After cooling to room temperature, 30 mL of methanol and 150 mL of water were added. The solid was filtered, washed with water and methanol before being purified by column chromatography (silica, petroleum ether/dichloromethane 3:10) to give the desired materials as a blue solid in 85 % yield (782 mg, 0.84 mmol).

10.2.9 *N,N'*-Bis(1-heptyloctyl)-2,5,10,13-tetrakis[3,3-dimethylbutyl]terrylene-3,4:11,12-tetracarboxylic acid diimide (C7SW-alk-TDI)
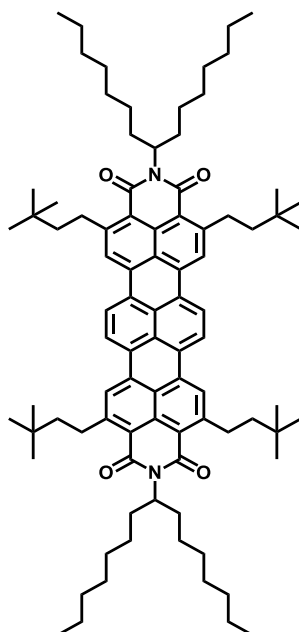
N,N'-Bis(1-heptyloctyl)-terrylene-3,4:11,12-tetracarboxylic acid diimide (0.30 g, 0.32 mmol), and 3,3-dimethyl-1-butene (0.54 g, 6.42 mmol) were mixed in 10 mL of dry mesitylene in an oven dried round bottom flask. Argon was bubbled through the solution for 30 minutes, and successively $RuH_2(CO)(PPh_3)_3$ (15.0 mg, 0.02 mmol) was added. The reaction was stirred under argon at 185 °C (bath temperature) for 18 hours. After removal of the solvent, the crude product was purified by column chromatography (silicagel CH_2Cl_2/petroleum ether 1:2), to give the desired compound as a blue solid (66 % yield, 0.27 g, 0.21 mmol).

^{1}H-NMR (500 MHz, 373 K, $C_2Cl_4D_2$): δ (ppm): 8.50 (s, 2H), 8.18 (s, 2H), 5.43–5.10 (m, 1H), 3.61–3.41 (m, 4H), 2.55–2.19 (m, 2H), 2.09–1.77 (m, 2H), 1.76–1.62 (m, 4H), 1.60–1.28 (m, 21H), 1.15 (s, 18H), 0.97–0.86 (m, 6H).

^{13}C-NMR (126 MHz, 373 K, $C_2Cl_4D_2$): δ (ppm): 164.1, 150.9, 133.6, 132.0, 130.4, 128.3, 124.9, 123.5, 123.3, 119.7, 54.0, 45.7, 32.6, 32.0, 31.6, 30.6, 29.4, 29.3, 29.0, 26.9, 22.3, 13.7.

FD Mass Spectrum (8kV): m/z= 1272.2 (100 %) [M+].

IR spectrum (ATR): ν_{max} [cm^{-1}]= 2953; 2924; 2857; 1683; 1648; 1594; 1542; 1460; 1416; 1331; 1298; 1205; 871; 841; 817; 700.

UV-Vis (in toluene): λ_{max} (ε): 548 nm (1.98 x 10^4 M^{-1}cm^{-1}), 591 nm (5.79 x 10^4 M^{-1}cm^{-1}), 643 nm (1.05 x 10^5 M^{-1}cm^{-1}).

Fluorescence (in toluene, λ_{ex}=632 nm): 657 nm, 716 nm. φ_F: 0.95.

Elemental Analysis: calculated (%): C, 83.10; H, 9.67; N, 2.20;
experimental (%): C, 82.83; H, 9.53; N, 2.18.

10.2.10 *N,N'*-Bis(1-heptyloctyl)-2,5,8,11-tetrakis[3,3-dimethylbutyl]perylene-3,4:9,10-tetracarboxylic acid diimide (C7SW-alk-PDI)
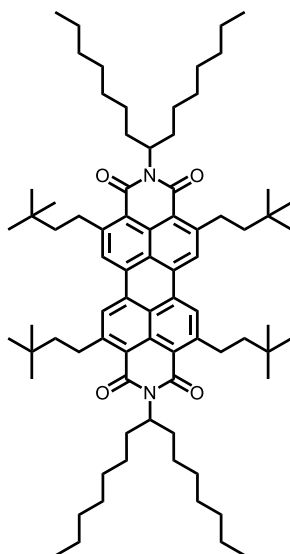
N,N'-Bis(1-heptyloctyl) perylene-3,4:9,10-tetracarboxylic acid diimide (0.20 g, 0.25 mmol), and 3,3-dimethyl-1-butene (0.42 g, 4.93 mmol) were mixed in 2 mL of dry mesitylene in an oven dried round bottom flask. Argon was bubbled through the solution for 30 minutes, and successively $RuH_2(CO)(PPh_3)_3$ (11 mg, 12 µmol) was added. The reaction was stirred under argon at 185 °C (bath temperature) for 14 hours. After removal of the solvent, the crude product was purified by column chromatography (silica, CH_2Cl_2/petroleum ether 1:2), to give the desired compound (89 % yield, 0.25 g, 0.22 mmol) as a bright orange solid.

¹H-NMR (300 MHz, CD_2Cl_2): δ (ppm): 8.34 (s, 4H), 5.28–5.11 (m, 2H), 3.70–3.37 (m, 8H), 2.39–2.19 (m, 4H), 1.94–1.68 (m, 4H), 1.67–1.54 (m, 8H), 1.45–1.17 (m, 40H), 1.10 (s, 36H), 0.82 (t, J = 6.2 Hz, 12H).

¹³C-NMR (75 MHz, CD_2Cl_2): δ (ppm): 164.9, 151.8, 133.4, 132.5, 127.4, 124.6, 121.2, 54.6, 46.3, 33.1, 32.9, 32.4, 31.4, 30.2, 29.9, 29.8, 27.6, 23.2, 14.4.

FD Mass Spectrum (8kV): m/z= 1148.9 (100 %) [M+].

IR spectrum (ATR): ν_{max} [cm⁻¹]= 2952; 2922; 2855; 1689; 1648; 1604; 1546; 1466; 1430; 1365; 1327; 1258; 1247; 1227; 1213; 881; 753; 721; 632.

UV-Vis (in toluene): λ_{max}(ε): 456 nm (1.62 x 10⁴ $M^{-1}cm^{-1}$), 486 nm (4.16 x 10⁴ $M^{-1}cm^{-1}$), 522 nm (6.12 x 10⁴ $M^{-1}cm^{-1}$).

Fluorescence (in toluene): λ_{max}: (λ_{ex}=522 nm): 535 nm, 574 nm. φ_F: 0.58.
(λ_{ex}=503 nm): 535 nm, 574 nm. φ_F: 1.00.

Elemental Analysis: calculated (%): C, 81.62; H, 10.36; N, 2.44;
experimental (%): C, 81.43; H, 9.94; N, 2.40.

10.2.11 *N,N'*-Bis(2,4-dimethylpent-3-yl)-2,5,8,11-tetrakis[3,3-dimethylbutyl]perylene-3,4:9,10-tetracarboxylic acid diimide (HB-alk-PDI)
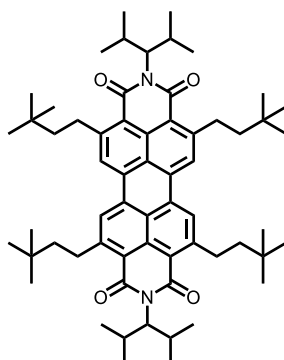
N,N'-Bis(2,4-dimethylpent-3-yl) perylene-3,4:9,10-tetracarboxylic acid diimide (0.50 g, 0.85 mmol) and 3,3-dimethyl-1-butene (1.43 g, 17.0 mmol) were mixed in 10 mL of dry mesitylene in an oven dried round bottom flask. Argon was bubbled through the solution for 30 minutes, and successively $RuH_2(CO)(PPh_3)_3$ (39 mg, 0.04 mmol) was added. The reaction was stirred under argon at 185 °C (bath temperature) for 20 hours. After removal of the solvent, the crude product was purified by column chromatography (silicagel CH_2Cl_2/petroleum ether 1:2), to give the desired compound (73 % yield, 0.57 g, 0.62 mmol) as a bright orange solid.

^{1}**H-NMR** (500 MHz, 373 K, $C_2Cl_4D_2$): δ (ppm): 8.33 (s, 4H), 4.83 (t, *J* = 8.2 Hz, 2H), 3.67–3.52 (m, 8H), 2.82–2.68 (m, 8H), 1.80–1.64 (m, 8H), 1.19 (d, *J* = 6.6 Hz, 12H), 1.16 (s, 36H), 1.03 (d, *J* = 6.7 Hz, 12H).

^{13}**C-NMR** (126 MHz, 373 K, $C_2Cl_4D_2$): δ (ppm): 164.4, 151.0, 132.7, 131.6, 126.2, 123.9, 120.6, 45.7, 32.0, 30.7, 29.3, 29.2, 21.7, 20.6.

FD Mass Spectrum (8kV): m/z= 923.0 (100 %) [M+].

IR spectrum (ATR): v_{max} [cm^{-1}]= 2954; 2865; 1691; 1654; 1604; 1546; 1465; 1430; 1403; 1388; 1362; 1322; 1258; 1218; 1111; 930; 891; 880; 829; 769; 751; 694; 659; 638; 625.

UV-Vis (in toluene): λ_{max}(ε): 455 nm (1.51 x 10^4 M^{-1}cm^{-1}), 485 nm (4.07 x 10^4 M^{-1}cm^{-1}), 521 nm (6.04 x 10^4 M^{-1}cm^{-1}).

Fluorescence (in toluene): λ_{max}: (λ_{ex}=521 nm): 535 nm, 571 nm. φ_F: 0.56.
$\qquad\qquad\qquad\qquad$ (λ_{ex}=501 nm): 535 nm, 571 nm. φ_F: 1.00.

Elemental Analysis: calculated (%): C, 80.65; H, 9.39; N, 3.03;
$\qquad\qquad\qquad\qquad$ experimental (%): C, 80.48; H, 9.54; N, 3.03.

10.2.12 *N,N'*-Bis(1-octyl)-2,5,8,11-tetrakis[3,3-dimethylbutyl]perylene-3,4:9,10-tetracarboxylic acid diimide (8-alk-PDI)
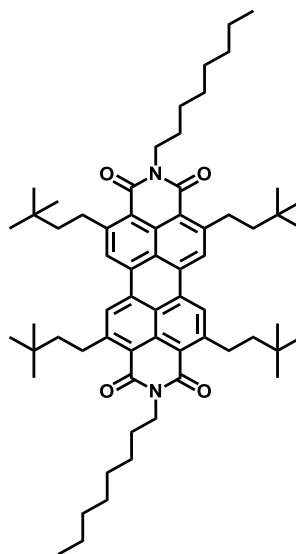
N,N'-Bis(1-octyl)-perylene-3,4:9,10-tetracarboxylic acid diimide (0.50 g, 0.81 mmol) and 3,3-dimethyl-1-butene (1.37 g, 16.3 mmol) were mixed in 20 mL of dry mesitylene in an oven dried round bottom flask. Argon was bubbled through the solution for 30 minutes and successively RuH$_2$(CO)(PPh$_3$)$_3$ (40 mg, 0.04 mmol) was added. The reaction was stirred under argon at 185 °C (bath temperature) for 20 hours. After removal of the solvent, the crude product was purified by column chromatography (silicagel CH$_2$Cl$_2$/petroleum ether 1:1), to give the desired compound (93 % yield, 0.72 g, 0.76 mmol) as a bright red solid.

^{1}H-NMR (300 MHz, CD$_2$Cl$_2$): δ (ppm): 7.98 (s, 4H), 4.12 (m, 4H), 3.48–3.25 (m, 8H), 1.81 –1.51(m, 4H), 1.59 –1.52 (m, 4H), 1.50– 1.23 (m, 24H), 1.11 (s, 36H), 0.94–0.84 (m, 6H).

^{13}C-NMR (75 MHz, CD$_2$Cl$_2$): δ (ppm): 163.5, 151.7, 133.0, 132.1, 127.0, 124.2, 120.3, 45.8, 40.9, 33.2, 32.5, 31.4, 30.0, 29.9, 29.8, 28.6, 27.9, 23.3, 14.5.

FD Mass Spectrum (8kV): m/z= 950.7 (100 %) [M+].

IR spectrum (ATR): ν_{max} [cm^{-1}]= 2954; 2926; 2857; 1686; 1652; 1603; 1548; 1465; 1436; 1394; 1363; 1330; 1245; 1204; 880; 752.

UV-Vis (in toluene): λ_{max} (ε): 455 nm (1.62 x 10^4 M^{-1}cm^{-1}), 485 nm (4.04 x 10^4 M^{-1}cm^{-1}), 521 nm (5.92 x 10^4 M^{-1}cm^{-1}).

Fluorescence (in toluene) λ_{max}: (λ_{ex}=521 nm): 532 nm, 571 nm. φ_F: 0.58.
                                  (λ_{ex}=501 nm): 532 nm, 571 nm. φ_F: 1.00.

Elemental Analysis: calculated (%): C, 80.79; H, 9.53; N, 2.94;
                            experimental (%): C, 80.67; H, 9.68; N, 2.94.

10.2.13 *N,N'*-Bis(2-ethylhexyl)-2,5,8,11-tetrakis[3,3-dimethylbutyl]perylene-3,4:9,10-tetracarboxylic acid diimide (EH-alk-PDI)
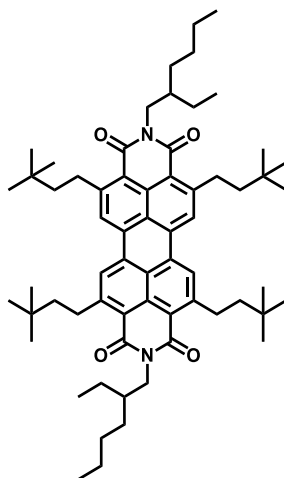
N,N'-Bis(2-ethylhexyl)-perylene-3,4:9,10-tetracarboxylic acid diimide (0.50 g, 0.81 mmol), and 3,3-dimethyl-1-butene (1.37 g, 16.3 mmol) were mixed in 15 mL of dry mesitylene in an oven dried round bottom flask. Argon was bubbled through the solution for 30 minutes, and successively $RuH_2(CO)(PPh_3)_3$ (40 mg, 0.04 mmol) was added. The reaction was stirred under argon at 185 °C (bath temperature) for 20 hours. After removal of the solvent, the crude product was purified by column chromatography (silicagel, CH_2Cl_2/petroleum ether 1:1), to give the desired compound (81 % yield, 0.63 g, 0.66 mmol) as a red solid.

^{1}H-NMR (500 MHz, 373 K, $C_2Cl_4D_2$): δ (ppm): 8.34 (s, 4H), 4.29–4.13 (m, 4H), 3.62 (dd, *J* = 9.8, 6.9 Hz, 8H), 2.07–1.96 (m, 2H), 1.79–1.67 (m, 8H), 1.58–1.32 (m, 16H), 1.18 (s, 36H), 1.03 (t, *J* = 7.4 Hz, 6H), 0.96 (t, *J* = 7.1 Hz, 6H).

^{13}C-NMR (126 MHz, 373 K, $C_2Cl_4D_2$): δ (ppm): 163.4, 151.3, 132.8, 131.8, 126.4, 124.0, 120.1, 45.4, 43.6, 38.1, 32.2, 31.1, 30.6, 29.3, 28.6, 24.4, 22.8, 13.7, 10.6.

FD Mass Spectrum (8kV): m/z= 950.9 (100 %) [M+].

IR spectrum (ATR): ν_{max} [cm^{-1}]= 2954; 2863; 1686; 1652; 1603; 1548; 1463; 1435; 1394; 1364; 1330; 1245; 1207; 880; 751.

UV-Vis (in toluene): λ_{max} (ε): 455 nm (1.77 x 10^4 M^{-1}cm^{-1}), 486 nm (4.41 x 10^4 M^{-1}cm^{-1}), 521 nm (6.46 x 10^4 M^{-1}cm^{-1}).

Fluorescence (in toluene) λ_{max}: (λ_{ex}=521 nm): 532 nm, 571 nm. φ_F: 0.56.
                              (λ_{ex}=501 nm): 532nm, 571 nm. φ_F: 1.00.

Elemental Analysis: calculated (%): C, 80.79; H, 9.53; N, 2.94;
                     experimental (%): C, 80.70; H, 9.37; N, 2.97.

10.2.15 *N*-1-Ethylpropyl-perylene-3,4-dicarboxylic acid imide (C2SW-PMI)
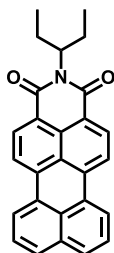
Perylene-3,4-dicarboxylic acid anhydride (1.00 g, 3.10 mmol), 3-amino-pentane (1.35 g, 15.5 mmol) and imidazole (10 g) were mixed and heated under argon atmosphere at 130 °C for 16 hours. After cooling the reaction to room temperature, the mixture was sonicated in HCl (1.0 M), to remove the imidazole. The residual solid was then filtered and purified via column chromatography (silica gel, first CH₂Cl₂/AcOEt 50/1). The desired product was obtained as a dark red crystalline powder (0.95 g, 2.42 mmol, 78 % yield).

¹H-NMR (300 MHz, CD₂Cl₂): δ (ppm): 8.43–8.23 (m, 2H), 8.08 (d, *J* = 7.4 Hz, 2H), 8.04 (d, *J* = 8.1 Hz, 2H), 7.71 (d, *J* = 7.9 Hz, 2H), 7.43 (t, *J* = 7.8 Hz, 2H), 5.03 (tt, *J* = 9.4, 6.0 Hz, 1H), 2.37–2.14 (m, 2H), 2.05–1.84 (m, 2H), 0.94 (t, *J* = 7.5 Hz, 6H).

¹³C-NMR (75 MHz, CD₂Cl₂): δ (ppm): 165.0, 136.9, 134.6, 131.5, 131.1, 130.1, 129.4, 128.1, 127.3, 126.8, 123.8, 121.6, 120.4, 57.7, 25.6, 11.8.

FD Mass Spectrum (8kV): m/z= 390.4 (100 %) [M+].

IR spectrum (ATR): ν_{max} [cm⁻¹]=2960; 2930; 2873; 1682;1643;1590; 1570; 1501; 1458; 1409; 1390; 1374; 1350; 1291; 1243; 1199; 1181; 1161; 1136; 1082; 914; 876; 835; 806; 794; 782; 760; 748; 667; 613; 563; 543.

UV-vis (in toluene): λ_{max} (ε): 478 nm (2.96 x 10⁴ M⁻¹cm⁻¹), 504 nm (3.06 x 10⁴ M⁻¹cm⁻¹).

Fluorescence (in toluene): λ_{max}: (λ_{ex}=479 nm): 529 nm, 562 nm. φ_F: 0.44.
                                        (λ_{ex}=504 nm): 529 nm, 562 nm. φ_F: 0.86.

Elemental Analysis: theoretical (%): C, 82.84; H, 5.41; N, 3.58;
                experimental (%): C, 82.57; H, 5.34; N, 3.47.

10.2.16 *N*-1-Ethylpropyl-2,5-di[3,3-dimethylbutyl]-perylene-3,4-dicarboxylic acid imide (C2SW-alk-PMI)
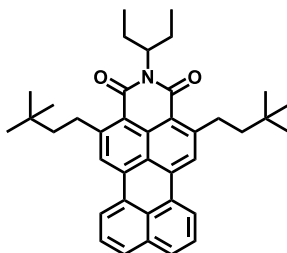
N-1-Ethylpropyl-perylene-3,4-dicarboxylic acid imide (1.85 g, 4.73 mmol) and 3,3-dimethyl-1-butene (3.98 g, 47.3 mmol) were mixed in 30 mL dry mesitylene in an oven dried round bottom flask. Argon was bubbled through the solution for 30 minutes, and successively RuH$_2$(CO)(PPh$_3$)$_3$ (0.11 g, 0.11 mmol) was added. The reaction was stirred under argon at 185 °C (bath temperature) for 10 hours. After removal of the solvent, the crude product was purified by crystallization from *iso*-propanol to give the desired compound as a bright orange solid (93 % yield, 2.46 g, 4.40 mmol).

¹H-NMR (250 MHz, CD$_2$Cl$_2$): δ (ppm): 8.29 (d, *J* = 7.4 Hz, 2H), 8.03 (s, 2H), 7.79 (d, *J* = 7.8 Hz, 2H), 7.53 (t, *J* = 7.8 Hz, 2H), 5.07 (tt, *J* = 9.5, 5.9 Hz, 1H), 3.53–3.23 (m, 4H), 2.43–2.14 (m, 2H), 2.05–1.76 (m, 2H), 1.72–1.45 (m, 4H), 1.08 (s, 18H), 0.93 (t, *J* = 7.5 Hz, 6H).

¹³C-NMR (63 MHz, CD$_2$Cl$_2$): δ (ppm): 165.2, 151.5, 135.3, 134.6, 132.9, 130.6, 129.6, 128.4, 127.3, 124.9, 124.8, 123.4, 119.5, 57.5, 46.2, 32.9, 31.3, 29.7, 25.7, 11.8.

FD Mass Spectrum (8kV): m/z= 558.0 (100 %) [M+].

IR spectrum (ATR): ν_{max} [cm^{-1}]= 2950; 2900; 2875; 1682; 1644; 1599; 1545; 1462; 1411; 1391; 1363; 1337; 1284; 1218; 1147; 1086; 909; 869; 836; 821; 801; 755; 670; 607; 562.

UV-vis (in toluene): λ_{max} (ε): 470 nm (2.81 x 10^4 M^{-1}cm^{-1}), 497 nm (2.66 x 10^4 M^{-1}cm^{-1}).

Fluorescence (in toluene): λ_{max}: (λ_{ex}=470 nm): 522 nm, 555 nm. φ_F: 0.46.

Elemental Analysis: calculated (%): C, 83.68; H, 8.10; N, 2.50;
experimental (%) C, 83.20; H, 7.69; N, 2.47.

10.2.17 2,5-Bis[3,3-dimethylbutyl]-perylene-3,4-dicarboxylic acid anhydride (alk-PMA)
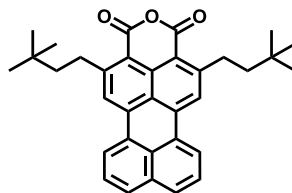
N-1-Ethylpropyl-2,5-di[3,3-dimethylbutyl]-perylene-3,4-dicarboxylic acid imide (2.00 g, 3.57 mmol) and KOH (8.02 g, 143 mmol) were suspended in 175 2-methyl-2-butanol. The reaction was refluxed for 16 hours. After cooling to room temperature, the reaction was poured into a mixture of 40 mL acetic acid, 40 mL MeOH and 400 mL cold water with ice. After stirring for 20 minutes, the red solid was filtered, washed with methanol and successively dissolved in 400 mL CH_2Cl_2 and 20 mL acetic acid. The mixture was stirred for 40 hours, then the dichloromethane evaporated, 200 mL of water were added and the precipitate was filtered and washed with methanol. The product was isolated as an orange crystalline solid after crystallization from toluene (yield 92 %, 1.61 g, 3.28 mmol).

^{1}H NMR (500 MHz, 373 K, $C_2Cl_4D_2$): δ (ppm): 8.49 (d, *J* = 7.5 Hz, 2H), 8.23 (s, 2H), 7.98 (d, *J* = 8.1 Hz, 2H), 7.70 (t, *J* = 7.8 Hz, 2H), 3.54 – 3.39 (m, 4H), 1.79 – 1.63 (m, 4H), 1.16 (s, 18H).

^{13}C NMR (126 MHz, 373 K, $C_2Cl_4D_2$): δ (ppm): 159.4, 153.5, 137.0, 135.1, 134.1, 131.0, 128.5, 127.9, 126.9, 124.5, 123.8, 123.7, 113.9, 45.1, 31.8, 30.6, 29.2.

FD Mass Spectrum (8kV): m/z= 489.3 (100 %) [M+].

IR spectrum (ATR): ν_{max} [cm^{-1}]= 3074; 2951; 2898; 2862; 1741; 1709; 1594; 1574; 1545; 1464; 1358; 1334; 1298; 1274; 1179; 1158; 1140; 1028; 878; 856; 839; 818; 773; 757; 663; 612; 557.

UV-vis (in toluene): λ_{max} (ε): 473 nm (2.39 x 10^4 M^{-1}cm^{-1}), 499 nm (2.17 x 10^4 M^{-1}cm^{-1}).

Fluorescence (in toluene): λ_{max}: (λ_{ex}=473 nm): 525 nm, 558 nm. φ_F: 0.49.

Elemental Analysis: calculated: C, 83.23; H, 6.98;
experimental C, 83.40; H, 6.98.

10.2.18 *N*-(2-Carboxyphenyl)-2,5-bis[3,3-dimethylbutyl]perylene-3,4-dicarboxylic acid imide (B-alk-PMI)
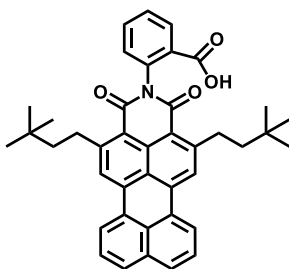
A mixture of 2,5-bis[3,3-dimethylbutyl]-perylene-3,4-dicarboxylic acid anhydride (0.30 g, 0.61 mmol), and methyl 2-aminobenzoate (0.46 g, 3.06 mmol) and imidazole (3 g) were mixed and heated at 130 ℃ under argon atmosphere for 16 hours. After cooling the reaction to room temperature, the solid obtained was sonicated in HCl (1.0 M), to remove the imidazole. The red solid was filtered and purified via column chromatography (silica gel, first CH_2Cl_2/AcOEt 50/1, then THF). The desired product was isolated as a red waxy solid (0.24 g, 0.39 mmol, 64 % yield).

¹H NMR (250 MHz, THF): δ (ppm): 8.54 (d, J = 7.4 Hz, 2H), 8.30 (s, 2H), 8.20 (d, J = 7.7 Hz, 1H), 7.91 (d, J = 8.2 Hz, 2H), 7.73 – 7.54 (m, 3H), 7.49 (t, J = 7.6 Hz, 1H), 7.35 (d, J = 7.5 Hz, 1H), 3.53 – 3.33 (m, 4H), 1.69 – 1.54 (m, 4H), 1.02 (s, 18H).

¹³C NMR (63 MHz, THF): δ (ppm): 166.3, 164.5, 152.3, 139.7, 136.4, 135.5, 134.2, 133.6, 132.6, 132.2, 131.2, 130.3, 130.2, 129.0, 128.6, 127.9, 125.9, 125.6, 124.5, 120.0, 46.3, 33.3, 30.8, 30.0.

FD Mass Spectrum (8kV): m/z= 690.0 (100 %) [M+].

IR spectrum (ATR): v_{max} [cm^{-1}]= 3050; 2946; 2901; 2863; 1715; 1689; 1653; 1630; 1595; 1545; 1452; 1349; 1284; 1224; 1164; 1134; 1077; 1046; 916; 875; 837; 822; 757; 739; 661; 646; 632; 608; 555.

UV-vis (in THF): λ_{max} (ε): 468 nm (3.02 x 10^4 M^{-1}cm^{-1}), 493 nm (2.84 x 10^4 M^{-1}cm^{-1}).

Fluorescence (in THF): λ_{max}: (λ_{ex}=468 nm): 525 nm, 552 nm. φ_F: 0.46.

HR-MS (ESI-MS) of (C41H40NO4)+ ([M + H]+): m/z calculated = 610.2957, experimental= 610.2946.

10.2.19 *N*-(2-Carboxyphenyl)-2,5-bis[3,3-dimethylbutyl]-9-bromo-perylene-3,4-dicarboxylic acid imide (B-9-Br-alk-PMI)
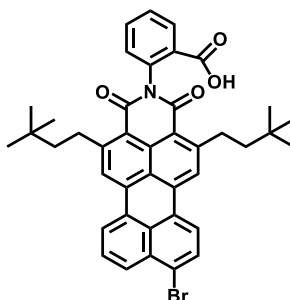
N-(2-Carboxyphenyl)-2,5-bis[3,3-dimethylbutyl]perylene-3,4-dicarboxylic acid imide (0.28 g, 0.45 mmol) and N-bromosuccinimide (0.16 g, 1.36 mmol) were dissolved in 30 mL of THF. The reaction was heated up to 110 °C and monitored via FD-MS analysis. After fifteen hours the system was cooled to room temperature and N-bromosuccinimide (0.16 g, 1.36 mmol) was added once again. The process was repeated until from via FD-MS analysis only the target compound was detected. After removal of the solvent, the desired product was isolated via precipitation in hexane from THF as an orange waxy solid in 83 % yield (0.26 g, 2.46 mmol).

^{1}H NMR (500 MHz, THF-d_8): δ (ppm): 8.48 (d, J = 7.6 Hz, 1H), 8.30 (d, J = 8.2 Hz, 1H), 8.23 − 8.15 (m, 4H), 7.86 (d, J = 8.1 Hz, 1H), 7.71 − 7.60 (m, 2H), 7.51 (t, J = 7.7 Hz, 1H), 7.37 (d, J = 7.7 Hz, 1H), 3.48 − 3.33 (m, 4H), 1.65 − 1.54 (m, 4H), 1.01 (s, 9H), 1.00 (s, 9H).

^{13}C NMR (63 MHz, THF): δ (ppm): 166.3, 164.5, 152.4, 139.6, 135.7, 135.6, 134.0, 133.7, 133.6, 132.6, 132.2, 132.2, 130.8, 130.4, 130.2, 130.0, 129.9, 129.2, 128.7, 126.2, 126.0, 125.8, 125.4, 125.2, 124.8, 120.4, 120.4, 46.2, 33.3, 31.7, 30.0.

FD Mass Spectrum (8kV): m/z= 690.0 (100 %) [M+].

IR spectrum (ATR): v_{max} [cm^{-1}]= 3072; 2949; 2902; 2864; 1724; 1691; 1645; 1597; 1545; 1491; 1438; 1393; 1345; 1225; 1163; 1133; 1076; 1047; 923; 874; 836; 819; 754; 672; 630; 554.

UV-vis (in THF): λ_{max} (ε): 469 nm (2.89 x 10^4 M^{-1}cm^{-1}), 495 nm (2.89 x 10^4 M^{-1}cm^{-1}).

Fluorescence (in THF): λ_{max}: (λ_{ex} = 469 nm): 525 nm, 552 nm. φ_F: 0.51.

HR-MS (ESI-MS) of (C41H38NO4NaBr)+ ([M+Na]+): m/z calculated = 710.1882, experimental = 710.1907.

10.2.20 *N*-(2-Carboxyphenyl)-2,5-bis[3,3-dimethylbutyl]-9-((p-cyanophenyl)amino)perylene-3,4-dicarboxylic acid imide (B-9-amino-alk-PMI)
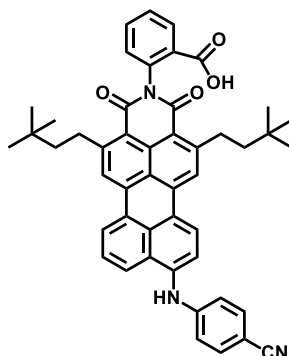
N-(2-Carboxyphenyl)-2,5-bis[3,3-dimethylbutyl]-9-bromo-perylene-3,4-dicarboxylic acid imide (0.22 g, 0.32 mmol), 4-aminobenzonitrile (49 mg, 0.42 mmol) tris-(dibenzylideneacetone)-dipalladium(0) (17 mg, 18 μmol), tris-tert-butylphosphine (4.0 mg, 4.3 μmol) and sodium-tert-butoxide (13 mg, 0.13 mmol) were dissolved in dry toluene (20 mL) under argon atmosphere. The reaction was then stirred at 80 °C under argon overnight. After cooling, the solvent was removedand the remaining solid was dissolved in THF and filtered over silica. The desired product was finally isolated after purification via gel permeation chromatography (BioBeads, THF) as a violet solid in 54 % yield (0.13 g, 0.17 mmol).

^{1}H NMR (700 MHz, THF-d_8): δ (ppm): 8.44 (d, J = 8.2 Hz, 1H), 8.38 (d, J = 7.4 Hz, 1H), 8.25 (dd, J = 8.0, 1.6 Hz, 1H), 8.13 (s, 1H), 8.10 (s, 1H), 8.07 − 8.00 (m, 1H), 7.69 (td, J = 7.6, 1.6 Hz, 1H), 7.58-7.51 (m, 4H), 7.39-7.36 (m, 2H), 7.18 (d, J = 8.3 Hz, 2H), 3.53 − 3.35 (m, 3H), 3.33 − 3.18 (m, 1H), 1.67-1.58 (m, 4H), 1.00 (s, 9H), 0.99 (s, 9H).

^{13}C NMR (176 MHz, THF): δ (ppm): 167.1, 164.7, 164.6, 152.4, 152.5, 149.3, 140.9, 140.1, 136.7, 136.5, 134.5, 134.3, 133.9, 132.7, 132.3, 130.3, 130.0, 129.9, 128.8, 127.1, 125.3, 125.3, 125.1, 125.1, 124.4, 119.9, 119.6, 118.8, 118.1, 103.9, 46.4, 46.2, 33.4, 31.6, 30.0.

FD Mass Spectrum (8kV): m/z= 725.3 (100 %) [M+].

IR spectrum (ATR): ν_{max} [cm^{-1}]= 3373; 3060; 2947; 2904; 2864; 2217; 1690; 1670; 1633; 1605; 1573; 1535; 1512; 1447; 1348; 1327; 1291; 1250; 1222; 1174; 1049; 911; 874; 816; 755; 742; 703; 633; 544.

UV-vis (in THF): λ_{max} (ε): 515 nm (2.59 x 10^4 M^{-1}cm^{-1}).

Fluorescence (in THF): λ_{max}: (λ_{ex}=515 nm): 640 nm. φ_F: 0.20.

HR-MS (ESI-MS) of (C48H43N3O4Na)+ ([M+Na]+): m/z calculated = 748.3151, experimental= 748.3125.

10.2.21 *(E)*-4-((7,16-bis(3,3-dimethylbutyl)-6,18-dioxo-6*H*-benzo[4,5][1,3]oxazino[2,3-a]benzo[5,10]anthra[2,1,9-*def*]isoquinolin-12(18*H*)-ylidene)amino)benzonitrile (Quinoid)

**(The structure of the compound may not correspond to the material obtained from the reaction)**
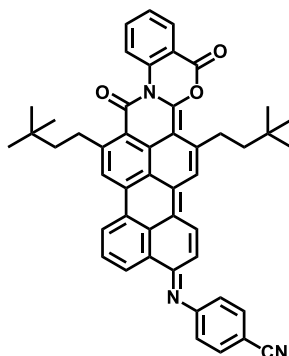
N-(2-Carboxyphenyl)-2,5-bis[3,3-dimethylbutyl]-9-((p-cyanophenyl)amino)perylene-3,4dicarboxylic acid imide (25 mg, 34.5 μmol) was suspended in 4 mL of freshly distilled thionyl chloride and the reaction mixture was refluxed under argon for 4 hours. After removal of the solvent, the solid was dissolved in 5 mL anhydrous THF. The solution was then added dropwise to a suspension of sodium hydride (90 mg, 60 % in mineral oil) in 5 mL of anhydrous THF at 0 °C. After stirring for 1 hour at 0 °C, the excess of sodium hydride was destroyed by dropwise addition of methanol and successively of water. In the solution a precipitate was formed, which was then filtered and washed with methanol and water to give 20 mg of a red solid.

Most of the characterization methods failed, most probably due to the strong aggregation of the material.

IR spectrum (ATR): ν_{max} [cm^{-1}]=2941, 2920, 2852, 2332, 2317, 2214, 1653, 1572, 1506, 1439, 1360, 1201, 1161, 1039, 1007, 887, 839, 759, 644.

UV-vis (in THF): λ_{max} : 461 nm.

10.2.22 *N*,*N'*-Bis(1-ethylpropyl)-2,5,8,11-tetrakis[2-(diethoxyphosphoryl)ethyl]perylene-3,4:9,10-tetracarboxylic acid diimide (C2SW-4PO(OEt)$_2$-PDI)
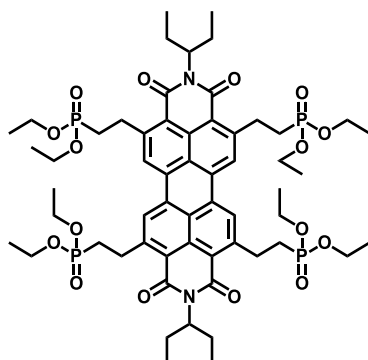
N,*N'*-Bis(1-ethylpropyl) perylene-3,4:9,10-tetracarboxylic acid diimide (100 mg, 0.19 mmol) and diethyl vinylphosphonate (619 mg, 3.77 mmol) were dissolved in 4 mL anhydrous mesitylene. Argon was bubbled through the solution for 30 minutes. RuH$_2$(CO)(PPh$_3$)$_3$ (9 mg, 0.01 mmol) was added to the mixture and the reaction was heated at 180 °C for 12 hours. After cooling the system to room temperature, the solvent was removed. The reaction mixture was dissolved in 10 mL of methanol and poured into 100 ml water. The precipitate was filtered and the desired compound obtained as a red solid with 95 % yield (213 mg, 0.18 mmol).

^{1}H-NMR (500 MHz, CD$_2$Cl$_2$): δ (ppm): 8.63 (s, 4H), 5.08 (m, 2H), 4.24–4.08 (m, 16H), 3.73 (dd, J = 15.8, 9.3 Hz, 8H), 2.35–2.15 (m, 12H), 1.94 (m, 4H), 1.34 (t, J = 6.9 Hz, 24H), 0.92 (t, J = 7.2 Hz, 12H).

^{13}C-NMR (126 MHz, CD$_2$Cl$_2$): δ (ppm): 164.7, 149.3, 133.7, 132.3, 128.3, 125.3, 121.1, 62.3, 58.0, 30.9, 27.1, 25.6, 16 9, 11.8.

FD/MS (8kV): m/z= 1183.6 (100 %) [M+].

UV-Vis (in CH$_2$Cl$_2$): λ$_{max}$(ε): 524 nm (5.70 x 10^4 M^{-1}cm^{-1}), 488 nm (3.81 x 10^4 M^{-1}cm^{-1}), 458 nm (1.50 x 10^4 M^{-1}cm^{-1}).

Fluorescence (in CH$_2$Cl$_2$, λ$_{ex}$=524 nm): 532 nm. φ$_F$: 0.88.

IR spectrum (ATR): ν$_{max}$ [cm^{-1}]= 3441; 2981; 2934; 2876; 1685; 1645; 1609; 1548; 1437; 1402; 1340; 1322; 1288; 1212; 1161; 1094; 1051; 1024; 963; 885; 831; 815; 783; 751; 634; 586; 555.

Elemental Analysis: theoretical (%): C: 58.68; H: 6.96; N: 2.36;
experimental (%): C: 58.45; H: 6.90; N: 2.24.

10.2.23 *N,N'*-Bis(1-ethylpropyl)-2,5,8,11-tetrakis[2-(dihydroxyphosphoryl)ethyl]perylene-3,4:9,10-tetracarboxylic acid diimide (C2SW-4PO(OH)₂-PDI)
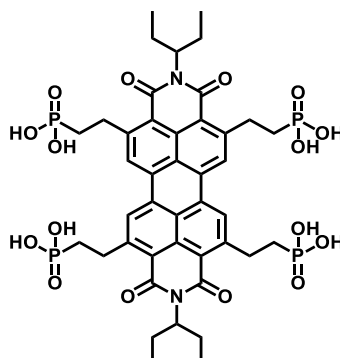
N,N'-Bis(1-ethylpropyl)-2,5,8,11-tetrakis[2-(diethoxyphosphoryl)ethyl]perylene-3,4:9,10-tetracarboxylic acid diimide (150 mg, 0.13 mmol) and bromotrimethylsilane (309 mg, 0.266 mL, 2.02 mmol) were mixed together in 25 mL anhydrous dichloromethane and stirred in a sealed vessel for 2 days at room temperature. After evaporating the solvent, the solid was dissolved in 50 mL methanol and stirred at room temperature for 2 days. Afterwards the precipitate was filtered and washed with 50 mL methanol and afterwards with 50 mL dichloromethane. The desired product was isolated as an orange solid with 84 % yield (102 mg, 0.11 mmol).

¹H-NMR (250 MHz, DMF-d₄): δ (ppm): 8.70 (s, overlapping with the water signal), 4.89 (m, 2H), 3.67 (s, 8H), 2.47–1.76 (m, 16H), 0.89 (t, J = 7.0 Hz, 12H).

¹³C-NMR (75 MHz, DMF-d₄): δ (ppm): 164.9, 150.1, 133.5, 133.0, 129.3, 124.8, 120.4, 58.1, 27.9, 25.8, 12.4.

MALDI-TOF analysis (m/z): 962.21 (100%) [M+].

UV-Vis (in water): $\lambda_{max}(\varepsilon)$: 531 nm (5.45 x 10⁴ M⁻¹cm⁻¹), 495 nm (2.45 x 10⁴ M⁻¹cm⁻¹), 458 nm (1.57 x 10⁴ M⁻¹cm⁻¹).

Fluorescence (in water): λ_{max}: (λ_{ex}=531 nm): 548 nm. φ_F: 0.76.

IR spectrum (ATR): ν_{max} [cm⁻¹]= 3494; 2967; 2936; 2878; 2234; 1689; 1635; 1604; 1548; 1433; 1403; 1340; 1288; 1222; 1090; 989; 924; 881; 794; 750; 728; 627; 582; 548.

HR-MS (ESI-MS) ([M + H]+): m/z calculated = 963.2208, experimental= 963.2189.

10.2.24 *N,N'*-Bis(1-ethylpropyl)-2,5,8,11-tetrakis[4,4,5,5-tetramethyl-1,3,2-dioxaborolan-2-y]perylene-3,4:9,10-tetracarboxylic acid diimide (C2SW-4bor-PDI)[n]
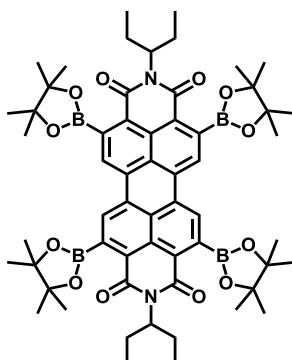
N,N'-Bis(1-ethylpropyl) perylene-3,4:9,10-tetracarboxylic acid diimide (100 mg, 0.19 mmol) and bis(pinacolato)diboron (383 mg, 1.51 mmol) were mixed together and dissolved in 2 mL anhydrous toluene and 0.15 mL anhydrous acetone. Argon was bubbled through the solution for 30 minutes. $RuH_2(CO)(PPh_3)_3$ (87 mg, 0.09 mmol) was added to the mixture, the vial selaed and the reaction heated at 140 °C for 3 and half hours in microwave oven. After cooling the system to room temperature, the solvent was evaporated and the desired compound purified by successive reprecipitation from dichloromethane in methanol. The desired product was obtained as an orange bright solid with 60 % yield (117 mg, 0.11 mmol).

^{1}H-NMR (250 MHz, CD_2Cl_2): δ (ppm): 8.59 (s, 4H), 4.94 (tt, *J* = 9.2, 6.0 Hz, 2H), 2.33–2.10 (m, 4H), 2.04–1.84 (m, 4H), 1.51 (s, 48H), 0.92 (t, *J* = 7.4 Hz, 12H).

^{13}C-NMR (126 MHz, CD_2Cl_2): δ (ppm): 166.4, 139.5, 133.8, 128.9, 127.3, 126.3, 84.9, 58.5, 25.6, 25.3, 11.8.

FD/MS (8kV): m/z= 1033.33 (100 %) [M+].

UV-Vis (in toluene): $\lambda_{max}(\varepsilon)$: 468 nm (1.64 x 10^4 $M^{-1}cm^{-1}$), 500 nm (4.55 x 10^4 $M^{-1}cm^{-1}$), 538 nm (7.30 x 10^4 $M^{-1}cm^{-1}$).

**Fluorescence** (in toluene): λ_{max} (λ_{ex}=538 nm): 548 nm, 591nm. φ_F: 0.89.

IR spectrum (ATR): ν_{max} [cm^{-1}]= 2972; 2935; 2878; 1687; 1650; 1609; 1550; 1438; 1389; 1312; 1234; 1194; 1138; 1090; 1012; 983; 963; 878; 855; 822; 793; 754; 678; 577.

Elemental Analysis: theoretical (%): C: 67.34; H: 7.21; N: 2.71;
experimental (%): C: 67.29; H: 7.40; N: 2.96.

---

[n] The here reported synthesis is an improved version of the protocol published on: Battagliarin, G., Li, C., Enkelmann, V., & Müllen, K. (2011). *Organic Letters*, *13*(12), 3012-3015.

10.2.25 *N,N'*-Bis(1-heptyloctyl)-2,5,8,11-tetrakis[4,4,5,5-tetramethyl-1,3,2-dioxaborolan-2-y]perylene-3,4:9,10-tetracarboxylic acid diimide (C7SW-4bor-PDI)[o]
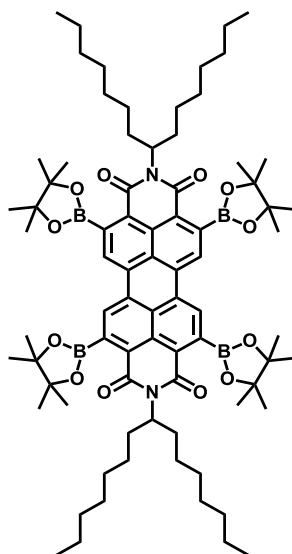
N,N'-Bis(1-heptyloctyl) perylene-3,4:9,10-tetracarboxylic acid diimide (1.00 g, 1.23 mmol) and bis(pinacolato)diboron (2.50 g, 9.86 mmol) were mixed together and dissolved in 10 mL anhydrous toluene and 1.5 mL anhydrous acetone. Argon was bubbled through the solution for 30 minutes. $RuH_2(CO)(PPh_3)_3$ (0.57 g, 0.62 mmol) was added to the mixture and the reaction was heated at 140 °C for 3 and half hours in microwave oven. After cooling the system to room temperature, the solvent was evaporated and the desired compound purified by successive reprecipitation from dichloromethane in methanol. The product was isolated as an orange crystalline solid with 70 % yield (1.13 g, 0.86 mmol).

^{1}H-NMR (250 MHz, CD_2Cl_2): δ (ppm): 8.58 (s, 4H), 5.06 (s, 2H), 2.35–2.06 (m, 4H), 1.98–1.72 (m, 4H), 1.50 (s, 48H), 1.24 (s, 40H), 0.84 (t, *J* = 6.5 Hz, 12H).

^{13}C-NMR (126 MHz, CD_2Cl_2): δ (ppm): 166.2, 139.3, 133.8, 128.8, 127.6, 127.3, 126.3, 84.9, 55.2, 32.8, 32.5, 30.0, 29.8, 27.4, 25.4, 23.2, 14.4.

FD/MS (8kV): m/z= 1312.4 (100 %) [M+].

UV-Vis (in toluene): $\lambda_{max}(\epsilon)$: 468 nm (1.62 x 10^4 $M^{-1}cm^{-1}$),500 nm (4.49 x 10^4 $M^{-1}cm^{-1}$), 538 nm (7.30 x 10^4 $M^{-1}cm^{-1}$).

Fluorescence (in toluene): λ_{max}: (λ_{ex}=538 nm): 548 nm, 591nm. φ_F: 0.83.

IR spectrum (ATR): v_{max} [cm^{-1}]= 2972; 2935; 2926; 2856; 1687; 1649; 1607; 1547; 1438; 1388; 1335; 1311; 1236; 1138; 1111; 963; 892; 868; 822; 797; 755; 678; 636; 577.

Elemental Analysis: theoretical (%): C: 71.24; H: 8.74; N: 2.13;
experimental (%): C: 70.97; H: 8.41; N: 2.28.

---

[o] The here reported synthesis is an improved version of the protocol published on: Battagliarin, G., Li, C., Enkelmann, V., & Müllen, K. (2011). *Organic Letters*, *13*(12), 3012-3015.

10.2.26 *N,N'*-Bis(1-heptyloctyl)-2,5,10,13-tetrakis[4,4,5,5-tetramethyl-1,3,2-dioxaborolan-2-yl]terrylene-3,4:11,12-tetracarboxylic acid diimide (C7SW-4bor-TDI)
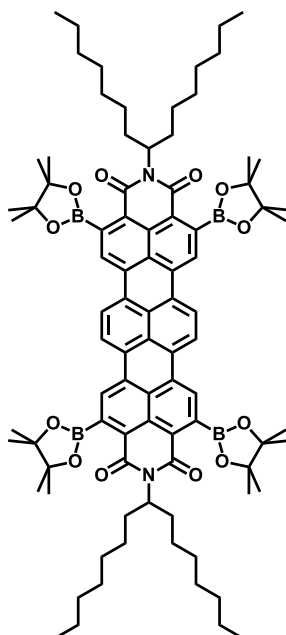
N,N'-Bis(1-heptyloctyl)-terrylene-3,4:11,12-tetracarboxylic acid diimide (0.80 g, 0.86 mmol) and bis(pinacolato)diboron (1.74 g, 6.84 mmol) were mixed together and dissolved in 60 mL anhydrous toluene and 2 mL anhydrous acetone in a pressure vial. Argon was bubbled through the solution for 30 minutes. $RuH_2(CO)(PPh_3)_3$ (0.40 g, 0.43 mmol) was added to the mixture, the vial sealed and the reaction heated at 140 °C for 24 hours. After cooling the system to room temperature, the solvent was evaporated and 400 mL of methanol were added to the remaining liquid. The precipitate was filtered, dissolved in dichloromethane and precipitated once again in methanol. The desired product was isolated after gel permeation chromatography (BioBeads, dichloromethane) as dark blue solid with 60 % yield (840 mg, 0.58 mmol).

^{1}H-NMR (500 MHz, CD_2Cl_2): δ (ppm): 8.74 (s, 4H), 8.53 (s, 4H), 5.19–4.99 (m, 2H), 2.32–2.15 (m, 4H), 1.95–1.75 (m, 4H), 1.39–1.15 (m, 40H), 0.85 (t, *J* = 6.9 Hz, 12H)

^{13}C-NMR (126 MHz, 393 K, $C_2D_2Cl_4$): δ (ppm): 165.5, 133.9, 131.0, 129.0, 128.1, 126.0, 125.7, 124.1, 123.8, 120.2, 84.1, 54.5, 32.4, 31.6, 29.2, 28.8, 26.6, 24.8, 22.3, 13.6.

FD Mass Spectrum (8kV): m/z= 1438.1 (100 %) [M+].

IR spectrum (ATR): ν_{max} [cm^{-1}]= 2925; 2854; 1678; 1644; 1541; 1430; 1369; 1342; 1303; 1237; 1141; 1095; 1007; 962; 867; 847; 816; 781; 719; 699; 661; 617; 577.

UV-vis (in chloroform): λ_{max} (ε): 663 nm (1.30 x 10^5 M^{-1}cm^{-1}), 608 nm (6.57 x 10^4 M^{-1}cm^{-1}), 563 nm (2.11 X 10^4 M^{-1}cm^{-1}).

Fluorescence (in chloroform): λ_{max}: (λ_{ex} = 632 nm): 680 nm, 739 nm. φ_F: 1.00.

HR-MALDI (ESI-MS) ([M + H]+): m/z calculated = 1438.9057; experimental 1438.9071.

10.2.27 N-(1-Ethylpropyl)-2,5-bis[4,4,5,5-tetramethyl-1,3,2-dioxaborolan-2-yl]perylene-3,4-dicarboxylic acid monoimide (C2SW-2,5-bor-PMI)
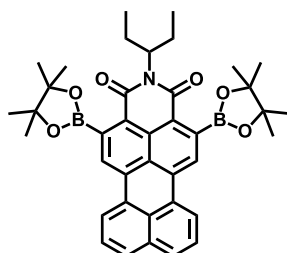
N-1-Ethylpropyl-perylene-3,4-dicarboxylic acid imide (0.50 g, 1.28 mmol), and bis(pinacolato)diboron (1.30 g, 5.11 mmol) were mixed together and dissolved in 20 mL anhydrous toluene and 1 mL anhydrous acetone in a 48 mL pressure vial. Argon was bubbled through the solution for 30 minutes. RuH$_2$(CO)(PPh$_3$)$_3$ (0.29 g, 0.32 mmol) was added to the mixture, the vial sealed and the reaction heated at 140 °C for 18 hours. After cooling the system to room temperature, the solvent was evaporated and to the remaining liquid were added 250 mL methanol. The solid was filtered, dissolved in dichloromethane and precipitated once again in methanol. The desired product was obtained as an orange solid in 76 % yield (630 mg, 0.98 mmol)

^{1}H-NMR (250 MHz, CD$_2$Cl$_2$): δ (ppm): 8.44 (d, J = 7.1 Hz, 2H), 8.32 (s, 2H), 7.86 (d, J = 7.8 Hz, 2H), 7.59 (t, J = 7.8 Hz, 2H), 4.94 (tt, J = 9.1, 6.1 Hz, 1H), 2.34–2.09 (m, 2H), 2.07–1.82 (m, 2H), 1.51 (s, 24H), 0.93 (t, J = 7.5 Hz, 6H).

^{13}C-NMR (63 MHz, CD$_2$Cl$_2$): δ (ppm): 166.7, 139.4, 135.9, 134.9, 131.2, 129.7, 129.1, 128.6, 127.4, 127.3, 125.2, 124.1, 123.5, 84.7, 58.1, 25.5, 25.3, 11.8.

FD Mass Spectrum (8kV): m/z= 643.4 (100 %) [M+]

IR spectrum (ATR): v$_{max}$ [cm^{-1}]= 2972; 2931; 2878; 1675; 1642; 1618; 1605; 1545; 1462; 1422; 1352; 1289; 1236; 1210; 1136; 1069; 1006; 986; 964; 916; 879; 866; 839; 818; 800; 789; 754; 655; 616.

UV-vis (in toluene): λ$_{max}$ (ε): 484 nm (3.14 x 10^4 M^{-1}cm^{-1}), 511 nm (3.26 x 10^4 M^{-1}cm^{-1}).

Fluorescence (in toluene) λ$_{max}$: (λ$_{ex}$=485 nm): 535 nm, 568 nm. φ$_F$: 0.53.
(λ$_{ex}$=510 nm): 535 nm, 568 nm. φ$_F$: 0.78.

Elemental Analysis: calculated (%): C, 72.81; H, 6.74; N, 2.18;
experimental (%): C, 72.58; H, 6.58; N, 2.20.

10.2.28 *N,N'*-Bis(1-ethylpropyl)-2,5,8,11-tetrakis[4-methylbenzoate] perylene-3,4:9,10-tetracarboxylic acid diimide (C2SW-4PhCOOMe-PDI)
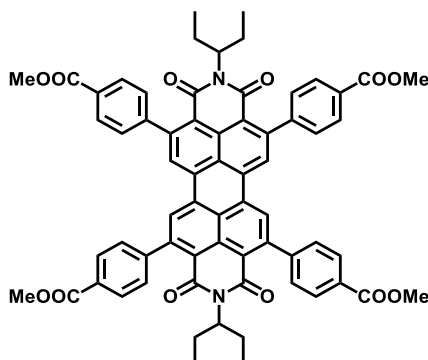
N,N'-Bis(1-ethylpropyl)-2,5,8,11-tetrakis[4,4,5,5-tetramethyl-1,3,2-dioxaborolan-2-yl]perylene-3,4:9,10-tetracarboxylic acid diimide (180 mg, 0.17 mmol) and methyl 4-bromobenzoate (224 mg, 1.04 mmol) were dissolved in 35 mL of dry tolune. A solution of potassium carbonate (577 mg in 3.5 mL of water) and ethanol (0.35 mL) were added to the reaction mixture and argon was bubbled for 30 minutes. After adding Pd(PPh$_3$)$_4$ (121 mg, 0.10 mmol) and bubbling argon for other 30 minutes, the reaction was heated at 80 °C under inert atmosphere for 48 hours. After cooling to room temperature the desired product was purified via column chromatography (silica gel, CH$_2$Cl$_2$/acetone 50/1) and isolated in 43 % yield as an orange solid (80 mg, 0.07 mmol).

¹H-NMR (500 MHz, CD$_2$Cl$_2$): δ (ppm): 8.42 (s, 4H), 8.14 (d, *J* = 8.2 Hz, 8H), 7.50 (d, *J* = 8.2 Hz, 8H), 4.77–4.68 (m, 2H), 3.94 (s, 12H), 2.06–1.89 (m, 4H), 1.80–1.64 (m, 4H), 0.84 (t, *J* = 7.4 Hz, 12H).

¹³C-NMR (126 MHz, CD$_2$Cl$_2$): δ (ppm): 167.2, 163.9, 147.7, 147.5, 133.3, 131.6, 130.0, 129.9, 128.6, 127.8, 126.3, 122.0, 58.3, 52.6, 25.3, 11.6.

FD/MS (8kV): m/z= 1066.6 (100 %) [M+].

UV-Vis (in CH$_2$Cl$_2$): λ$_{max}$ (ε): 459 nm (1.65 x 10^4 M^{-1}cm^{-1}), 491 nm (4.47 x 10^4 M^{-1}cm^{-1}), 528 nm (7.02 x 10^4 M^{-1}cm^{-1}).

Fluorescence (in CH$_2$Cl$_2$) λ$_{max}$: (λ$_{ex}$= 528 nm): 542 nm, 581 nm. φ$_F$: 0.43.

IR spectrum (ATR): ν$_{max}$ [cm^{-1}]= 3059; 2957; 2932; 2874; 1713; 1695; 1695; 1655; 1597; 1545; 1434; 1402; 1341; 1313; 1271; 1225; 1177; 1097; 1019; 962; 893; 857; 816; 800; 774; 745; 700; 618; 566.

Elemental Analysis: theoretical (%): C: 74.28; H: 5.10; N: 2.63;
experimental (%): C: 73.99; H: 5.34; N: 2.61.

10.2.29 *N,N'*-Bis(1-heptyloctyl)-2,5,8,11-tetrakis[4-benzonitril]perylene-3,4:9,10-tetracarboxylic acid diimide (C7SW-4PhCN-PDI)
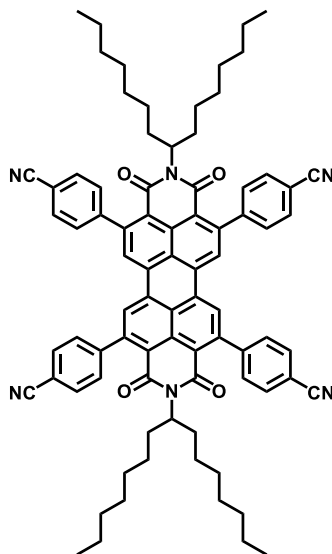
N,N'-Bis(1-heptyloctyl)-2,5,8,11-tetrakis[4,4,5,5-tetramethyl-1,3,2-dioxaborolan-2-y]perylene-3,4:9,10-tetracarboxylic acid diimide (100 mg, 0.08 mmol) and 4-bromo-benzonitrile (83 mg, 0.46 mmol) were mixed together and dissolved in 30 mL toluene and 0.3 mL ethanol. Potassium carbonate (252 mg, 1.83 mmol) was dissolved in 3 mL of water and added to the reaction mixture. After bubbling argon through the solution for 30 minutes, Pd(PPh$_3$)$_4$ (53 mg, 0,05 mmol) was added. Again argon was bubbled through the reaction mixture for 30 minutes. The reaction was then heated under argon atmosphere for 14 hours at 80 °C. After cooling the system to room temperature, the solvent was evaporated and the mixture purified by column chromatography (silica, CH$_2$Cl$_2$). The desired product was obtained as an orange solid with 70 % yield (65 mg, 0.05 mmol).

¹H-NMR (700 MHz, CD$_2$Cl$_2$): δ (ppm): 8.37 (s, 4H), 7.80 (d, *J* = 8.1 Hz, 8H), 7.52 (d, *J* = 8.1 Hz, 8H), 4.86–4.80 (m, 2H), 1.99–1.91 (m, 4H), 1.63 (m, 4H), 1.28–1.14 (m, 40H), 0.84 (t, *J* = 7.1 Hz, 12H).

¹³C-NMR (176 MHz, CD$_2$Cl$_2$): δ (ppm): 164.0, 163.1, 147.6, 146.8, 133.3, 132.6, 131.5, 129.3, 127.7, 126.5, 122.6, 121.9, 119.2, 112.2 55.4, 32.5, 32.4, 29.9, 29.8, 27.4, 23.2, 14.4.

FD/MS (8kV): m/z= 1216:3 (100 %) [M+].

UV-Vis (in CH$_2$Cl$_2$): λ$_{max}$ (ε): 460 nm (1.56 x 10^4 M^{-1}cm^{-1}), 491 nm (4.07 x 10^4 M^{-1}cm^{-1}), 528 nm (6.29 x 10^4 M^{-1}cm^{-1}).

Fluorescence (in CH$_2$Cl$_2$) λ$_{max}$: (λ$_{ex}$=528 nm): 542 nm, 581 nm. φ$_F$: 0.69.

IR spectrum (ATR): ν$_{max}$ [cm^{-1}]= 2923; 2853; 2227; 1696; 1657; 1598; 1541; 1433; 1403; 1339; 1315; 1225; 1109; 1021; 923; 842; 827; 750; 575.

Elemental Analysis: theoretical (%): C: 81.02; H: 6.80; N: 6.91;
experimental (%): C: 81.21; H: 6.78; N: 6.61.

10.2.30 *N,N'*-Bis(1-heptyloctyl)-2,5,8,11-tetrachloro-perylene-3,4:9,10-tetracarboxylic acid diimide (C7SW-4Cl-PDI)
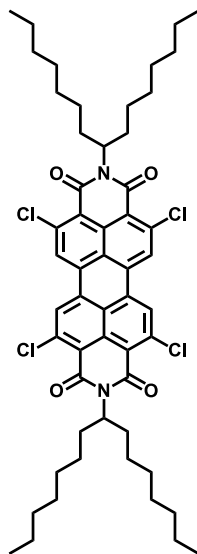
N,N'-Bis(1-heptyloctyl)-2,5,8,11-tetrakis[4,4,5,5-tetramethyl-1,3,2-dioxaborolan-2-yl]perylene-3,4:9,10-tetracarboxylic acid diimide (1.00 g, 0.76 mmol) and $CuCl_2$ (1.23 g, 9.13 mmol) were suspended in 160 ml of a 5/2/1 mixture of dioxane/methanol/water and heated at 120 °C for 12 hours in a sealed pressure vial. The reaction mixture was then cooled down, poured into HCl (1.0 M) and the precipitate filtered. The desired compound was isolated as a yellow solid after column chromatography (silica, dichloromethane: petrol ether 1:1) in 87 % yield (0.63 g, 0.66 mmol).

¹H-NMR (500 MHz, CD_2Cl_2): δ (ppm): 8.46 (s, 4H), 5.23–5.07 (m, 2H), 2.19 (m, 4H), 1.98–1.81 (m, 4H), 1.41–1.17 (m, 40H), 0.84 (t, *J* = 6.4 Hz, 12H).

¹³C-NMR (126 MHz, CD_2Cl_2): δ (ppm): 161.4 141.3, 133.1, 132.9, 128.5, 124.1, 120.6, 56.0, 32.8, 32.4, 30.0, 29.8, 27.6, 23.2, 14.5.

FD/MS (8kV): m/z= 947.7 (100 %) [M+].

UV-Vis (in CH_2Cl_2): λ_{max} (ε): 389 nm (9.21 x 10^3 $M^{-1}cm^{-1}$), 441 nm (1.50 x 10^4 $M^{-1}cm^{-1}$), 470 nm (3.86 x 10^4 $M^{-1}cm^{-1}$), 505 nm (5.70 x 10^4 $M^{-1}cm^{-1}$).

Fluorescence (in CH_2Cl_2): λ_{max}: (λ_{ex}= 505 nm): 515 nm, 552 nm. φ_F: 0.47.

IR spectrum (ATR): v_{max} [cm⁻¹]= 2951; 2920; 2852; 1699; 1659; 1593; 1575; 1543; 1426; 1328; 1289; 1253; 1229; 1187; 1115; 922; 908; 879; 855; 830; 816; 748; 712.

Elemental Analysis: theoretical (%): C: 68.35; H: 7.01; N: 2.95;
experimental (%): C: 68.48; H: 6.74; N: 2.57.

10.2.31 *N,N'*-Bis(1-heptyloctyl)-2,5,8,11-tetrabromo-perylene-3,4:9,10-tetracarboxylic acid diimide (C7SW-4Br-PDI)
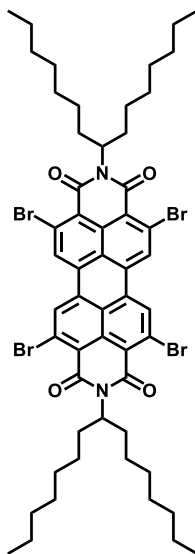
N,N'-Bis(1-heptyloctyl)-2,5,8,11-tetrakis[4,4,5,5-tetramethyl-1,3,2-dioxaborolan-2-y]perylene-3,4:9,10-tetracarboxylic acid diimide (1.00 g, 0.76 mmol) and $CuBr_2$ (2.04 g, 9.13 mmol) were suspended in 160 ml of a 5/2/1 mixture of dioxane/methanol/water and heated at 120 °C for 12 hours in a sealed pressure vial. The reaction mixture was then cooled down, poured into HCl (1.0 M) and the precipitate filtered. The desired compound was isolated as an orange solid after column chromatography (silica, dichloromethane: petrol ether 1:1) in 92 % yield (0.79 g, 0.70 mmol).

^{1}H-NMR (500 MHz, CD_2Cl_2): δ (ppm): 8.74 (s, 4H), 5.22–5.07 (m, 2H), 2.19 (m, 4H), 1.88 (m, 4H), 1.39–1.18 (m, 40H), 0.84 (t, *J* = 6.3 Hz, 12H).

^{13}C-NMR (126 MHz, CD_2Cl_2): δ (ppm): 161.7, 133.1, 132.8, 132.1, 129.4, 125.2, 122.1, 56.3, 32.8, 32.4, 30.0, 29.8, 27.5, 23.2, 14.4.

FD/MS (8kV): m/z= 1124.8 (100 %) [M+].

UV-Vis (in CH_2Cl_2): λ_{max} (ε): 395 nm (1.57 x 10^4 $M^{-1}cm^{-1}$), 445 nm (2.06 x 10^4 $M^{-1}cm^{-1}$), 474 nm (5.34 x 10^4 $M^{-1}cm^{-1}$), 509 nm (7.90 x 10^4 $M^{-1}cm^{-1}$).

Fluorescence (in CH_2Cl_2): λ_{max}: (λ_{ex}= 509 nm): 519 nm, 558 nm. φ_F: 0.21.

IR spectrum (ATR): v_{max} [cm^{-1}]= 2953; 2921; 2853; 1659; 1588; 1567; 1540; 1462; 1423; 1399; 1372; 1326; 1283; 1229; 1189; 1113; 902; 878; 815; 746; 722; 679.

Elemental Analysis: theoretical (%): C: 57.56; H: 5.90; N: 2.49;
experimental (%): C: 57.25; H: 6.27; N: 2.52.

10.2.32 *N,N'*-Bis(1-heptyloctyl)-2,5,8,11-tetraiodo-perylene-3,4:9,10-tetracarboxylic acid diimide (C7SW-4I-PDI)
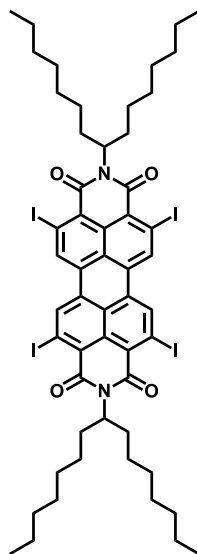
Synthetic Route 1

N,N'-Bis(1-heptyloctyl)-2,5,8,11-tetrakis[4,4,5,5-tetramethyl-1,3,2-dioxaborolan-2-y]perylene-3,4:9,10-tetracarboxylic acid diimide (100 mg, 0.08 mmol) was suspended in 50 mL of a 1/3 water/THF mixture. Chloramine-T (600 mg, 4.53 mmol) and sodium iodide (680 mg, 4.53 mmol) were added to the reaction, the vessel sealed and heated at 55 °C for 12 hours without light. After cooling the reaction to room temperature, 10 mL of a saturated solution of sodium sulfite were added. Successively the reaction mixture was thrown in 100 mL of water, the solid filtered, dried and purified by column chromatography (1/1 PE/CH$_2$Cl$_2$). The target molecule was obtained as a red solid with 42 % yield (42 mg, 0.03 mmol).

Synthetic Route 2

N,N'-Bis(1-heptyloctyl)-2,5,8,11-tetrakis[4,4,5,5-tetramethyl-1,3,2-dioxaborolan-2-y]perylene-3,4:9,10-tetracarboxylic acid diimide (100 mg, 0.08 mmol) and HBF$_2$ (142 mg, 1,82 mmol) were suspended in 24 ml of isopropanol and heated at 55 °C for 45 minutes. After cooling the reaction to room temperature, 30 ml of petrol ether were added and the precipitate filtered. The so obtained material was suspended in 50 mL of a 1/1 water/THF mixture. Chloramine-T (600 mg, 4.53 mmol) and sodium iodide (680 mg, 4.53 mmol) were added to the reaction, the vessel sealed and heated at 55 °C for 12 hours without light. After cooling the reaction to room temperature, 10 mL of a saturated solution of sodium sulfite were added to the reaction. Successively the reaction mixture was thrown in 100 mL of water, the solid filtrated, dried and purified by column chromatography (1/1 PE/CH$_2$Cl$_2$). The target compound was obtained as a red solid with 51 % yield (52 mg, 0.04 mmol).

^{1}H-NMR (700 MHz, CD$_2$Cl$_2$): δ (ppm): 9.10 (s, 4H), 5.22–5.11 (m, 2H), 2.26–2.14 (m, 4H), 1.95–1.87 (m, 4H), 1.40–1.18 (m, 40H), 0.84 (t, *J* = 7.0 Hz, 12H).

^{13}C-NMR (176 MHz, CD$_2$Cl$_2$): δ (ppm): 161.3, 139.1, 138.6, 132.4, 131.7, 126.3, 124.1, 56.6, 32.8, 32.4, 30.0, 29.8, 27.5, 23.2, 14.4.

FD/MS (8kV): m/z= 1315.4 (100 %) [M+].

UV-Vis (in CH$_2$Cl$_2$): λ$_{max}$(ε): 425 nm (2.00 x 10^4 M^{-1}cm^{-1}), 451 nm (2.47 x 10^4 M^{-1}cm^{-1}), 483 nm (4.95 x 10^4 M^{-1}cm^{-1}), 518 nm (7.23 x 10^4 M^{-1}cm^{-1}).

IR spectrum (ATR): ν$_{max}$ [cm^{-1}]= 2952; 2919; 2850; 1699; 1650; 1581; 1559; 1531; 1458; 1424; 1370; 1331; 1276; 1230; 1115; 879; 843; 811; 761; 743; 721; 658; 593; 528.

Elemental Analysis: theoretical (%): C: 49.33; H: 5.06; N: 2.13;
                        experimental (%): C: 49.68; H: 5.01; N: 2.24.

10.2.33   *N,N'*-Bis(1-heptyloctyl)-2,5,8,11-tetrafluoro-perylene-3,4:9,10-tetracarboxylic acid diimide (C7SW-4F-PDI)
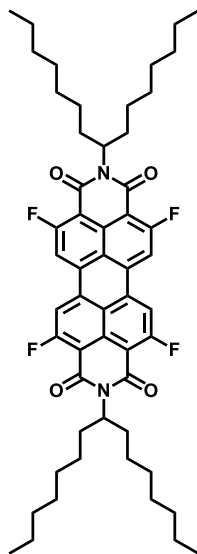
N,N'-Bis(1-heptyloctyl)-2,5,8,11-tetrachloro-perylene-3,4:9,10-tetracarboxylic acid diimide (200 mg, 0.21 mmol) and potassium fluoride (244 mg, 4.20 mmol) were suspended in 2 mL dioxane and 1 ml diglyme and heated at 150 °C for 20 hours in a sealed vessel in a microwave oven. The reaction mixture was then cooled down, the solvent removed and the remaining solid purified by column chromatography (silica gel, dichloromethane/petrol ether 2/1). The desired compound was obtained as a yellow solid in 2 % yield (3 mg, 3 μmol).

¹H-NMR (250 MHz, CD$_2$Cl$_2$): δ (ppm): 8.23 (d, *J* = 12.4 Hz, 4H), 5.15 (m, 2H), 2.18 (m, 4H), 1.82 (m, 4H), 1.25 (m, 40H), 0.92–0.73 (m, 12H).
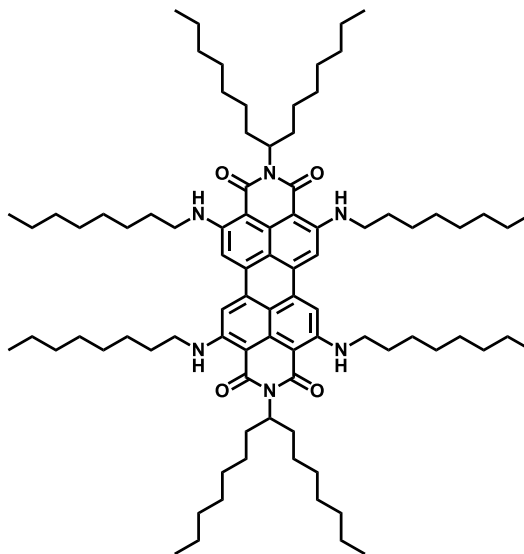
FD Mass Spectrum (8kV): m/z= 882.9 (100 %) [M+].

UV-Vis (in dichloromethane): λ$_{max}$: 500 nm.

Fluorescence (in dichloromethane): λ$_{max}$: (λ$_{ex}$= 500 nm): 509 nm.

The missing characterizations could not be performed, due to the small amounts of materials.

10.2.34 *N,N'*-Bis(1-heptyloctyl)-2,5,8,11-tetrakis[octylamino]perylene-3,4:9,10-tetracarboxylic acid diimide (C7SW-4N-PDI)

N,N'-Bis(1-heptyloctyl)-2,5,8,11-tetraiodo-perylene-3,4:9,10-tetracarboxylic acid diimide (100 mg, 0.08 mmol) was suspended in 10 mL octylamine. The reaction mixture was heated at 130 °C under argon atmosphere for 3 hours. After cooling the reaction to room temperature, 50 mL of water were added and the precipitate filtrated and dried. The target compound was isolated as a dark red solid with 96 % yield (96 mg, 0.07 mmol).

The same experimental procedure can be applied to *N,N'*-Bis(1-heptyloctyl)-2,5,8,11-tetrabromo-perylene-3,4:9,10-tetracarboxylic acid diimide.

^{1}H-NMR (500 MHz, $C_2Cl_4D_2$, 373 K): δ (ppm): 10.18 (s, 4H), 7.43 (s, 4H), 5.19 (m, 2H), 3.44 (d, *J* = 5.7 Hz, 8H), 2.16 (m, 4H), 1.84–1.70 (m, 12H), 1.45 (m, 8H), 1.23 (m, 72H), 0.78 (dd, *J* = 25.2, 6.6 Hz, 24H).

^{13}C-NMR (126 MHz, $C_2Cl_4D_2$, 373 K): δ (ppm): 166.7, 153.7, 135.6, 134.8, 110.8, 103.8, 99.8, 53.5, 43.1, 32.7, 31.8, 31.8, 29.7, 29.6, 29.4, 29.2, 29.2, 27.4, 27.1, 22.6, 22.5, 13.9.

FD/MS (8kV): m/z= 1319.4 (100 %) [M+].

UV-Vis (in CH_2Cl_2): $\lambda_{max}(\varepsilon)$: 512 nm (5.42 x 10^4 $M^{-1}cm^{-1}$).

Fluorescence (in CH_2Cl_2): λ_{max}: (λ_{ex}=512 nm): 608 nm, 654 nm. φ_F: 0.05.

IR spectrum (ATR): ν_{max} [cm^{-1}]= 3207; 2953; 2919; 2849; 1639; 1606; 1582; 1507; 1484; 1466; 1441; 1399; 1369; 1343; 1227; 1209; 1150; 883; 827; 814; 749; 721; 662; 620.

Elemental Analysis: calculated (%): C: 78.25; H: 10.54; N: 6.37;
experimental (%): C: 78.51; H: 10.73; N: 6.30.

10.2.35 *N,N'*-Bis(1-ethylpropyl)-2,5,8,11-tetracyano-perylene-3,4:9,10-tetracarboxylic acid diimide (C2SW-4CN-PDI)
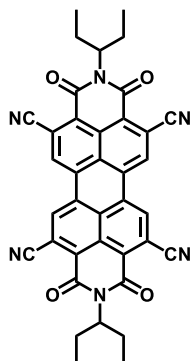
N,N'-Bis(1-ethylpropyl)-2,5,8,11-tetrakis[4,4,5,5-tetramethyl-1,3,2-dioxaborolan-2-y]perylene-3,4:9,10-tetracarboxylic acid diimide (50 mg, 0.048 mmol), zinc cyanide (68 mg, 0.58 mmol), cesium fluoride (29 mg, 0,19 mmol) and copper nitrate (90 mg, 0.38 mmol) were suspended in a mixture of water, methanol and dioxane (1 ml, 1 ml and 1 ml). The reaction vessel was closed and heated in a microwave oven for 1 hour at 100 °C. The reaction was then thrown in a saturated solution of ammonium chloride and extracted with dichloromethane. The organic phase was dried over magnesium sulfate and the solvent evaporated. The product was purified via column chromatography (silica, dichloromethane/acetone 50/1) and obtained as a red-orange solid (yield 30 %, 9.0 mg, 0.014 mmol).

^{1}H-NMR (250 MHz, CD_2Cl_2): δ (ppm): 8.98 (s, 4H), 5.09 (m, 2H), 2.38–2.16 (m, 4H), 2.11–1.90 (m, 4H), 0.96 (t, *J* = 7.5 Hz, 12H).

^{13}C-NMR: due to the strong aggregation of the molecule, the spectrum could not be measured.

FD Mass Spectrum (8kV): m/z= 630,9 (100 %) [M+].

UV-Vis (in CH_2Cl_2): λ_{max}(ε): 517 nm (7,31 x 10^4 $M^{-1}cm^{-1}$).

Fluorescence (in CH_2Cl_2): λ_{max}: (λ_{ex}=517 nm): 525 nm; φ_F: 0.52.

Elemental Analysis: calculated (%): C: 72.37; H: 4.13; N: 13.33;
experimental (%): C: 70.51; H: 4.44; N: 14.30.

Elemental analyses of several batches of the material were measured, however deviations were always observed, probably due to incomplete combustion of the solid.

10.2.36   *N,N'*-Bis(1-heptyloctyl)-2,5,8,11-tetracyano-perylene-3,4:9,10-tetracarboxylic acid diimide (C7SW-4CN-PDI)
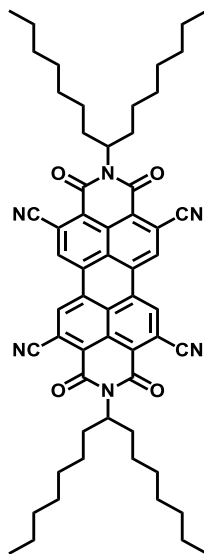
Synthetic Route 1

N,N'-Bis(1-heptyloctyl)-2,5,8,11-tetrakis[4,4,5,5-tetramethyl-1,3,2-dioxaborolan-2-yl]perylene-3,4:9,10-tetracarboxylic acid diimide (63 mg, 0.05 mmol), cesium fluoride (29 mg, 0.19 mmol) zinc cyanide (68 mg, 0.58 mmol) and copper(II) nitrate ·2.5 H$_2$O (89 mg, 0.38 mmol) were suspended in 3 ml of a 5/1 mixture of dioxane/methanol and heated in a microwave vessel at 80 °C for 5 minutes. The reaction mixture was then poured in a saturated solution of ammonium chloride and extracted with dichloromethane. The organic phase was dried over magnesium sulfate and the solvent evaporated. The desired compound was isolated as a brownish solid after column chromatography (silica, dichloromethane) in 40 % yield (18 mg, 0.019 mmol).

Synthetic Route 2

N,N'-Bis(1-heptyloctyl)-2,5,8,11-tetrabromo-perylene-3,4:9,10-tetracarboxylic acid diimide (1.00 g, 0.89 mmol) and copper(I) cyanide (1.59 g, 17.8 mmol) were suspended in 170 ml of anhydrous DMF and heated under argon atmosphere at 130 °C for 30 minutes. The reaction was then cooled down and 170 mL of a saturated solution of Mohrsches salt added. The mixture was then heated to 60 °C for 3 hours and then cooled again to room temperature. After extracting the mixture with chloroform, the organic phases were collected and dried over magnesium sulfate. The chloroform was then removed via rotary evaporation and from the remaining DMF solution a red precipitate was filtered and dried. The product was isolated after column chromatography (silica, dichloromethane) as a brownish solid in 82 % yield (0.66 g, 0.72 mmol).

^{1}H-NMR (500 MHz, CD$_2$Cl$_2$): δ (ppm): 8.99 (s, 4H), 5.25–5.14 (m, 2H), 2.30–2.12 (m, 4H), 1.93 (m, 4H), 1.29 (m, 40H), 0.84 (t, J = 5.7 Hz, 12H).

^{13}C-NMR (126 MHz, CD$_2$Cl$_2$): δ (ppm): 161.3, 133.2, 131.0, 129.9, 128.7, 127.4, 117.6, 117.3, 57.2, 32.6, 32.3, 30.0, 29.7, 27.5, 23.2, 14.4.

FD/MS (8kV): m/z= 909.9 (100 %) [M+].

UV-Vis (in CH$_2$Cl$_2$): λ$_{max}$ (ε): 451 nm (1.30 x 10^3 M^{-1}cm^{-1}), 482 nm (3.99 x 10^4 M^{-1}cm^{-1}), 518 nm (7.00 x 10^4 M^{-1}cm^{-1}).

Fluorescence (in CH$_2$Cl$_2$): λ$_{max}$: (λ$_{ex}$= 518 nm): 528 nm, 568 nm. φ$_F$: 0.55.

IR spectrum (ATR): ν$_{max}$ [cm^{-1}]= 2954; 2924; 2855; 2236; 2221; 1705; 1659; 1602; 1560; 1498; 1455; 1434; 1412; 1398; 1349; 1310; 1264; 1230; 1205; 1115; 925; 906; 823; 746; 721; 622; 595; 552.

Elemental Analysis: theoretical (%): C: 76.45; H: 7.30; N: 9.22;
experimental (%): C: 76.80; H: 6.98; N: 9.50.

10.2.37 *N,N'*-Bis(1-heptyloctyl)-2,5,10,13-tetrabromo-terrylene-3,4:11,12-tetracarboxylic acid diimide (*o*-C7SW-4Br-TDI)
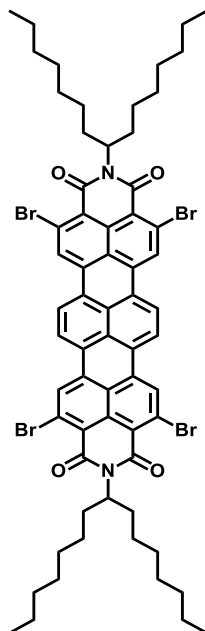
N,N'-Bis(1-heptyloctyl)-2,5,10,13-tetrakis[4,4,5,5-tetramethyl-1,3,2-dioxaborolan-2-yl]terrylene-3,4:11,12-tetracarboxylic acid diimide (0.40 g, 0.28 mmol) and CuBr$_2$ (0.75 g, 3.33 mmol) were suspended in 100 ml of a 8/1/1 mixture of dioxane/methanol/water and heated at 120 °C for 12 hours in a sealed pressure vial. The reaction mixture was then cooled down, poured in 0.1 M HCl and filtered. The desired compound was obtained after column chromatography (silica, toluene) as a blue solid in 78 % yield (0.27 g, 0.22 mmol).

^{1}H-NMR (250 MHz, CD$_2$Cl$_2$): δ (ppm): 8.41 (s, 4H), 8.10 (s, 4H), 5.25–5.04 (m, 2H), 2.41–2.10 (m, 4H), 2.10–1.85 (m, 4H), 1.30 (m, 40H), 0.87 (t, *J* = 6.6 Hz, 12H).

^{13}C-NMR (126 MHz, CD$_2$Cl$_2$): δ (ppm): 161.3, 134.0, 132.9, 129.6, 129.5, 128.9, 127.5, 124.4, 124.1, 120.3, 56.3, 32.9, 32.5, 30.2, 29.9, 27.9, 23.3, 14.5.

FD/MS (8kV): m/z= 1251.9 (100 %) [M+].

UV-vis (in CHCl$_3$): λ_{max} (ε): 640 nm (1.52 x 10^5 M^{-1}cm^{-1}), 588 nm (8.23 x 10^4 M^{-1}cm^{-1}), 545 nm (2.69 x 10^4 M^{-1}cm^{-1}).

Fluorescence (in CHCl$_3$) λ_{max}: (λ_{ex}=632 nm): 654 nm, 713 nm. φ_F: 0.89.

IR spectrum (ATR): ν_{max} [cm^{-1}]=2952; 2919; 2850; 1701; 1654; 1581; 1533; 1494; 1441; 1417; 1326; 1261; 1236; 1199; 1084; 1033; 904; 871; 856; 839; 809; 760; 724; 692; 638; 595.

Elemental Analysis: theoretical (%): C, 61.45; H, 5.64; N, 2.24;
experimental (%): C: 61.28; H: 5.92; N: 2.40.

10.2.38 *N,N'*-Bis(1-heptyloctyl)-2,5,10,13-tetracyano-terrylene-3,4:11,12-tetracarboxylic acid diimide (*o*-C7SW-4CN-TDI)
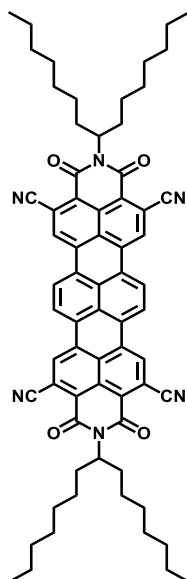
N,N'-Bis(1-heptyloctyl)-2,5,10,13-tetrabromo-terrylene-3,4:11,12-tetracarboxylic acid diimide (70 mg, 56 µmol) and copper(I) cyanide (0.10 g, 1.12 mmol) were mixed together and suspended in 20 mL anhydrous DMF in argon atmosphere. The reaction was heated at 130 °C for 30 minutes. After cooling the system to room temperature, 40 mL of saturated solution of ammonium iron(II) sulfate were added and the mixture heated to 60 °C for 2 hours. After cooling to room temperature the solution was extracted with chloroform (3 x 80 mL), the organic phases were collected, extracted with brine (3 x 80 mL) and dried over magnesium sulfate. Chloroform was evaporated and the solid precipitating from the remaining solution was filtered and purified via column chromatography (silica, CH$_2$Cl$_2$). The desired product was obtained as a dark blue solid with 42 % yield (24 mg, 24 µmol).

^{1}H-NMR (250 MHz, C$_2$D$_2$Cl$_4$): δ (ppm): 8.89 (s, 4H), 8.77 (s, 4H), 5.19 (m, 2H), 2.20 (m, 4H), 1.98 (m, 4H), 1.25 (m, 40H), 0.85 (m, 12H).

^{13}C-NMR (126 MHz, deuterated orthodichlorobenzene, 373 K): δ (ppm): 191.2, 161.4, 135.9, 131.0, 130.2, 128.7, 127.9, 126.3, 125.2, 117.6, 117.5, 33.3, 32.5, 30.2, 29.9, 27.9, 23.2, 14.4.

FD/MS (8kV): m/z= 1033.4 (100 %) [M+].

UV-vis (in CHCl$_3$): λ$_{max}$ (ε): 661 nm (1.48 x 10^5 M^{-1}cm^{-1}), 607 nm (6.40 x 10^4 M^{-1}cm^{-1}), 560 nm (1.79 x 10^4 M^{-1}cm^{-1}).

Fluorescence (in c CHCl$_3$): λ$_{max}$: (λ$_{ex}$=632 nm): 680 nm, 739 nm. φ$_F$: 1.00.

IR spectrum (ATR): ν$_{max}$ [cm^{-1}]= 2924; 2853; 2226; 1702; 1655; 1588; 1553; 1460; 1422; 1382; 1339; 1327; 1287; 1263; 1231; 1211; 1112; 1028; 908; 880; 847; 816; 766; 722; 694; 672; 648; 617; 575.

Elemental Analysis: theoretical (%): C, 78.89; H, 6.81; N, 8.12;
experimental (%): C: 78.54; H: 6.47; N: 8.01.

10.2.39 *N,N'*-Bis(1-heptyloctyl)-1,6,9,14-tetrabromo-terrylene-3,4:11,12-tetracarboxylic acid diimide (*b*-C7SW-4Br-TDI)
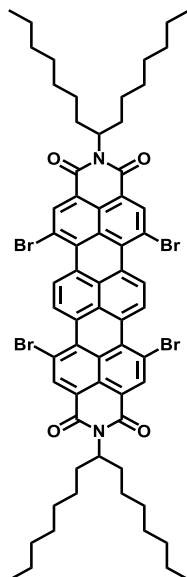
N,N'-Bis(1-heptyloctyl)-terrylene-3,4:11,12-tetracarboxylic acid diimide (1.50 g, 1.60 mmol) was dissolved in 620 mL chloroform. Successively 17 mL of bromine were added to the solution and the reaction was heated in exclusion of light for 12 hours. After cooling the system to room temperature, 400 mL of a saturated solution of Na_2SO_3 were added and, after stirring the mixture for 30 minutes, the phases were separated. The organic solution was then dried over anhydrous magnesium sulfate and afterwards solvent was evaporated. The desired product was separated from the three times brominated TDI derivative by dissolving the solid in 200 mL of dichloromethane and afterwards precipitating it by addition of petrol ether (300 mL) and methanol 200 mL. The process was repeated until the triply cyanated derivative was completely removed (monitored via TLC, SiO_2, toluene). The desired product was obtained as a dark blue solid (1.71 g, 1.37 mmol, 85 % yield).

^{1}H-NMR (500 MHz, 373 K, $C_2Cl_4D_2$): δ (ppm): 9.56 (s, 4H), 8.95 (s, 4H), 5.19 (m, 2H), 2.42–2.13 (m, 4H), 2.05-1.85 (m, 4H), 1.58–1.25 (m, 40H), 0.92 (s, br, 12H).

^{13}C-NMR (126 MHz, 373 K, $C_2Cl_4D_2$): δ (ppm): 162.6 137.9, 133.5, 131.1, 129.8, 129.0, 127.3, 126.3, 121.9, 120.1, 55.1, 32.3, 31.6, 29.2, 28.9, 26.8, 22.3, 13.7.

FD/MS (8kV): m/z= 1251.9 (100 %) [M+].

UV-vis (in $CHCl_3$): λ_{max} (ε): 651 nm (8.75 x 10^4 $M^{-1}cm^{-1}$), 599 nm (4.86 x 10^4 $M^{-1}cm^{-1}$).

Fluorescence (in $CHCl_3$): λ_{max}: (λ_{ex}=632 nm): 683 nm. φ_F: 0.79.

IR spectrum (ATR): ν_{max} [cm^{-1}]= 2951; 2921; 2853; 1701; 1657; 1583; 1492; 1459; 1407; 1342; 1306; 1235; 1176; 976; 917; 845; 808; 765; 722; 699; 690; 629.

Elemental Analysis: theoretical (%): C, 61.45; H, 5.64; N, 2.24;
experimental (%): C: 61.35; H: 5.55; N: 2.25.

10.2.40 *N,N'*-Bis(1-heptyloctyl)-1,6,9,14-tetracyano-terrylene-3,4:11,12-tetracarboxylic acid diimide (*b*-C7SW-4CN-TDI)
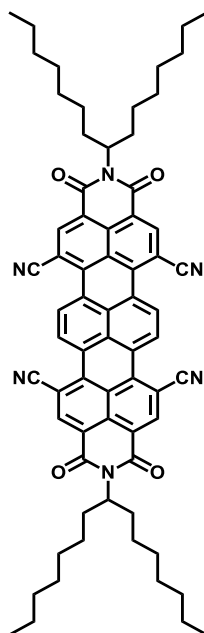
N,N'-Bis(1-heptyloctyl)-1,6,9,14-tetrabromo-terrylene-3,4:11,12-tetracarboxylic acid diimide (0.43 g, 0.34 mmol) and copper(I) cyanide (0.62 g, 6.88 mmol) were suspended in 130 mL anhydrous DMF in argon atmosphere. The reaction was heated at 150 °C for 4 hours. After cooling the system to room temperature, 120 mL of saturated solution of ammonium iron(II) sulfate were added and the mixture was heated to 60 °C for 2 hours. After cooling to room temperature, the solution was extracted with chloroform (3 x 80 mL), the organic phases were collected and dried over magnesium sulfate. Successively chloroform was evaporated and the solution cooled down to room temperature. The precipitate was filtered and purified via column chromatography (silica, dichloromethane). The desired product was obtained as a dark blue solid with 70 % yield (0.25 g, 0.24 mmol).

^{1}H-NMR (500 MHz, $C_2Cl_4D_2$, 373 K): δ (ppm): 9.88 (s, 4H), 9.07 (s, 4H), 5.21 (tt, *J* = 8.9, 6.0 Hz, 2H), 2.38–2.21 (m, 4H), 2.06–1.89 (m, 4H), 1.46–1.23 (m, 40H), 0.92 (t, *J* = 6.9 Hz, 12H).

^{13}C-NMR (126 MHz, $C_2Cl_4D_2$, 373 K): δ (ppm): 161.6, 137.8, 137.2, 130.7, 129.6, 128.8, 128.0, 126.5, 123.1, 118.8, 108.5, 55.8, 32.2, 31.5, 29.2, 28.9, 26.7, 22.3, 13.7.

FD/MS (8kV): m/z= 1032.5 (100 %) [M+].

UV-vis (in $CHCl_3$): λ_{max} (ε): 657 nm (1.12 x 10^5 $M^{-1}cm^{-1}$), 602 nm (5.98 x 10^4 $M^{-1}cm^{-1}$), 558 nm (1.97 x 10^4 $M^{-1}cm^{-1}$).

Fluorescence (in $CHCl_3$): λ_{max}: (λ_{ex}=632 nm): 673 nm, 732 nm. φ_F: 1.00.

IR spectrum (ATR): ν_{max} [cm^{-1}]=2953; 2922; 2853; 2218; 1705; 1657; 1599; 1537; 1464; 1412; 1375; 1353; 1314; 1254; 1179; 1123; 1056; 928; 852; 813; 769; 724; 696; 676; 615; 578.

Elemental Analysis: theoretical (%): C, 78.89; H, 6.81; N, 8.12;
experimental (%): C: 78.85; H: 6.74; N: 8.02.

## 10.2.41 Perylenetetracarboxylic 3,4:9,10-diimide (NH-PDI)
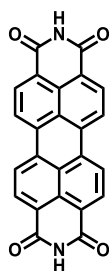
N,N'-Bis(1-ethylpropyl) perylene-3,4:9,10-tetracarboxylic acid (70 mg, 0.13 mmol) was sealed under vacuum in a glass ampoule. The system was then put into an oven and heated according to the following ramp: 40 °C to 420 °C in 90 minutes, 420 °C for 90 minutes and cooling to room temperature over 90 minutes.

After reaction the ampoule was opened. The dark violet solid was separated from the glass and dried in an oven under vacuum at 110 °C for 12 hours to remove traces of the alkene developed during the reaction. The desired material was obtained as a dark solid in quantitative yield.

The product could also be synthesized starting from *N,N'*-Bis(1-heptyloctyl) perylene-3,4:9,10-tetracarboxylic acid (0,10 g,) and applying the same procedure as above.

The experimental data agree with those reported in the literature.

10.2.42 Terrylene-3,4:11,12-tetracarboxylic acid diimide (NH-TDI)
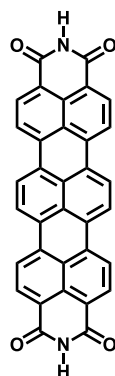
N,N'-Bis(1-heptyloctyl)-terrylene-3,4:11,12-tetracarboxylic acid diimide (0.80 g, 0.86 mmol) was sealed under vacuum in a glass ampoule. The system was then put into an oven and heated according to the following ramp: 40 °C to 440 °C in 90 minutes, 44 °C for 90 minutes and cooled to room temperature in 90 minutesAfter reaction the ampoule was opened. The dark violet solid was separated from the glass and dried in an oven under vacuum at 110 °C for 12 hours to remove traces of the alkene developed during the reaction. The desired material was obtained as a dark blue solid in quantitative yield.

¹H-NMR (500 MHz, Chloroform-d₃): δ (ppm): 10.62 (s, 8H), 10.42 (d, *J* = 8.4 Hz, 8H), 10.33 (d, *J* = 8.1 Hz, 8H).

¹³C-NMR (126 MHz, D_2SO_4): δ (ppm): 164.4 (set as standard), 144.9, 138.3, 135.0, 133.4, 132.3, 127.8, 127.4, 125.7, 115.1.

MALDI-TOF analysis (m/z): 514.53 (100 %) [M+].

IR spectrum (ATR): ν_{max} [cm⁻¹] = 3138; 3090; 3014; 2845; 1662; 1571; 1505; 1424; 1377; 1362; 1302; 1272; 1213; 1117; 1009; 880; 839; 807; 787; 743; 729; 689; 679; 665; 647; 526.

Elemental Analysis: calculated: C, 79.37; H, 2.74; N, 5.44;
experimental C, 79.38; H, 2.98; N, 5.22.

### 10.2.43 2,5,8,11-Tetracyano-perylene-3,4:9,10-tetracarboxylic acid diimide (NH-4CN-PDI)
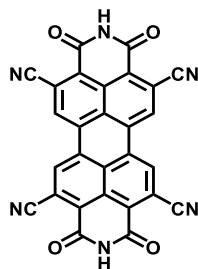
N,N'-Bis(1-heptyloctyl)-2,5,8,11-tetracyano-perylene-3,4:9,10-tetracarboxylic acid diimide was sealed under vacuum in a glass ampoule. The system was then put into an oven and heated according to the following ramp: 40 °C to 380 °C in 90 minutes, 380 °C for 90 minutes and cooled to room temperature in 90 minutes. After reaction the ampoule was opened. The dark violet solid was separated from the glass and dried in an oven under vacuum at 110 °C for 12 hours to remove traces of the alkene developed during the reaction. The material was obtained as a dark solid.

Elemental Analysis: calculated (%): C, 68.58; H, 1.23; N, 17.14;
experimental (%): C, 69.81; H, 2.66; N, 13.38.

Elemental analysis was repeated several times, not providing any matching results. Other characterization techniques were not applicable due to the extreme insolubility of the material.

10.2.44 *N*-(1-Ethylpropyl)-2,5-bis[3,3-dimethylbutyl]-8,11-bis[4,4,5,5-tetramethyl-1,3,2-dioxaborolan-2-y]-perylene-3,4-dicarboxylic acid monoimide (C2SW-alk-8,11-bor-PMI)
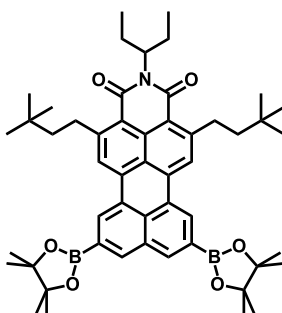
N-(1-Ethylpropyl)-2,5-bis[3,3-dimethylbutyl]perylene-3,4-dicarboxylic acid monoimide (0.100 g, 0.179 mmol), bis(pinacolato)diboron (0.10 g, 0.39 mmol), [Ir(OMe)cod]$_2$ (5.9 mg, 8.9 μmol) and dtbpy (4.8 mg, 18 μmol) were mixed in an oven dried flask under argon atmosphere. Anhydrous cyclohexane (3 ml) was added and the reaction heated for 1 hour at 80 °C in a microwave oven. After cooling down to room temperature, the solvent was evaporated and the solid purified by column chromatography (silica gel, first CH$_2$Cl$_2$/AcOEt 50/1 and afterwards CH$_2$Cl$_2$/acetone/MeOH 30/5/1). The desired compound was isolated as an orange powder in 74 % yield (0.11 g, 0.13 mmol).

^{1}H-NMR (250 MHz, CD$_2$Cl$_2$): δ (ppm): 8.78 (s, 2H), 8.40 (s, 2H), 8.26 (s, 2H), 5.19–4.99 (m, 1H), 3.47 (dt, *J* = 24.7, 10.7 Hz, 4H), 2.44–2.16 (m, 2H), 2.00–1.77 (m, 2H), 1.65–1.52 (m, 4H), 1.44 (s, 24H), 1.09 (s, 18H), 0.92 (t, *J* = 7.4 Hz, 6H).

^{13}C-NMR (63 MHz, CD$_2$Cl$_2$): δ (ppm): 165.4, 152.0, 139.5, 135.8, 133.7, 133.3, 131.5, 129.4, 129.2, 128.3, 125.4, 125.4, 119.6, 85.2, 57.6, 46.6, 33.2, 31.6, 30.0, 25.9, 25.6, 12.0.

FD Mass Spectrum (8kV): m/z= 815.0 (100 %) [M+].

IR spectrum (ATR): ν_{max} [cm^{-1}]= 2956; 2872; 1687; 1648; 1589; 1547; 1517; 1449; 1416; 1379; 1331; 1302; 1269; 1215; 1141; 1004; 968; 871; 855; 829; 763; 708; 689; 667.

UV-vis (in toluene): λ_{max} (ε): 474 nm (2.87 x 10^4 M^{-1}cm^{-1}), 501 nm (2.59 x 10^4 M^{-1}cm^{-1}).

Fluorescence (in toluene): λ_{max}: (λ_{ex}= 474 nm): 529 nm, 561 nm. φ_F: 0.56.

HR-MS (ESI-MS) ([M + H]+): m/z calculated = 812.5257, experimental= 812.5233.

10.2.45 *N*-(1-Ethylpropyl)-8,11-bis[4,4,5,5-tetramethyl-1,3,2-dioxaborolan-2-y]-perylene-3,4-dicarboxylic acid monoimide (C2SW-8,11-bor-PMI)
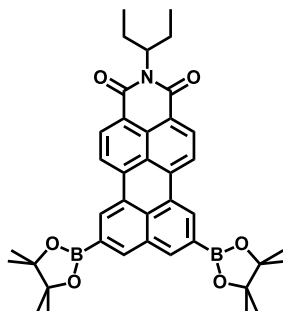
N-(1-Ethylpropyl) perylene-3,4-dicarboxylic acid monoimide (2.00 g, 5.11 mmol), bis(pinacolato) diboron (3.11 g, 12.3 mmol), [Ir(OMe)cod]$_2$ (0.17 g, 0.26 mmol) and dtbpy (0.14 g, 0.51 mmol) were mixed in an oven dried flask under argon atmosphere. Anhydrous THF (80 ml) was added and the reaction heated for 18 hours at 60 °C. After cooling to room temperature, the solvent was evaporated and residue dissolved in dichloromethane, precipitated in methanol and filtered. The process was repeated three times. Final purification was done by GPC column (dichlormethane, Bio-Beads S-X1 Beads 200-400 mesh). The desired product was obtained as a red solid (68 % yield, 2,24 g, 3.47 mmol).

^{1}H-NMR (250 MHz, CD$_2$Cl$_2$): δ (ppm): 8.78 (s, 2H), 8.57–8.44 (m, 4H), 8.35 (s, 2H), 5.15–4.94 (m, 1H), 2.40–2.15 (m, 2H), 2.02–1.78 (m, 2H), 1.44 (s, 24H), 0.91 (t, *J* = 7.5 Hz, 6H).

^{13}C-NMR (63 MHz, CD$_2$Cl$_2$): δ (ppm): 164.9, 139.5, 137.4, 133.5, 132.6, 131.2, 130.6, 129.9, 128.8, 128.2, 127.3, 121.7, 120.9, 85.0, 57.6, 25.6, 25.3, 11.7.

FD Mass Spectrum (8kV): m/z= 642,6 (100 %) [M+]

IR spectrum (ATR): ν_{max} [cm^{-1}]= 2972; 2933; 2876; 1687; 1650; 1584; 1457; 1412; 1388; 1347; 1296; 1283; 1270; 1243; 1209; 1139; 1087; 1010; 966; 891; 867; 848; 828; 806; 788; 775; 751; 706; 686; 668; 627; 590; 563.

UV-vis (in toluene): λ_{max} (ε): 481 nm (2.98 x 10^4 M^{-1}cm^{-1}), 509 nm (2.83 x 10^4 M^{-1}cm^{-1}).

Fluorescence (in toluene): λ_{max}: (λ_{ex} = 481 nm): 532 nm, 568 nm. φ_F: 0.51.

Elemental Analysis: calculated (%): C, 72.81; H, 6.74; N, 2.18;
experimental (%): C, 72.72; H, 6.84; N, 2.11.

10.2.46 *N*-(1-Heptyloctyl)-8,11-bis[4,4,5,5-tetramethyl-1,3,2-dioxaborolan-2-y]-perylene-3,4-dicarboxylic acid monoimide (C7SW-8,11-bor-PMI)
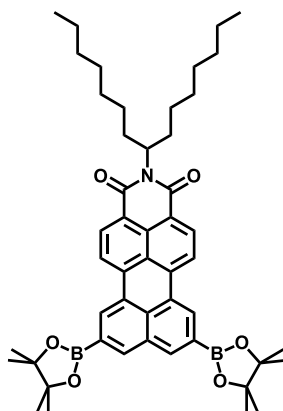
N-(1-Heptyloctyl)-perylene-3,4-dicarboxylic acid monoimide (0.76 g, 1.42 mmol), bis(pinacolato) diboron (0.87 g, 3.43 mmol), [Ir(OMe)cod]$_2$ (0.047 g, 0.26 mol) and dtbpy (0.137 g, 0.51 mmol) were mixed in an oven dried flask under argon atmosphere. Anhydrous THF (80 ml) was added and the reaction heated for 18 hours at 60 °C. After cooling to room temperature, the solvent was evaporated and the residue dissolved in dichloromethane, precipitated in methanol and filtered. The process was repeated three times. Afterwards the material was purified by GPC column (dichlormethane, Bio-Beads S-X1 Beads 200-400 mesh). The desired product was isolated as a red powder (71 % yield, 2,24 g, 3.47 mmol).

¹H-NMR (250 MHz, CD$_2$Cl$_2$): δ (ppm): 8.51 (s, 2H), 8.34 (d, *J* = 5.5 Hz, 2H), 8.23 (d, *J* = 8.2 Hz, 2H), 8.16 (s, 2H), 5.20 (tt, *J* = 9.2, 5.9 Hz, 1H), 2.41–2.17 (m, 4H), 1.98-1.81 (m, 2H), 1.48 (s, 24H), 1.41–1.12 (m, 20H), 0.84 (t, *J* = 6.6 Hz, 6H).

¹³C-NMR (63 MHz, CD$_2$Cl$_2$): δ (ppm): 165.3, 164.4, 139.4, 137.0, 133.2, 131.9, 131.2, 130.8, 130.3, 129.6, 128.5, 128.1, 127.0, 122.0, 121.2, 120.6, 84.9, 54.6, 33.0, 32.5, 30.2, 29.9, 27.7, 25.4, 23.2, 14.5.

FD Mass Spectrum (8kV): m/z= 785.1 (100 %) [M+].

IR spectrum (ATR): ν_{max} [cm^{-1}]=2975; 2925; 2855; 1650; 1584; 1457; 1416; 1389; 1371; 1346; 1296; 1269; 1243; 1207; 1141; 1111; 1088; 1008; 966; 895; 851; 829; 775; 753; 705; 685; 667.
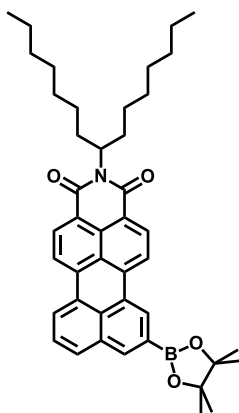
UV-vis (in toluene): λ_{max} (ε): 482 nm (3.24 x 10^4 M^{-1}cm^{-1}), 510 nm (3.06 x 10^4 M^{-1}cm^{-1}).

Fluorescence (in toluene): λ_{max}:(λ_{ex} = 482 nm): 532 nm, 568 nm. φ_F: 0.53.

Elemental Analysis: calculated: C, 75.10; H, 8.10; N, 1.79;
experimental: C, 75.06; H, 7.69; N, 1.78.

10.2.47 *N*-(1-Heptyloctyl)-8-[4,4,5,5-tetramethyl-1,3,2-dioxaborolan-2-y]-perylene-3,4-dicarboxylic acid monoimide (C7SW-8-bor-PMI)

N-(1-Heptyloctyl)-perylene-3,4-dicarboxylic acid monoimide (0.50 g, 0.94 mmol), bis(pinacolato) diboron (0.26 g, 1.03 mmol), [Ir(OMe)cod]$_2$ (0.016 g, 24 μ mol) and dtbpy (0.013 g, 47 μmol) were mixed in an oven dried flask under argon atmosphere. Anhydrous cyclohexane (50 ml) was added and the reaction heated for 18 hours at 60 °C. Solvent wasevaporated and the residue was dissolved in dichloromethane, precipitated in methanol and filtered. The process was repeated several times until the N-(1-heptyloctyl)-9-[4,4,5,5-tetramethyl-1,3,2-dioxaborolan-2-y]-perylene-3,4-dicarboxylic acid monoimide was not more visible on TLC. The solid was then purified by GPC column (THF, Bio-Beads S-X1 Beads 200-400 mesh). The desired product was obtained as a red powder (26 % yield, 0.16 g, 0.24 mmol).

¹H-NMR (300 MHz, CD$_2$Cl$_2$): δ (ppm): 8.79 (s, 1H), 8.59–8.46 (m, 6H), 8.43 (d, *J* = 8.1 Hz, 1H), 8.36 (s, 1H), 7.99–7.91 (m, 1H), 7.65 (t, *J* = 7.8 Hz, 1H), 2.45–2.10 (m, 2H), 1.95–1.70 (m, 2H), 1.42 (s, 12H), 1.37–1.13 (m, 20H), 0.81 (t, *J* = 6.6 Hz, 6H).

¹³C-NMR (63 MHz, CD$_2$Cl$_2$): δ (ppm): 165.6, 138.9, 137.4, 134.2, 131.9, 130.5, 129.8, 129.7, 129.0, 128.9, 127.5, 127.2, 126.0, 125.0, 120.9, 120.6, 85.0, 34.7, 32.9, 32.4, 30.6, 30.1, 29.8, 27.5, 25.4, 23.2, 14.4.

FD Mass Spectrum (8kV): m/z= 657.8 (100 %) [M+].

IR spectrum (ATR): ν$_{max}$ [cm^{-1}]=2924; 2854; 1689; 1650; 1584; 1468; 1418; 1348; 1312; 1287; 1244; 1210; 1139; 1106; 968; 884; 850; 799; 752; 688; 617; 575.

UV-vis (in toluene): λ$_{max}$ (ε): 480 nm (3.75 x 10^4 M^{-1}cm^{-1}), 508 nm (3.66 x 10^4 M^{-1}cm^{-1}).

Fluorescence (in toluene): λ$_{max}$: (λ$_{ex}$=480 nm): 529 nm, 565 nm. φ$_F$: 0.69.

Elemental Analysis: calculated: C, 78.53; H, 7.97; N, 2.13;
experimental C, 78.42; H, 7.88; N,2.15.

10.2.48 *N*-(1-Ethylpropyl)-8,11-bis-chloro-perylene-3,4-dicarboxylic acid monoimide (C2SW-8,11-Cl-PMI)
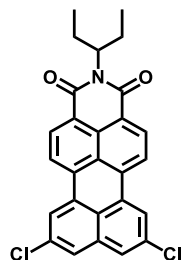
N-(1-Ethylpropyl)-8,11-bis[4,4,5,5-tetramethyl-1,3,2-dioxaborolan-2-y]-perylene-3,4-dicarboxylic acid monoimide (0.60 g, 0.93 mmol) was suspended in a mixture of dioxane (100 ml), methanol (10 ml) and water (10 ml) in a 210 mL pressure vial. Copper(II) chloride (1.25 g, 9.33 mmol) was added, the vessel sealed and heated up to 120 °C for 12 hours. The reaction mixture was poured into 200 mL of 1.0 M hydrochloric acid and filtered. After column chromatography (silica, toluene) and crystallization from toluene, the desired compound was isolated as a dark orange powder (yield 54 %, 0.23 g, 0.50 mmol).

^{1}H-NMR (250 MHz, $C_2D_2Cl_4$): δ (ppm): 8.51 (d, *J* = 8.0 Hz, 2H), 8.26 (d, *J* = 8.2 Hz, 2H), 8.13 (d, *J* = 1.7 Hz, 2H), 7.62 (d, *J* = 1.5 Hz, 2H), 4.98 (d, *J* = 6.0 Hz, 1H), 2.31–2.08 (m, 2H), 2.02–1.81 (m, 2H), 0.89 (t, *J* = 7.4 Hz, 6H).

^{13}C-NMR (126 MHz, D_2SO_4, 373 K): δ (ppm): 164.7, 164.4, 149.1, 148.9, 140.4, 139.0, 138.4, 138.1, 137.2, 135.2, 131.7, 129.0, 126.1, 125.5, 122.4, 112.0, 111.8, 71.8, 25.7, 11.2 (signal at 11.15 set as reference using the chemical shift of the same carbon obtained from a ^{13}C-NMR in tetrachloroethane).

FD Mass Spectrum (8kV): m/z= 460,6 (100 %) [M+].

IR spectrum (ATR): $ν_{max}$ [cm^{-1}]= 3069; 2964; 2929; 2873; 1688; 1647; 1614; 1587; 1489; 1458; 1397; 1357; 1341; 1280; 1242; 1200; 1158; 1113; 1083; 1001; 916; 863; 848; 825; 813; 784; 750; 638; 621.

UV-vis (in toluene): $λ_{max}$ (ε): 494 nm (2.61 x 10^4 M^{-1}cm^{-1}), 465 nm (2.00 x 10^4 M^{-1}cm^{-1}).

Fluorescence (in toluene): $λ_{max}$: ($λ_{ex}$=474 nm): 512 nm, 545 nm. $φ_F$: 0.67.
($λ_{ex}$=494 nm): 512 nm, 545 nm. $φ_F$: 0.64.

Elemental Analysis: calculated: C, 70.44; H, 4.16; N, 3.04;
experimental C, 70.66; H, 3.99; N, 2.94.

10.2.49 *N*-(1-Ethylpropyl)-8,11-bis-bromo-perylene-3,4-dicarboxylic acid monoimide (C2SW-8,11-Br-PMI)
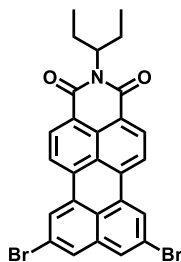
N-(1-Ethylpropyl)-8,11-bis[4,4,5,5-tetramethyl-1,3,2-dioxaborolan-2-y]-perylene-3,4-dicarboxylic acid monoimide (0.60 g, 0.93 mmol) was suspended in a mixture of dioxane (100 ml), methanol (10 ml) and water (10 ml) in a 210 mL pressure vial. Copper(II) bromide (2.08 g, 9.33 mmol) was added, the vessel sealed and heated up to 120 °C for 12 hours. The reaction mixture was poured into 200 mL of 1.0 M hydrochloric acid and filtered. After column chromatography (silica, toluene) and crystallization from toluene, the desired compound was isolated as an orange solid (yield 48 %, 0.25 g, 0.48 mmol).

^{1}H-NMR (500 MHz, $C_2Cl_4D_2$, 373 K): δ (ppm): 8.64 (d, *J* = 5.2 Hz, 2H), 8.50 (s, 2H), 8.43 (d, *J* = 6.0 Hz, 2H), 7.98 (s, 2H), 5.20–4.94 (m, 1H), 2.35–2.21 (m, 2H), 2.08–1.95 (m, 2H), 1.03–0.96 (m, 6H).

^{13}C-NMR (126 MHz, D_2SO_4, 373 K): δ (ppm): 164.7, 164.4, 148.8, 148.6, 145.8, 143.7, 143.5, 139.9, 139.0, 138.2, 135.5, 131.6, 128.9, 126.0, 125.6, 125.5, 125.4, 122.7, 112.1, 111.9, 71.6, 25.7, 11.1 (Signal at 11.1 set as reference using the chemical shift of the same carbon obtained from a ^{13}C-NMR in tetrachloroethane).

FD Mass Spectrum (8kV): m/z= 549.6 (100 %) [M+].

IR spectrum (ATR): v_{max} [cm^{-1}]= 3055; 2966; 2939; 2873; 1686; 1686; 1642; 1612; 1585; 1355; 1320; 1283; 1241; 1203; 1083; 1062; 906; 864; 851; 833; 825; 800; 787; 771; 749; 631; 592; 573; 561.

UV-vis (in toluene): λ_{max} (ε): 495 nm (3.21 x 10^4 M^{-1}cm^{-1}), 466 nm (2.45 x 10^4 M^{-1}cm^{-1}).

Fluorescence (in toluene): λ_{max}: (λ_{ex}=475 nm): 512 nm, 548 nm. φ_F: 0.63.
(λ_{ex}=495 nm): 512 nm, 548 nm. φ_F: 0.63.

Elemental Analysis: calculated: C, 59.04; H, 3.49; N, 2.55;
experimental: C, 59.12; H, 3.62; N, 2.51.

10.2.50 *N*-(1-Heptyloctyl)-8,11-bis-bromo-perylene-3,4-dicarboxylic acid monoimide (C7SW-8,11-Br-PMI)
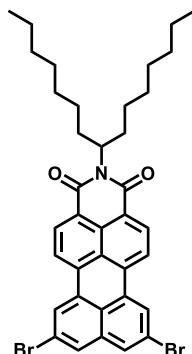
N-(1-Heptyloctyl)-8,11-bis[4,4,5,5-tetramethyl-1,3,2-dioxaborolan-2-y]-perylene-3,4-dicarboxylic acid monoimide (1.00 g, 1.28 mmol) was suspended in a mixture of THF (90 ml), methanol (10 ml) and water (10 ml) in a 210 mL pressure vial. Copper(II) bromide (2.85 g, 12.8 mmol) was added, the vessel sealed and heated up to 120 °C for 12 hours. After cooling to room temperature, the reaction mixture was poured into 200 mL of 1.0 M hydrochloric acid and filtered to obtain a red solid. The desired compound was isolated after column chromatography (silica, toluene) as a bright orange powder (yield 38 %, 0.34 g, 0.49 mmol).

^{1}H-NMR (500 MHz, CD$_2$Cl$_2$): δ (ppm): 8.32 (s, br, 2H), 7.80 (d, *J* = 8.0 Hz, 2H), 7.73 (s, 2H), 7.35 (s, 2H), 5.21–5.06 (m, 1H), 2.31–2.17 (m, 2H), 1.94–1.77 (m, 2H), 1.42–1.20 (m, 20H), 0.86 (t, *J* = 6.6 Hz, 6H).

^{13}C-NMR (126 MHz, CD$_2$Cl$_2$): δ (ppm): 165.0, 136.3, 134.2, 131.7, 131.1, 130.8, 129.7, 126.2, 126.1, 124.7, 123.4, 122.5, 121.2, 54.9, 32.9, 32.5, 30.2, 29.9, 27.7, 23.2, 14.5.

FD Mass Spectrum (8kV): m/z= 549.6 (100 %) [M+].

IR spectrum (ATR): ν_{max} [cm^{-1}]=2922; 2853; 1695; 1649; 1613; 1589; 1456; 1399; 1355; 1339; 1323; 1282; 1243; 1174; 1108; 1084; 864; 849; 826; 808; 783; 749; 722; 632.

UV-vis (in toluene): λ_{max} (ε): 496 nm (3.68 x 10^4 M^{-1}cm^{-1}), 467 nm (2.84 x 10^4 M^{-1}cm^{-1}).

Fluorescence (in toluene): λ_{max} :(λ_{ex}=475 nm): 512 nm, 548 nm. φ_F: 0.64.
                              (λ_{ex}=496 nm): 512 nm, 548 nm. φ_F: 0.65.

HR-MS (ESI-MS) ([M + H]+): m/z calculated = 688.1426, experimental = 688.1393.

10.2.51 *N*-(1-Heptyloctyl)-8-(4-benzonitril)-perylene-3,4-dicarboxylic acid monoimide (C7SW-8-PhCN-PMI)
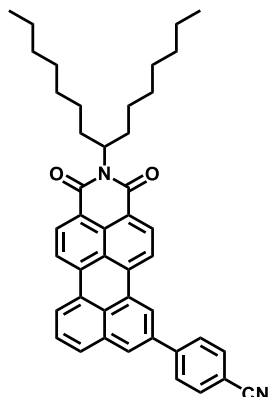
N-(1-Heptyloctyl)-8-[4,4,5,5-tetramethyl-1,3,2-dioxaborolan-2-y]-perylene-3,4-dicarboxylic acid monoimide (40 mg, 0.08 mmol) and 4-bromo-benzonitrile (21 mg, 0.11 mmol) were dissolved in 10 mL toluene and 0.1 mL ethanol. Potassium carbonate (63 mg, 0.46 mmol) was dissolved in 1 mL of water and added to the reaction mixture. After bubbling argon through the solution for 30 minutes, $Pd(PPh_3)_4$ (9 mg, 7.6 μmol) was added. After further bubbling for 30 minutes, the reaction was heated under inert atmosphere for 28 hours at 80 °C. Cooled the reaction mixture to room temperature, the solvent was evaporated. The desired compound was obtained after chromatographic purification (silica, CH_2Cl_2) as an orange solid with 88 % yield (33 mg, 0.05 mmol).

^{1}H-NMR (700 MHz, CD_2Cl_2): δ (ppm): 8.45–8.36 (m, 3H), 8.27 (d, *J* = 8.0 Hz, 1H), 8.22 (d, *J* = 7.5 Hz, 1H), 8.20 (d, *J* = 7.9 Hz, 1H), 7.98 (s, 1H), 7.89–7.79 (m, 5H), 7.54 (t, *J* = 7.7 Hz, 1H), 5.20–5.11 (m, 1H), 2.30–2.16 (m, 2H), 1.86 (ddt, *J* = 14.6, 10.9, 5.3 Hz, 2H), 1.42–1.13 (m, 20H), 0.83 (t, *J* = 6.9 Hz, 6H).

^{13}C-NMR (63 MHz, CD_2Cl_2): δ (ppm): 165.3, 164.4, 145.0, 138.1, 136.6, 136.5, 135.0, 133.4, 131.9, 131.4, 130.6, 130.3, 129.6, 129.3, 128.5, 128.2, 127.9, 127.0, 124.3, 122.6, 122.0, 120.9, 119.3, 112.3, 54.7, 32.4, 30.1, 29.9, 27.6, 23.2, 14.4.

FD Mass Spectrum (8kV): m/z= 633.1 (100 %) [M+].

IR spectrum (ATR): v_{max} [cm^{-1}]= 2924; 2854; 2226; 1691; 1648; 1593; 1575; 1494; 1455; 1369; 1348; 1295; 1242; 1173; 1135; 1109; 838; 827; 797; 765; 751; 627; 606.

UV-vis (in toluene): λ_{max} (ε): 476 nm (3.31 x 10^4 M^{-1}cm^{-1}), 504 nm (3.65 x 10^4 M^{-1}cm^{-1}).

Fluorescence (in toluene): λ_{max}: (λ_{ex}= 504 nm): 522 nm, 561 nm. φ_F: 0.56.

HR-MS (ESI-MS) ([M + H]+): m/z calculated = 633.3481, experimental= 633.3462.

10.2.52 *N*-(1-Heptyloctyl)-8,11-di[2-nitrophenyl]-perylene-3,4-dicarboxylic acid monoimide (C7SW-8,11-PhNO₂-PMI)
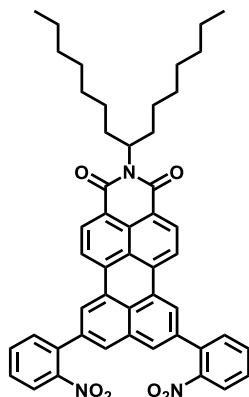
N-(1-Heptyloctyl)-8,11-bis[4,4,5,5-tetramethyl-1,3,2-dioxaborolan-2-y]-perylene-3,4-dicarboxylic acid (0.070 g, 0.09 mmol) and 1-bromo-2-nitrobenzene (0.054 g, 0.27 mmol) were dissolved in 15 mL toluene and 0.15 mL ethanol. Potassium carbonate (148 mg, 1.07 mmol) was dissolved in 1.5 mL of water and added to the reaction mixture. After bubbling argon through the solution for 30 minutes, Pd(PPh₃)₄ (28 mg, 18 μmol) was added. After bubbling argon through the solution for other 30 minutes, the reaction was heated under argon atmosphere for 28 hours at 80 °C. After cooling to room temperature, the solvent was evaporated. The reaction mixture was dissolved in dichloromethane and filtered over silica. Finally, after gel permeation chromatography using THF as eluent, the desired compound was isolated in 82 % yield (57 mg, 0.07 mmol).

¹H-NMR (250 MHz, CD₂Cl₂): δ (ppm): 8.46 (s, 2H), 8.44–8.29 (m, 4H), 8.04 (dt, *J* = 8.1, 1.8 Hz, 2H), 7.86 (t, *J* = 1.8 Hz, 2H), 7.83–7.73 (m, 2H), 7.73–7.58 (m, 4H), 5.15 (tt, *J* = 9.1, 5.8 Hz, 1H), 2.34–2.12 (m, 1H), 1.94–1.74 (m, 2H), 1.38–1.11 (m, 20H), 0.82 (t, *J* = 6.4 Hz, 6H).

¹³C-NMR (63 MHz, CD₂Cl₂): δ (ppm): 149.5, 138.0, 136.4, 136.0, 134.8, 133.6, 132.9, 132.1, 131.4, 130.5, 130.4, 129.9, 129.7, 127.4, 127.3, 125.1, 124.3, 121.4, 54.8, 32.9, 32.4, 30.1, 29.8, 27.5, 23.2, 14.4.

FD Mass Spectrum (8kV): m/z= 773.9 (100 %) [M+].

IR spectrum (ATR): ν_{max} [cm⁻¹]=2925; 2855; 1687; 1647; 1587; 1522; 1455; 1402; 1345; 1302; 1240; 1108; 878; 855; 829; 782; 752; 704; 675; 650; 627; 611; 606.

UV-vis (in CH₂Cl₂): λ_{max} (ε): 476 nm (3.81 x 10⁴ M⁻¹cm⁻¹), 501 nm (4.20 x 10⁴ M⁻¹cm⁻¹).

Fluorescence (in CH₂Cl₂): λ_{max}: (λ_{ex}= 501 nm): 529 nm. φ_F: 0.01.

Elemental Analysis: calculated (%): C, 76.05; H, 6.12; N, 5.43;
experimental (%): C, 75.58; H, 6.41; N, 5.30.

10.2.53 *N*-(1-Heptyloctyl)-8,11-bis(bis(4-(2,4,4-trimethylpentane-2-yl)phenyl)amino)-perylene-3,4-dicarboxylic acid monoimide (C7SW-8,11-diamino-PMI)
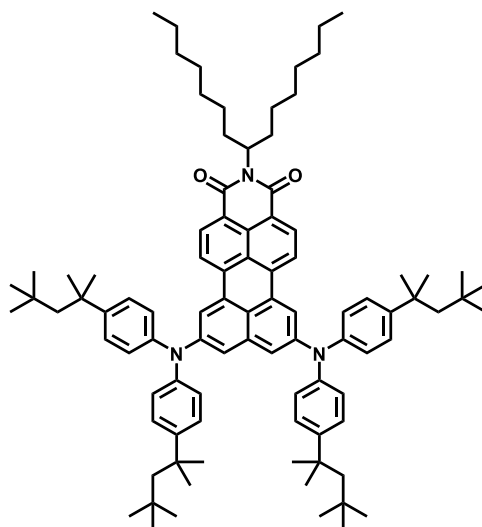
N-(1-Heptyloctyl)-8,11-bis-bromo-perylene-3,4-dicarboxylic acid monoimide (70 mg, 0.10 mmol) and bis(4-(2,4,4-trimethylpentan-2-yl)phenyl)amine (0.11 mg, 0.27 mmol) were mixed together with sodium-tert-butylate (60 mg, 6.24 mmol) tris(dibenzylideneacetone)dipalladium(0) (18 mg, 20 μmol) and tri(tert-butyl)phosphine (7 mg, 35μmol) in 7 mL anhydrous toluene under nitrogen atmosphere. The reaction was successively heated at 80 °C for 36 hours. After cooling the reaction mixture to room temperature, the solvent was removed and the product purified via column chromatography (silica gel, PE:dichloromethane 2:1) The target compound was isolated as a red solid after reprecipitation in methanol from dichloromethane. (72 % yield, 96 mg, 0.07 mmol).

^{1}H-NMR (250 MHz, CD_2Cl_2): δ (ppm): 8.37 (s, 2H), 8.06–7.86 (m, 1H), 7.34 (d, *J* = 8.6 Hz, 1H), 7.14–7.02 (m, 2H), 5.22–5.02 (m, 1H), 2.27–2.08 (m, 2H), 1.84-1.67 (m, 10H), 1.38 (s, 24H), 1.32–1.11 (m, 20H), 0.84-0.72 (m, 42H).

^{13}C-NMR (63 MHz, CD_2Cl_2): δ (ppm): 165.5, 148.0, 146.1, 144.9, 137.5, 137.2, 131.9, 131.1, 130.4, 130.1, 128.0, 127.2, 124.9, 120.7, 120.1, 119.7, 118.7, 57.6, 38.7, 32.7, 32.4, 32.0, 31.8, 30.1, 29.8, 27.4, 23.2, 14.4.

FD Mass Spectrum (8kV): m/z= 773.9 (100 %) [M+].

IR spectrum (ATR): ν_{max} [cm^{-1}]=2952; 2926; 2860; 1694; 1655; 1620; 1592; 1507; 1465; 1404; 1364; 1349; 1328; 1253; 1216; 1192; 1096; 1016; 853; 828; 802; 754; 603.

UV-vis (in toluene): λ_{max} (ε): 457 nm (2.27 x 10^4 M^{-1}cm^{-1}), 473 nm (2.23 x 10^4 M^{-1}cm^{-1}), 550 nm (1.84 x 10^4 M^{-1}cm^{-1}).

Fluorescence (in toluene): λ_{max}: (λ_{ex}= 473 nm): 637 nm. φ_F: 0.05.

HR-MS (ESI-MS) ([M + H]+): m/z calculated = 1314.9694, experimental = 1314.9727.

11 List of Publications

11.1 Publications

1. Kamm, V., Battagliarin, G., Howard, I. A., Pisula, W., Mavrinskiy, A., Li, C., Müllen, K. & Laquai, F. (2011). Polythiophene: Perylene Diimide Solar Cells–the Impact of Alkyl-Substitution on the Photovoltaic Performance. *Advanced Energy Materials*, *1*(2), 297-302.

2. Battagliarin, G., Li, C., Enkelmann, V., & Müllen, K. (2011). 2, 5, 8, 11-Tetraboronic ester perylenediimides: a next generation building block for dye-stuff synthesis. *Organic Letters*, *13*(12), 3012-3015.

3. Battagliarin, G., Zhao, Y., Li, C., & Müllen, K. (2011). Efficient Tuning of LUMO Levels of 2, 5, 8, 11-Substituted Perylenediimides via Copper Catalyzed Reactions. *Organic Letters*, *13*(13), 3399-3401.

4. Xu, X., Stöttinger, S., Battagliarin, G., Hinze, G., Mugnaioli, E., Li, C., Müllen, K. & Basché, T. (2011). Assembly and separation of semiconductor quantum dot dimers and trimers. *Journal of the American Chemical Society*, *133*(45), 18062-18065.

5. Papadopoulos, P., Deng, X., Mammen, L., Drotlef, D. M., Battagliarin, G., Li, C., Müllen, K., Landfester, K., del Campo, A., Butt, H. J. & Vollmer, D. (2012). Wetting on the microscale: shape of a liquid drop on a microstructured surface at different length scales. *Langmuir*, *28*(22), 8392-8398.

6. Battagliarin, G., Davies, M., Mackowiak, S., Li, C., & Müllen, K. (2012). Ortho-Functionalized Perylenediimides for Highly Fluorescent Water-Soluble Dyes. *ChemPhysChem*, *13*(4), 923-926.

7. Puniredd, S. R., Kiersnowski, A., Battagliarin, G., Zajączkowski, W., Wong, W. W., Kirby, N., Müllen, K., and Pisula. W., "Polythiophene–perylene diimide heterojunction field-effect transistors." *Journal of Materials Chemistry C* (2013). (2013). Polythiophene–perylene diimide heterojunction field-effect transistors. *Journal of Materials Chemistry C.*

8. Beverina, L., Sanguineti, A., Battagliarin, G., Ruffo, R., Roberto, D., Righetto, S., Soave, R., Lo Presti, L., Ugo, R., & Pagani, G. A. (2011). UV absorbing zwitterionic pyridinium-tetrazolate: exceptional transparency/optical nonlinearity trade-off. *Chemical Communications*, *47*(1), 292-294.

9. De Luca, G., Liscio, A., Battagliarin, G., Chen, L., Scolaro, L. M., Müllen, K., Samorì, P. & Palermo, V. (2013). Orthogonal self-assembly and selective solvent vapour annealing: simplified processing of a photovoltaic blend. *Chemical Communications*.

10. Dorresteijn, R., Ragg, R., Rago, G., Billecke, N., Bonn, M., Parekh, S. H., Battagliarin, G., Peneva, K., Wagner, M. Klapper, M., & Müllen, K. (2013). Biocompatible Polylactide-block-Polypeptide-block-Polylactide Nanocarrier. *Biomacromolecules*, *14*(5), 1572-1577.

11.2 Poster Presentations

1. G. Battagliarin, C. Li, K. Müllen, "Efficient Tuning of LUMO Levels via Ortho-Substitution of Rylenediimides", *10ᵗʰ International Symposium on Functional p-Electron Systems*, Beijing, China, **2011**.

2. G. Battagliarin, C. Li, K. Müllen, "Efficient Tuning of Molecular Orbitals of 2,5,8,11-Substituted Perylenediimides", *10th International Conference on Materials Chemistry*, Manchester, UK, **2011**.

3. G. Battagliarin, Z. Liu, C. Li, K. Müllen, "A Perylene Monoimide Based Sensor for Selective Recognition of Zinc(II) Ions Via Intramolecular Charge Transfer", *9ᵗʰ International Symposium on Functional p-Electron Systems*, Atlanta, GA, U.S.A, **2010**.

11.3 Patent Applications

1. Reichelt, H., Geßner, T., Li, C., Müllen, K., & Battagliarin, G. (2012). *U.S. Patent No. 20,120,289,703*. Washington, DC: U.S. Patent and Trademark Office.

2. Geßner, T., Reichelt, H., Battagliarin, G., Li, C., & Müllen, K. (2013). *WIPO Patent No. 2013024026*. Geneva, Switzerland: World Intellectual Property Organization.

3. Reichelt, H., Geßner, T., Müllen, K., Li, C., & Battagliarin, G. (2012). *U.S. Patent No. 20,120,226,042*. Washington, DC: U.S. Patent and Trademark Office.

4. Reichelt, H., Geßner, T., Li, C., Müllen, K., & Battagliarin, G. (2012). *WIPO Patent No. 2012152598*. Geneva, Switzerland: World Intellectual Property Organization.